

6-23-2016

Interaction of Cementitious Systems with Chemical Admixtures

Natallia Shanahan

University of South Florida, nkashalo@mail.usf.edu

Follow this and additional works at: <http://scholarcommons.usf.edu/etd>

 Part of the [Civil Engineering Commons](#)

Scholar Commons Citation

Shanahan, Natallia, "Interaction of Cementitious Systems with Chemical Admixtures" (2016). *Graduate Theses and Dissertations*.
<http://scholarcommons.usf.edu/etd/6386>

This Thesis is brought to you for free and open access by the Graduate School at Scholar Commons. It has been accepted for inclusion in Graduate Theses and Dissertations by an authorized administrator of Scholar Commons. For more information, please contact scholarcommons@usf.edu.

Interaction of Cementitious Systems with Chemical Admixtures

by

Natallia G. Shanahan

A dissertation submitted in partial fulfillment
of the requirements for the degree of
Doctor of Philosophy
Department of Civil and Environmental Engineering
College of Engineering
University of South Florida

Major Professor: A. Zayed, Ph.D.
Gray Mullins, Ph.D.
Aydin Sunol, Ph.D.
Mahmood Nachabe, Ph.D.
Kyle Riding, Ph.D.

Date of Approval:
June 23, 2016

Keywords: accelerator, heat of hydration, autogenous shrinkage, rheology, microstructure

Copyright © 2016, Natallia G. Shanahan

DEDICATION

To Nicholas. You are my inspiration, and the reason behind everything I do. Love, mom.

ACKNOWLEDGMENTS

I would like to express my gratitude to everyone who helped and guided me along the way and made this endeavor possible. I would first like to thank my advisor Dr. Zayed for her advice, support and encouragement through my PhD study. You've always pushed me out of my comfort zone to become a better researcher and a better engineer. I would also like to thank my supervisory committee for their guidance: Dr. Riding, Dr. Sunol, Dr. Nachabe, Dr. Sen and Dr. Mullins. Additionally, I would like to offer special thanks Dr. Riding. You were always available for questions and problem-solving, thank you for reviewing my papers, your advice and for sharing your extensive knowledge with me. Also, my deep appreciation to Dr. Sunol for the use of his lab and Autosorb-1, which was critical to my research.

I would like to thank all of my friends and colleagues, Dr. Ahmadreza Sedaghat, Andre Bien-Aime, Dan Buidens, Thomas Meagher, Victor Tran, Andrew Williams, Dr. Yuri Stetsko, Ananya Markandeya, and Ahmed Elnihum for their support and assistance in my research. I would like to thank the Florida Department of Transportation (FDOT) and US DOT for providing funds for this research. I would also like to express my appreciation to Dr. DeFord at the FDOT State Materials Office for training and the use of their equipment, as well as my to Robert Tufts, Jay Bieber, and Dr. Emirov for training and the use of NREC equipment.

I would like to thank my parents for their unconditional support and encouragement, I couldn't have done it without you. A special thank you to the Children's Cancer Center, Leanne Vaughn and all the oncology families for your support and encouragement to continue my studies and not give up during this difficult time.

TABLE OF CONTENTS

LIST OF TABLES.....	iii
LIST OF FIGURES	v
ABSTRACT.....	ix
CHAPTER 1: INTRODUCTION.....	1
CHAPTER 2: INTERACTION OF CEMENT MINERALOGY AND CALCIUM CHLORIDE-BASED ACCELERATOR.....	7
2.1 Introduction.....	7
2.2 Experimental Procedures	8
2.2.1 Materials	8
2.2.2 Methodology.....	10
2.3 Results and Discussion	11
2.3.1 As-Received Cements.....	11
2.3.1.1 Isothermal Calorimetry	14
2.3.1.1.1 As-Received Cements.....	14
2.3.1.1.2 Doped Cements.....	18
2.3.1.2 Compressive Strength	29
2.3.1.3 X-ray Diffraction	36
2.4 Conclusions.....	43
CHAPTER 3: EFFECT OF CHLORIDE-BASED ACCELERATOR IN THE PRESENCE OF WATER-REDUCING AND RETARDING ADMIXTURE ON AUTOGENOUS SHRINKAGE	44
3.1 Introduction.....	44
3.2 Experimental Procedures	47
3.2.1 Materials	47
3.2.2 Methodology.....	50
3.3 Results and Discussion	54
3.3.1 Isothermal Calorimetry and Setting Time.....	54
3.3.2 Autogenous Shrinkage Measurements.....	56
3.3.3 Autogenous Shrinkage and Mechanical Property Development	59
3.3.4 X-ray Diffraction Measurements	61
3.3.5 Mercury Intrusion Porosimetry.....	62
3.3.6 Nitrogen Adsorption Porosity Measurements.....	64
3.4 Conclusions.....	68

CHAPTER 4: INFLUENCE OF SCMs ON RHEOLOGY OF PASTE AND ITS DEPENDENCE ON PARTICLE CHARACTERISTICS OF THE MIXTURE	69
4.1 Introduction	69
4.2 Experimental Procedures	72
4.3 Results and Discussion	75
4.3.1 Materials Characterization	75
4.4 Rheology Measurements	77
4.5 Conclusions	95
 CHAPTER 5: MODELING HEAT OF HYDRATION REDUCTION FOR CEMENT REPLACEMENT BY SCMs	97
5.1 Introduction	97
5.2 Experimental Procedures	100
5.3 Results and Discussion	108
5.3.1 Model Development	108
5.3.2 Model Validation	115
5.4 Conclusions	116
 CHAPTER 6: MULTI-TECHNIQUE INVESTIGATION OF METAKAOLIN AND SLAG BLENDED PORTLAND CEMENT PASTES	118
6.1 Introduction	118
6.2 Experimental Procedures	122
6.2.1 Materials	122
6.2.2 Methodology	122
6.2.2.1 Isothermal Calorimetry	122
6.2.2.2 Sample Preparation for X-Ray Diffraction, Nanoindentation and Nitrogen Adsorption	124
6.2.2.3 X-Ray Diffraction and Rietveld Analysis	124
6.2.2.4 Nitrogen Adsorption	125
6.2.2.5 Nanoindentation	126
6.3 Results and Discussion	127
6.3.1 Isothermal Calorimetry	127
6.3.2 Hydration Products	128
6.3.3 Porosity Measurement with Nitrogen Adsorption	129
6.3.4 Nanoindentation	133
6.4 Conclusions	139
 CHAPTER 7: CONCLUSIONS	140
 REFERENCES	144
 APPENDIX A: COPYRIGHT PERMISSIONS	165

LIST OF TABLES

Table 2.1. Commercial accelerator composition	9
Table 2.2. Chemical oxide composition of as-received cements.....	12
Table 2.3. Mineralogical composition and physical properties of as-received cements	13
Table 3.1. Cement composition and physical properties	47
Table 3.2. Concrete mixture proportions	49
Table 4.1. Chemical admixture addition rates	73
Table 4.2. Cement replacement levels for binary, ternary and quaternary mixtures.....	74
Table 4.3. Oxide chemical analysis for as-received cement and mineral admixtures	76
Table 4.4. Cement and mineral admixture densities.....	76
Table 4.5. Particle size analysis of as-received cement and mineral admixtures	77
Table 5.1. Experimental design addition levels.....	103
Table 5.2. Fractional factorial design matrix.....	104
Table 5.3. Additional axial points design matrix.....	104
Table 5.4. Admixture addition rates for validation mixtures.....	106
Table 5.5. Validation mixtures coded levels for each factor	107
Table 5.6. Parameter estimates of the statistical models based on coded values.....	109
Table 5.7. Parameter estimates of the statistical models based on natural values.....	109
Table 6.1. Summary of published elastic moduli values for C-S-H and CH.....	120
Table 6.2. Mixture proportions	123
Table 6.3. Degree of hydration calculated from isothermal calorimetry at 7 days.....	127

Table 6.4. Rietveld analysis of the pastes at the age of 7 days	128
Table 6.5. Consumption of individual clinker phases at the age of 7 days.....	129
Table 6.6. BET surface areas at 7 days.....	132
Table 6.7. Average nanoindentation values.....	133
Table 6.8. Adjusted average values after excluding indentations with E above 40 GPa.....	134
Table 6.9. Results of the deconvolution analysis.....	138

LIST OF FIGURES

Figure 2.1. Heat of hydration curves for as-received Cement 1 pastes	15
Figure 2.2. Heat of hydration curves for as-received Cement 2 pastes	16
Figure 2.3. Heat of hydration curves for as-received Cement 3 pastes	17
Figure 2.4. Effect of increased C ₃ A content on heat of hydration with pure CaCl ₂ and commercial accelerator	20
Figure 2.5. Effect of SO ₃ content on heat of hydration with pure CaCl ₂ and commercial accelerator	21
Figure 2.6. Effect of NaOH on heat of hydration with pure CaCl ₂ and commercial accelerator	22
Figure 2.7. Effect of KOH on heat of hydration with pure CaCl ₂	23
Figure 2.8. Effect Na ₂ SO ₄ on heat of hydration with pure CaCl ₂	24
Figure 2.9. Effect of K ₂ SO ₄ on heat of hydration with pure CaCl ₂ and commercial accelerator	25
Figure 2.10. Effect of C ₃ A and K ₂ SO ₄ on heat of hydration with commercial accelerator	26
Figure 2.11. Effect of K ₂ SO ₄ and gypsum on heat of hydration with pure CaCl ₂	27
Figure 2.12. Combined effect of C ₃ A, K ₂ SO ₄ and gypsum on heat of hydration with pure CaCl ₂ and commercial accelerator.....	28
Figure 2.13. Compressive strength development for Cement 1.....	30
Figure 2.14. Compressive strength development for Cement 2.....	30
Figure 2.15. Compressive strength development for Cement 3.....	31
Figure 2.16. Compressive strength development as a function of degree of hydration.....	33
Figure 2.17. Compressive strength development for non-accelerated mortars	34

Figure 2.18. Compressive strength development for mortars with pure CaCl ₂	34
Figure 2.19. Compressive strength development for mortars with commercial accelerator	35
Figure 2.20. XRD scan of Cement 1 samples at 4 hours	37
Figure 2.21. XRD scan of Cement 1 samples at 24 hours	38
Figure 2.22. XRD scan of Cement 2 samples at 4 hours	39
Figure 2.23. XRD scan of Cement 2 samples at 24 hours	40
Figure 2.24. XRD scan of Cement 3 samples at 4 hours	41
Figure 2.25. XRD scan of Cement 3 samples at 24 hours	42
Figure 3.1. Coarse aggregate grading curve	48
Figure 3.2. Fine aggregate grading curve	49
Figure 3.3. Free shrinkage frame	52
Figure 3.4. Heat flow of cement pastes normalized per gram of cement	54
Figure 3.5. Total heat evolved of cement pastes normalized per gram of cement	55
Figure 3.6. Setting time curves	56
Figure 3.7. Free shrinkage measurements under isothermal conditions at 23°C as a function of time.....	57
Figure 3.8. Free shrinkage measurements under isothermal conditions at 23°C as a function of degree of hydration.....	59
Figure 3.9. Relationship between free shrinkage and tensile strength development	60
Figure 3.10. Relationship between free shrinkage and elastic modulus development	61
Figure 3.11 X-ray diffraction scans of the CHA and CDA mixtures at 3 days	62
Figure 3.12. Pore size distribution of concrete samples determined by mercury intrusion porosimetry at 3 days.....	63
Figure 3.13. Effect of accelerator addition on pore size distribution of concrete determined by MIP at 3 days	64

Figure 3.14. Pore size distribution of cement paste calculated from nitrogen adsorption at the age of 3 days	65
Figure 4.1. Effect of Class F fly ash on rheology of non-plasticized (Ref) and plasticized pastes.....	78
Figure 4.2. Effect of slag on rheology of non-plasticized (Ref) and plasticized pastes	79
Figure 4.3. Effect of silica fume on rheology of non-plasticized (Ref) and plasticized pastes.....	80
Figure 4.4. Effect of metakaolin on rheology of non-plasticized (Ref) and plasticized pastes.....	81
Figure 4.5. Effect of fly ash/silica fume combination on rheology of plasticized paste.....	83
Figure 4.6. Effect of fly ash/metakaolin combination on rheology of plasticized paste	84
Figure 4.7. Effect of slag/metakaolin combination on rheology of plasticized paste.....	85
Figure 4.8. Effect of metakaolin/silica fume/slag combination on rheology of plasticized paste	86
Figure 4.9. Relationship between mean particle size of the OPC and OPC/SCM binary blends and apparent yield stress in the absence of chemical admixtures	87
Figure 4.10. Relationship between mean particle size of the OPC/SCM binary, ternary and quaternary blends and apparent yield stress in the presence of chemical admixtures.....	88
Figure 4.11. Relationship between BET specific surface area of the OPC and OPC/SCM binary blends and apparent yield stress in the absence of chemical admixtures.....	89
Figure 4.12. Relationship between BET specific surface area of the OPC/SCM binary, ternary and quaternary blends and apparent yield stress in the presence of chemical admixtures	90
Figure 4.13. Relationship between packing density of the OPC and OPC/SCM binary blends and apparent yield stress in the absence of chemical admixtures	92
Figure 4.14. Relationship between percent cement replacement and normal consistency for all the pastes	94
Figure 4.15. Relationship between BET surface area and normal consistency for all the pastes.....	95

Figure 5.1.	Two-dimensional central composite design (CCD) representation.....	102
Figure 5.2.	Response surface plot for the change in FA and SL content using Equation 5.8	111
Figure 5.3.	Contour plot of the total heat reduction with the change in FA and SL content.....	112
Figure 5.4.	Contour plot for the change in FA, SL and SF content using Equation 5.8	113
Figure 5.5.	Contour plot of the total heat reduction with the change in MK, SL and SF content using Equation 5.8	114
Figure 5.6.	Contour plot of the total heat reduction with the change in MK, FA and SF content using Equation 5.8	115
Figure 5.7.	Measured versus predicted total heat reduction calculated using Equation 5.8	116
Figure 6.1.	Total heat of hydration	127
Figure 6.2.	BJH pore size distribution at 7 days	130
Figure 6.3.	BJH pore volumes for each paste sample at 7 days.....	132
Figure 6.4.	Relationship between compressive strength and average nanoindentation modulus of hydration products at 7 days	134
Figure 6.5.	Relationship between a) LGP pore volume and b) BET surface area and average nanoindentation modulus of hydration products at 7 days.....	135
Figure 6.6.	Probability density functions of a) control, b) 10MK and c) 52SL paste at 7 days	137
Figure 6.7.	Relationship between volume fraction of CH obtained from nanoindentation and weight percent of CH calculated from XRD measurements.....	138

ABSTRACT

The use of supplementary cementitious materials (SCMs) in commercial construction have been increasing over the last several decades as climate change and sustainability has been gaining global attention. Incorporation of SCMs into concrete mixtures provides several environmental benefits. Since most SCMs are waste by-products of other industries, their use in concrete reduces waste disposal. Additionally, cements substitution with SCMs reduces the carbon footprint of the construction industry. Cement production generates large amounts of CO₂ emissions; the use of SCMs reduces the amount of cement in a concrete mixture thereby reducing emissions from its production.

In addition to SCMs, modern concretes typically incorporate a combination of chemical admixtures. Adverse interaction of admixtures with cement, with or without the SCMs, or with each other is one of the most common reasons for early-age concrete issues. Since the possible combinations of admixtures are numerous and there is a variety of cements on the market, testing all possible chemical/mineral/cement admixture combinations is impractical.

The aim of this research was to cover a broad base of admixture-related issues, each addressing a specific need of the construction industry. There is currently no explanation for why calcium chloride-based accelerator is not always effective when used with high tricalcium aluminate (C₃A) cements. It was determined that increasing C₃A or gypsum content alone did not appear to significantly affect acceleration; however, the presence of alkalis reduced the effectiveness of CaCl₂ accelerator.

When CaCl_2 -based accelerators are used in concrete, they are typically used in combination with other chemical admixtures, such as water-reducing and retarding admixtures (WRRRA) to allow for the use of a low water-cementitious material ratio. In order to avoid premature hardening, CaCl_2 accelerator is most often added onsite, rather than at the concrete batching plant. Onsite addition can lead to accidental overdose of accelerator. It was found that increasing dosages of calcium chloride-containing accelerating admixtures in the presence of WRRRA has a non-linear effect on the pore size distribution and consequently a non-linear increase on the autogenous shrinkage, which can contribute to early-age concrete cracking.

Water-reducing admixtures and superplasticizers are added to concrete to improve workability, which decreases not only with a decrease in water-cementitious material ratio, but also with addition of some SCMs. Silica fume and metakaolin are known to decrease workability; fly ash and slag addition improve it. The effect of SCM combinations on workability is typically assumed to be additive. However, this investigation revealed that combining SCMs does not have an additive effect on workability, measured in terms of apparent yield stress and plastic viscosity; consequently, these parameters cannot be estimated from their respective values.

Cement replacement with SCMs affects not only workability, but also heat of hydration, and is commonly used to reduce concrete temperature rise in concrete. Prediction and control of concrete temperature rise due to cement hydration is of great significance for mass concrete structures since large temperature gradients between the surface and the core of the structure can lead to cracking thus reducing durability of the structure. A number of equations have been proposed to predict the heat of hydration of cement and cement/SCM blends. However, these equations do not include metakaolin, which is a relatively new mineral admixture. Based on statistical experimental design, an equation was developed to predict the reduction of total

hydration heat at 24, 48 and 72 hours with addition of SCMs compared to a plain ordinary portland cement (OPC)-water mixture. The developed equation allows the evaluation of the contribution of Class F fly ash (FA), blast furnace slag (BFS), silica fume (SF) and metakaolin (MK) as well as their combinations.

Since metakaolin has been on the market for only about 10 years, the current knowledge on its effect on hydration products and paste microstructure remains incomplete. The effect of MK on the nature of hydration products was evaluated through x-ray diffraction. Its effect on the microstructure was assessed by measuring porosity with nitrogen adsorption and determining nanoindentation modulus as well as the volume fraction of calcium silicate hydrates (C-S-H) with variable packing densities. No significant effect was observed on the nature of hydration products with MK or BFS addition. However, nitrogen-accessible porosity increased with MK and BFS addition, the increase being larger with BFS. The average indentation modulus for the hydration products decreased with addition of MK and BFS, which corresponded to increasing nitrogen accessible pores. The results of this study indicate that phase quantification by quantitative x-ray diffraction (QXRD) of the hydrated paste may not be sufficient to assess the impact of metakaolin or BFS addition on the hydrating cementitious systems, and a multi-technique approach that provides information not only on the amount of hydration products, but also their morphology is preferable.

CHAPTER 1: INTRODUCTION

The cement and concrete industry has experienced several drastic changes in the last 100 years. Cement fineness has increased dramatically from typical values of approximately 1600 cm^2/g in 1917 [1] to values of 6000 cm^2/g not being uncommon today. Invention of chemical admixtures was a technological break-through that resulted in acceleration of typical construction schedules and production of such “exotic” concrete mixes as high-strength high-performance concrete and self-compacting concrete to name a few. Chemical admixtures are able to modify fresh and hardened concrete properties, such as acceleration of setting time and strength development, increasing workability to allow the use of very low water to cement (w/c) ratios resulting in very high early compressive strengths as in high-strength high-performance concrete, and producing flowable concrete with normal compressive strength while preventing segregation of the mixture. In addition to chemical admixtures, supplementary cementitious materials (SCMs) have gained popularity and are now widely used by the construction industry. Most of the SCMs, except for metakaolin, are waste by-products from other industries, and their incorporation in concrete reduces the amount of cement needed, thus reducing the carbon footprint of the construction industry in addition to lowering the cost of concrete in most cases. Addition of SCMs also improves durability thus resulting in fewer repairs and lower maintenance costs for the structure.

Since the introduction of chemical admixtures to the market, a number of cases of negative interactions between chemical admixture and cement/SCMs combination have been reported [2]–

[4]. Although the use of combinations of mineral and chemical admixtures is very wide-spread in modern construction, current standards or practice guidelines do not necessarily provide adequate guidance, if any, on predicting negative interactions between the admixtures. Wang et al. [4] point out that “the certification processes for mineral admixtures, chemical admixtures and cement do not require consideration of combination of these components.” There are a great number of possible combinations of admixtures, and it is impractical if not impossible for admixture manufacturers or cement producers to test all the different combinations of chemical admixtures and mineral admixtures with cements of different chemistries.

Chemical or mineral admixtures are incorporated in concrete mixtures to enhance or improve concrete fresh and hardened properties. Two main properties of interest are the heat generated during hydration and fresh mixtures workability. Chemical reactions occurring when cement comes in contact with water are exothermic; the total heat evolution during the cement hydration process is referred to as heat of hydration (HOH). The HOH can serve as an indication of setting and compressive strength development and can be used to measure the degree of hydration of a cementitious system [5], [6], [7]. Additionally, the total amount of heat evolved affects the temperature rise in concrete, which can be a serious issue in mass concrete structures. Since concrete is a poor conductor of heat, large temperature gradients can develop between the core and the surface of the structure leading to thermal cracking and consequently reduced durability and service life of the structure. With respect to fresh concrete properties, the parameters that are of most importance during construction are adequate workability that allows concrete to be properly placed and consolidated and setting time that occurs during the expected period of time. Addition of chemical and mineral admixtures is known to modify workability and setting time of concrete. With the use of low w/c ratio concrete mixtures, below 0.4, autogenous shrinkage

becomes a practical concern. Autogenous shrinkage is the bulk volume change that occurs without moisture loss to the environment or temperature change [16]–[18]. This volume change results from the consumption of pore water and chemical shrinkage during hydration. Although there is no clear agreement in the literature on which mechanism is responsible for autogenous shrinkage, it is clear that changes in porosity or in C-S-H morphology are likely to affect autogenous shrinkage.

This research focused on identifying potential negative or significant interactions between cements of different mineralogy and commonly used admixture combinations on properties of cementitious systems. The emphasis of this study was placed on HOH of the mixtures due to its implications on temperature rise and thermal stresses, which are a major durability issue and rheology as a measure of workability. Additionally, this study examined the effect of SCMs and chemical admixtures on microstructure development due to its implications on durability and service life of concrete structures. This study had five objectives with the first two objectives focusing on calcium chloride (CaCl_2), which is used to accelerate the setting and strength gain of concrete.

CaCl_2 is the oldest and arguably the most studied chemical admixture. CaCl_2 is an accelerator that reduces setting time and increases early strength gain of concrete and is the most widely used accelerator for non-reinforced concrete due to its low cost and high effectiveness. The accelerating effect of CaCl_2 on cement hydration has been primarily studied in terms of its effect on tricalcium silicate (C_3S) hydration. However, the exact mechanism by which CaCl_2 modifies cement hydration is still not well established. As such, it is difficult to extend the conclusions of existing phenomenological studies to cements of varying physical and chemical characteristics. There have been reports in the literature that CaCl_2 does not have the same effect on cements of

different mineralogy, typically cements with high C_3A content [5], [13]–[16], although this topic has not received much attention and the studies did not produce a unified theory explaining the variation in $CaCl_2$ performance with different cements. The first part examined the effect of chemical admixture ($CaCl_2$) on heat of hydration (HOH) of cements with different mineralogical composition that will include a variation in C_3A content. An article based on this work has been submitted to Elsevier and is currently under review for the Cement and Concrete Composites Journal.

Since most of the research on $CaCl_2$ has been conducted in the 1970s, prior to concrete mixtures with low w/c ratios and prior to autogenous shrinkage being recognized as being of practical concern, there is a lack of information in the literature regarding the effects of variable dosages of $CaCl_2$ -based accelerating admixture on concrete autogenous shrinkage. $CaCl_2$ has been shown to affect porosity [16]–[19], particularly in the range of fine pores [20]–[22]; however, this has not been related to autogenous shrinkage even though there are several proposed mechanisms in the literature that relate autogenous shrinkage to porosity [8]–[12]. It has been recently shown that accelerator dosage had a non-linear effect on autogenous shrinkage [23], although this study did not investigate the relationship between accelerator dosage and microstructural modifications of concrete. The second part focused on explaining the effect of $CaCl_2$ on concrete properties, specifically autogenous shrinkage. The findings have been published in the Journal of the American Ceramic Society [24].

Structural concrete mixtures used in Florida typically contain not only chemical admixtures, but also SCMs, which themselves modify the binder mineralogy and consequently cement hydration reactions. The SCMs typically used in Florida are Class F fly ash (FA), granulated blast furnace slag (SL), silica fume (SF) and metakaolin (MK). Cement replacement

with SCMs is not only beneficial in terms of reducing the carbon footprint of cement production, but each of the SCMs can result in improvement in certain concrete qualities. As mentioned previously, heat release during hydration of a cementitious system can be a serious issue as it can lead to thermal cracking. In Florida, due to the warmer climate, thermal gradients can lead to cracking even in structures, such as concrete pavement [25], that would not normally be considered mass concrete. Several models have been proposed in the literature to predict the hydration behavior of OPC/SCM systems [26]–[28]; however, these models did not include metakaolin. The only guidance regarding the HOH of MK comes from Gajda [29] who states that it can be approximated as “100% to 125% that of Portland cement.” This, however, applies only to OPC/MK mixtures, and it is unclear how the total heat evolution of ternary or quaternary systems will be modified by addition of MK with chemical admixtures. This part of the research evaluated the effect of combinations of chemical admixtures and SCMs on heat of hydration in order to identify significant interactions between SCMs and/or chemical admixtures in terms of HOH. A model was constructed in order to predict the total heat of hydration reduction for OPC/SCM/chemical admixture combinations including MK compared to a plain OPC mixture. An article has been submitted to the Journal of Thermal Analysis and Calorimetry for publication consideration.

As mentioned previously, workability and setting time are the most important fresh concrete properties. Loss of workability, rapid or prolonged setting can be indicative of admixture incompatibilities. Although some mineral admixtures can improve workability, it is not clear what specifically is responsible for this improvement. As Ferraris et al. [30] point out, currently testing is the only way to evaluate the effect of mineral admixtures on concrete workability. Typical tests used to assess the compatibility of different chemical and mineral admixtures are setting time and

rheological measurements. A manuscript based on the findings of this portion of the study have been submitted to Elsevier and is currently under review by the Construction and Building Materials Journal. The next part of the study investigated the effect of SCM and chemical admixture combinations.

Microstructural changes can have a significant effect on hardened concrete properties. Addition of SCMs and chemical admixtures is expected to affect both the chemical composition and the morphology of the hydration products. For example, addition of superplasticizer has been shown to change the morphology of ettringite. In most cases, the effect of SCMs and chemical admixtures on hydration is studied using a “one admixture at a time” approach [31]–[35]. This approach does not represent complex interactions between the binder mineralogy, which has been modified by addition of one or more SCMs, and chemical admixtures. This portion of the research evaluated the effect of SCMs with chemical admixtures on microstructure development by evaluating the effect of these combinations on hydration kinetics using HOH, formation of hydration phases through x-ray diffraction (XRD), microstructural changes by studying pore structure modification with nitrogen adsorption and examining the changes elastic modulus of hydration products of select mixtures through nanoindentation. A manuscript based on the findings of this portion of the research have been submitted to the Applied Clay Science Journal and are currently under review.

This work was conducted as part of funded studies by the US Department of Transportation and the Florida Department of Transportation under contract numbers BDV25-977-01 and BDV25-977-02.

CHAPTER 2: INTERACTION OF CEMENT MINERALOGY AND CALCIUM CHLORIDE-BASED ACCELERATOR¹

2.1 Introduction

Calcium chloride has been used for decades to accelerate cement hydration. Although its effect on setting and strength development has been studied at length, the mechanism of acceleration of cement hydration by CaCl_2 is still not well-established. As such, it is difficult to extend the conclusions of existing phenomenological studies to cements of varying physical and chemical characteristics. Since it was concluded early on that the main effect of CaCl_2 is due to the acceleration of C_3S hydration, a number of studies have been conducted on pure C_3S pastes, which does not take into account the complex interactions between different ionic species occurring during cement hydration as have been pointed out by Jupe et al. [13].

There are indications in the literature that CaCl_2 does not have the same effect on cements of different mineralogy, although this topic has not received much attention. Shideler [14] reported in 1952 that CaCl_2 is considerably less effective in accelerating Type III cement hydration compared to other cement types. Price also stated that CaCl_2 “reacts differently with different cements” [15]. Oey et al. [5] observed that generally CaCl_2 is “more efficient at accelerating set in the Type II/V OPC compared to the Type I/II OPC.” Suryavanshi et al. [16] compared the effect of CaCl_2 on OPC and sulfate resistant portland cement (SRPC) mortars. The authors attributed greater effect of chlorides on SRPC mortars to lower chloride-binding capacity of SRPC due to its

¹ This chapter has been submitted as a manuscript to the Cement and Concrete Composites Journal and is currently under review.

lower C_3A content. Jupe et al. [13] compared performance of $CaCl_2$ on two oil well cements, Class H and A, of similar C_3S content and variable C_3A/C_4AF composition (0.65/17.00 % and 11.00/7.00 % respectively) and observed that the accelerating effect was greater for cement with low C_3A content. The authors attributed this to the possible formation of “ferrihydrite gel” in the Class H slurries, as $CaCl_2$ has been reported to accelerate the reaction of C_4AF with gypsum [36]. This study points to a more complex interaction between phases in the presence of $CaCl_2$ rather than merely acceleration of C_3S hydration. Although it was not remarked on by the authors, another major difference between the two cements investigated by Jupe et al. [13] was their alkali, more specifically K_2O , content, which for Class A cement was almost double that of Class H. Alkalis are known to modify cement hydration [37], and their impact on $CaCl_2$ efficiency deserves attention.

The purpose of this portion of the study was to investigate the influence of cement mineralogy, more specifically C_3A and alkali content, on the accelerating efficiency of pure $CaCl_2$ and commercial chloride-based accelerator. Identification of specific cement compounds affecting $CaCl_2$ performance can enable the engineers to make informed decisions on the appropriate materials selection for concrete mixtures in different construction applications.

2.2 Experimental Procedures

2.2.1 Materials

Three cements of similar fineness (in terms of Blaine fineness and mean particle size) and similar C_3S content, but variable C_3A , C_4AF composition and variable alkali content were selected for this study. Their density was determined following ASTM C188, while the fineness was measured using a Blaine air-permeability apparatus in accordance with ASTM C204. Particle size distribution was determined using the LA-950 laser scattering particle size analyzer manufactured

by Horiba, which was then used to calculate the mean particle size (MPS). MPS has been shown to have a better correlation with heat of hydration of Portland cements compared to Blain fineness at 1, 3 and 7 days [38].

The chemical oxide composition was determined by x-ray fluorescence (XRF) in accordance with ASTM C114, and mineralogical composition was obtained from Rietveld refinement performed with HighScore Plus software 3.0 from Panalytical. X-ray diffraction scans for Rietveld refinement were collected on X'Pert 3040Pro diffractometer with Cu K α radiation manufactured by Panalytical. The tension and current were set to 45 kV and 40 mA respectively. The following optics settings were used: 1° divergence slit, 0.2 mm receiving slit and 1° anti-scatter slit. Rietveld analysis was carried out using the HighScore Plus 3.0 software by Panalytical.

Two accelerators were used in this study: a pure reagent grade CaCl₂ and a commercial CaCl₂-based Type E accelerating admixture (ASTM C494). The composition of the Type E admixture was obtained from the materials safety data sheet provided by the manufacturer and is listed in Table 2.1. A 4% volumetric solution was prepared with pure CaCl₂ and was used in place of the mixing water. This corresponded to 2% CaCl₂ addition by mass of cement. The commercial accelerator was used at the dosage that is typically used for rapid-repair concrete mixtures for jointed plain concrete pavement. This dosage corresponded to 1-2% CaCl₂ addition by mass of cement based on the ranges listed in Table 2.1.

Table 2.1. Commercial accelerator composition

Component	Percentage
Calcium Chloride	25-50
Potassium Chloride	1-10
Sodium Chloride	1-10
Triethanolamine	1-10

2.2.2 Methodology

Acceleration of early-age hydration by CaCl_2 and commercial accelerator was evaluated by measuring the heat of hydration (HOH) for each cement with and without addition of CaCl_2 /accelerator. TAMAIR isothermal conduction calorimeter manufactured by TA Instruments was used to measure the heat flow and the total heat evolved following ASTM C1702, Method A, internal mixing.

The degree of hydration $\alpha(t)$ was calculated based on the total heat evolution measured by isothermal calorimetry according to:

$$\alpha(t) = \frac{H(t)}{H_u} \quad \text{Equation 2.1}$$

where $H(t)$ is the total heat released at time t and H_u is the ultimate heat of the mixture, which is calculated based on the cementitious content of the mixture [26], [39]. Since the mixtures in this study did not contain any supplementary cementitious materials (SCMs), H_u was equal to the total heat of hydration of cement H_{cem} , which is a function of cement composition.

$$H_{cem} = 500P_{C3S} + 260P_{C2S} + 866P_{C3A} + 420P_{C4AF} + 624P_{SO3} + 1186P_{FreeCaO} + 850P_{MgO} \quad \text{Equation 2.2}$$

where P is the mass of i^{th} component to total cement content ratio.

Compressive strength testing for as-received cements was performed on mortar mixes prepared in accordance with ASTM C109. 50 mm mortar cubes were tested at the ages of 4, 8, 12 and 24 hours, and 3 and 7 days following ASTM C305.

As-received Cement 2 was doped with C_3A , gypsum and alkali sulfates and alkali hydroxides to the levels of Cement 3 in order to identify the compounds responsible for the reduced acceleration with addition of CaCl_2 /Type E admixture. C_3A (purity of 97.6% cubic based on Rietveld refinement) was obtained from CTL. C_3A was weighed out, added to Cement 2 and mixed by hand to a homogeneous appearance prior to conducting isothermal calorimetry

measurements. The rest of the doping compounds were reagent-grade chemicals. Gypsum and alkalis were also added to cement in the form of dry powder and mixed by hand. When cement was doped with more than one compound, the same procedure was adopted.

The accelerating ability of CaCl_2 and commercial accelerator was evaluated by comparing the time of occurrence and the magnitude of the main hydration peak of the accelerated sample to its counterpart with no accelerator. For example, time and peak magnitude of Cement 2+ K_2SO_4 sample was subtracted respectively from time and peak magnitude of Cement 2+ K_2SO_4 + CaCl_2 sample in order to evaluate the accelerating ability of CaCl_2 with increasing potassium content.

2.3 Results and Discussion

2.3.1 As-Received Cements

The elemental oxide composition, mineralogical composition and physical properties of the as-received cements are depicted in Tables 2.2 and 2.3 where it can be seen that all cements had similar Blaine fineness, MPS and C_3S content. The density for all three cements was similar as well.

It is also noted that cements had variable C_3A and alkali contents which increased from 2.5% and 0.58% respectively for Cement 1 to 9.3% and 1.13% for Cement 3. The ferrite phase content and $\text{SO}_3/\text{Al}_2\text{O}_3$ ratio were very similar for Cements 1 and 2. Cement 3 had the highest C_3A , highest alkali content, highest $\text{SO}_3/\text{Al}_2\text{O}_3$ ratio, and lowest C_4AF . Although the total Al_2O_3 content of all cements was similar, the Al_2O_3 present in C_4AF is expected to be less reactive than Al_2O_3 present in C_3A , and therefore is not expected to have a major effect on the heat of hydration during the first 24 hours.

Table 2.2. Chemical oxide composition of as-received cements

Analyte	Cement 1	Cement 2	Cement 3
SiO ₂ (wt. %)	20.74	20.01	18.67
Al ₂ O ₃ (wt. %)	4.45	5.15	5.7
Fe ₂ O ₃ (wt. %)	4.07	3.86	2.63
CaO (wt. %)	64.83	63.52	60.15
MgO (wt. %)	0.92	0.92	2.92
SO ₃ (wt. %)	2.58	3.18	4.83
Na ₂ O (wt. %)	0.07	0.12	0.41
K ₂ O (wt. %)	0.28	0.42	1.1
TiO ₂ (wt. %)	0.26	0.26	0.25
P ₂ O ₅ (wt. %)	0.1	0.13	0.26
Mn ₂ O ₃ (wt. %)	0.08	0.01	0.07
SrO (wt. %)	0.04	0.06	0.28
Cr ₂ O ₃ (wt. %)	0.01	0.01	0.01
ZnO (wt. %)	0.05	0.01	0.06
L.O.I(950°C)	1.22	2.4	2.58
Total (wt. %)	99.72	100.07	99.91
Alkalis as Na ₂ O _{eq} (wt. %)	0.25	0.40	1.13
SO ₃ /Al ₂ O ₃	0.58	0.62	0.85

Table 2.3. Mineralogical composition and physical properties of as-received cements

Cement Phase/Property	Cement 1	Cement 2	Cement 3
Alite (%)	58.9	61.9	59.5
Belite (%)	19.6	13.9	13.7
Brownmillerite (%)	10.1	9.7	5.5
C ₃ A cubic (%)	2.5	5.8	9.3
C ₃ A orthorhombic (%)	0.0	1.0	0.0
Periclase (%)	0.0	0.0	1.6
Arcanite (%)	0.0	0.1	0.0
Syngenite (%)	0.9	1.5	2.1
Aphthitalite (%)	0.0	0.0	0.3
Portlandite (%)	1.3	0.1	0.5
Calcite (%)	3.5	1.7	1.6
Gypsum (%)	0.3	4.2	4.4
Hemihydrate (%)	0.6	0.0	1.5
Anhydrite (%)	1.9	0.0	0.0
Blaine Fineness (m ² /kg)	414	417	405
Mean Particle Size (μm)	13.15	12.9	14.35
Density (Mg/m ³)	3.16	3.14	3.14

2.3.1.1 Isothermal Calorimetry

2.3.1.1.1 As-Received Cements

Heat of hydration curves for Cements 1, 2 and 3 are presented in Figures 2.1-2.3. Isothermal calorimetry of cement pastes typically shows three peaks on the heat flow curves. The first peak is due to rapid initial dissolution of cement phases. The second, or main hydration peak, is typically associated with the hydration of silicates, while the following peak, which can be seen as a shoulder on the right side of the main hydration peak, is attributed to the reaction of aluminates [40]. This shoulder is also referred to as the sulfate depletion point. In a properly sulfated cement, the sulfate depletion point is expected to occur after the main hydration peak [41]. Appearance of the aluminate peak on the left side of the main hydration peak is an indication that the system does not contain enough sulfate to adequately control the aluminate reaction, which can have a retarding effect on C_3S hydration [42].

The heat flow curve for Cement 1 non-accelerated sample showed a shoulder occurring on the left side of the main hydration peak suggesting that this cement was undersulfated (Figure 2.1). Addition of both $CaCl_2$ and Type E admixture significantly accelerated Cement 1 hydration as evidenced by the increased heat flow rate, increased magnitude of the main hydration peak and reduced timing of its occurrence. Only two peaks are present in these samples with no discernable aluminate peak. $CaCl_2$ is known to accelerate the C_3S hydration [43]–[45]. It has also been shown to accelerate the reaction of C_3A with gypsum [36], [46], [47]. The accelerating effect of pure $CaCl_2$ and commercial accelerator on Cement 1 hydration appears to be very similar; only minor differences are observed in the timing and magnitude of the main hydration peaks in these samples.

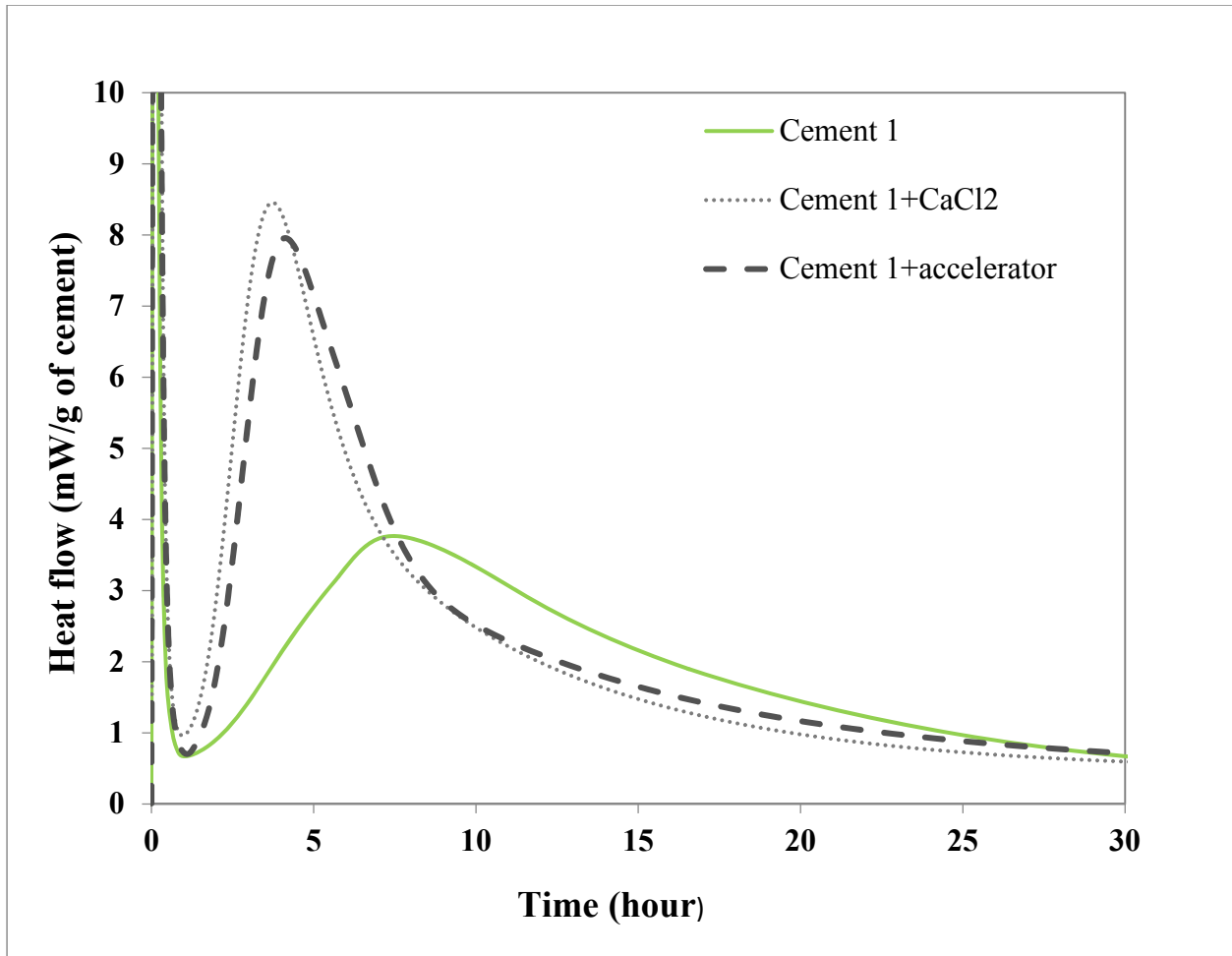


Figure 2.1. Heat of hydration curves for as-received Cement 1 pastes

The sulfate depletion point in Cement 2 non-accelerated sample appears on the right side of the main hydration peak indicating that this cement was properly sulfated (Figure 2.2). For the Cement 2 sample with pure CaCl_2 , only two peaks are visible similar to the Cement 1+ CaCl_2 sample. However, for the sample with commercial accelerator, a third peak appears after the main hydration peak, which is most likely due to the reaction of aluminates. While the main hydration peak shifted to shorter times, from 10 hours to 5 hours after mixing with addition of accelerator, the sulfate depletion point only moved by 2 hours, from 14 hours to 12 hours. It appears that, at least in this case, the commercial accelerator has a much greater effect on the silicate hydration

compared to the aluminates. In contrast to Cement 1 samples, there is a clear difference in the magnitudes of the main hydration peaks in Cement 2+CaCl₂ and Cement 2+accelerator samples.

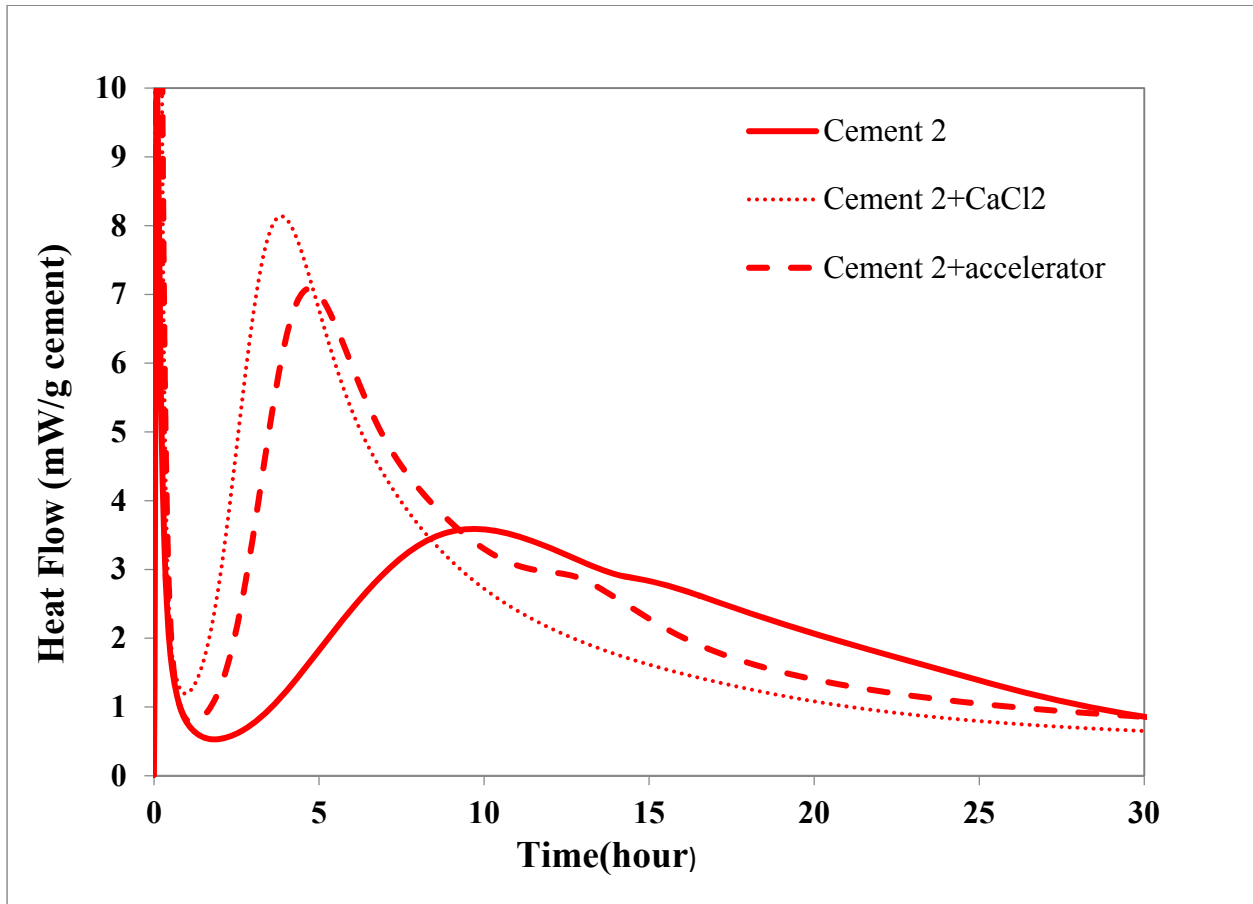


Figure 2.2. Heat of hydration curves for as-received Cement 2 pastes

Cement 3 also appeared to be properly sulfated (Figure 2.3). Additions of pure CaCl₂ or Type E admixture produced main hydration peaks of equal magnitude, however, they were not significantly higher than the main hydration peak of the non-accelerated sample indicating a significant reduction in CaCl₂ accelerator efficiency with this cement. Only two hydration peaks were discernable with either addition of pure CaCl₂ or commercial accelerator.

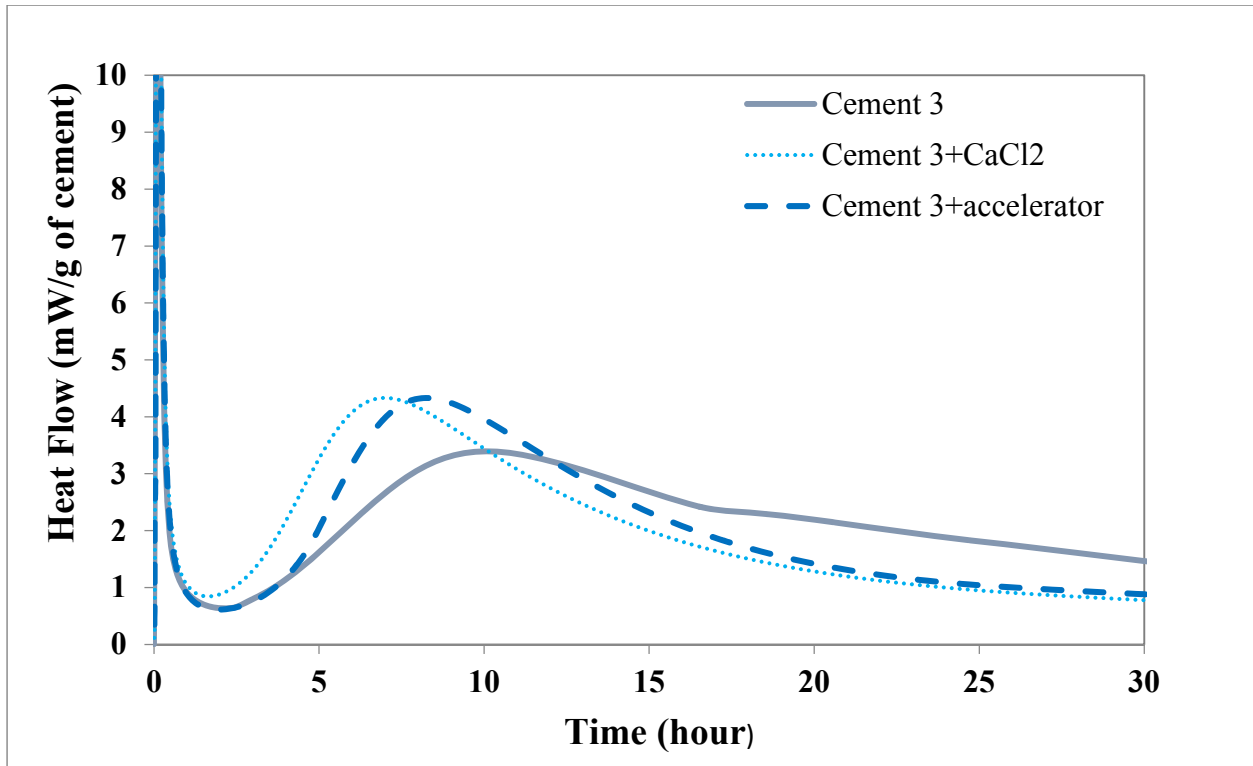


Figure 2.3. Heat of hydration curves for as-received Cement 3 pastes

Based on these results, it seems that pure CaCl_2 is not sensitive to the mineralogical differences between Cements 1 and 2, as the timing and magnitude of the main hydration peak were very similar, but is sensitive to the differences between these two cements and Cement 3. However, for the commercial accelerator, the heat of hydration measurements show sensitivity to mineralogical and chemical oxide composition between Cements 1 and 2 as well as Cement 3.

First, considering Cements 1 and 2, the chemical oxide content of these cements is very similar (Table 2.2), although there are differences in their mineralogical composition (Table 2.3). While Cement 1 had 2.5% C_3A present in the cubic form, Cement 2 had cubic and orthorhombic C_3A (5.8% cubic and 1.0% orthorhombic). Their reactivity is known to be different with the latter being more reactive. Although the $\text{SO}_3/\text{Al}_2\text{O}_3$ ratio of these cements was very similar, the majority of sulfates in Cement 1 were present as natural anhydrite, while Cement 2 contained gypsum. While solubility of anhydrite obtained through dehydration of gypsum during the grinding process

(also referred to as soluble anhydrite) is higher than solubility of gypsum [48], solubility of natural anhydrite is lower than that of gypsum [49], which explains why the sulfate depletion point occurs on the left side of the main hydration peak for Cement 1 despite a seemingly adequate $\text{SO}_3/\text{Al}_2\text{O}_3$ ratio. Therefore, it appears that for a C_3A content in the range of 2.5 to 6.8%, the availability of sulfate ions or the presence of a small amount of orthorhombic C_3A has no significant effect on the accelerating efficiency of pure CaCl_2 .

Comparing the composition of Cements 2 and 3 can help identify the phases or oxides that may be responsible for the reduced performance of pure CaCl_2 observed with Cement 3. Cement 3 had a high C_3A (cubic) content of 9.3%, high alkali content (1.13% as $\text{Na}_2\text{O}_{\text{eq}}$), mostly due to high K_2O , and higher $\text{SO}_3/\text{Al}_2\text{O}_3$ ratio (0.85), which is expected since high-alkali cements require higher sulfate amounts to adequately control the aluminate reaction [41]. Cement 3 also had lower ferrite phase content. While C_4AF is generally considered to have a much lower reactivity compared to C_3A , Wang et al. [50] recently showed that hydration of ferrites in industrial clinkers can contribute notable amounts of heat during early-age cement hydration. Additionally, CaCl_2 has been shown to accelerate C_4AF reaction with gypsum [36].

As for the variation in performance of the commercial accelerator, it can possibly be attributed to increasing C_3A content, increasing the amount of readily-available sulfates, and increasing alkali content. Since the C_4AF content of Cement 1 and Cement 2 was very similar, it does not seem likely to be responsible for reduced acceleration of Cement 2 with commercial accelerator addition compared to Cement 1.

2.3.1.1.2 Doped Cements

In order to test the hypothesis that high C_3A content, or increased sulfate or alkali content of Portland cements may be responsible for reduced effectiveness of pure CaCl_2 and chloride-

based commercial accelerator, Cement 2 was doped with these compounds to the levels of Cement 3. Cement 2 was selected over Cement 1 for the following reasons: it was properly sulfated, its C_3A content was more typical of a Type I/II cement than that of Cement 1, and the heat flow curve of the non-accelerated Cement 2 sample was very similar to that of Cement 3.

First, Cement 2 was doped with C_3A to 9.3%. Addition of C_3A is expected to increase the aluminate peak and shift the sulfate depletion point to an earlier time, which can be seen in Figure 2.4 for the non-accelerated sample. A slight reduction in the main hydration peak is also expected as increasing amounts of aluminate ions in solution reduces the reactivity of the silicates [51]. The same effects were observed for the sample containing commercial accelerator, although the effect on the aluminate peak was more pronounced. However, the heat flow rate during the acceleration period as well as the timing and magnitude of the main hydration peak remained unaffected. Increasing the C_3A content did not have a significant effect in the presence of pure $CaCl_2$. Increase in the C_3A content does not appear to result in reduced accelerating effect of either pure $CaCl_2$ or commercial accelerator.

Cement 2 was also doped with gypsum to increase its SO_3 content from 3.18% to the level of Cement 3 cement (4.83%). Addition of gypsum delayed the sulfate depletion point in the non-accelerated paste sample and increased the rate of the silicate reaction as evidenced by the increased rate of heat flow during the acceleration period and a higher magnitude of the main hydration peak (Figure 2.5). This was consistent with the previous observations that in a properly sulfated system, C_3S hydration is accelerated by the presence of gypsum [41], [42]. The aluminate peak was significantly decreased in the doped sample with commercial accelerator, while no change in the main hydration peak was observed. However, addition of gypsum in the presence

of pure CaCl_2 slightly decreased the rate of heat flow during the acceleration period and the magnitude of the main hydration peak.

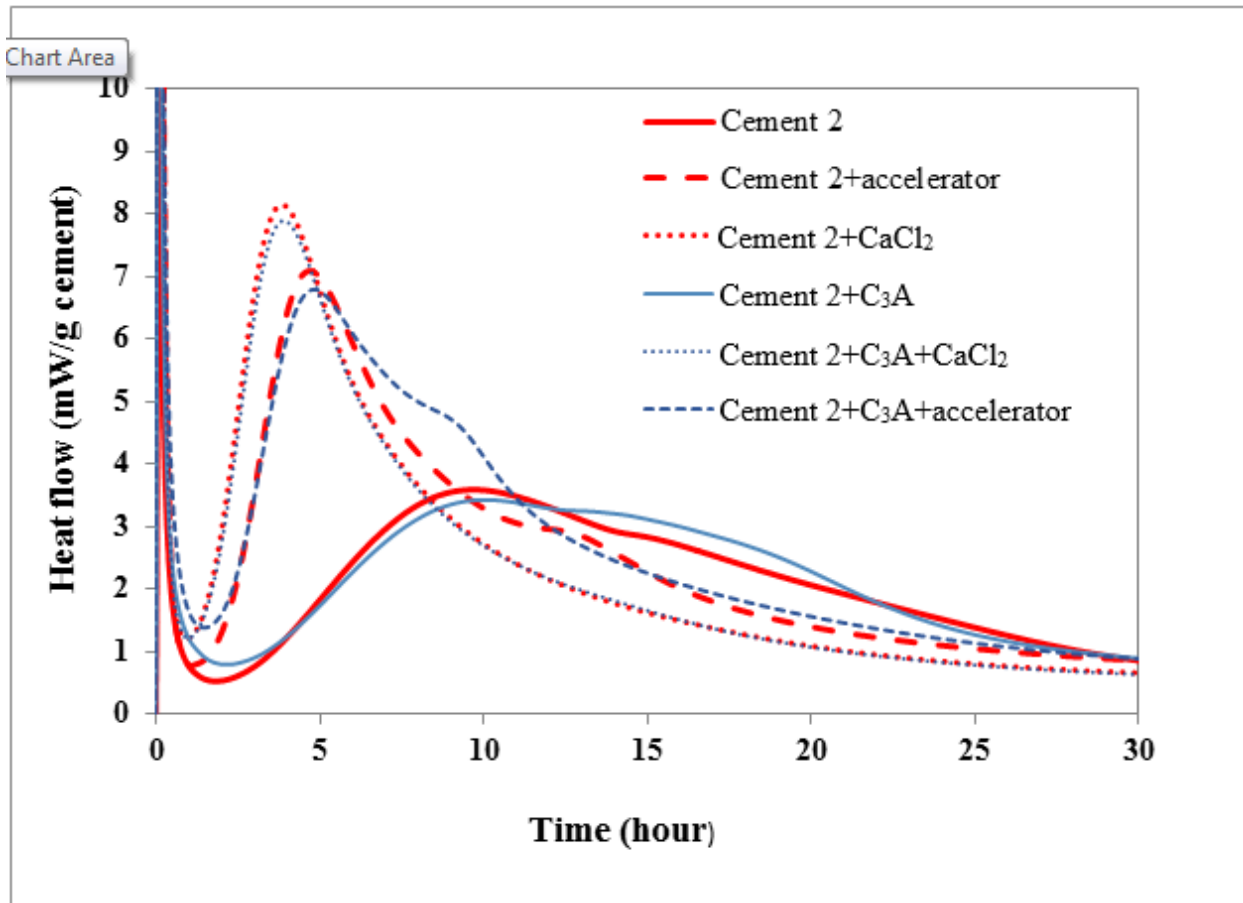


Figure 2.4. Effect of increased C_3A content on heat of hydration with pure CaCl_2 and commercial accelerator

Figures 2.6- 2.9 show the heat flow profiles for Cement 2 doped with alkalis. Alkalis can be present in cement in the form of sulfates or as oxides incorporated into the crystal structure of cement phases [48]. Although the main difference in the equivalent alkali content of the cements used in this study was due to the presence of potassium, addition of both sodium and potassium was evaluated to determine if the possible reduction of acceleration due to an increase in the alkali content was cation-specific. Both alkali hydroxides and alkali sulfates were used for the doping. Potassium compounds were added to increase the K_2O content of Cement 2 cement to the level of

Cement 3; sodium compounds were added to increase the equivalent alkali content ($\text{Na}_2\text{O}_{\text{eq}}$) to the level of Cement 3 since the Na_2O content of all three cements were not significantly different.

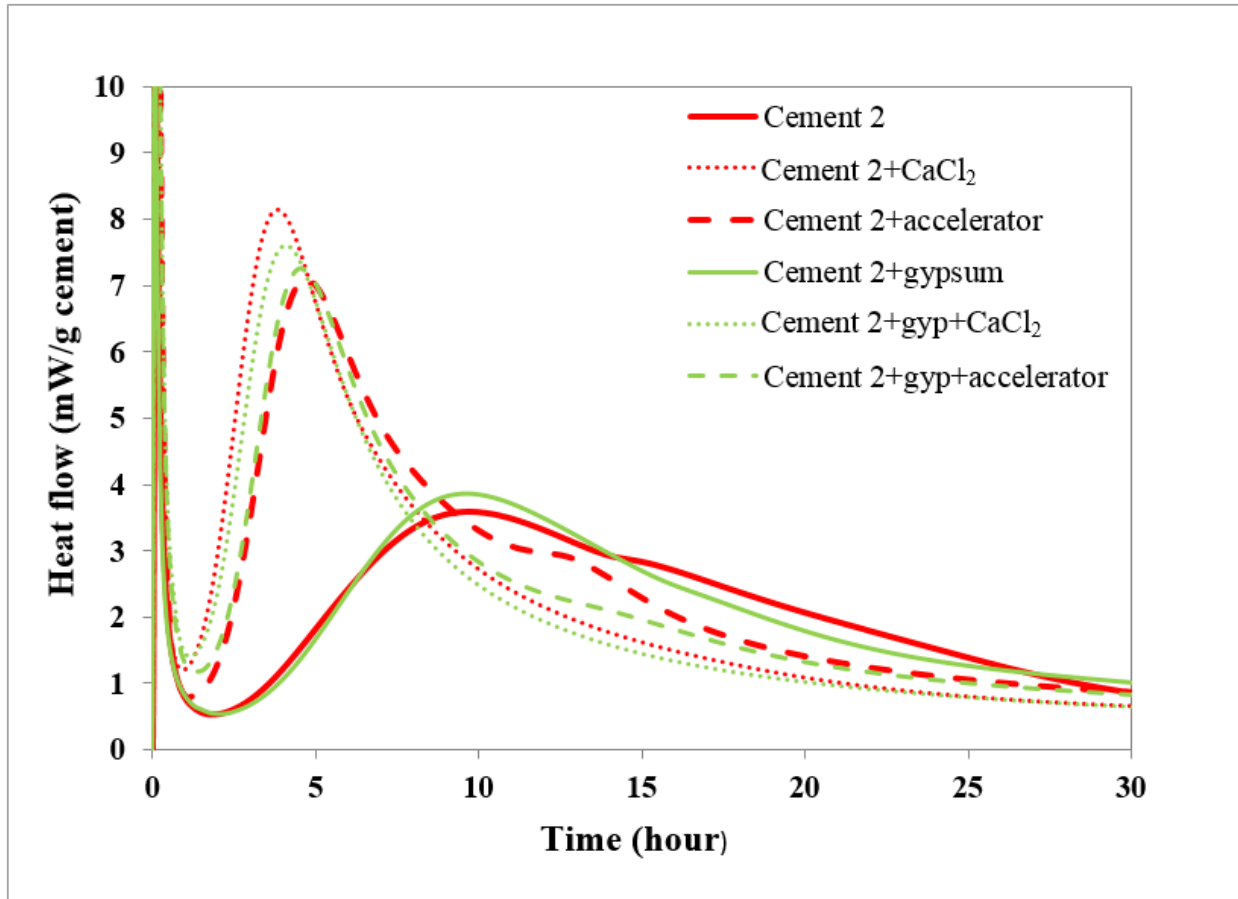


Figure 2.5. Effect of SO_3 content on heat of hydration with pure CaCl_2 and commercial accelerator

Addition of NaOH increased both reactions of silicates and aluminates in the non-accelerated sample, although this increase appeared to be more significant for the aluminate hydration (Figure 2.6). Acceleration of C_3S [52], [53] and cement hydration [54], [55] with NaOH addition has been previously reported. Bu and Weiss [54] attributed the increase in the hydration rate to the decrease in the solubility of CH with NaOH addition, which causes finer CH crystals to precipitate thus increasing the nucleation rate. As for the C_3A hydration, increased dissolution of C_3A has been reported with increase in alkali content [56]. It has also been well established that

high-alkali cements require higher sulfate amounts to properly control the reaction of aluminates [41], possibly due to the increase aluminate dissolution. The increase in the aluminate peak, therefore, can be explained by the reduced ability of the sulfate present in the Cement 2 to control the aluminate reaction with increased alkali content. In the presence of commercial accelerator, a slight reduction in the magnitude of the main hydration peak was observed, while in the presence of pure CaCl_2 , the magnitude of the main hydration peak was reduced by half. Since commercial accelerator contains NaCl , further addition of sodium ions did not appear to compromise accelerator effectiveness.

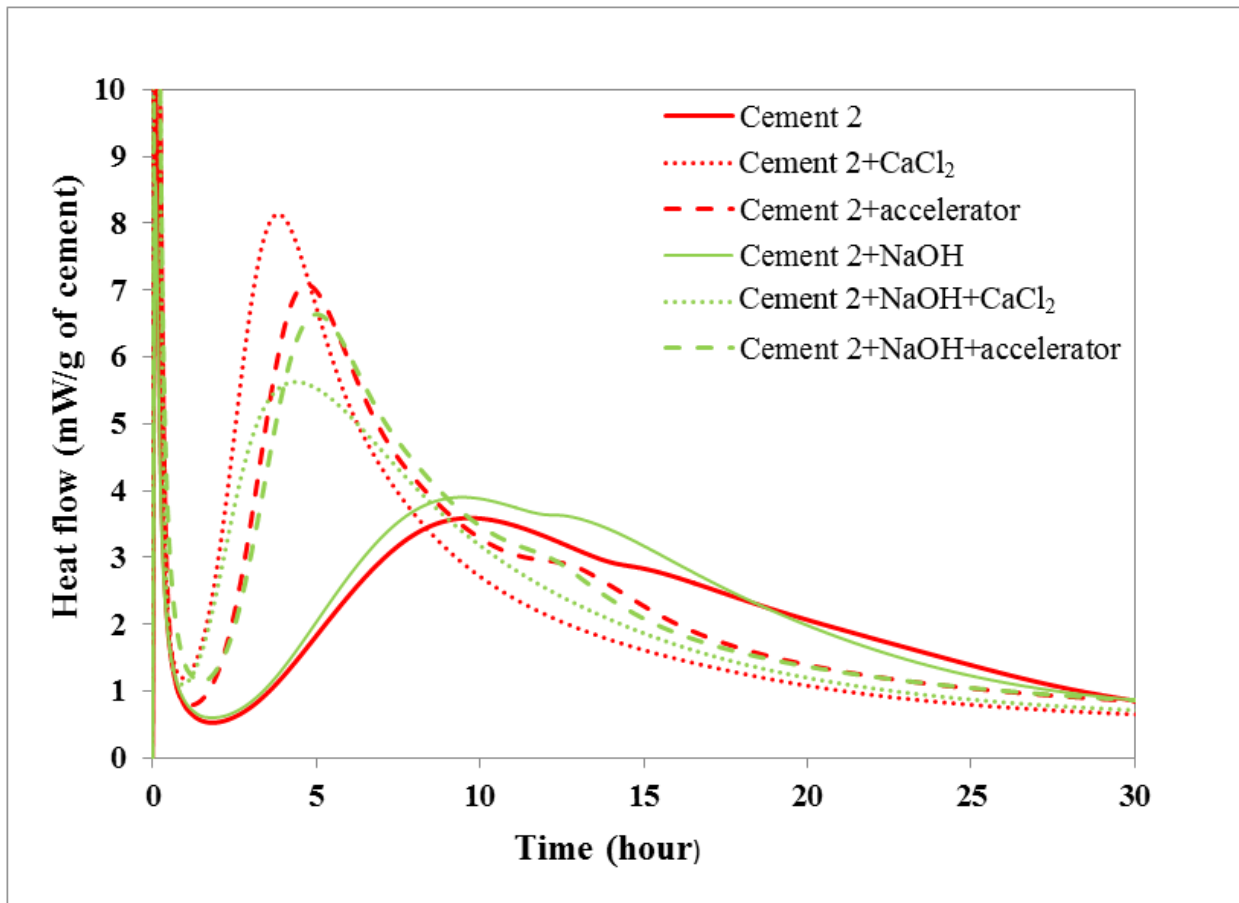


Figure 2.6. Effect of NaOH on heat of hydration with pure CaCl_2 and commercial accelerator

KOH addition to the non-accelerated sample also increased the aluminate peak and shifted the sulfate depletion point to the left, but it did not affect the main hydration peak (Figure 2.7). In the presence of pure CaCl_2 , the main hydration peak was reduced as in the case of NaOH, however, the decrease in its magnitude was not as drastic. Additionally, the time of occurrence of the peak maximum was delayed by approximately one hour, while no shift was observed with the addition of NaOH.

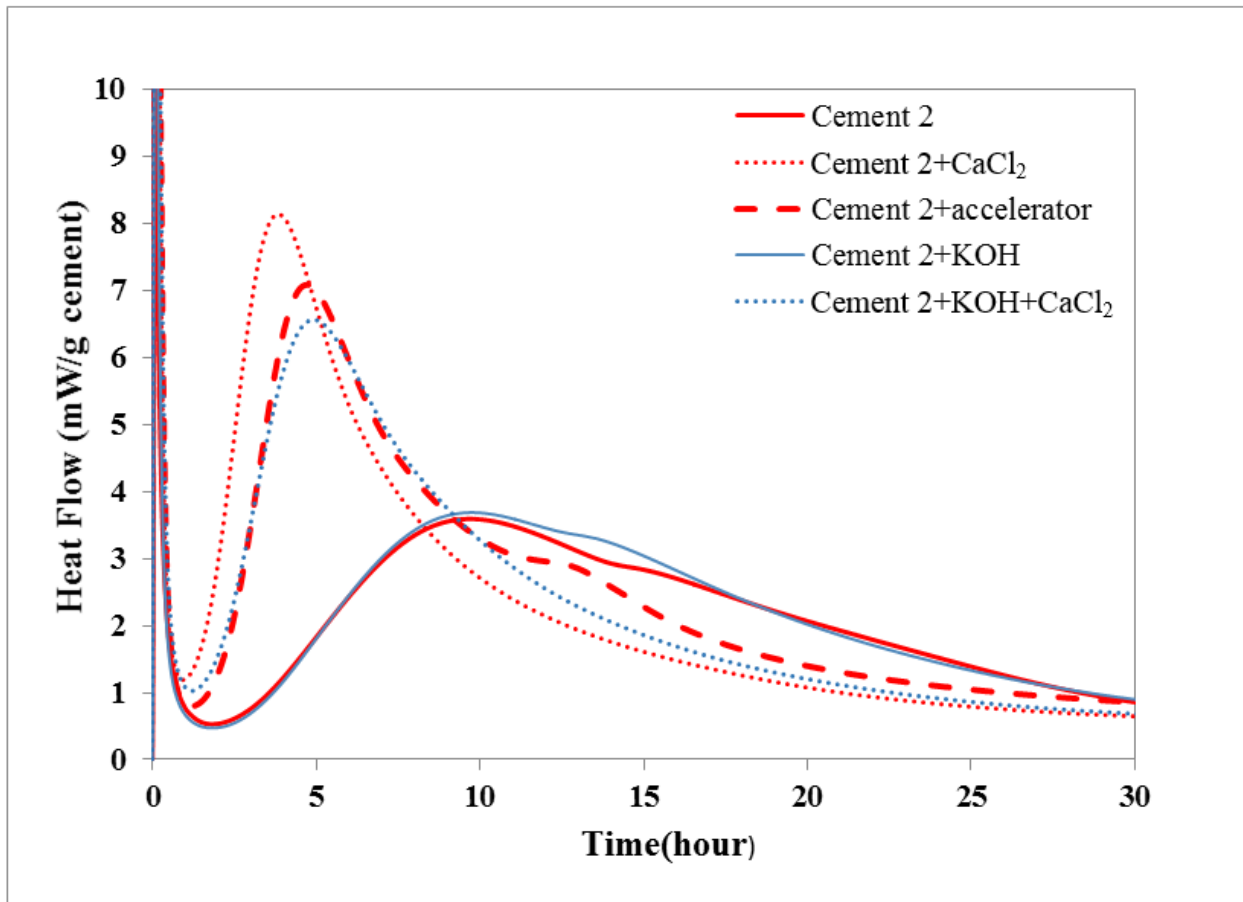


Figure 2.7. Effect of KOH on heat of hydration with pure CaCl_2

Na_2SO_4 added to the non-accelerated sample acted as an accelerator. It increased the rate of heat flow during the acceleration period, the magnitude of the main hydration peak, and shifted the timing of its occurrence to the left by approximately one hour (Figure 2.8). This is consistent with previous reports that alkali sulfates accelerate hydration [57]. However, in the presence of

pure CaCl_2 , Na_2SO_4 decreased both the rate of heat flow during the acceleration period and the magnitude of the main hydration peak and delayed its time of occurrence by approximately 0.5 hours.

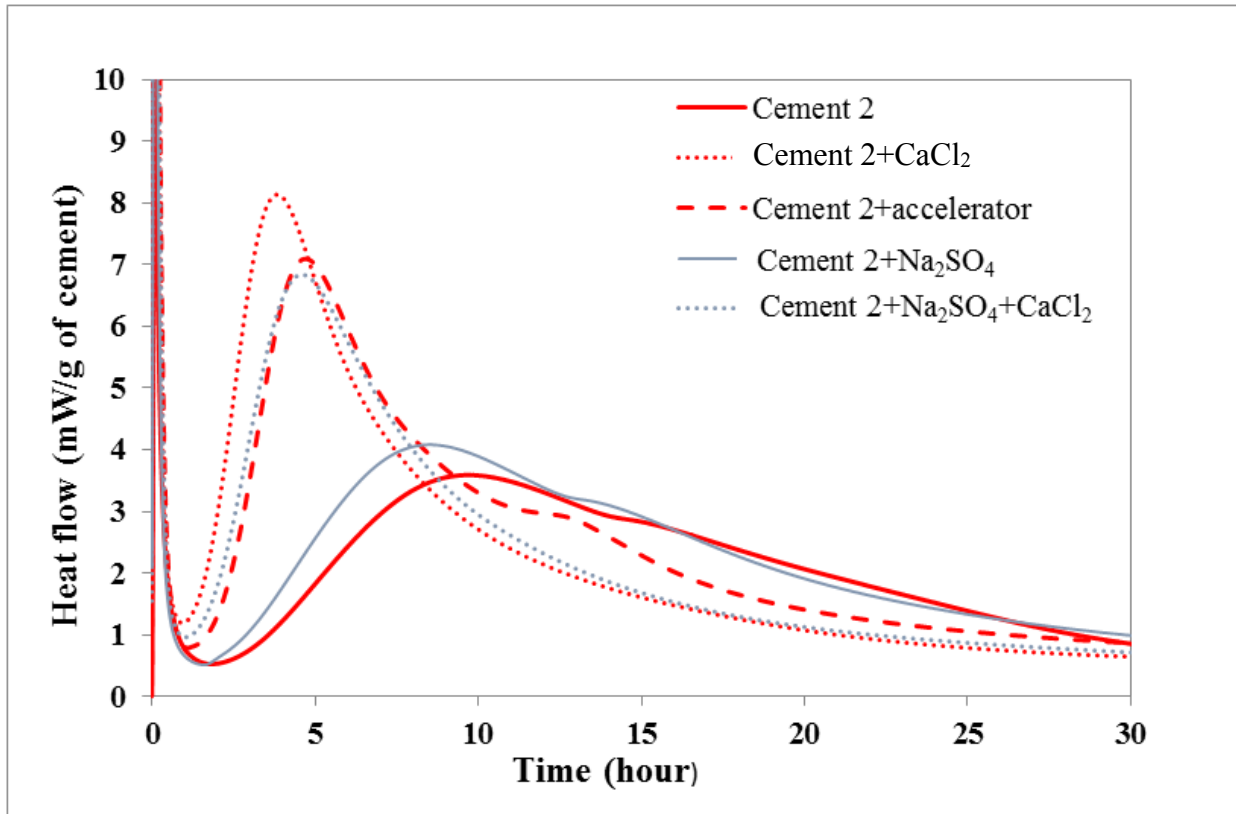


Figure 2.8. Effect Na_2SO_4 on heat of hydration with pure CaCl_2

K_2SO_4 addition produced similar effects to Na_2SO_4 (Figure 2.9). In the non-accelerated sample, both the silicate and aluminate reactions were accelerated, although very slightly and to a much lesser degree than in the presence of Na_2SO_4 . In the presence of pure CaCl_2 , K_2SO_4 addition retarded the main hydration peak, same as Na_2SO_4 addition, although the decrease in its magnitude was greater than with Na_2SO_4 . In the presence of commercial accelerator, K_2SO_4 addition also reduced the heat flow rate and the magnitude of the main hydration peak, although its timing was unaffected.

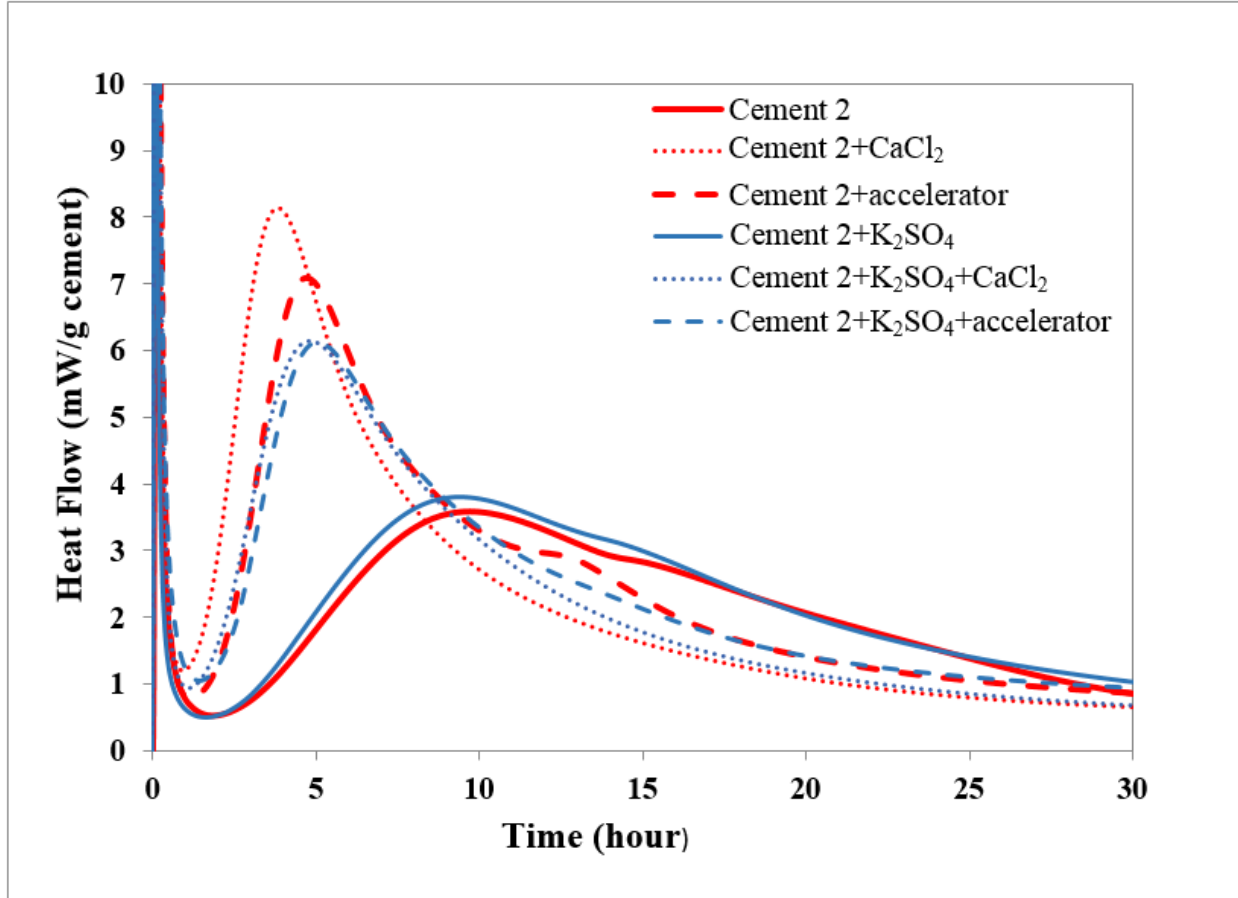


Figure 2.9. Effect of K_2SO_4 on heat of hydration with pure $CaCl_2$ and commercial accelerator

The findings indicate that for non-accelerated pastes, both alkali sulfates and hydroxides have an accelerating effect on cement hydration, with sodium salts being more effective than potassium salts. With accelerator addition, both pure $CaCl_2$ and commercial Type E admixture, the reverse effect is observed: increasing the alkali content reduces the magnitude of the main hydration peak.

After the examining the effect of individual factors, the effect of C_3A /gypsum/ K_2SO_4 combinations was examined by doping the Cement 2 cement with two of these phases at a time in order to identify any synergistic interactions between these phases. Figure 2.10 shows the combined effect of C_3A and K_2SO_4 on heat flow. In the non-accelerated sample both the silicate

and aluminate hydration is accelerated compared not only to the as-received Cement 2 sample, but also with respect to Cement 2+C₃A and Cement 2+K₂SO₄ pastes. In the presence of commercial accelerator, increased C₃A and increased alkali content translated to a greater reduction of the main hydration peak compared to Cement 2, Cement 2+C₃A and Cement 2+K₂SO₄ samples and a greater shift to the right in its timing.

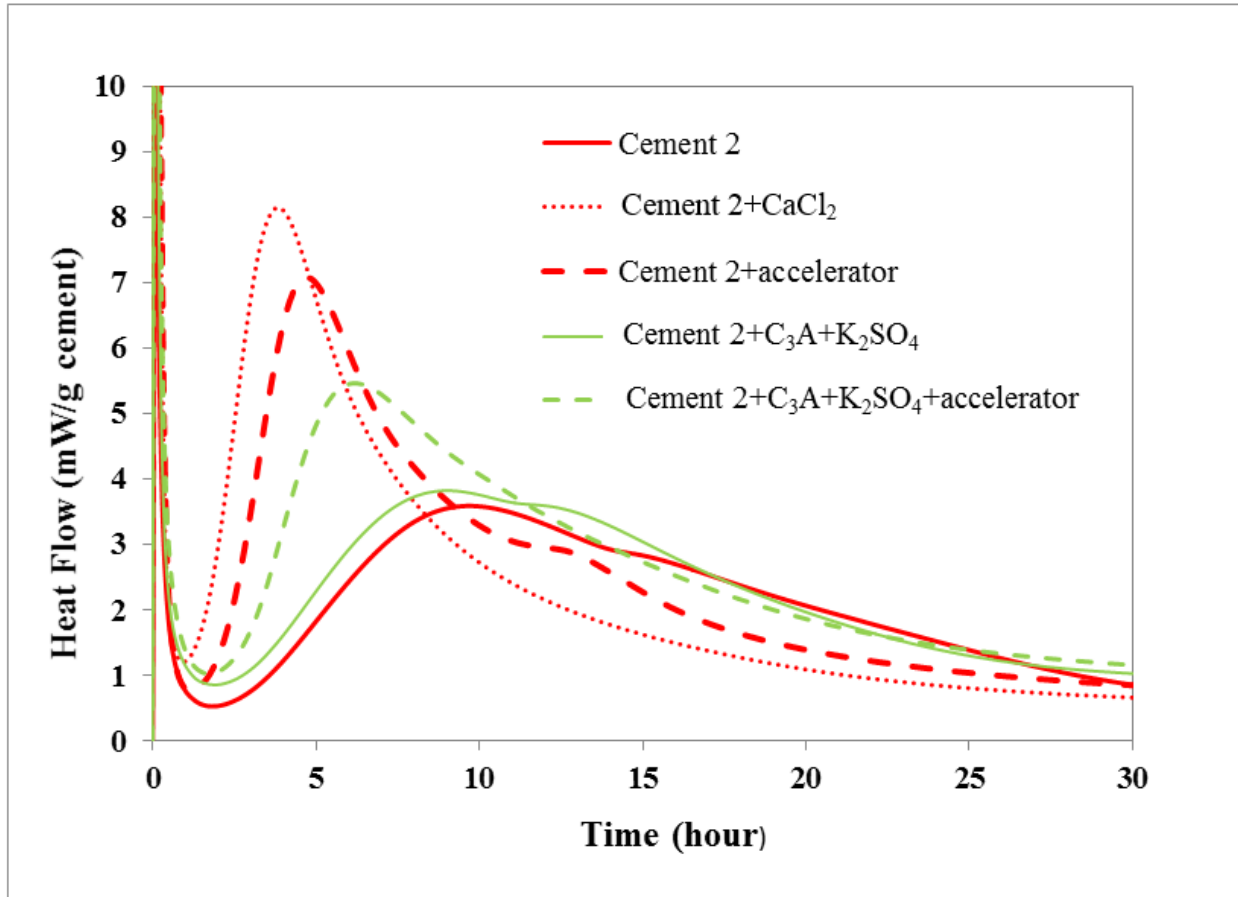


Figure 2.10. Effect of C₃A and K₂SO₄ on heat of hydration with commercial accelerator

Figure 2.11 shows the effect of K₂SO₄ and gypsum addition on heat flow. In the non-accelerated sample there was no significant effect on the main hydration peak compared to the as-received Cement 2; however, the aluminate peak was suppressed with no visible sulfate depletion point. In the sample with pure CaCl₂, greater reduction in the magnitude of the main peak is observed compared to the Cement 2, Cement 2+gypsum and Cement 2+K₂SO₄; in this case the

effect appears to be additive. The reduction in the maximum heat flow is approximately the same as the sum of the reductions achieved with K_2SO_4 and gypsum additions separately. This is in contrast to the C_3A and K_2SO_4 combination, where the reduction in the maximum heat flow was greater than the combined sum, which suggests an interaction between C_3A and K_2SO_4 and no significant interaction between K_2SO_4 and gypsum. This is further confirmed by the timing of the main hydration peak, which was the same as for the Cement 2+ K_2SO_4 sample with pure $CaCl_2$.

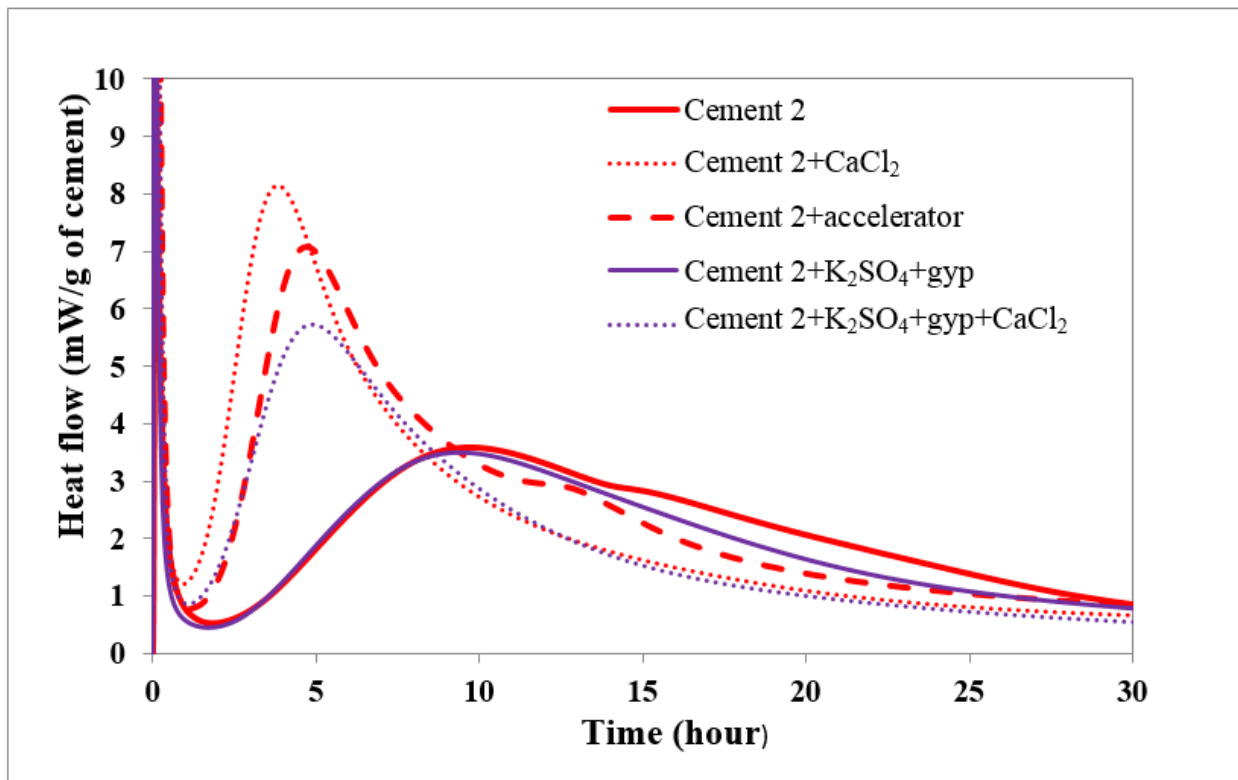


Figure 2.11. Effect of K_2SO_4 and gypsum on heat of hydration with pure $CaCl_2$

A combined effect of high C_3A , high alkali content and high sulfate content was examined as well (Figure 2.12). In the non-accelerated sample, the main hydration peak is similar to that of the Cement 2+ C_3A + K_2SO_4 sample, except the aluminate peak is suppressed by the addition of gypsum. In the presence of pure $CaCl_2$, the magnitude and timing of the main hydration peak are very similar to those of the Cement 2+ K_2SO_4 +gypsum, although the peak shape is broader, most

likely due to the reaction of aluminates. In the case of commercial accelerator, the main hydration peak is very similar to that of the Cement 2+C₃A+K₂SO₄ sample, except in the Cement 2+C₃A+K₂SO₄ with accelerator sample the peak is broader than in Cement 2+C₃A+K₂SO₄+gypsum sample with accelerator due to the lower sulfate content of Cement 2+C₃A+K₂SO₄.

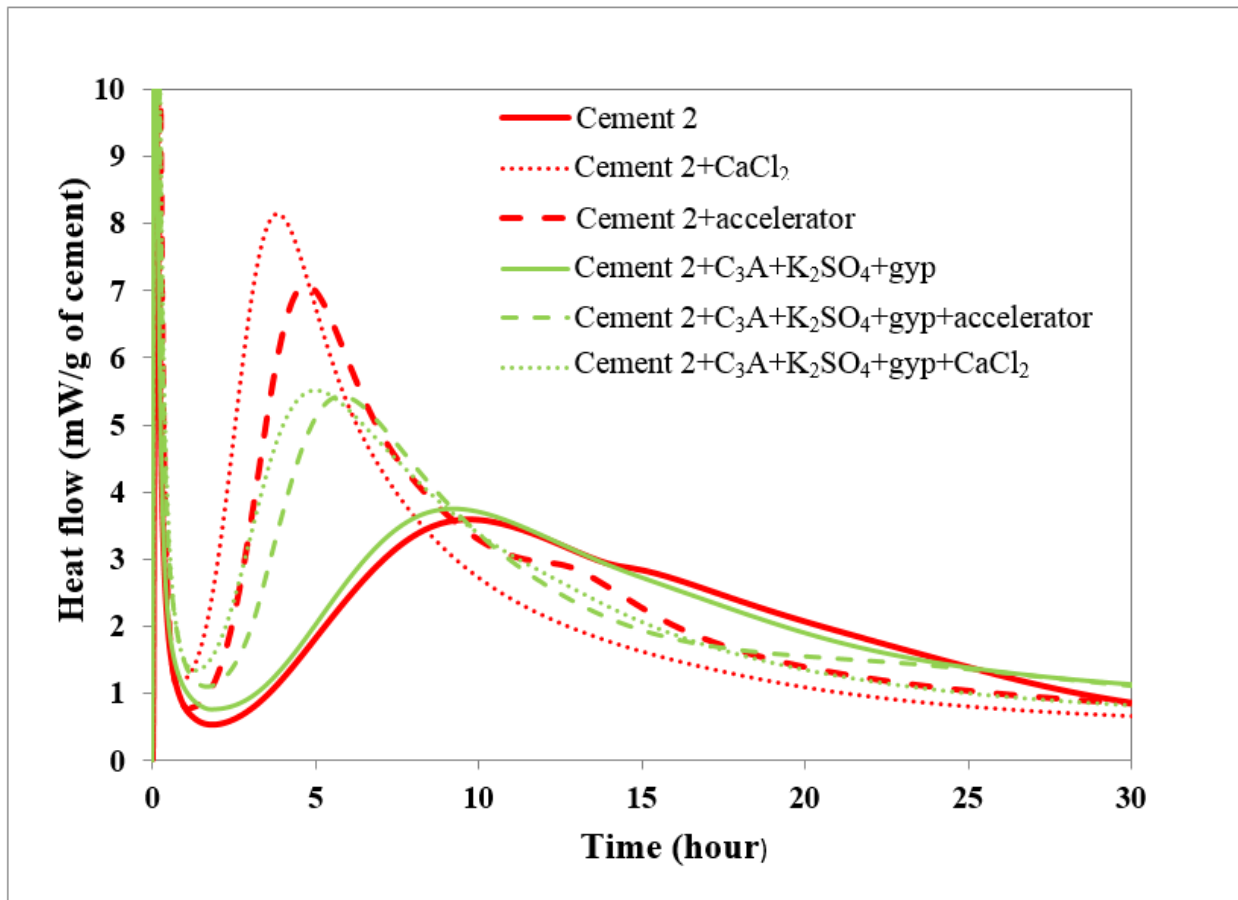


Figure 2.12. Combined effect of C₃A, K₂SO₄ and gypsum on heat of hydration with pure CaCl₂ and commercial accelerator

In summary, in the case of pure CaCl₂, increasing C₃A did not have an effect on the rate of heat flow, the magnitude of the main hydration peak or the timing of its occurrence. Increasing gypsum content slightly decreased the magnitude of the peak, but the rest of the parameters were unaffected. Addition of alkalis, both as sulfate salts and as hydroxides decreased the magnitude of the hydration peak and delayed the time of its occurrence by approximately an hour, except in

the case of NaOH where the timing was unaffected despite a significant reduction in the peak magnitude.

In the presence of commercial accelerator, increasing C_3A , gypsum content and addition of NaOH did not have an effect on the rate of heat flow during the acceleration period, the magnitude of the main hydration peak or the time of its occurrence. Addition of K_2SO_4 alone reduced the magnitude of the main peak, but its timing was unaffected. A further reduction in the peak magnitude and a slight delay in its timing were observed when both C_3A and K_2SO_4 were added to Cement 2. No further changes in the timing or the magnitude of the main hydration peak were achieved by adding $C_3A+K_2SO_4$ +gypsum.

2.3.1.2 Compressive Strength

While isothermal calorimetry is an excellent tool for following the progress of cement hydration through heat released, it is the early-age compressive strength which is often the parameter of interest in practice, especially with addition of accelerators.

Compressive strength measured for the as-received cements is shown in Figures 2.13-2.15. Significant increase in compressive strength at all ages was observed for Cement 1 with pure $CaCl_2$ addition (Figure 2.13). Increase in the early-age strength with commercial accelerator was slight, somewhat increasing after 24 hours, although the 7-day strength showed a slight decrease when compared to the mixture with no accelerator.

Pure $CaCl_2$ significantly increased compressive strengths of Cement 2 as well (Figure 2.14.). Commercial accelerator produced higher strengths at early ages (up to 24 hours) compared to Cement 1, although the strength drop at 7 day was more pronounced.

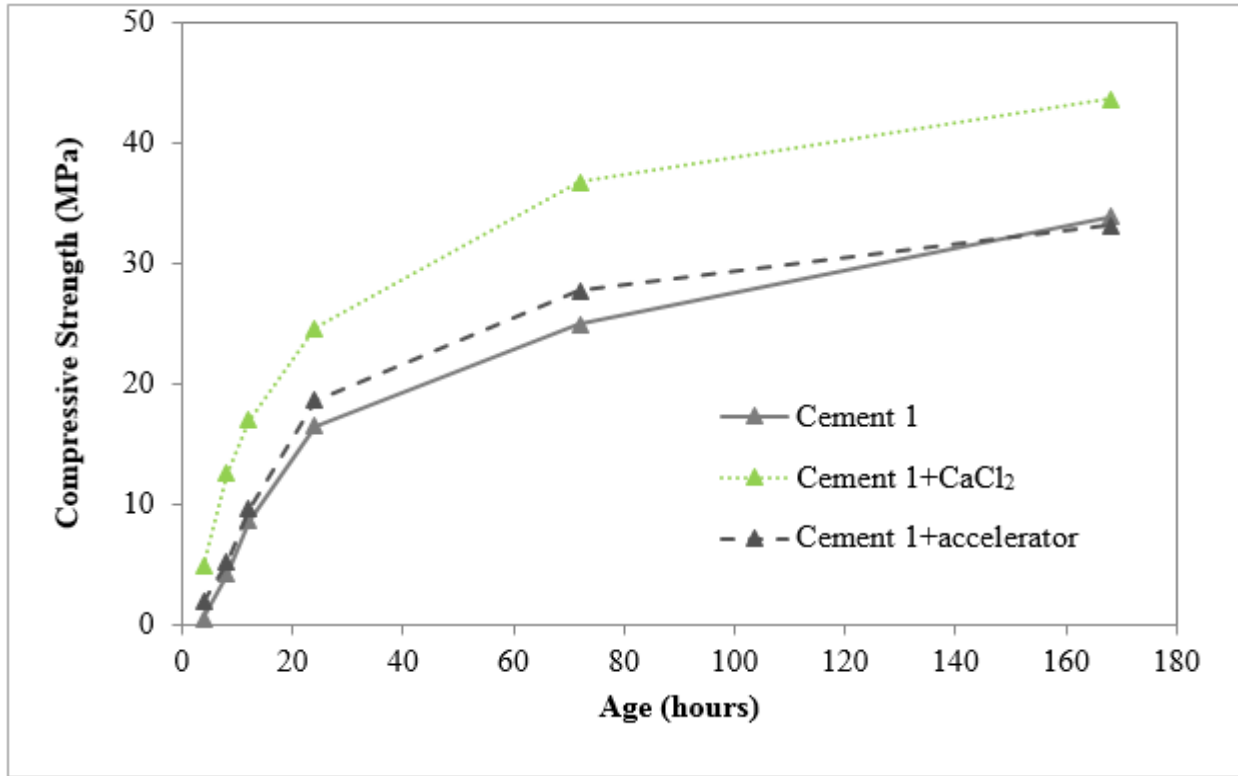


Figure 2.13. Compressive strength development for Cement 1

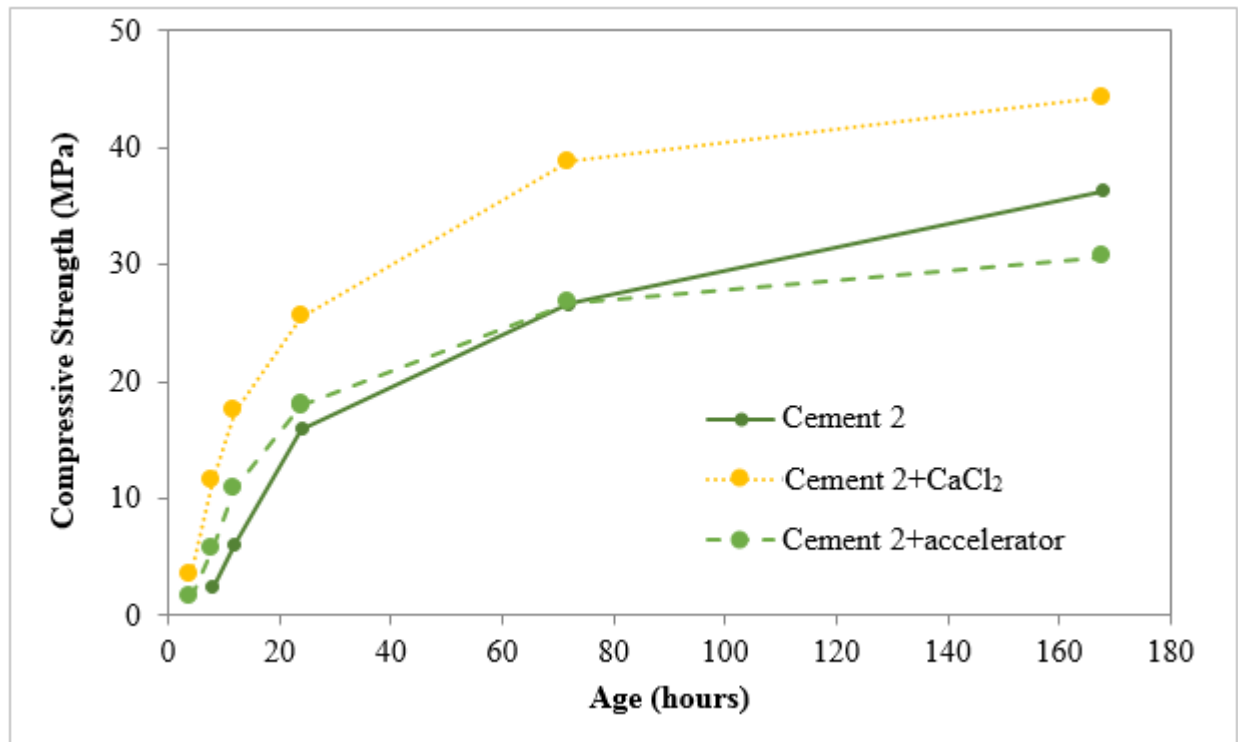


Figure 2.14. Compressive strength development for Cement 2

For Cement 3, addition of pure CaCl_2 increased early strengths only slightly (Figure 2.15), although after 24 hours strength gain began to improve and at 7 days exceeded that of the non-accelerated sample by almost 7 MPa, which is comparable to the other cements at this age. Commercial accelerator had minimal effect on early-age strength, although at 72 and 168 hours an increase was observed compared to the non-accelerated sample.

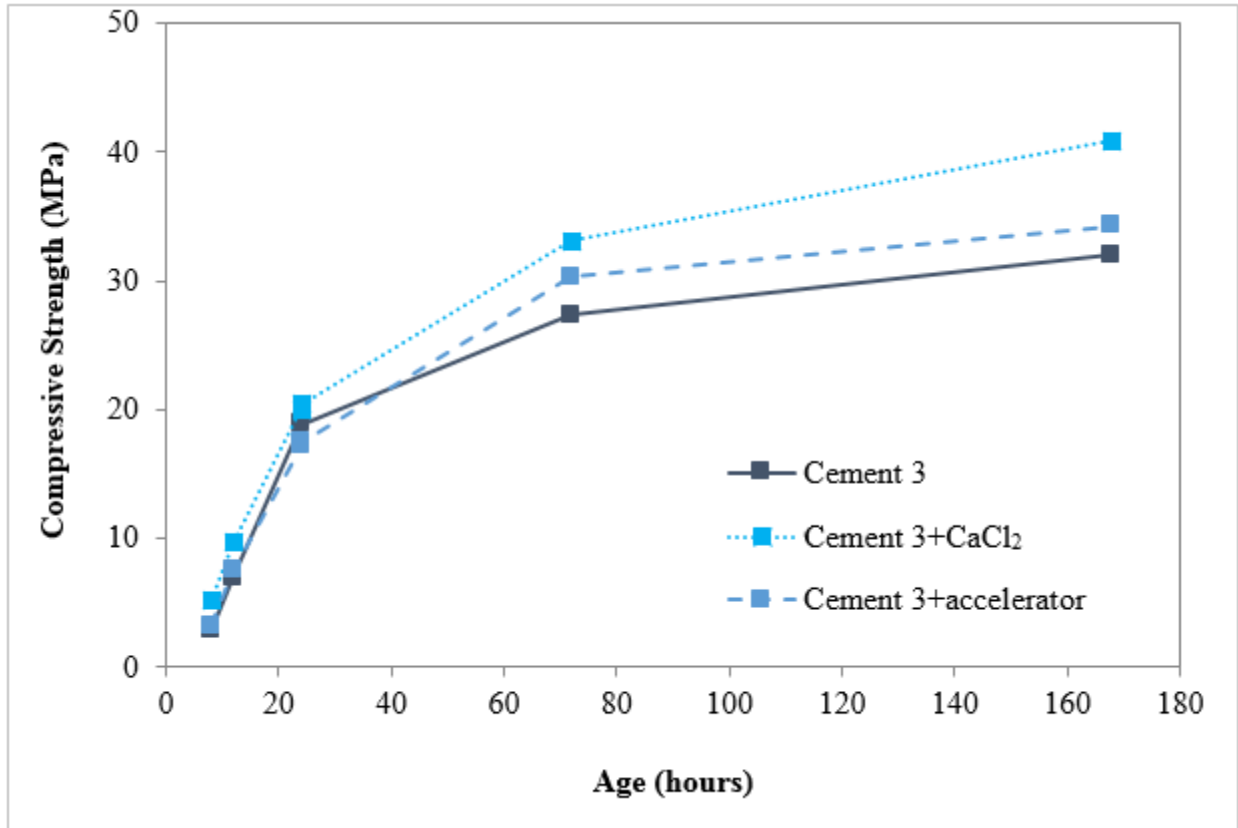


Figure 2.15. Compressive strength development for Cement 3

For mixtures with constant w/c ratio, curing temperature and similar cement fineness, the early-age compressive strength is primarily a function of the C_3S content of cement. It is not surprising, therefore, that compressive strengths of non-accelerated samples were generally similar at all ages except at 7 days, when Cement 3 mortar showed a decrease in compressive strength compared to the other samples. Odler and Wonnemann [58] reported a significant decrease in

compressive strength in the presence of alkali sulfates at all ages up to 28 days, so the decrease in Cement 3 strength at 7 days could be due to its higher syngenite content .

Similar to isothermal calorimetry results, higher strengths were observed with addition of CaCl_2 than commercial accelerator for Cements 1 and 2. When CaCl_2 was added to the samples, compressive strengths of Cement 1 and Cement 2 samples were very similar, while compressive strength of Cement 3 was lower at all ages. Addition of commercial accelerator, on the other hand, produced similar compressive strengths for all cements during the first 24 hours, after which time Cement 3 had the highest compressive strength.

Bentz et al. [6] showed that compressive strength of mortar mixtures prepared at different w/cm ratios is a linear function of $H(t)$ normalized by the amount of water present in the mixture. Oey et al. [5] applied this concept to OPC+SCM mixtures containing accelerator. Since all the mixtures in this study had the same w/c ratio, $H(t)$ was normalized per gram of cement. To further eliminate the between-cement variability, compressive strength data for all the mixes was plotted against the degree of hydration calculated from isothermal calorimetry using Equations 2.1 and 2.2 (Figure 2.16). The majority of the data falls in the $\pm 20\%$ error bounds (indicated by the dashed lines in Figure 2.16) with a few outliers which is consistent with the results reported by Bentz et al. [6] and Oey et al. [5].

Although a good coefficient of determination was obtained when all the dataset were combined (Figure 2.16), the fit was improved when the mixtures were plotted separately based on the accelerator used (Figures 2.17-2.19). Figures 2.17-2.19 show that the scatter in the data in Figure 2.16 was mostly due to the presence of accelerator/ CaCl_2 and not the differences in the mineralogical composition of cements. It is recognized that while the degree of hydration is a measure of the progress of chemical processes occurring during cement hydration, compressive

strength is a result of both chemical and physical changes. Nonetheless, Figures 2.17-2.19 provide a good correlation between these two parameters at a w/c ratio of 0.5.

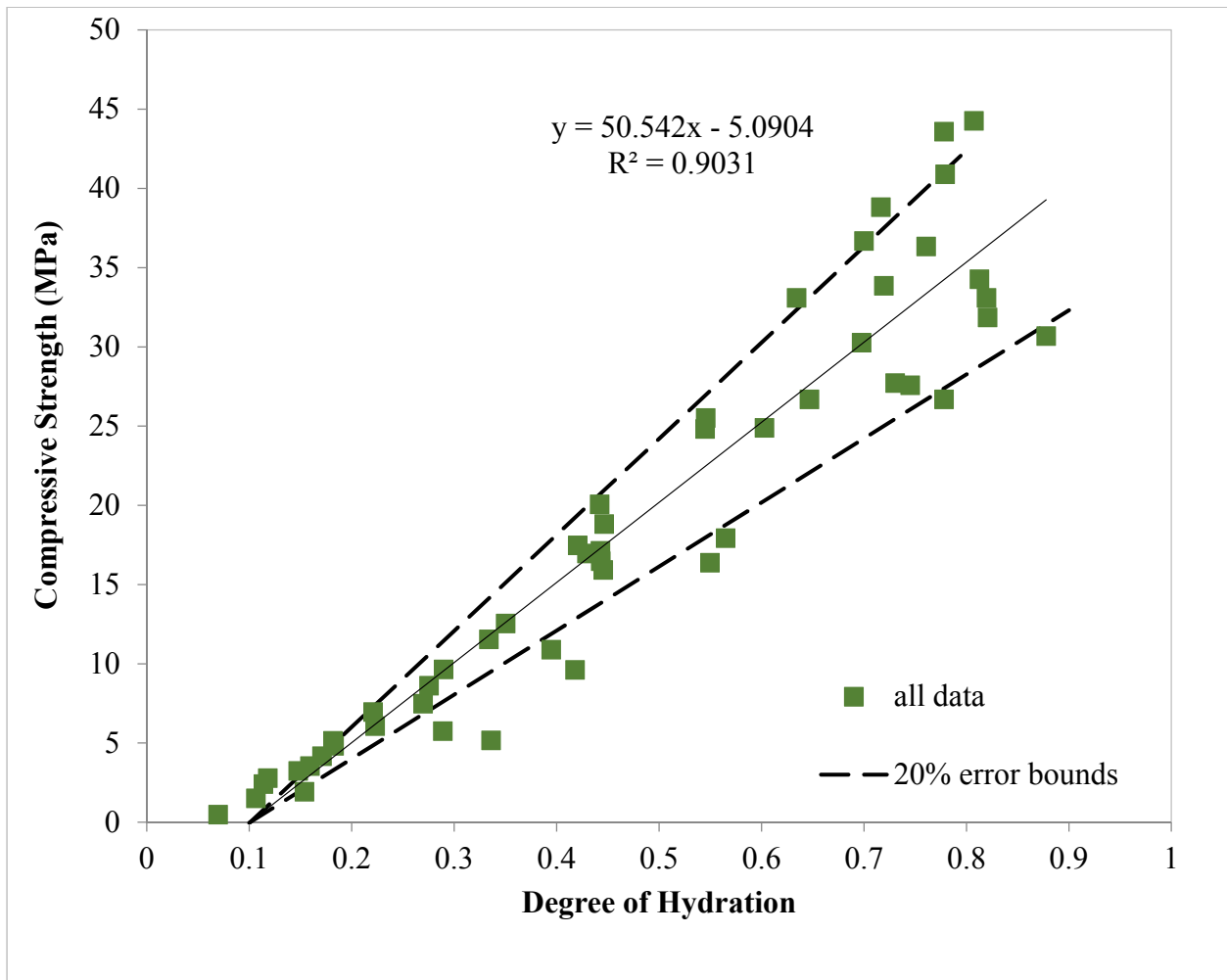


Figure 2.16. Compressive strength development as a function of degree of hydration. Data includes non-accelerated samples, samples with pure CaCl_2 and with commercial accelerator

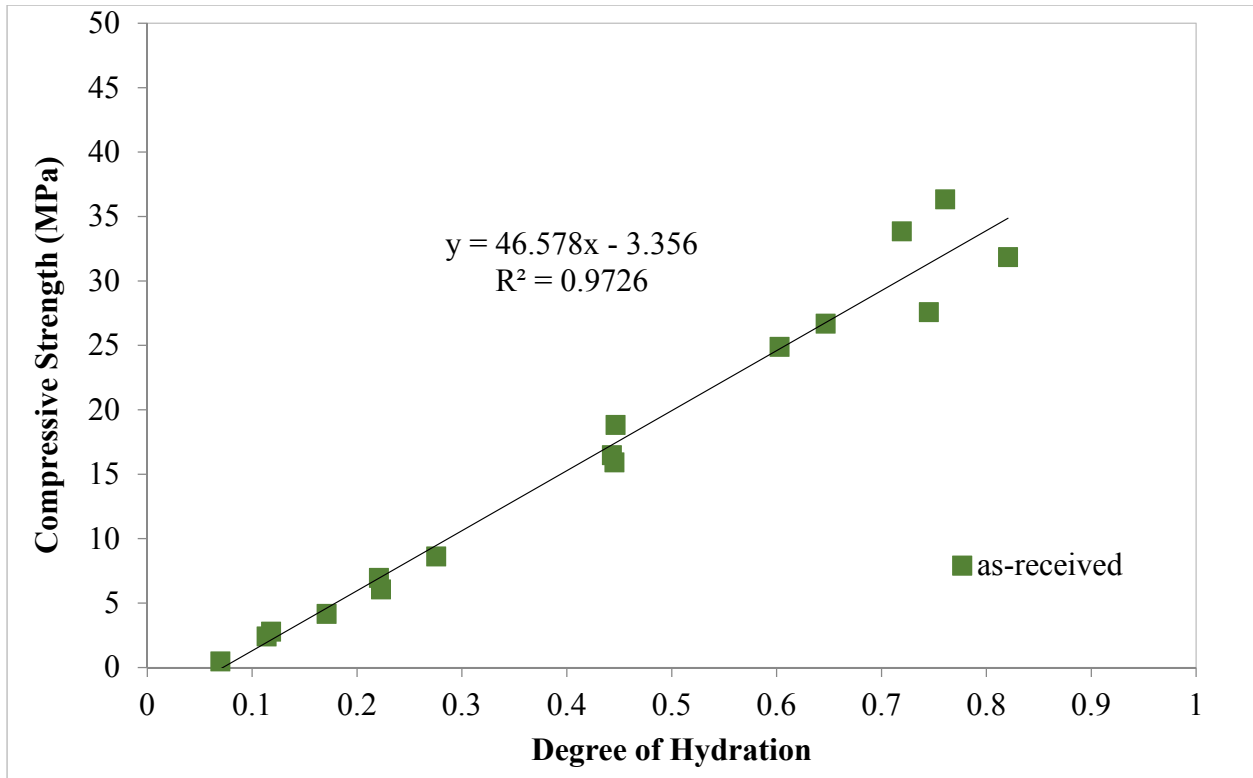


Figure 2.17. Compressive strength development for non-accelerated mortars

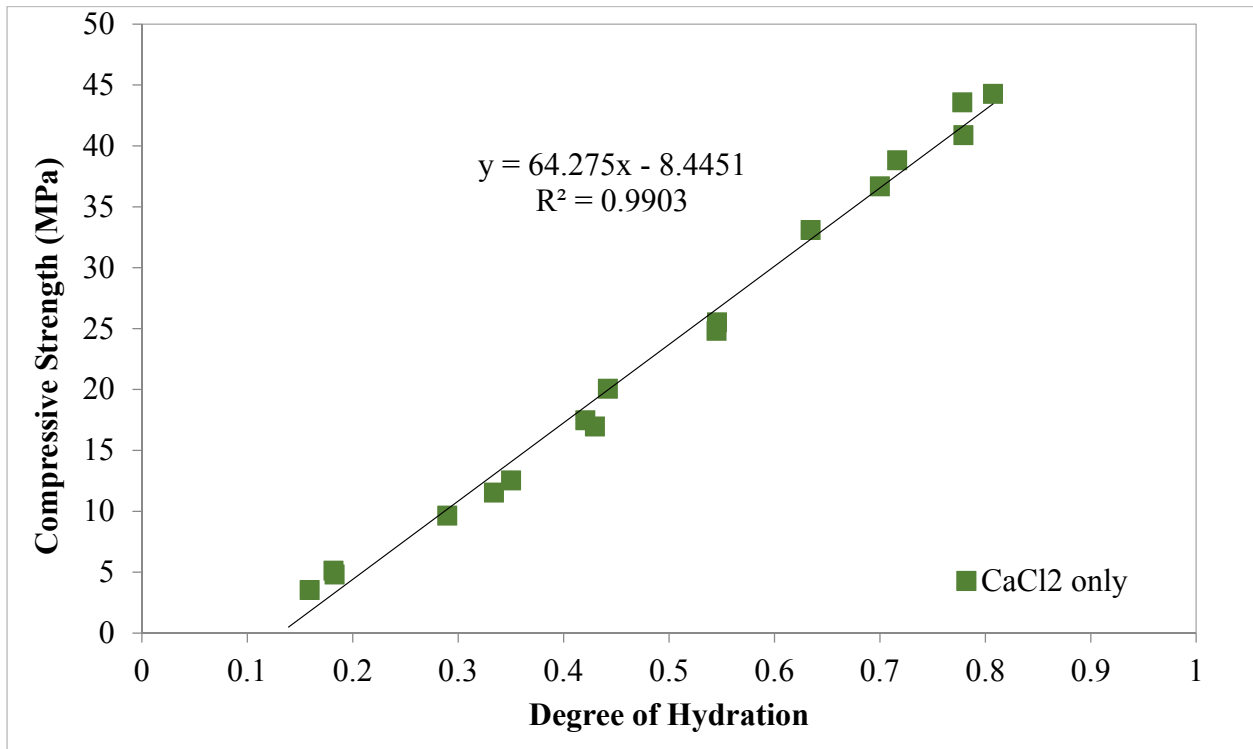


Figure 2.18. Compressive strength development for mortars with pure CaCl_2

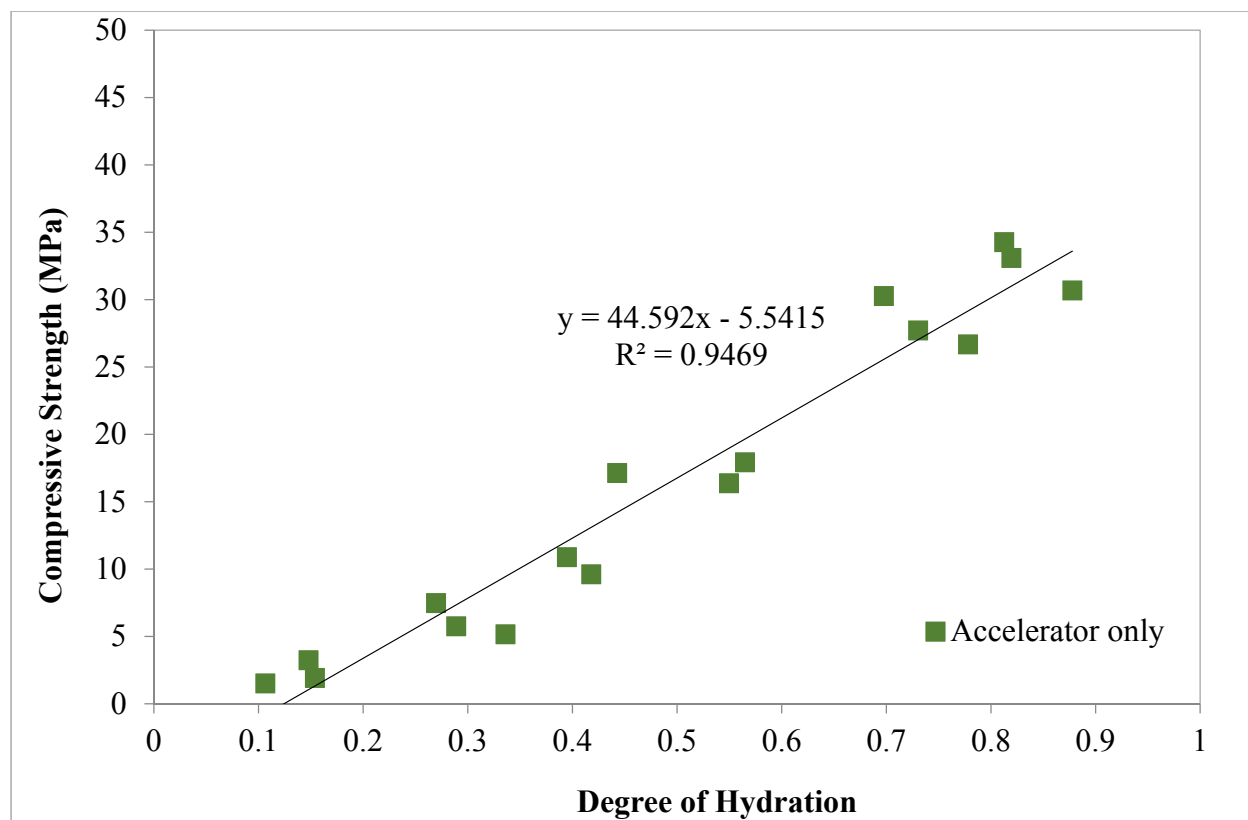


Figure 2.19. Compressive strength development for mortars with commercial accelerator

It is interesting to note that when pure CaCl₂ or a commercial CaCl₂-based accelerator were added, the minimum degree of hydration at which mortar begins to gain finite strength increased from 0.072 to 0.131 and 0.124, respectively. Bentz et al. [59], [60] had previously demonstrated that the degree of hydration at which setting occurs increases with increase in cement fineness even though setting time is decreased. The authors explained that when cement fineness increases, hydration products have to form an increased number of “particle-to-particle bridges” in order to develop a connected microstructure that is able to resist a force. Calcium chloride increases the number of hydration product nuclei [5], which explains the increase in the degree of hydration at which a connected microstructure is formed and strength developments begins. It can also be seen in Figures 2.17-2.18 that addition of pure CaCl₂ increased the rate of strength gain as expected. The rate of strength gain was essentially unchanged with the Type E accelerator addition compared

to the non-accelerated mixtures, which is consistent with observations by Oey et al. [5]. Although compressive strengths were not measured for the doped cements, it is expected that samples showing lower heat release will have lower compressive strengths.

2.3.1.3 X-ray Diffraction

Chloride ions are known to substitute for sulfate in the reaction of aluminates [61], [62]. It has been suggested that this abstraction of chlorides from the pore solution may be responsible for decreased effectiveness of CaCl_2 in high- C_3A cements [16]. XRD measurements were conducted on pastes of as-received cements with and without the addition of CaCl_2 /accelerator in order to identify any hydration products that may possibly be responsible for decreased effectiveness of chlorides.

X-ray diffraction patterns for the as-received cements were collected at 4 and 24 hours. For the non-accelerated samples, 4 hours corresponded to the beginning of acceleration period and low degree of hydration calculated from isothermal calorimetry (0.07 for Cement 1, 0.04 for Cement 2 and 0.05 for Cement 3). With addition of pure CaCl_2 or commercial accelerator, the degree of hydration of Cements 1 and 2 more than doubled, although only a slight effect was observed for Cement 3. A comparison at equal age was selected rather than equal degree of hydration as it is of more practical importance since accelerators are added to shorten setting and strength gain.

The 24-hour testing age was selected based on Shideler's work [14] which states that "CaCl₂ is only active during the first 24 hours." Twenty-four hours was selected as a second point of comparison. If CaCl_2 is ineffective beyond this time, it was expected that XRD measurements may show evidence of removal of chloride ions from solution through formation of Cl-containing phases.

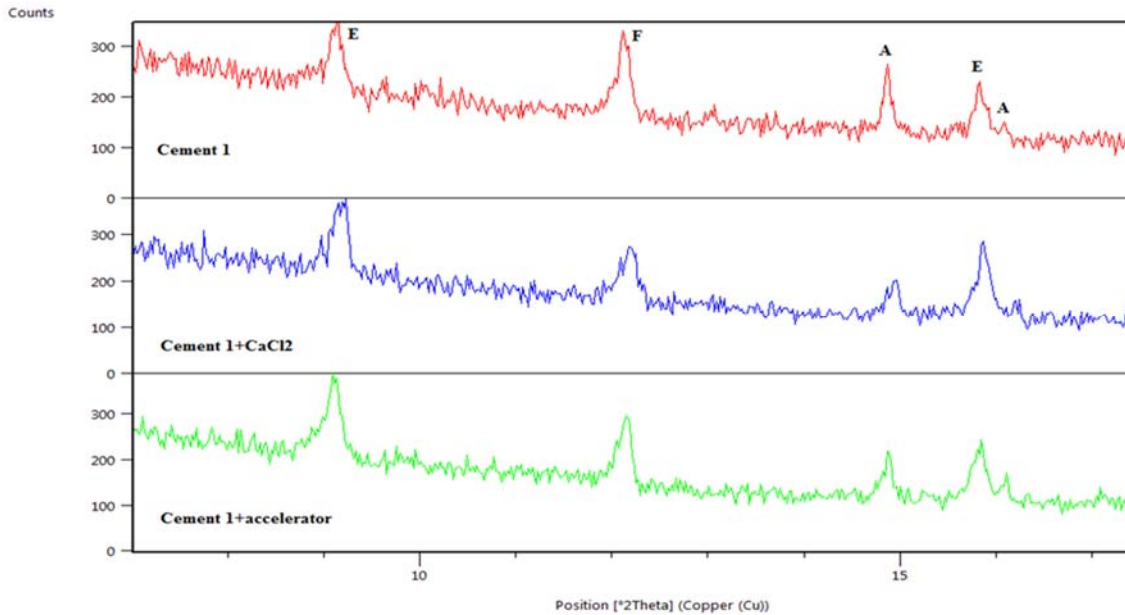


Figure 2.20. XRD scan of Cement 1 samples at 4 hours. Notation: E= ettringite, F=ferrite, A=alite

Figures 2.20 through 2.25 show diffractograms in the 2θ angular range of $7-17^\circ$, which is the region of the strongest diffraction peaks for chloroaluminate hydrates. Figures 2.20 and 2.21 show collected diffractograms for Cement 1 samples at 4 and 24 hours respectively. No significant differences in hydration phases were observed at 4 hours (Figure 2.20) between the accelerated and non-accelerated sample apart from the decrease in the alite peak, which is consistent with isothermal calorimetry results.

At 24 hours (Figure 2.21), formation of Friedel's salt is observed in the samples with CaCl_2 or commercial accelerator. Only a slight decrease is observed in the peak of the ferrite phase, bringing into question the hypothesis proposed by Jupe et al. [13] that greater accelerating effect of CaCl_2 on low- C_3A oilwell cements is due to formation of "ferrihydrite gel."

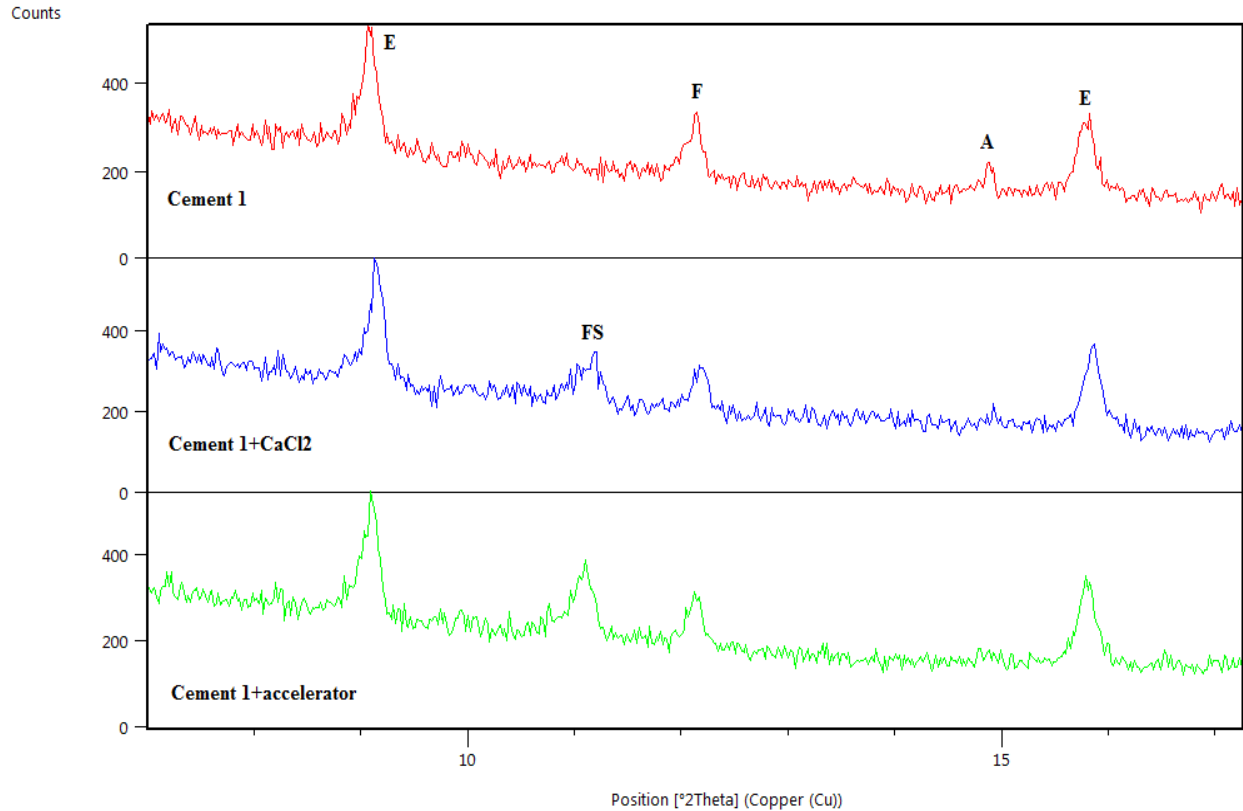


Figure 2.21. XRD scan of Cement 1 samples at 24 hours. Notation: E= ettringite, F=ferrite, A=alite, FS=Friedel's salt

As for Cement 2 diffractograms, the most notable differences at 4 hours (Figure 2.22) are observed in the magnitudes of the ettringite and gypsum peaks for samples with pure CaCl₂ or commercial accelerator, which is consistent with findings by Tenoutasse [63], who reported that CaCl₂ accelerates the reaction of C₃A with gypsum. There is a clear increase in the magnitude of the ettringite peak with the addition of calcium chloride or commercial accelerator and a corresponding decrease in the magnitude of the gypsum peak.

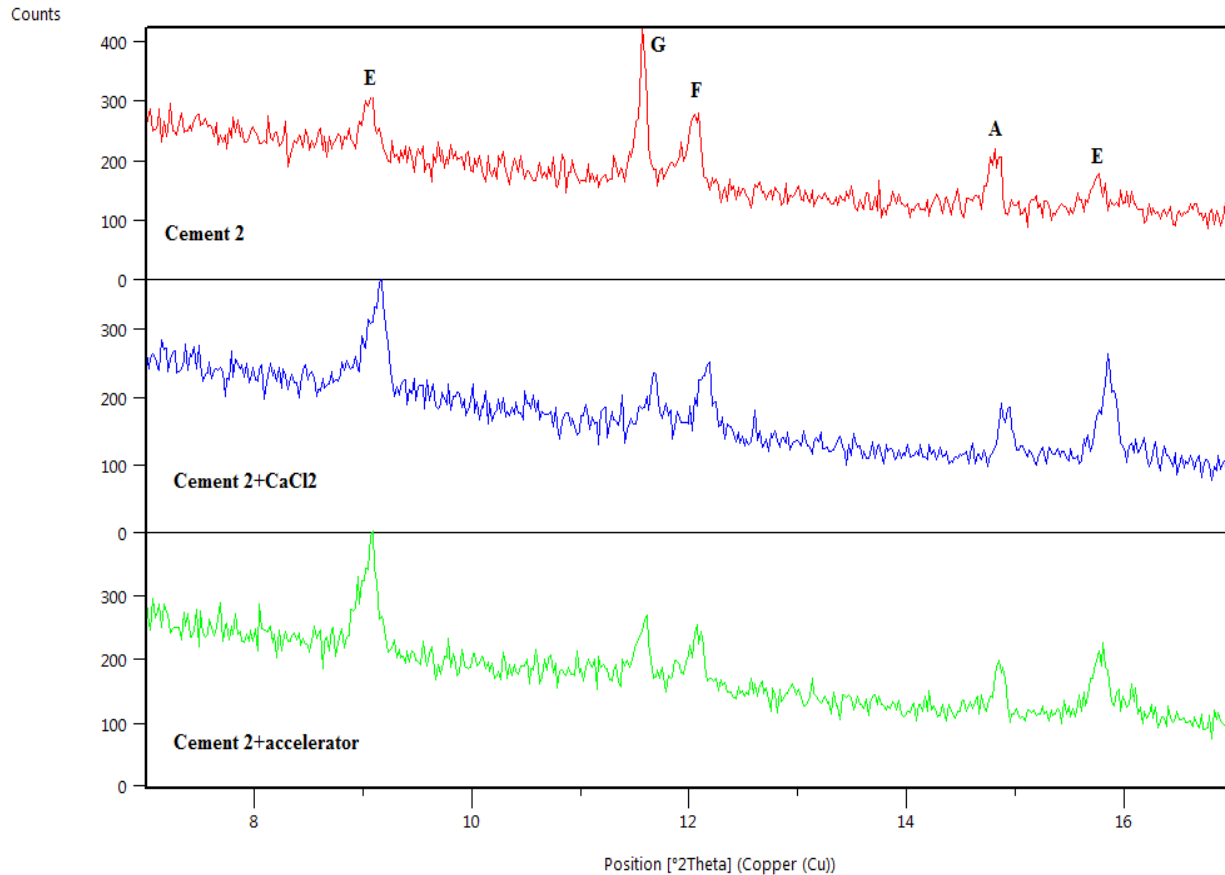


Figure 2.22. XRD scan of Cement 2 samples at 4 hours. Notation: E= ettringite, G=gypsum, F=ferrite, A=alite

At 24 hours (Figure 2.23), similar to Cement 1, Cement 2 samples had similar ferrite peaks. Also, accelerated samples showed the presence of Friedel's salt. This identification of Friedel's salt in Cement 1 and 2 accelerated samples is consistent with findings by Suryavanshi et al. [62] who measured the chloride ion concentration at 9 hours and 3 days. They showed that chloride binding is minimal at 9 hours, less than 2% of the total Cl^- ions. By 3 days, however, the percentage of bound chlorides increased to 38%. It appears that chloride binding did not occur during the early hydration stages, whether chlorides are added in the form of $NaCl$ [62] or $CaCl_2$.

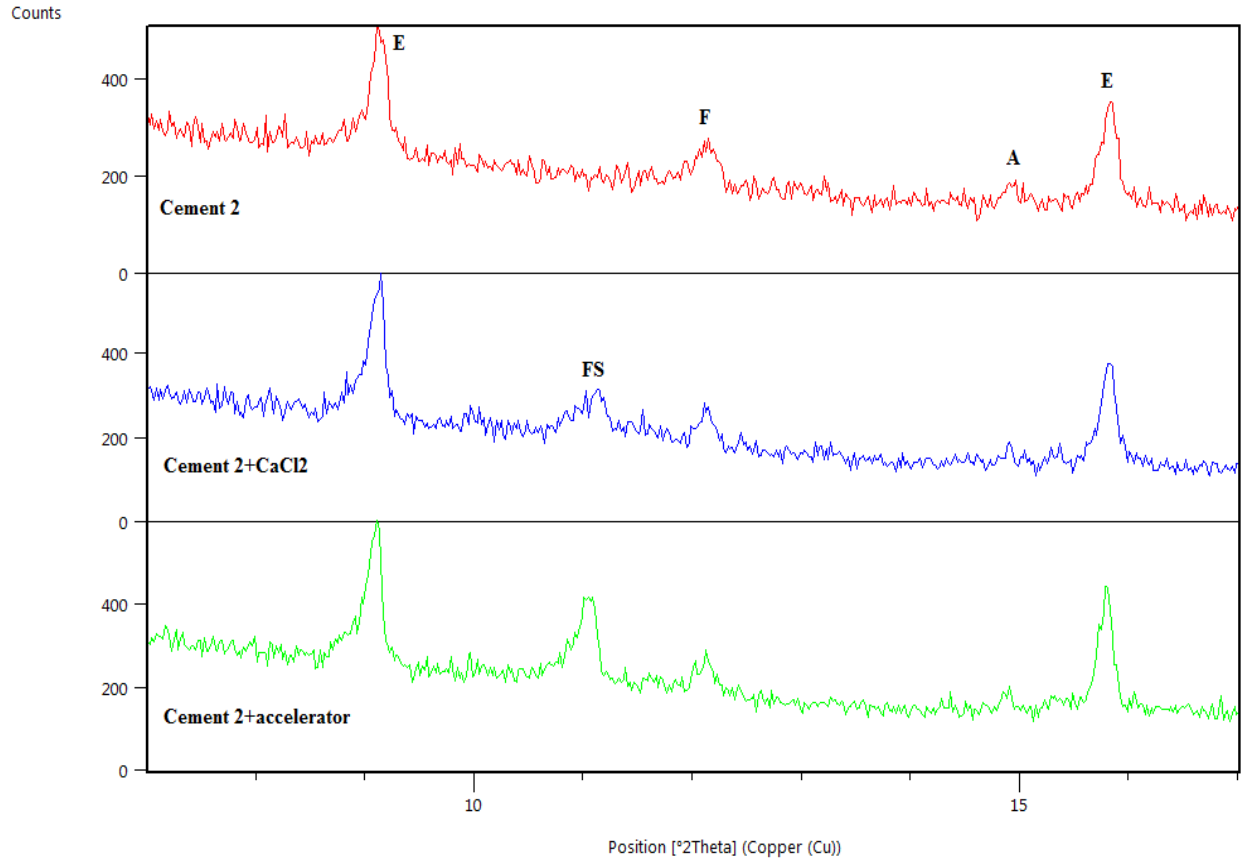


Figure 2.23. XRD scan of Cement 2 samples at 24 hours. Notation: E= ettringite, G=gypsum, F=ferrite, A=alite, FS=Friedel's salt

The most notable feature of Cement 3 diffractograms at 4 hours is the increase in the magnitude of the gypsum peak with CaCl_2 or commercial accelerator addition (note the difference in scales in Figure 2.24). Although gypsum structure is subject to preferred orientation [64], it may be possible for gypsum to precipitate from the reaction of CaCl_2 solution with K_2SO_4 [65]. However, by 24 hours, the gypsum is consumed in all the Cement 3 samples, similar to what was observed for Cement 2 at this age.

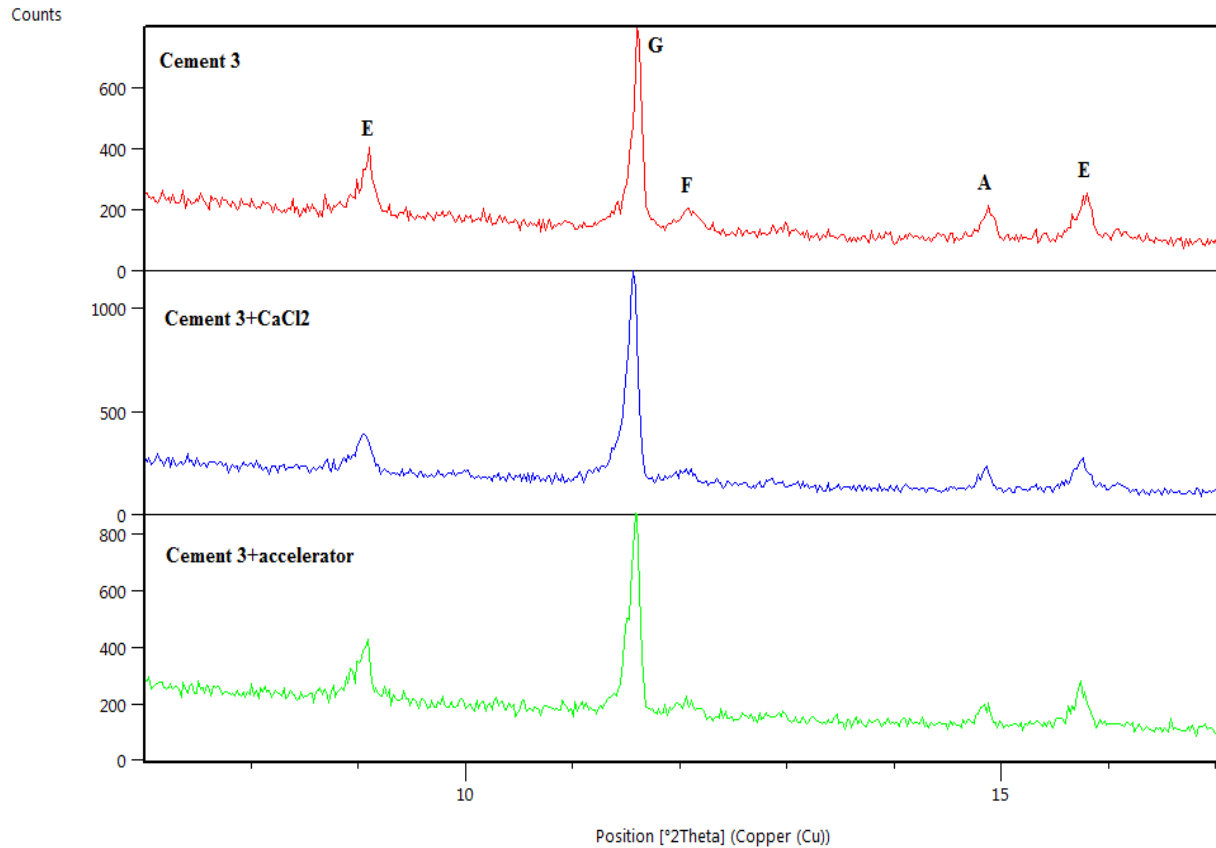


Figure 2.24. XRD scan of Cement 3 samples at 4 hours. Notation: E= ettringite, G=gypsum, F=ferrite, A=alite

Additionally, ettringite peaks in Cement 3 samples are similar regardless of the presence of accelerator as with the other cements. What is notable, however, is the absence of Friedel's salt in any of the Cement 3 samples (Figure 2.25). Therefore, it does not appear that the greater effect of chlorides on low- C_3A mixtures is due to their lower chloride-binding capacity through Friedel's salt formation. It is not clear what happened to the chlorides in Cement 3 samples as no other significant differences in mineralogy were detected at 24 hours.

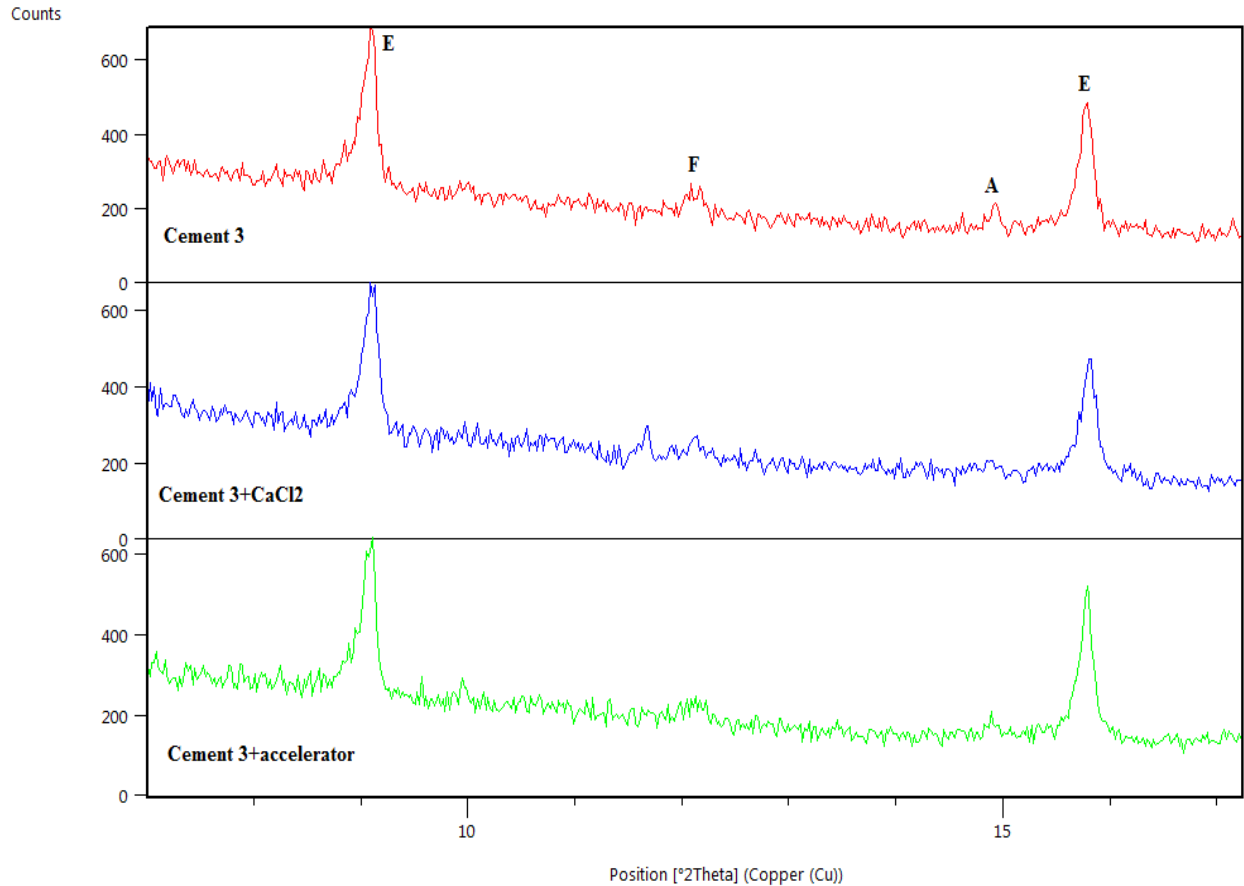


Figure 2.25. XRD scan of Cement 3 samples at 24 hours. Notation: E= ettringite, F=ferrite, A=alite

The reduced accelerating efficiency may possibly be explained by the increased adsorption of chloride ions by the C-S-H surface in high-alkali cements. pH is increased in the presence of alkalis. An increase in the pH corresponds to an increase in the negative surface charge of C-S-H, which in turn leads to an accumulation of positively charged calcium ions [66]. Labbez et al. [66] state that a larger amount of calcium ions are adsorbed than what is required to neutralize the surface charge, which makes the apparent charge of the C-S-H positive. Negatively charged chloride ions are in turn attracted to the now positively charged C-S-H surface in order to achieve charge neutrality. Several studies have previously reported adsorption of chlorides by C-S-H [67]–[69]. Although the chloride ions are not chemically bound to C-S-H [66], the attractive forces may

be sufficient to make these ions unavailable for acceleration of further hydration. This hypothesis is in agreement with the absence chloride-containing crystalline hydration products in Cement 2 samples with CaCl₂ or commercial accelerator. However, further study, such as pore solution analysis at various ages would be required to confirm this hypothesis.

2.4 Conclusions

It is clear that alkalis, specifically K₂SO₄, have a significant effect on chloride-based accelerators performance whether pure CaCl₂ or Type E commercial admixture. Increased C₃A or gypsum content of cement alone did not appear to reduce accelerator performance; however, in combination with high alkali content, these phases can have a notable effect on chloride-based accelerator efficiency in terms of heat release as measured by isothermal calorimetry. Further investigation is needed to determine the cause of this reduction in the accelerating efficiency in the presence of alkalis. Cement alkali content needs to be taken into account prior to accelerator selection as reduced heat release in high-alkali cements with chloride-based accelerator is expected to correlate with reduced compressive strength.

CHAPTER 3: EFFECT OF CHLORIDE-BASED ACCELERATOR IN THE PRESENCE OF WATER-REDUCING AND RETARDING ADMIXTURE ON AUTOGENOUS SHRINKAGE²

3.1 Introduction

Modern construction often requires concrete to achieve high strengths at early ages. In order to meet this requirement, mixtures are proportioned with low w/c ratio and large amount of accelerator. To maintain workability, water-reducing admixtures (WRA) are added as well. Autogenous shrinkage is a known cause of early-age concrete cracking for mixtures with water-cementitious (w/cm) ratios below 0.4. The effect of w/c ratio, supplementary cementitious materials (SCMs), and shrinkage-reducing admixtures (SRAs) on autogenous shrinkage has been extensively studied [70]–[80]. Oliviera et al. [81] showed the advantages of using a combination of SRA and expansive admixture in reducing autogenous shrinkage in concrete. The effect of other admixtures or their combinations, however, has not received much attention.

Recently, Meagher et al. [82] measured free shrinkage deformation in concretes containing an accelerator, as well as air-entraining admixture (AEA) and WRA. However, since the authors compared the performance of two types of accelerator, chloride-based and chloride-free, in combination with AEA and WRA, only one accelerator dosage was evaluated in this study. Additionally, free shrinkage measurements were performed under variable temperature profiles

² This chapter was published in the Journal of the American Ceramic Society [24]. The citation style and numbering was modified from the published version to match the rest of the dissertation chapters. Permission is included in Appendix A.

meant to simulate the initial concrete temperature rise due to hydration as well as temperature variation due to the diurnal temperature cycles. Since addition of accelerator increases the rate of hydration and therefore the peak concrete temperature, resulting in higher thermal expansion with addition of accelerator, it is difficult to draw conclusions regarding the effect of accelerator on autogenous shrinkage specifically, as it cannot be separated from the effect of thermal dilation under these conditions. Meagher et al. [82] were only able to comparatively assess the effect of accelerator on autogenous shrinkage after the first 20 hours when the temperature profiles of different concrete mixtures became similar.

Calcium chloride-based accelerators are frequently used in rapid repair concrete mixtures for jointed plain concrete pavement (JPCP) [83]. In addition to large amounts of accelerator, these mixtures have low w/c ratios and high cement contents to ensure that pavement can be quickly opened to traffic. Consequently, autogenous shrinkage and its contribution to microcracking is a concern [83]. Accelerators are most often used in conjunction with water-reducing admixtures, especially in rapid-repair concrete mixtures. Lignosulfonate water reducing admixtures have been shown to reduce autogenous shrinkage when used as the only admixture [84], but it is unknown how much they contribute when used in combination with accelerating admixtures. The use of accelerators has been suggested as one of the practical measures of reducing early-age autogenous shrinkage caused by other admixtures [85]; however, this suggestion has not been evaluated for the calcium chloride-based accelerators. Additionally, when accelerators are added at the job site, erroneous dosages can be introduced by mistake, which may possibly affect autogenous shrinkage.

Since most of the research on calcium chloride has been conducted in the 1970s, prior to autogenous shrinkage being recognized as a practical concern, there is a need to examine the

effects of large dosages of calcium chloride-based accelerating admixtures in combination with water-reducing admixtures on concrete autogenous shrinkage.

Autogenous shrinkage is the bulk volume change that occurs without moisture loss to the environment or temperature change. This volume change results from the consumption of pore water and chemical shrinkage during hydration. Drying shrinkage is the change in concrete volume due to loss of moisture to the environment that occurs after final setting. The underlying mechanism for autogenous and drying shrinkage is essentially the same – removal and redistribution of water in the concrete pore structure. Several mechanisms have been discussed in the literature as responsible for concrete shrinkage: tension of capillary water, disjoining pressure and surface tension of colloidal particles also referred to as surface free energy [8]–[12]. Although there is no clear agreement in the literature on which of these mechanisms is ultimately responsible for autogenous shrinkage, it is clear that changes in porosity or in C-S-H morphology are likely to affect autogenous shrinkage.

It has been established that calcium chloride addition modifies C-S-H morphology and that this modification is dosage-dependent[86]. As for porosity, there are conflicting reports in the literature regarding the effect of CaCl_2 on porosity. Some authors reported that addition of CaCl_2 resulted in the coarsening of the pore structure or decrease in total porosity [16]–[19], while others observed an increase in the pore volume, specifically in the range of nitrogen-accessible porosity [20], [22]. Gouda et al. [20] showed an increase in the volume of pores with radii of 1-6 nm (which was the extent of reported data) with 2% CaCl_2 addition, while Juenger and Jennings [22] observed that the addition of 1% CaCl_2 increases the volume of pores with radii of 1-40 nm. The disagreement regarding the effect of CaCl_2 on total porosity can be reconciled by the work of Ramachandran and Feldman [86] who showed that this effect is dosage dependent. They observed

that 1% CaCl₂ addition resulted in lowest total porosity, and total porosity began to increase with calcium chloride dosage. However, they did not measure pore size distribution, and it is not clear how varying CaCl₂ dosages affect different pore size ranges. Li et al. [75] determined that the amount of pores in the 5-50 nm diameter range is strongly correlated to the amount of autogenous shrinkage. Therefore, it appears that addition of CaCl₂-based accelerator is likely to increase autogenous shrinkage, however, the dosage-dependency of the admixtures remains unclear, especially in the presence of other admixtures such as water-reducing admixtures.

3.2 Experimental Procedures

3.2.1 Materials

Materials and concrete mixture designs used in this study have been previously described in [25]. Table 3.1 shows the cement mineralogical composition and physical properties.

Table 3.1. Cement composition and physical properties

Cement Phase/ Property	Type I/II
Tricalcium Silicate, C ₃ S (%)	52.0
Dicalcium Silicate, C ₂ S (%)	20.7
Tricalcium Aluminate, C ₃ A (%)	10.2
Tetracalcium Aluminoferrite, C ₄ AF (%)	5.7
Gypsum	4.4
Hemihydrate	1.6
Anhydrite	0.2
Calcite	2.1
Lime	0.1
Portlandite	2.0
Quartz	0.9
ASTM C204-Blaine Fineness (m ² /kg)	442

Cement mineralogical composition was determined by x-ray diffraction (XRD). XRD scans were collected using X'Pert 3040Pro diffractometer manufactured by Panalytical, and Cu K α radiation. The following settings were used: 1° divergence slit, 0.2 mm receiving slit, 1° anti-scatter slit, 45 kV tension and 40 mA current. Cement mineralogy was determined by Rietveld refinement, using Panalytical HighScore Plus 3.0 software. Cement Blaine fineness was measured following ASTM C204.

The coarse aggregate used in this study was #57 limestone, and silica sand was used as fine aggregate. Their respective gradations are plotted in Figures 3.1 and 3.2 against the limits defined in ASTM C33. Table 3.2 shows the concrete mixture proportions used in this study.

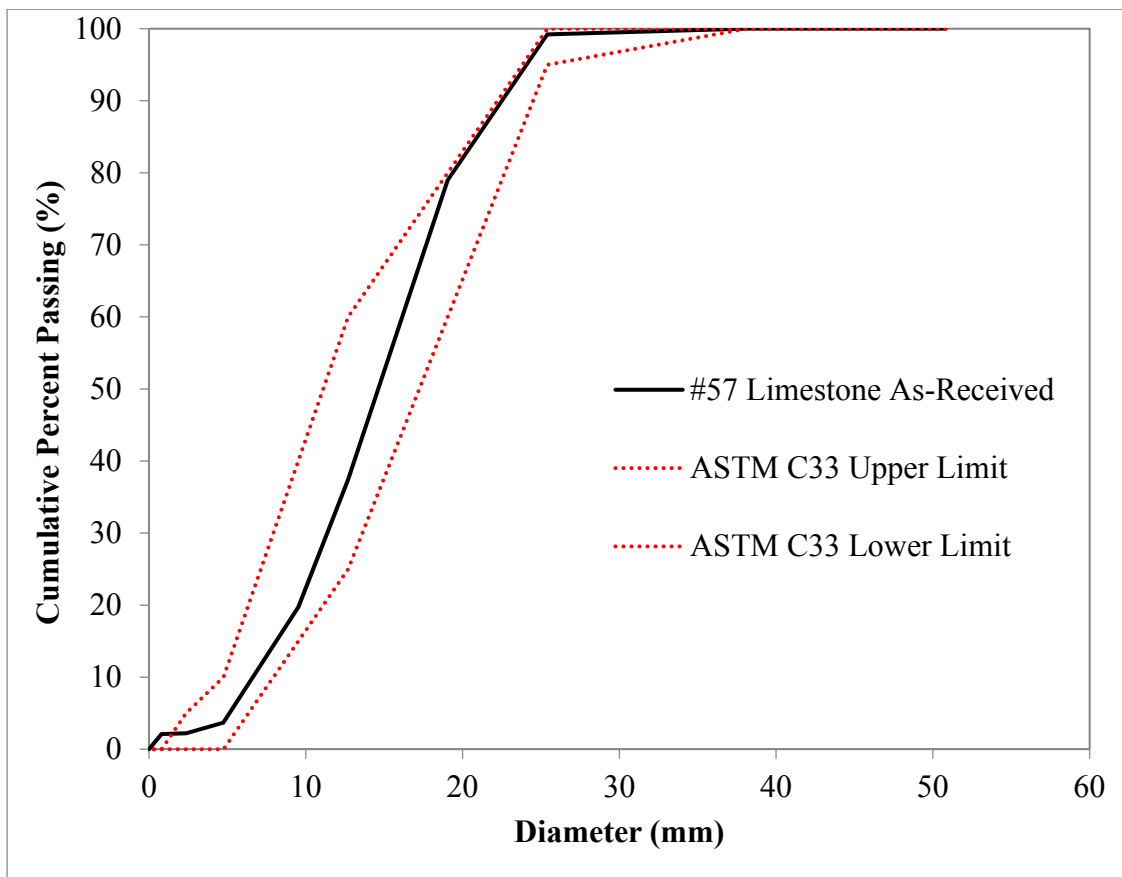


Figure 3.1. Coarse aggregate grading curve

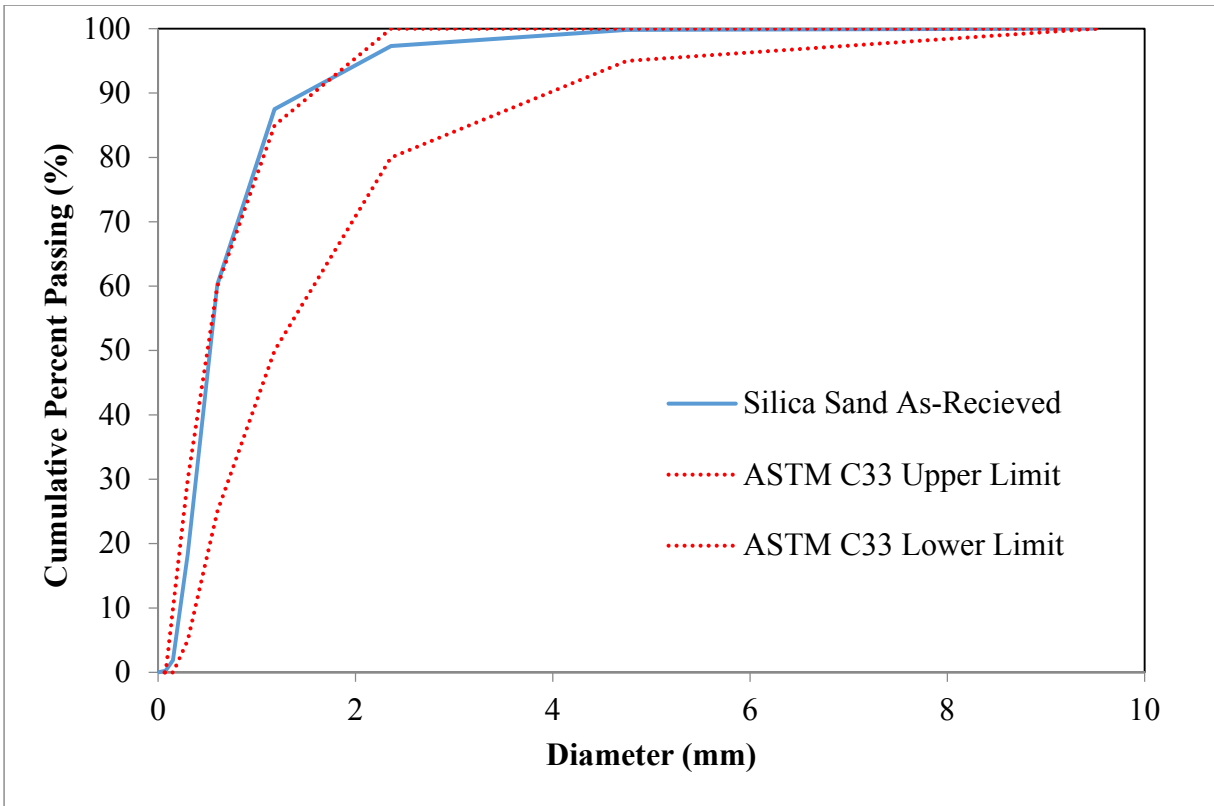


Figure 3.2. Fine aggregate grading curve

Table 3.2. Concrete mixture proportions

Mix ID	Cement (kg/m ³)	Coarse Aggregate (SSD) (kg/m ³)	Fine Aggregate (SSD) (kg/m ³)	Air-Ent. (ml/m ³)	Water-reducer (ml/m ³)	Water (kg/m ³)	Accelerator (ml/m ³)	CaCl ₂ Content (%)
C	534	997	493	0	0	205	0	0
CNA	534	997	493	116	1741	205	0	0
CHA	534	997	493	116	1741	199	7427	0.5-1
CA	534	997	493	116	1741	193	14853	1-2
CDA	534	997	493	116	1741	181	29707	2-4

Dosage of commercial calcium chloride-based accelerator was varied from no accelerator (CNA mixture) to 1375 ml/100 kg of cement (CHA mixture), which is in the middle of manufacturer’s recommended dosage range, to the upper limit of the recommended range at 2750 ml/100 kg (CA mixture), which is the actual dosage used in Florida for rapid repair concrete

pavement mixtures, to well above the recommended dosage at 5500 ml/100 kg (CDA mixture) representing the accidental overdose. Accelerator is added on-site to JPCP rapid repair mixtures; several instances of an accidental overdose have been reported in Florida. With the exception of the control mixture (C), all mixtures studied here contained the same amounts of air-entraining admixture (AEA) and lignosulfonate water-reducing and retarding admixture (WRRRA). In addition to calcium chloride, the accelerator contained small amounts of potassium and sodium chloride and triethanolamine. Water-to-cement ratio was maintained constant at 0.384. The mixing water was adjusted by the water contained in the accelerating admixture, in order to maintain a constant w/c. CaCl₂ amounts were approximated for each mixture based on the CaCl₂ percentage range listed in the material safety data sheet for the accelerator and are also included in Table 3.2.

3.2.2 Methodology

Isothermal calorimetry measurements were performed on paste samples at 23°C following the ASTM C1702 Method A, internal mixing and using TAM Air 8-twin channel calorimeter manufactured by TA Instruments. The mass of cement was 3.98 g and a constant w/c ratio was maintained at 0.384. Since accelerator dosage varied depending on the mixture, the water present in the accelerator was included in the calculation of the w/c ratio. The total mass of each sample varied from 5.51 g for C mixture to 5.67 g for CDA due to specific gravity of accelerating admixture (1.35). Two samples were tested for each mixture.

Isothermal calorimetry was used to calculate the degree of hydration $\alpha(t)$ for each mixture as a function of time to compare the mechanical property development and autogenous shrinkage on a degree of hydration basis, instead of age. The degree of hydration was calculated by dividing

the total heat $H(t)$ released by each mixture at time (t) by the total available heat H_u that can be generated by the cementitious components of the mixture:

$$\alpha(t) = \frac{H(t)}{H_u} \quad \text{Equation 3.1}$$

H_u is quantified as a function of cement composition, the amount of the phase, and type of supplementary cementing materials present in the system[26].

$$H_u = H_{cem} P_{cem} + 461 P_{slag} + 1800 P_{FA-CaO} P_{FA} \quad \text{Equation 3.2}$$

where

P_{slag} = Slag mass to total cementitious content ratio,

P_{FA} = Fly ash mass to total cementitious content

P_{FA-CaO} = Fly ash-CaO mass to total fly ash content ratio,

P_{cem} = Cement mass to total cementitious content ratio,

H_{cem} = Heat of hydration of the cement (J/gram).

Since the mixtures in this study only contained cement as a binder, H_u was equal to H_{cem} .

H_{cem} was calculated as follows:

$$H_{cem} = 500P_{C3S} + 260P_{C2S} + 866P_{C3A} + 420P_{C4AF} + 624P_{SO3} + 1186P_{FreeCaO} + 850P_{MgO} \quad \text{Equation 3.3}$$

where

H_{cem} = Total heat of hydration of Portland cement as describe above (J/gram)

P = Mass of i^{th} component to total cement content ratio.

Concrete mixtures were prepared following ASTM C192, except that the accelerator was added at the end of the mixing period specified by the standard after which concrete was mixed for an additional 30 seconds. As recommended by the manufacturer, the AEA was placed on the sand and WRRA was added to the mixing water. Tensile strength and elastic modulus of 100x200

mm concrete cylinders were measured following ASTM C496 and C469. Two specimens were tested in each case and their average value is reported.

Free shrinkage frame (FSF) was used to measure autogenous deformations of the concrete mixtures under isothermal conditions (23°C) during the first 72 hours. A detailed description of the FSF set-up used in this study can be found in [23]. Concrete was kept under isothermal conditions by circulating cooling water through the copper piping and sealed to prevent any moisture loss to the environment. Initial readings were taken at final setting after the movable steel plates were backed off (Figure 3.3).

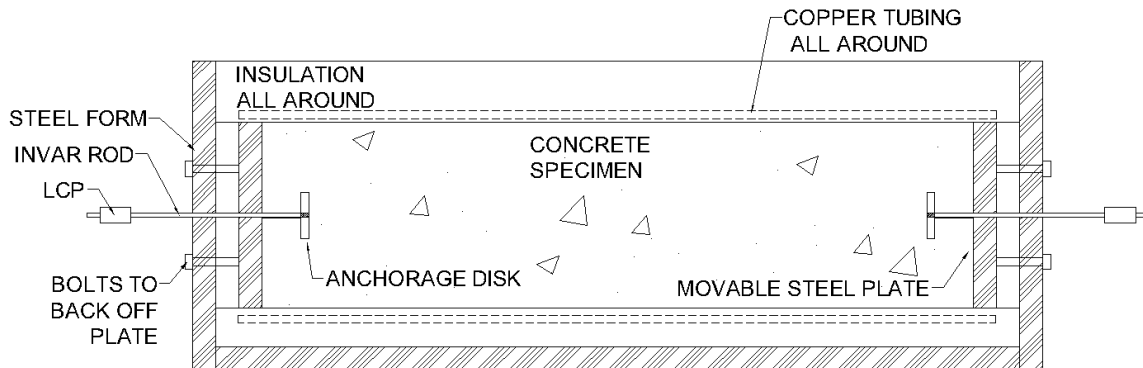


Figure 3.3. Free shrinkage frame

The setting time for each mixture was determined according to ASTM C403 prior to the FSF experiments. Linear deformation and concrete temperature readings were taken every minute for the duration of the free shrinkage test.

In conjunction with free shrinkage testing, paste samples were prepared for XRD analysis and porosity determination through nitrogen adsorption. Paste samples were sealed after mixing and cured for 3 days under isothermal conditions (23°C) to match the free shrinkage samples. For XRD measurements, samples were demolded at 72 hours and immediately crushed by hand with

mortar and pestle. XRD scans were collected immediately after powdering the samples using the settings described previously.

For nitrogen adsorption measurements, samples were crushed, sieved to separate the fraction with the size of 1-3 mm, and dried at 105°C under vacuum using the outgasser built into Autosorb-1 manufactured by Quantachrome Instruments. The paste drying procedure has been shown to have a significant effect on porosity determined by nitrogen adsorption [87], [88]. In this study, oven-drying at 105°C was combined with vacuum-drying. Drying time for each sample was in the range of 2-3 hours as suggested by Beaudoin [89]. Moreover, pastes were dried to a constant pressure, which ensures that the same pore size range was emptied for all the samples. After completion of drying, nitrogen adsorption/desorption isotherms were collected using Autosorb-1. Total pore volume and pore size distribution were calculated using the Barrett, Joyner, Hallenda (BJH) method. Both adsorption [90], [91] and desorption [87], [92] branches of the nitrogen adsorption isotherm have been used for BJH analysis of cement pastes. The adsorption branch of the isotherm was used for the BJH porosity calculation since it measures the size of the interior of the pore, while the desorption branch measures the pore entry size [93], [94]. Since pores in cement paste are expected to be bottle-necked, and autogenous shrinkage is affected by the size of the pore, not the size of the pore entry, adsorption branch was selected. Additionally, the adsorption branch is not influenced by the pore network effects to the same degree as the desorption branch [93], [95].

Porosity measurements were also performed on concrete samples for all mixtures using mercury intrusion porosimetry (MIP). MIP was selected for concrete analysis since nitrogen sorption is typically only used on pastes. Concrete cylinders, 100x200 mm, were prepared and cured for 3 days for all mixtures. For MIP measurements, a 5 cm long sample was saw-cut from

the middle of each cylinder. Samples were cut to fit the 5 cm diameter macro-cell used for MIP measurements. Prior to analysis, concrete samples were dried in the oven at 105°C for 14 hours. MIP measurements were carried out using the Quantachrome Poremaster mercury intrusion porosimeter. First, mercury was introduced into the sample at low pressure, up to 0.3 MPa, after which the analysis was continued in high pressure mode, where intrusion pressure was increased up to 414 MPa. Washburn equation was used for data analysis with a mercury contact angle of 140° and mercury tension of 0.48 N/m.

3.3 Results and Discussion

3.3.1 Isothermal Calorimetry and Setting Time

Isothermal calorimetry showed a reduction in the length of the dormant period and an increase in the rate of heat evolution during the acceleration period with increasing the accelerator dosage (Figure 3.4).

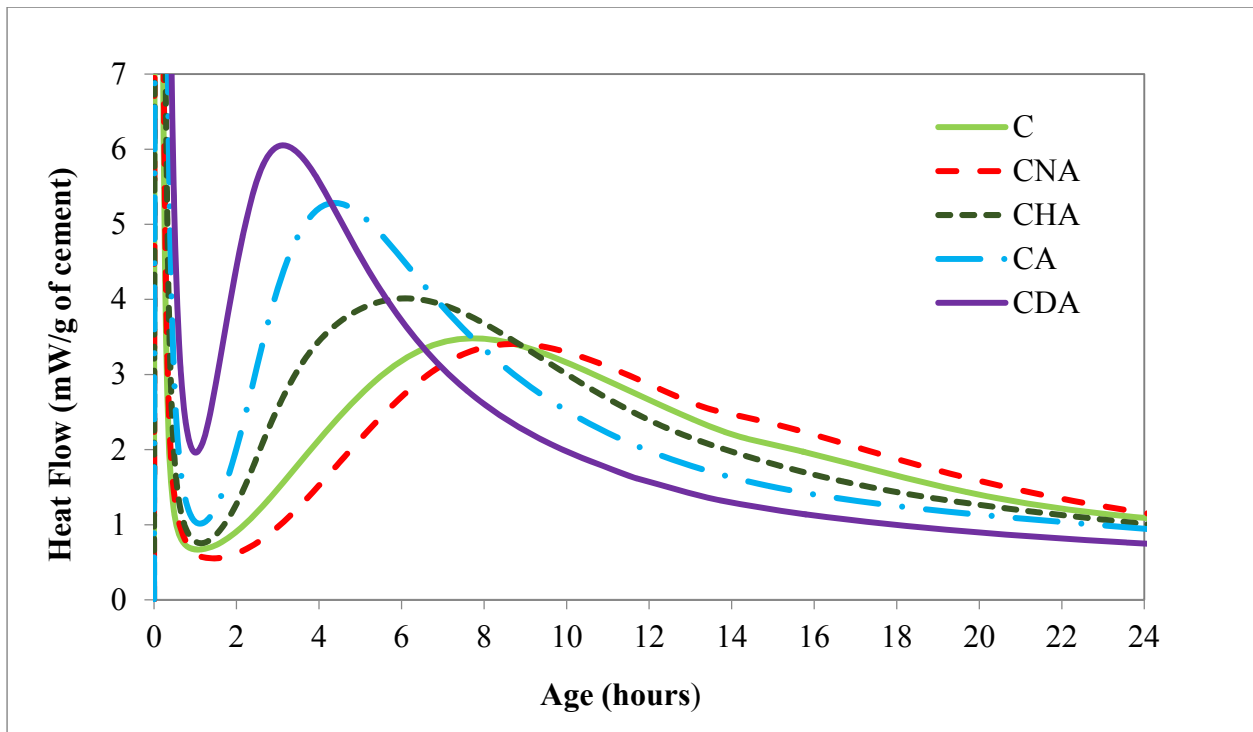


Figure 3.4. Heat flow of cement pastes normalized per gram of cement

It is interesting to note that although total heat evolved initially increases with accelerator dosage, after the first 24 hours there was a cross-over between CDA and CA total heat curves, and CDA total heat remained slightly below that of CA until 72 hours (Figure 3.5).

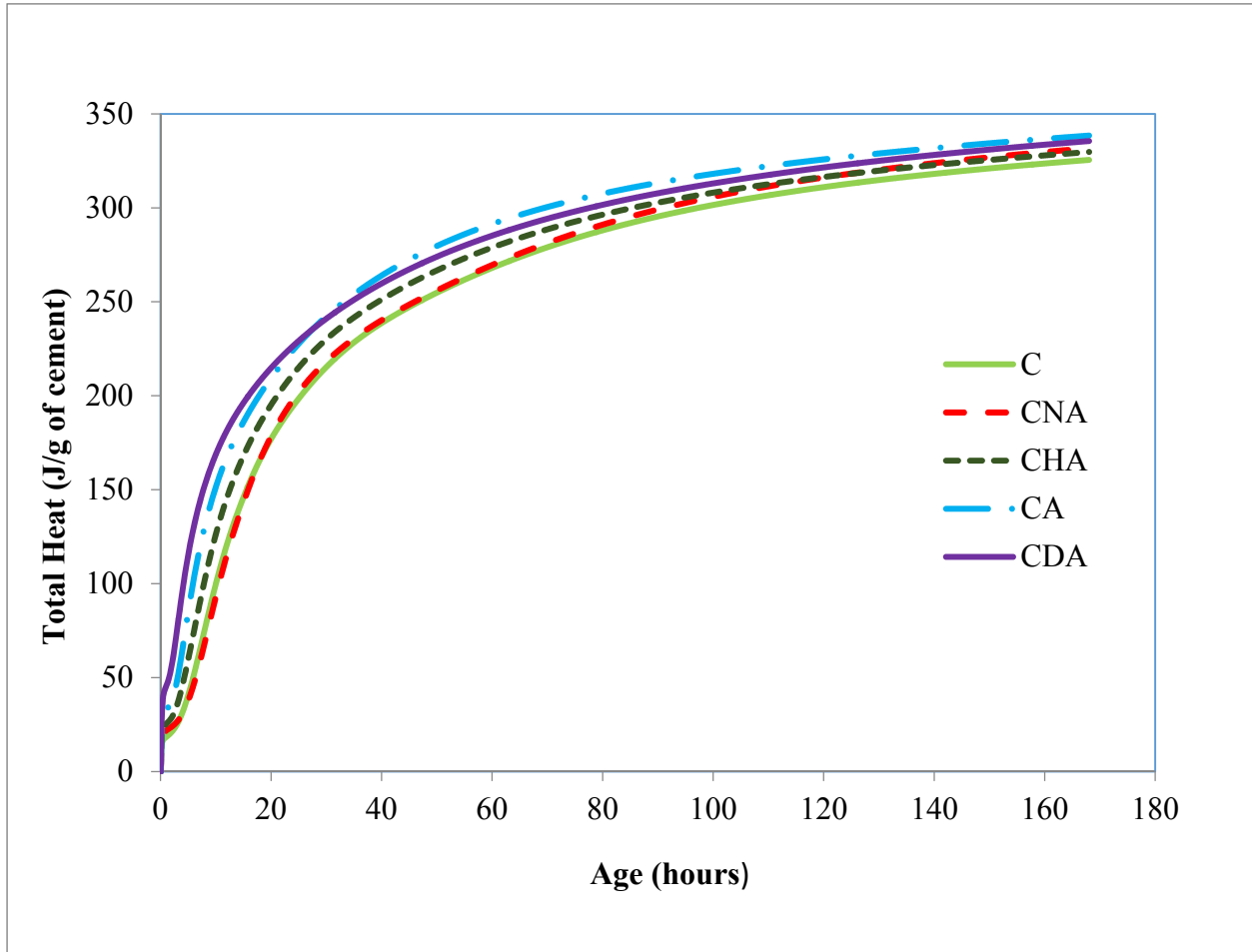


Figure 3.5. Total heat evolved of cement pastes normalized per gram of cement

Therefore, its degree of hydration at 72 hours was also slightly lower than that of CA. As expected, setting times followed the same trend as the heat flow curves with the CDA mixture having the shortest final setting and CNA the longest (Figure 3.6).

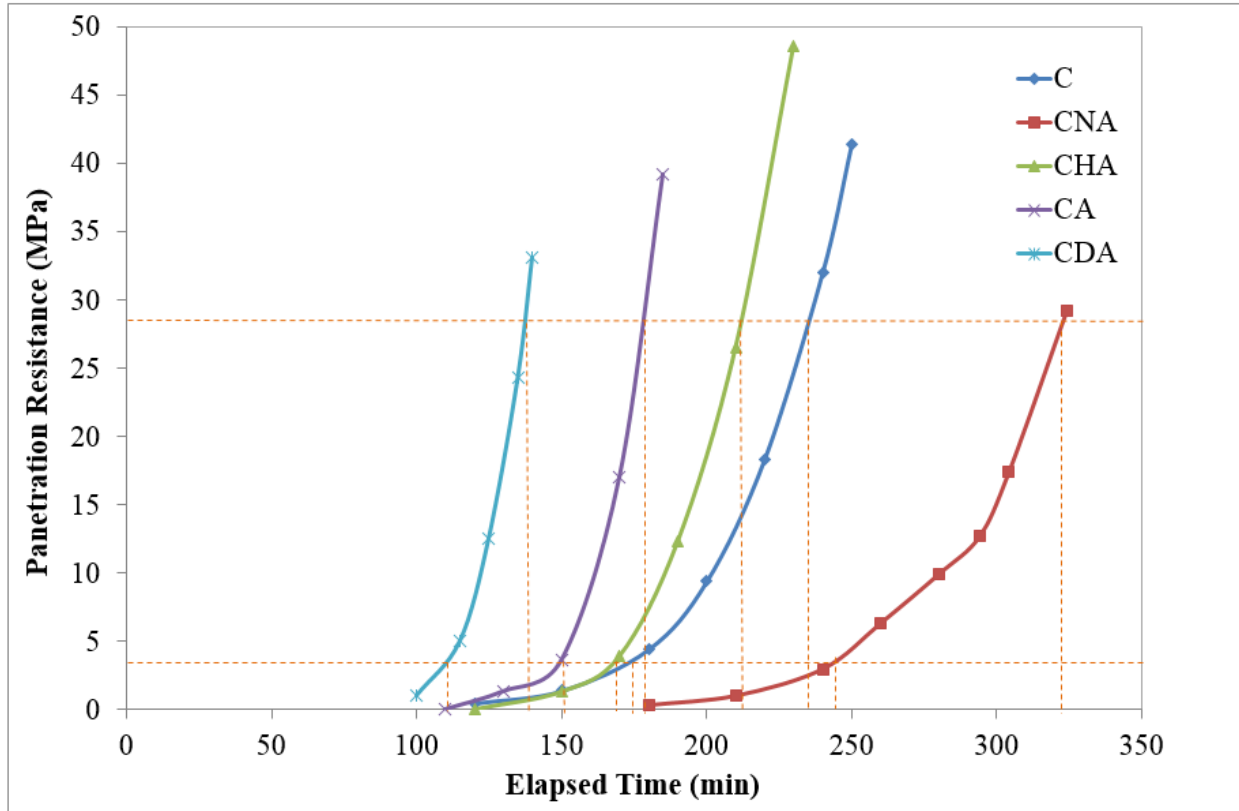


Figure 3.6. Setting time curves

3.3.2 Autogenous Shrinkage Measurements

Addition of WRRA did not significantly affect the amount of total shrinkage experienced by concrete at 3 days compared to the control sample C with no admixtures (Figure 3.7). Although water-reducer addition is expected to result in finer pores due to improved dispersion of cement particles, it is speculated that this effect was not significant enough to affect total shrinkage. However, the rate of initial autogenous shrinkage increased with addition of WRRA from $8 \mu\epsilon/\text{hr}$ for C mixture to $12.5 \mu\epsilon/\text{hr}$ for CNA. Shrinkage rates were calculated from the linear portion of the curves based on the time it takes each mix to reach $-100 \mu\epsilon$. The value of $-100 \mu\epsilon$ was chosen for convenience, since beyond this point some of the curves begin to deviate from linearity (CHA, CA, CDA). Retarders are known to accelerate hydration after the concrete does finally set, so the increased shrinkage rate of the CNA mixture may be due to the increased rate of hydration.

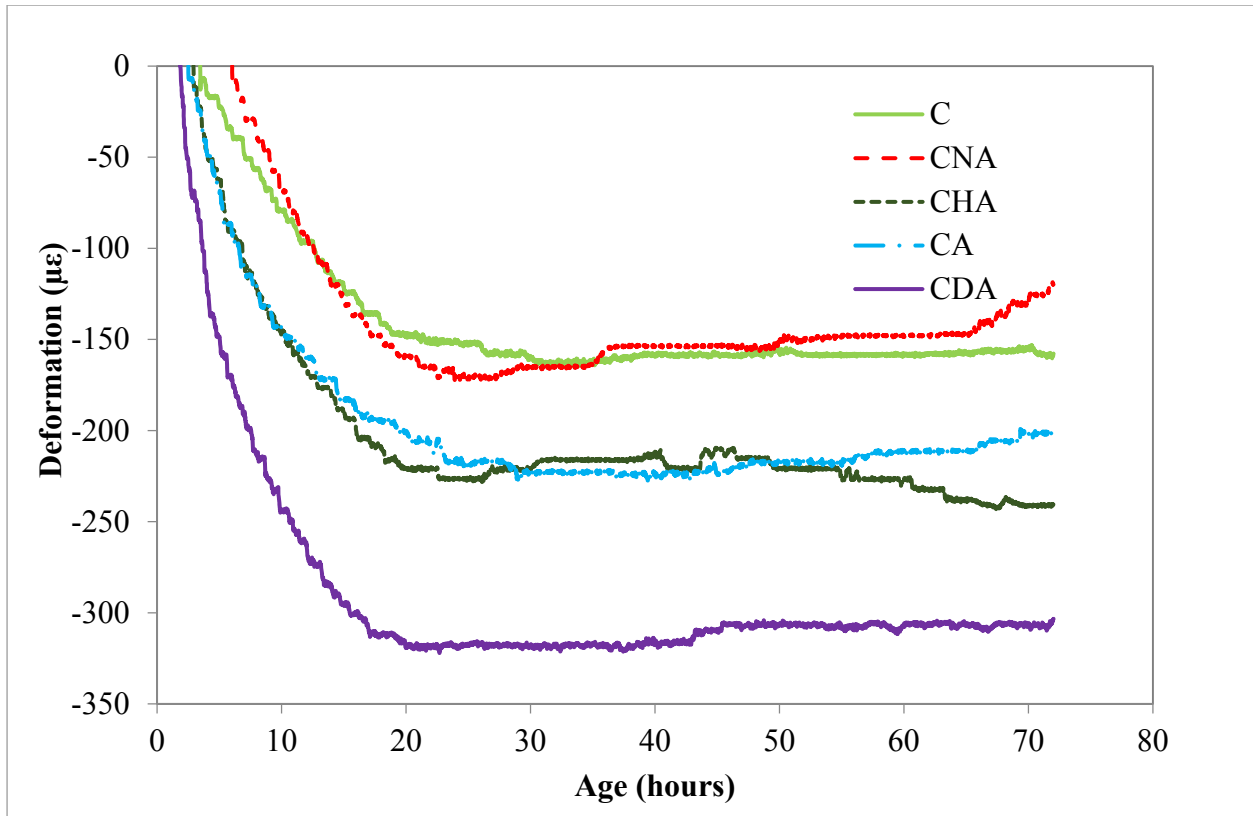


Figure 3.7. Free shrinkage measurements under isothermal conditions at 23°C as a function of time

It is interesting to note that there was no significant difference either in the total amount of autogenous shrinkage or in the rate of shrinkage (20 $\mu\epsilon/\text{hr}$) for the CHA and CA mixtures even though both isothermal calorimetry and setting time measurements clearly showed increased acceleration of cement hydration with increase in the accelerator dosage (Figures 3.4 and 3.6). However, increasing accelerator to CDA dosage increased both the rate (50 $\mu\epsilon/\text{hr}$) and the amount of total shrinkage. Since CHA and CA mixes show similar shrinkage values up to 3 days while CDA values are significantly higher, it appears that there may be a “critical dosage” of accelerator beyond which CaCl_2 -based accelerator begins to have a dosage-dependent effect on autogenous shrinkage. It should be noted that the suggestion by Holt [85] of accelerating the setting time as a means of reducing autogenous shrinkage was shown to be counter-productive for calcium

chloride-based accelerator as additions of the accelerator increased autogenous shrinkage despite reducing setting time.

Since accelerators increase the rate of hydration (α), it has been suggested that it is more appropriate to compare properties of accelerated and non-accelerated mixes on the basis of α rather than time [86]. Increase in hydration rate with accelerator addition would also mean that the pore water is consumed faster leading to a higher rate of autogenous shrinkage. It was not surprising that shrinkage rates increased with accelerator addition (Figure 3.7). However, Bentz et al. [59] showed that the differences in shrinkage rates can be eliminated by plotting autogenous shrinkage versus α . Nevertheless, Figure 3.8 shows that even when plotted against the degree of hydration, the shrinkage rate for CDA paste was still higher than that of the CNA, CHA and CA pastes pointing to a much different pore structure of this mixture. It appears that in addition to the accelerating effect on hydration reactions, accelerator may cause microstructural changes that can result in increased autogenous shrinkage independent of the degree of hydration.

It can also be noticed from Figure 3.8 that an increase in the accelerator dosage increased the degree of hydration at which setting occurred and autogenous shrinkage began. Bentz et al. [59] reported that decreasing cement particle size increases the degree of hydration at which setting occurs even though the time to achieve set is decreased because “more particle-to-particle bridges” have to be formed to achieve setting. Addition of CaCl_2 -based accelerator may have an effect on setting time akin to that of decreasing cement particle size. Oey et al. [96] state that as CaCl_2 dosage is increased, the number of nuclei of precipitated hydration products increases. If a large number of fine nuclei are formed rather than fewer nuclei that are larger in size due to the continued deposition of hydration products, a higher degree of hydration may be required to form particle-

to-particle connections and achieve setting. Higher degree of hydration of the CNA mixture is attributed to the retarding effect of the WRRA.

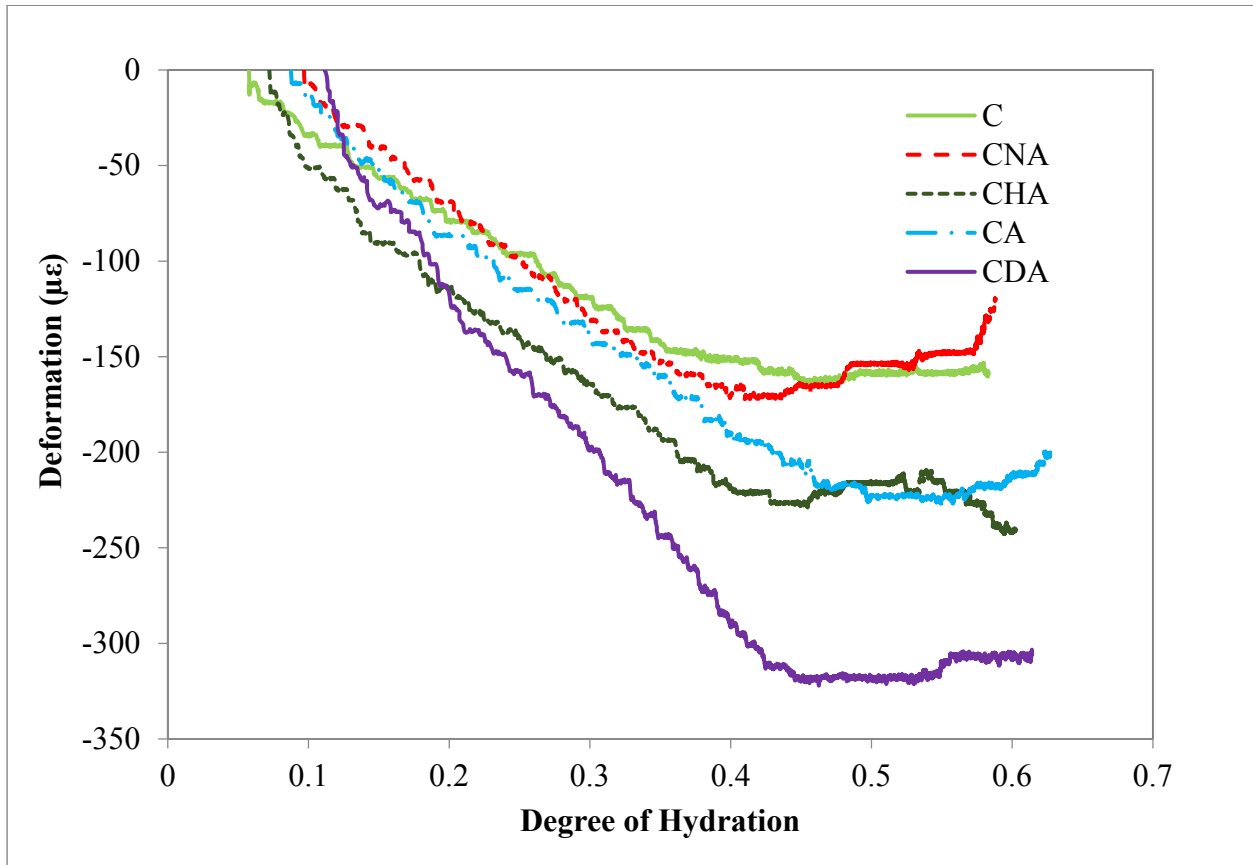


Figure 3.8. Free shrinkage measurements under isothermal conditions at 23°C as a function of degree of hydration

3.3.3 Autogenous Shrinkage and Mechanical Property Development

Autogenous shrinkage is frequently attributed to capillary tension [9]–[12]. Capillary tension is a function of internal relative humidity (RH) of concrete, which in turn depends on the degree of hydration. When autogenous shrinkage is plotted against α (Figure 3.8), the changes in RH due to varying hydration rates of the mixtures are taken out of the equation.

In order for capillary tension stresses to generate variable autogenous shrinkage as observed in this study, the tensile strength of the mixtures would have to be different. Figure 3.9 shows a plot of autogenous shrinkage versus tensile strength.

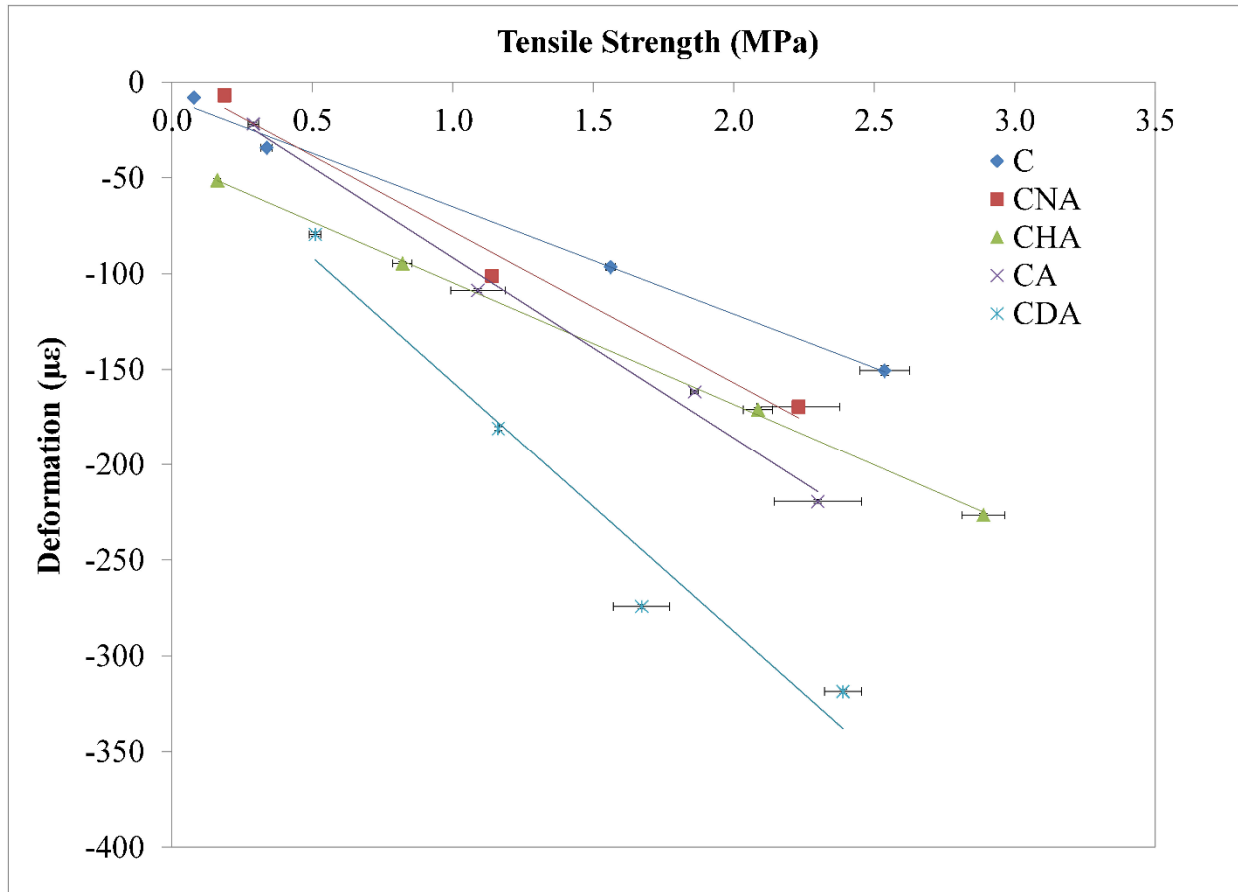


Figure 3.9. Relationship between free shrinkage and tensile strength development

For the same amount of shrinkage, tensile strength of CDA mixture was markedly lower compared to the other mixtures containing chemical admixtures and compared to the C mixture with no chemical admixtures. The same was observed for elastic modulus (Figure 3.10).

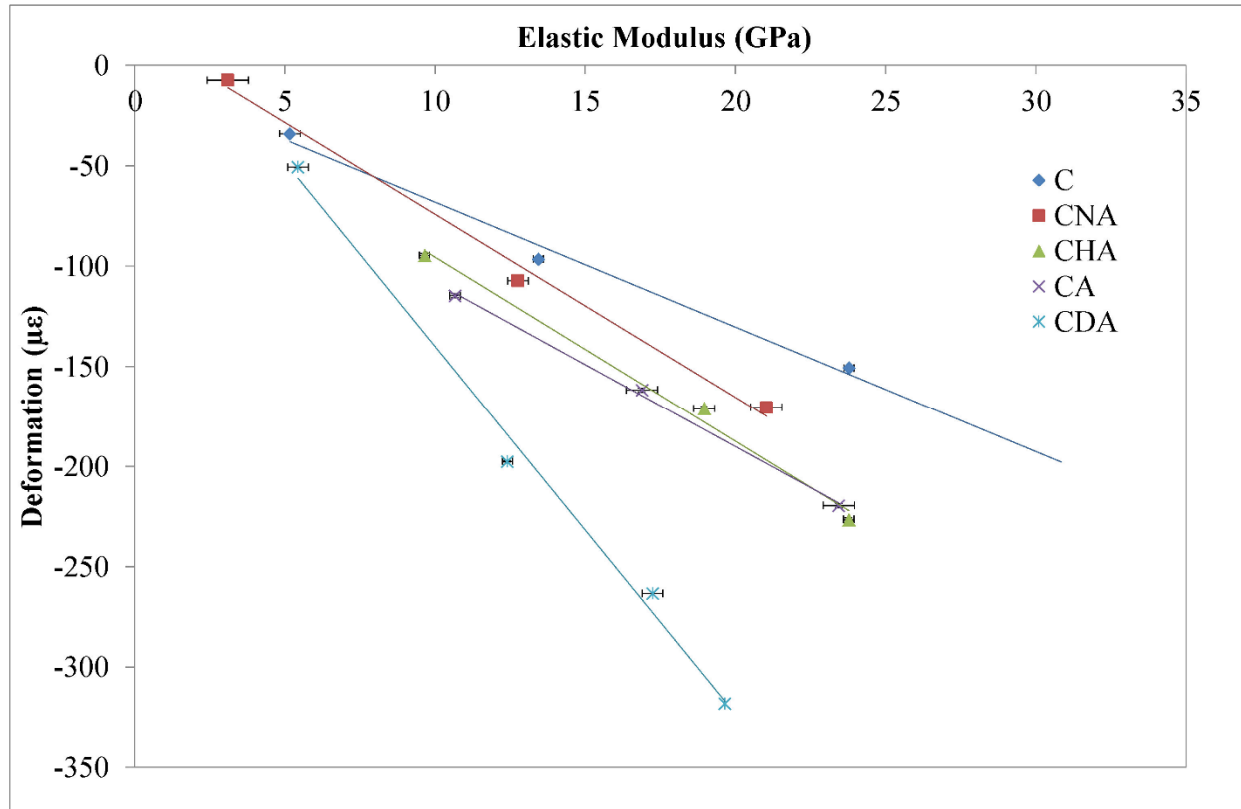


Figure 3.10. Relationship between free shrinkage and elastic modulus development

Several studies [86], [97], [98] demonstrated that addition of high CaCl_2 dosages increases the C/S ratio of C-S-H. Recently molecular simulations showed that increase in the C/S ratio of C-S-H results in the decrease in its mechanical properties [99]–[101].

3.3.4 X-ray Diffraction Measurements

Figure 3.11 shows XRD scans of CHA and CDA mixtures at 3 days. The two extreme accelerator dosages were selected to evaluate the effect of accelerator dosage on cement hydration products. The age of 3 days was selected in order to minimize differences in the degree of hydration between the mixtures – at this age the degree of hydration calculated using Equation 1 was approximately 0.6. Generally, the XRD patterns are very similar with comparable C_3S peak areas, which points to the similar degree of reaction of this phase in both mixtures. The main notable difference is the consistently lower calcium hydroxide (CH) peaks in the CDA mixture,

which is in agreement with previous studies [86], [97], [98]. These studies attributed the decrease in the CH peak to the increase in the C/S ratio of C-S-H with CaCl_2 addition. Apart from the effect on CH, increasing accelerator dosage to CDA level increased the amount of Friedel's salt formed, as expected, as well as increased dissolution of the ferrite phase.

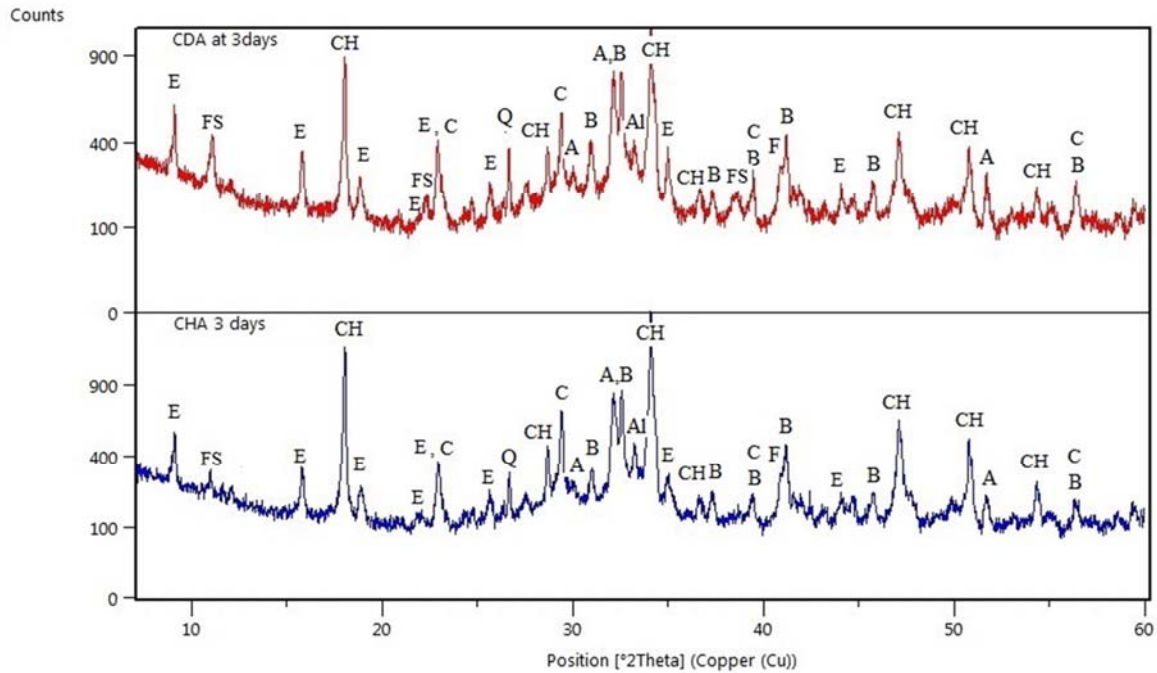


Figure 3.11. X-ray diffraction scans of the CHA and CDA mixtures at 3 days.

E=ettringite, FS=Friedel's salt, CH=calcium hydroxide, C=calcium carbonate, Q=quartz,

A=alite, B=belite, Al= C_3A , F= C_4AF

3.3.5 Mercury Intrusion Porosimetry

Although MIP has several known limitations, it is still widely used to analyze concrete porosity [75], [102], [103]. MIP measurements were performed on concrete samples for all mixtures at 3 days to determine if a particular pore size range could be related to the measured

autogenous deformation. Pore size distribution (Figure 3.12) indicates that pore volume in the 10-20 nm diameter range show the same trend as the autogenous deformation measurements.

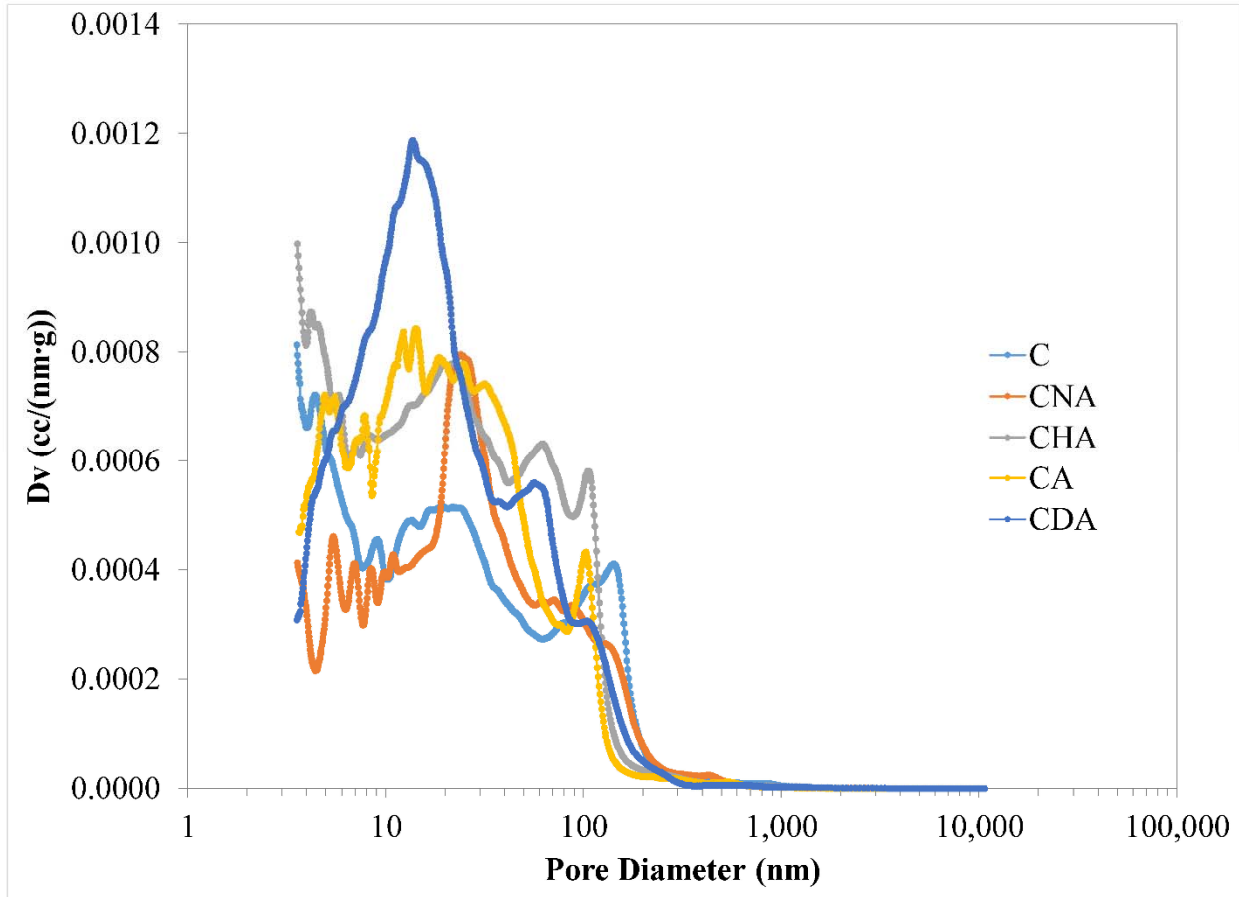


Figure 3.12. Pore size distribution of concrete samples determined by mercury intrusion porosimetry at 3 days

Intruded pore volumes for pores smaller than 50 nm were also plotted on a bar chart (Figure 3.13). Only this pore range was considered as pores below 50 nm diameter are known to be responsible for concrete shrinkage [7]. Figure 3.13 clearly shows that for 10-20 nm pores, pore volumes are the same for C and CNA mixtures and they are also the same for CHA and CA, which is consistent with the measured autogenous deformation (Figure 3.7). Additionally, increase in the intruded pore volume in this range corresponds to increased autogenous deformation, with CDA mixture having the largest pore volume and the largest deformation. For samples containing

accelerator, the increase in the 10-20 nm pore volume does not appear until the dosage of the CA mixture is exceeded, further supporting the hypothesis of a non-linear dosage-autogenous shrinkage response.

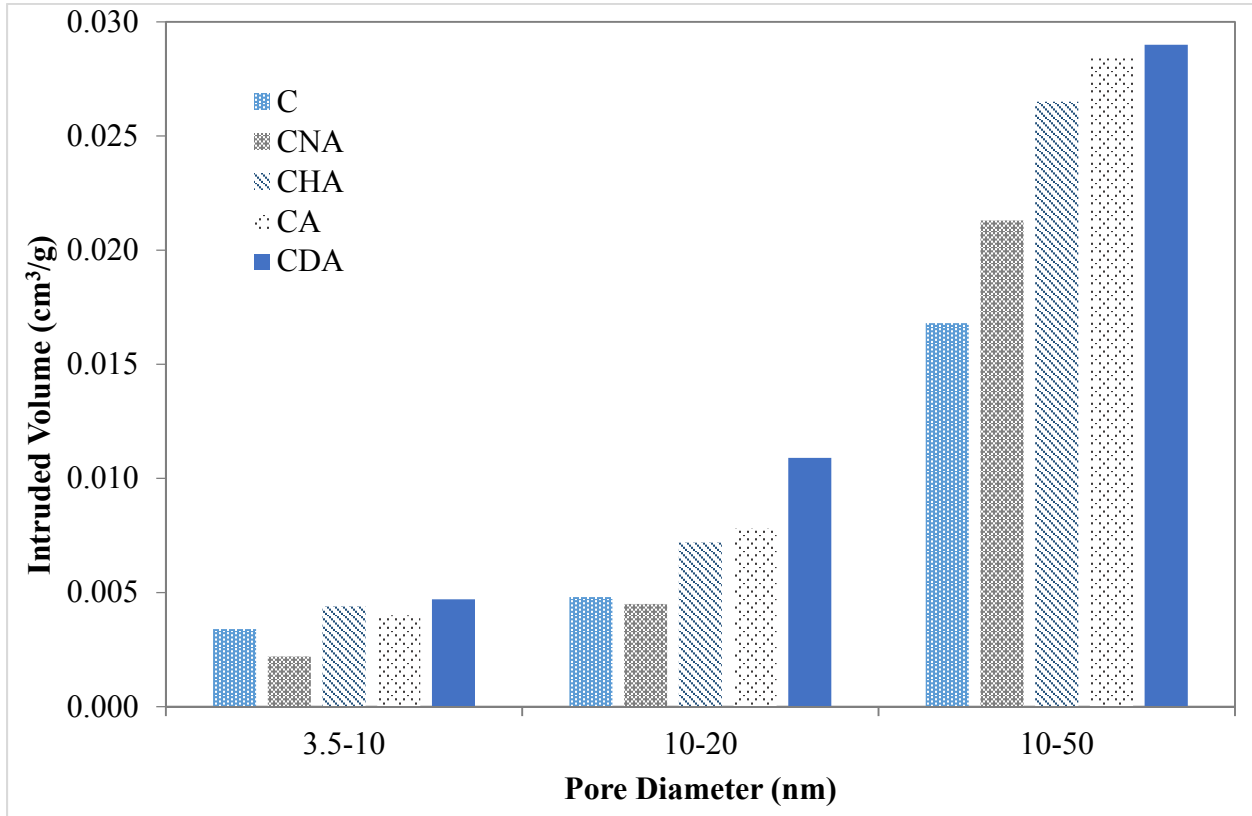


Figure 3.13. Effect of accelerator addition on pore size distribution of concrete determined by MIP at 3 days

3.3.6 Nitrogen Adsorption Porosity Measurements

In addition to MIP measurements, which predominantly measure large and medium capillary pores, nitrogen adsorption measurements were performed on selected paste samples (CNA, CHA and CDA) at 3 days in order to assess the effect of accelerator dosage on gel porosity. XRD results discussed in section 3.4 indicated a possibility of increasing C/S ratio with increasing accelerator dosage, which can result in a change in C-S-H morphology and gel porosity. The change in C-S-H morphology with CaCl₂ addition has been reported previously [21], [86]. Since

autogenous shrinkage profiles of C and CNA mixtures and CHA and CA mixtures were very similar, only one was selected for analysis from each pair.

Although MIP and nitrogen adsorption measure different pore size ranges, they do overlap in the 3.5-40 nm range. The same trend of increasing porosity with accelerator dosage in the 10-20 nm range was observed in Figure 3.14 as with MIP measurements.

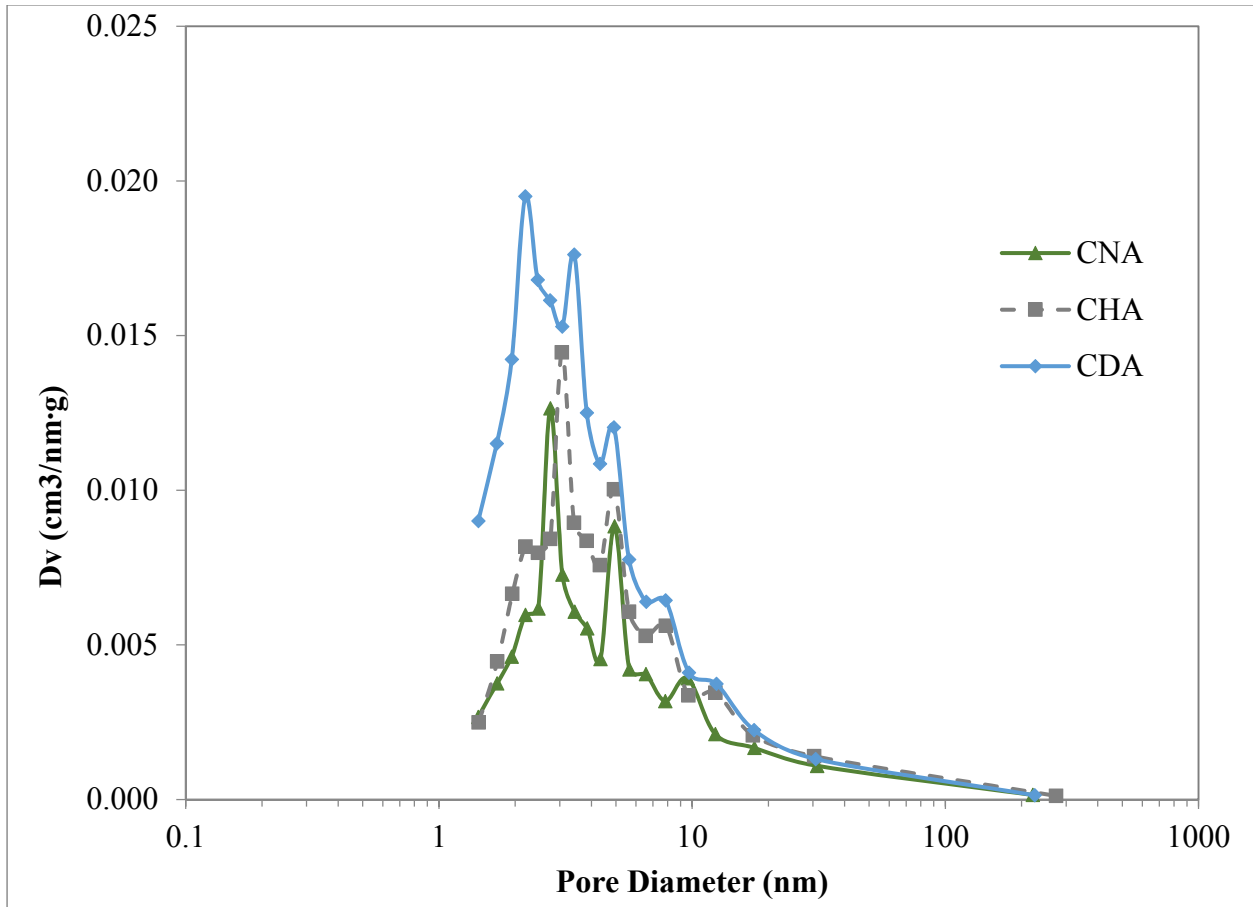


Figure 3.14. Pore size distribution of cement paste calculated from nitrogen adsorption at the age of 3 days

Additionally, there was a significant increase in the pores in the 1.5-10 nm range with increasing accelerator dosage from CNA (0% CaCl₂) to CHA (0.5-1% CaCl₂ as listed in Table 3.2), to CDA (2-4% CaCl₂).

It is interesting to note that porosity of CHA and CNA pastes was very similar up to approximately 3 nm, while for CDA it was notably higher. According to the CM-II C-S-H model proposed by Jennings [104], these are small gel pores (SGP) which represent the space between C-S-H particles or globules. Between 3 and 10 nm, CHA pore volumes increased compared to CNA. According to the CM-II model, these are large gel pores (LGP) that exist between C-S-H globules [104]. Jennings [104] estimated their size as 3-12 nm.

One possible explanation for the increase in the SGP volume is that there is more C-S-H in the CDA sample, although this should be unlikely considering that all the samples had a similar degree of hydration. A more plausible explanation may be a significant change in the C-S-H morphology at the CDA accelerator dosage. It appears that addition of CaCl₂-based accelerator at the CDA dosage increased the ratio of low density (LD) to high density (HD) C-S-H, while at the CHA dosage LD/HD ratio may not have been affected. LD C-S-H has a more open morphology, and, according to Jennings[105], it forms only during the early hydration period. Juenger and Jennings[22] have previously proposed that increase in the LD/HD ratio corresponds to an increase in drying shrinkage. It appears that an increase in the LD/HD ratio may also correspond to an increase in autogenous shrinkage and decrease in mechanical properties.

Although MIP measurements (section 3.5) and the mechanism of capillary tension can explain the differences in autogenous deformation between the mixtures when plotted against concrete age (Figure 3.7), capillary tension cannot explain the differences in autogenous shrinkage observed between CDA, CHA and CNA mixtures when plotted against the degree of hydration which eliminates differences in RH (Figure 3.8). Although the significantly lower tensile strength development of the CDA mixture (Figure 3.9) discussed in section 3.3 can be the cause of its higher deformation in Figure 3.8, tensile strength development for CNA and CHA mixtures was

fairly similar, which indicates that there may be another mechanism contributing to autogenous shrinkage.

Disjoining pressure has been cited as a mechanism of concrete shrinkage at high relative humidities (RH) [8], [106]–[108]. Although internal RH of concrete was not measured in this study, it can be reasonably assumed that the RH remained above 80% throughout the duration of the free shrinkage measurements with the low degree of hydration seen during the testing. A number of studies reported internal RH of concrete confirming this assumption [79], [109], [110]. It should be noted that all concrete samples were sealed during shrinkage measurements to prevent any moisture loss to the environment, so only the drop in RH due to self-desiccation is considered.

Although disjoining pressure has been reported to be constant in the range of 80-100% RH [9], Beltzung et al. [111] showed that it varies with the amounts of calcium and alkali ions in the pore solution. Since the addition of the accelerator increased both the amount of Ca^{2+} as well as Na^+ and K^+ in the pore solution (in addition to CaCl_2 accelerator contained small amounts of NaCl and KCl), an increase in autogenous shrinkage with accelerator addition may possibly be due to the variation in disjoining pressure due to modification in the pore solution chemistry.

Regardless of the specific mechanism, the volume of pores in the 1.5-3 nm range appears to correlate well with the shrinkage rates during the first 24 hours as a function of the degree of hydration, while the volume of 3-10 nm pores correlates with the total shrinkage observed at the end of 72 hours for CNA, CHA and CDA mixtures. Both autogenous shrinkage rates and pore size distribution determined by nitrogen adsorption indicate that an accidental overdose that doubles the intended amount of accelerator can result in significant microstructural changes of hydrated phases.

Since CDA experienced shrinkage strains that are significantly higher for a given tensile strength, when compared to the other mixtures, it is expected that the CDA mixture may have a higher cracking tendency. However, creep has to be taken into account, as CaCl_2 has been reported to increase creep [7], [14], [112]–[114], before definite conclusions can be made regarding the effect of increasing accelerator dosage on cracking tendency. Stress measurements on restrained specimens, using for example cracking frame testing, under isothermal conditions would be required to compare stresses generated by autogenous shrinkage in these concretes.

3.4 Conclusions

The addition of lignosulfonate-based water-reducing and retarding admixture changed little the autogenous shrinkage rate of concrete when the rate was compared on a degree of hydration basis. However, addition of CaCl_2 -based accelerator increased autogenous shrinkage in concretes containing water-reducing and air-entraining admixtures, when compared on a degree of hydration basis.

There was good agreement between autogenous deformation at 3 days and pore volume in the 10-20 nm range as determined by MIP on concrete and by nitrogen adsorption on paste samples. This increase in porosity appears to be dosage dependent; porosity increases with initial accelerator addition, however, it remains constant until a “critical” dosage is reached that results in a further porosity increase. This large increase in autogenous shrinkage with the larger dosages of accelerator highlights the importance of controlling accelerator additions on field sites for rapid repair concrete mixtures to reduce the risk of cracking.

CHAPTER 4: INFLUENCE OF SCMs ON RHEOLOGY OF PASTE AND ITS DEPENDENCE ON PARTICLE CHARACTERISTICS OF THE MIXTURE³

4.1 Introduction

Increased emphasis on sustainability and reducing the environmental impact of cement production have led to increased incorporation of mineral admixtures/supplementary cementitious materials (SCMs) into concrete on cement-replacement basis. Since most SCMs are waste by-products of other industries, with the exception of metakaolin, their utilization in concrete provides two-fold environmental benefits. It reduces the need for waste disposal and provides waste valorization and, at the same time, reduces cement content thus reducing CO₂ emission associated with its production. Even incorporation of metakaolin, which is a material produced by calcination of kaolin clay, has environmental benefits as calcination temperatures during its production are significantly lower than that of the clinkering process, so cement substitution with metakaolin reduces the carbon foot print of the construction industry as well. Additionally, it should not be overlooked that incorporation of SCMs typically increases durability concrete structures, thus reducing the need for repairs and extending their design life, which is also environmentally beneficial.

Most commonly used SCMs are fly ash, slag, silica fume and metakaolin. Each of these materials has different effects on setting time, compressive strength development, and other hardened properties. Recently, investigations into ternary and quaternary blends of these materials

³ This chapter has been submitted as a manuscript to the Construction and Building Materials Journal and is currently under review.

with ordinary portland cement (OPC) have been undertaken in order to optimize concrete fresh and hardened properties [115]–[127]. Typical fresh properties considered in these investigations are water demand [116] and superplasticizer dosage [115], [116], [127], setting time [116], [118], [123], [127], and slump [122], [123].

Although SCMs are typical used for modification of concrete hardened properties, their effect on workability of concrete cannot be overlooked. Workability issues can include honeycombing, voids inside the concrete, excessive bleeding and segregation [128], [129]. Depending on the type of concrete and method of placement, slump test, which is the most common measure of concrete workability used on site, may not provide adequate information about concrete flow behavior [30]. Ferraris et al. [30] state that rheological measurements are much better suited for this purpose. Although there are a number of equations that are used to describe concrete rheology, the most frequently used is the Bingham model [130]:

$$\tau = \tau_0 + \mu \gamma \quad \text{Equation 4.1}$$

where τ is the shear stress, τ_0 is the yield stress, μ is the plastic viscosity and γ is the shear rate. In terms of the practical meaning of these parameters, τ_0 is a yield stress that has to be applied to initiate flow. Roussel [131] relates the yield stress to formwork filling and “generally whether or not concrete will flow or stop flowing under an applied stress”, which for most concrete applications is due to gravity. Yield stress has been related to slump [30], [132], [133] and can also be thought of as the amount of stress needed for concrete mixing. Viscosity is related to the rate of concrete flow [128]. The specific target values of yield strength and plastic viscosity vary not only from one type of concrete to another but also with the method of placement [134]. Although in some applications, like self-consolidating concrete, a low yield stress is desirable, a yield stress and/or viscosity that are too low can result in segregation [130], [135]. High yield

stress and viscosity values can be problematic as well; high yield stress will require greater amount of energy to be imparted in order to adequately mix the concrete, while high viscosity will result in workability reduction [135].

From the rheological point of view, both concrete, mortar and cement paste can be treated as concentrated suspensions. Although the ranges of values for τ_0 and μ are very different [130], concrete rheology is influenced by the rheology of paste, and a relationship between the yield stress of the paste and that of concrete has been suggested [128]. Additionally, even when it is considered as a constituent of concrete, the importance of paste rheology itself should not be underestimated as low yield stress of paste can lead to concrete segregation [128].

Rheology of the paste is dominated by interparticle interactions. A number of studies have identified solid volume fraction, particle size and distribution, surface average diameter of particles, particle separation distance, and a ratio of actual to maximum packing density (packing fraction) as having a major effect on rheology of concentrated suspensions including cement paste as well as other particles suspended in solution [128], [133], [136]–[140]. Cement replacement with SCMs is likely to affect most, if not all of these parameters.

Banfill [130] states that the trends in concrete rheology with varying mixture parameters, including introduction of chemical and mineral admixtures, are “generally additive.” At the same time, he also notes that inter-particle interactions in concrete are diluted by the presence of aggregates. With increasing research into ternary and quaternary combination of OPC/SCMs, the question remains if the effect of SCM combinations on rheology is indeed additive and if so, can the rheology of ternary and quaternary blends be predicted based on results obtained from their respective binary combinations. The objective of this part of the study was to evaluate the effect of OPC/SCM combinations on paste rheology, compare them to binary mixtures in order to

evaluate if the effects on rheology are additive and to relate the obtained results to the particle characteristics of the blends.

4.2 Experimental Procedures

A commercially available (Type I/II) portland cement, four SCMs (Class F FA, BFS, SF and MK) and four chemical admixtures, air-entraining admixture (AEA), water-reducing and retarding admixture (WRR) and two superplasticizers (SP), that are commonly used in structural concrete mixtures in the state of Florida were selected for this study. Both superplasticizers, SP1 and SP2, were polyacrylate-based with SP1 being more concentrated according to manufacturer's safety data sheets. SP1 is used in the field in concrete mixtures containing metakaolin while all other mixtures use SP2. Same SP1 and SP2 usage was followed in this study. Cement and SCMs were characterized in terms of their oxide chemical composition, specific gravity, particle size distribution (PSD) and fineness. The oxide chemical composition was determined using X-ray fluorescence spectroscopy (XRF) according to ASTM C114 and specific gravity was measured following ASTM C188. PSD was determined using an LA-950 laser scattering particle size analyzer manufactured by HORIBA Instruments using the dry method. Triplicate tests were conducted on all of the as-received materials and the averages of the 3 tests are reported here. For silica fume, the PSD was measured using the wet method as well.

Fineness of cement and mineral admixtures was determined by nitrogen adsorption using Autosorb-1 analyzer manufactured by Quantachrome Instruments. The samples were outgassed under vacuum at 80°C immediately prior to analysis in order to remove any moisture or contaminants from the sample surface. The Brunauer-Emmett-Teller (BET) method [141] was used for the specific surface area (SSA) calculations. Multipoint BET was selected over the single point BET for greater accuracy [142].

Based on the measured MPS and BET SSA values for each of the materials, MPS and BET surface area were calculated for all the OPC/SCM combinations as well using the following relationship:

$$y_b = \sum_{i=0}^n y_i x_i \quad \text{Equation 4.2}$$

where y_b is the property of interest for the OPC/SCM mixture, y_i is the measured value for the property of i th component of the mixture, x_i is the volumetric fraction of the i th component, and n is the total number of components in the mixture. For a binary mixture $n=2$, for a ternary mixture $n=3$ and for a quaternary mixture $n=4$.

Rheology and normal consistency were determined for binary, ternary and quaternary cement-mineral admixture combinations prepared with chemical admixtures. Chemical admixture dosages were maintained constant and are listed in Table 4.1.

Table 4.1. Chemical admixture addition rates

Chemical Admixture	Addition Rate (ml/100 kg cementitious)
AEA	2.5
WRRA	110
SP1	155
SP2	110

Binary OPC/SCM combinations were tested without chemical admixtures as well. A fixed w/cm ratio of 0.485 was used for all pastes, taking into account the water present in the chemical admixtures. Cement replacement levels by SCMs for binary, ternary, and quaternary mixtures are listed in Table 4.2.

Table 4.2. Cement replacement levels for binary, ternary and quaternary mixtures

Fly Ash (weight %)	Slag (weight %)	Silica Fume (weight %)	Metakaolin (weight %)
<i>Binary Mixtures</i>			
10	10	10	10
21	21	21	21
30	30	-	-
-	52	-	-
<i>Ternary Mixtures</i>			
21	21	-	-
21	30	-	-
21	40	-	-
21	-	10	-
10	-	-	10
40	-	-	10
-	52	-	10
<i>Quaternary Mixture</i>			
-	20	10	10

Rheology measurements were performed using TA Instruments AR 2000ex rheometer with a helical ribbon impeller. Strain rate sweep was used in this study to assess the effect of mineral and chemical admixtures on rheological properties in the first several minutes after mixing. Since concrete is subjected to various shearing conditions between mixing and placement, no single test can characterize all the rheological properties of cement paste [143]. Strain rate sweep is typically used to measure cement paste properties under conditions that concrete is subjected to during mixing and transport to site. Helical ribbon geometry was selected as it simulates the mixing action of a commercial impeller and is therefore most suitable to evaluate rheological changes

during the mixing process. Helical ribbon impellers have also been recognized as one of the best systems for homogenizing non-Newtonian fluids [144]. All measurements were performed at an isothermal temperature of 23°C. Pastes were mixed in an IKA-Werke RW16 low shear mixer manufactured by IKA Werke for 3 minutes, after which they were transferred into a rheometer cup. Pastes were sheared in the rheometer for 2 minutes at a constant shear rate of 50 Hz followed by a 2 minute equilibration period. After the equilibration period, a shear rate sweep was performed from 0.5 to 50 Hz. Shear rate sweep was performed under steady state flow conditions.

Normal consistency for pastes was determined following ASTM C187. Normal consistency in this case refers to the amount of water needed to make a standard paste of similar workability. The paste is considered to be at normal consistency when after the dropping of the rod it settles at 10 ± 1 mm below the original paste surface. The paste was mixed using the procedure in ASTM C305.

4.3 Results and Discussion

4.3.1 Materials Characterization

Table 4.3 lists the results of the chemical oxide analysis. Cement selected for this study had a low equivalent alkali content ($\text{Na}_2\text{O}_{\text{eq}}$) and so did the mineral admixtures, except for fly ash.

Cement and mineral admixture densities (Table 4.4) are in agreement with those published in the literature [145], except for metakaolin. The metakaolin density of 2.23 Mg/m^3 is below the typical values reported in the literature, which is generally around 2.50 Mg/m^3 [145]–[147]. This could be attributed to the lower Fe_2O_3 content of metakaolin used in this study compared to the published values [145]–[147]. The oxide chemical composition of the rest of the mineral admixtures is in agreement with the published values [145]. Fly ash used in the study complied

with the ASTM C618 Class F classification, slag satisfied ASTM C989, silica fume complied with ASTM C1240, while metakaolin met the requirements of Class N pozzolan.

Table 4.3. Oxide chemical analysis for as-received cement and mineral admixtures

Analyte	Cement (w/o)	MK (w/o)	SF (w/o)	SL (w/o)	FA (w/o)
SiO ₂	20.40	51.29	92.90	35.15	55.48
Al ₂ O ₃	5.20	44.16	0.31	14.25	27.46
Fe ₂ O ₃	3.20	0.49	0.10	0.48	6.70
CaO	63.10	<0.01	0.78	41.45	0.99
MgO	0.80	0.14	0.18	5.21	0.88
SO ₃	3.60	<0.01	<0.01	1.86	0.05
Na ₂ O	0.10	0.26	0.10	0.22	0.29
K ₂ O	0.38	0.27	0.52	0.32	2.28
Total	100.10	99.22	99.63	99.83	99.93
Na ₂ O _{eq}	0.35	0.44	0.44	0.43	1.80

Table 4.4. Cement and mineral admixture densities

Material	Density (Mg/m ³)
Cement	3.14
Class F Fly Ash	2.25
Metakaolin	2.23
Slag	2.91
Silica Fume	2.22

Table 4.5 shows the mean particle sizes (MPS) for cement and SCMs used in this study. It can be seen that the MPS of slag and fly ash were very similar to that of cement, while MPS of metakaolin was finer. However, MPS of silica fume was significantly coarser compared to other materials. Typically, over 95% of the silica fume particles are reported to be finer than 1 µm [145].

Since the silica fume used in this study is densified, it appears that the dry process of particle size analysis is unable to provide sufficient dispersion of the silica fume particles. SF was analyzed using the wet method as well; however, the wet method results (not shown here) were very similar to those obtained by the dry method. It is believed that the true fineness of SF, once completely dispersed, is significantly higher than what was indicated by the particle size analysis, which is supported by the BET results (Table 4.5). This was previously observed by Yajun and Cahyadi [148] with densified silica fume. They concluded “the laser diffraction measures the agglomeration size while nitrogen measures the original size.” Since the BET method is based on the physical adsorption of nitrogen gas molecules on the sample surface, it is not affected by agglomeration and is able to measure the true SF fineness. BET results confirm the similar fineness of cement, fly ash and slag.

Table 4.5. Particle size analysis of as-received cement and mineral admixtures

Physical Properties	Cement	FA	MK	SL	SF
Mean size (MPS) (μm)	15.1	14.1	6.2	12.6	79.4
Multipoint BET SSA (m^2/kg)	2,140	2,270	14,970	3,700	21,410

4.4 Rheology Measurements

As mentioned previously, both the apparent yield stress and plastic viscosity need to be considered during concrete mixture design, and the optimum values will vary depending on the application. The best way to assess the effect of various mixture constituents on yield stress and plastic viscosity is by the use of rheographs [134]. Figures 4.1 through 4.4 present rheographs for the binary OPC/SCM combinations with and without chemical admixtures. Note the difference in the scale of the y-axis in these figures.

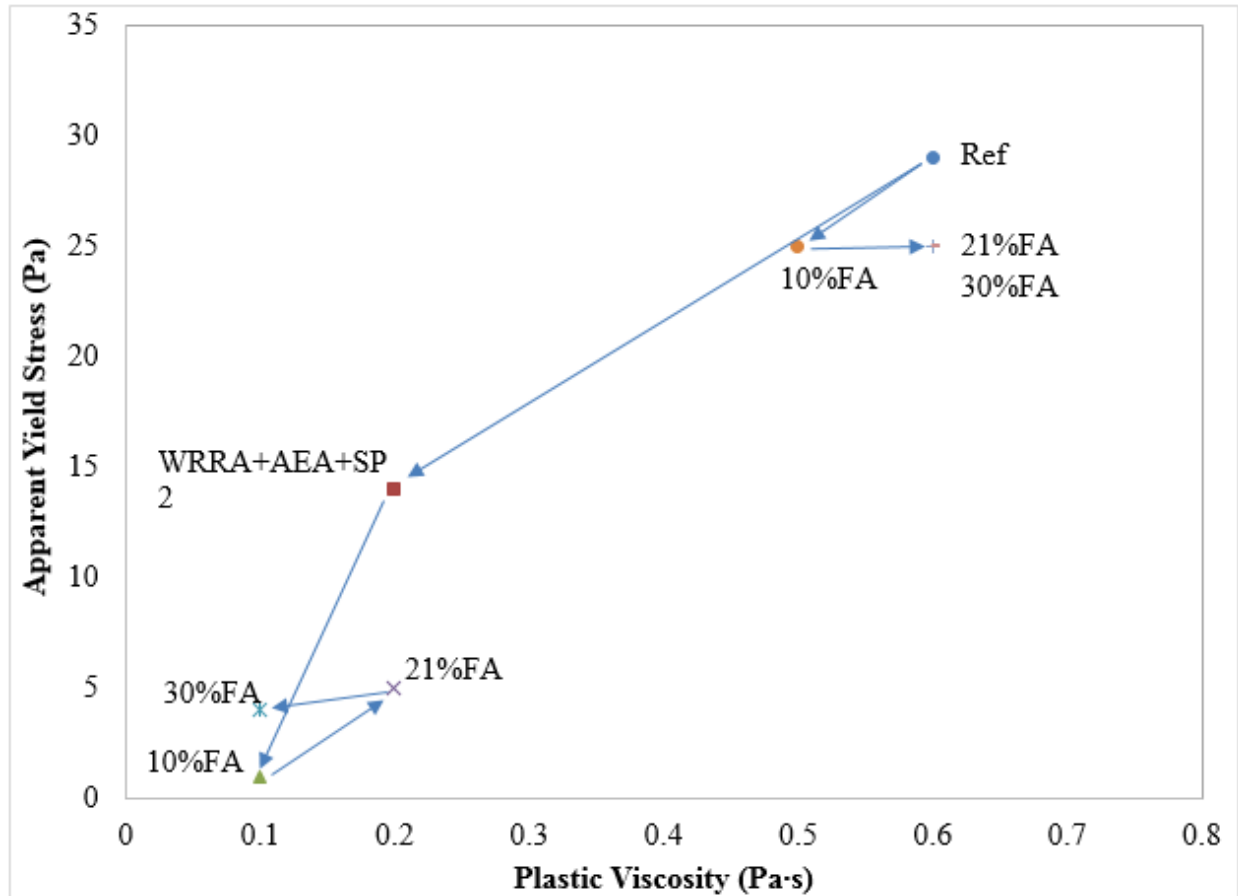


Figure 4.1. Effect of Class F fly ash on rheology of non-plasticized (Ref) and plasticized pastes

In the absence of chemical admixtures, cement replacement by 10% fly ash slightly decreases both the yield stress (τ_0) and plastic viscosity (μ) (Figure 4.1). Further increase in the fly ash content up to 30% does not have an effect on τ_0 , while plastic viscosity returns to the value of the reference paste. Addition of chemical admixtures significantly reduces both τ_0 and μ . Addition of fly ash to the plasticized paste further reduces τ_0 , with the amount of fly ash resulting in only minor variation in the values. There is a slight variation in μ between 0.1-0.2 Pa·s, which is notably lower than 0.5-0.6 Pa·s observed for the non-plasticized pastes.

Typically, an increase in fly ash content is reported to decrease the yield stress [145], [149], [150]. However, Park et al. [151] observed an initial decrease in yield stress with fly ash addition compared to control mix, but the values increased, although slightly, with increasing fly ash content. As for plastic viscosity, some researchers observed no change with fly ash incorporation [149], while others reported a decrease [150], [151]. However, an increase in viscosity with the introduction of fly ash has also been reported [145], [152]. The findings in this study for pastes with chemical admixtures are consistent with those reported by Park et al. [151]. In the absence of chemical admixtures the yield stress decreases compared to the reference paste; however, the yield stress value is not affected by the quantity of fly ash in the mixture in the range of 10-30%.

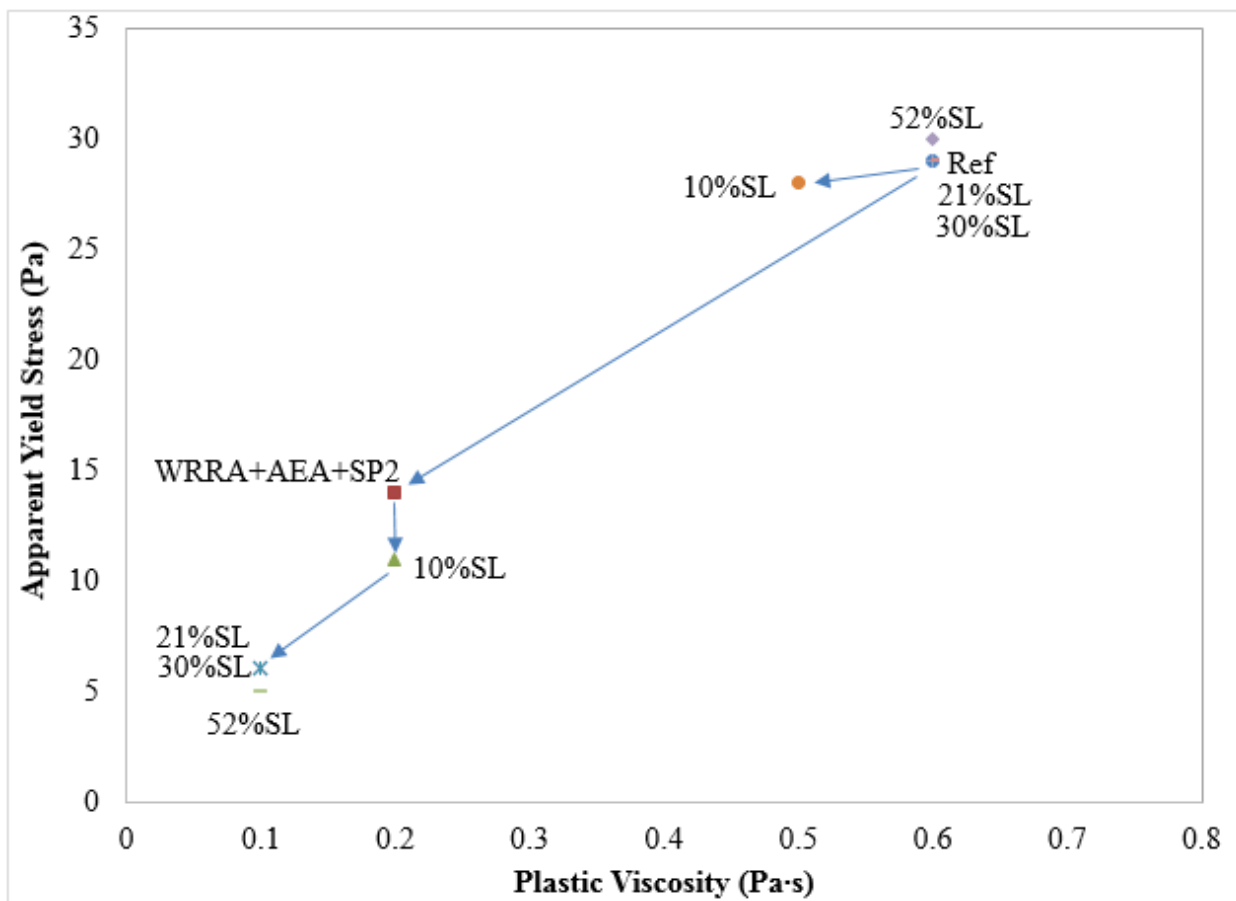


Figure 4.2. Effect of slag on rheology of non-plasticized (Ref) and plasticized pastes

Similar to fly ash, addition of slag to the reference paste, without chemical admixtures, has only a slight effect on μ at 10% cement replacement, while τ_0 remains unchanged up to 52% slag content (Figure 4.2). In the presence of chemical admixtures, μ decreases from 0.2 to 0.1 Pa·s at cement replacement levels over 10% while τ_0 gradually decreases with increasing slag content. Similar to the findings in this study, Zhang and Han [153] did not observe changes in yield stress with slag addition. Palacios et al. [154], on the other hand, reported an increase in yield stress with increasing slag content above 10%. However, similar to this study, they did not observe an effect on plastic viscosity.

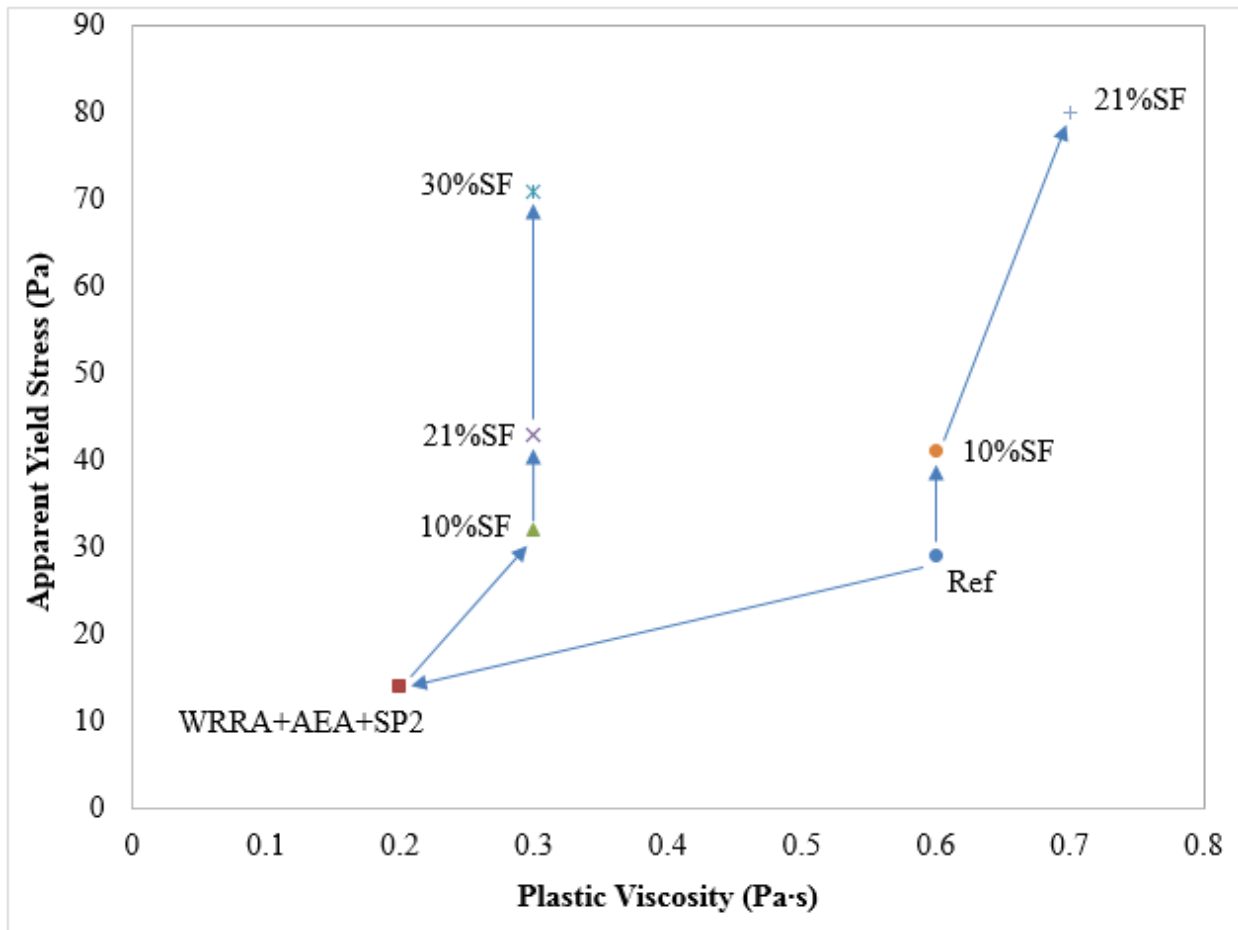


Figure 4.3. Effect of silica fume on rheology of non-plasticized (Ref) and plasticized pastes

Addition of silica fume to the reference paste increases τ_0 , with a significant increase at 21% cements replacement (Figure 4.3). In the presence of chemical admixtures, the increase in τ_0 with increase in SF content from 0 to 21% is less pronounced, although further increase in SF content results in a significant increase in τ_0 . This indicates that at the w/cm ratio used in this study, the fixed dosages of chemical admixtures were insufficient to maintain workability in increasing cement replacement level by silica fume.

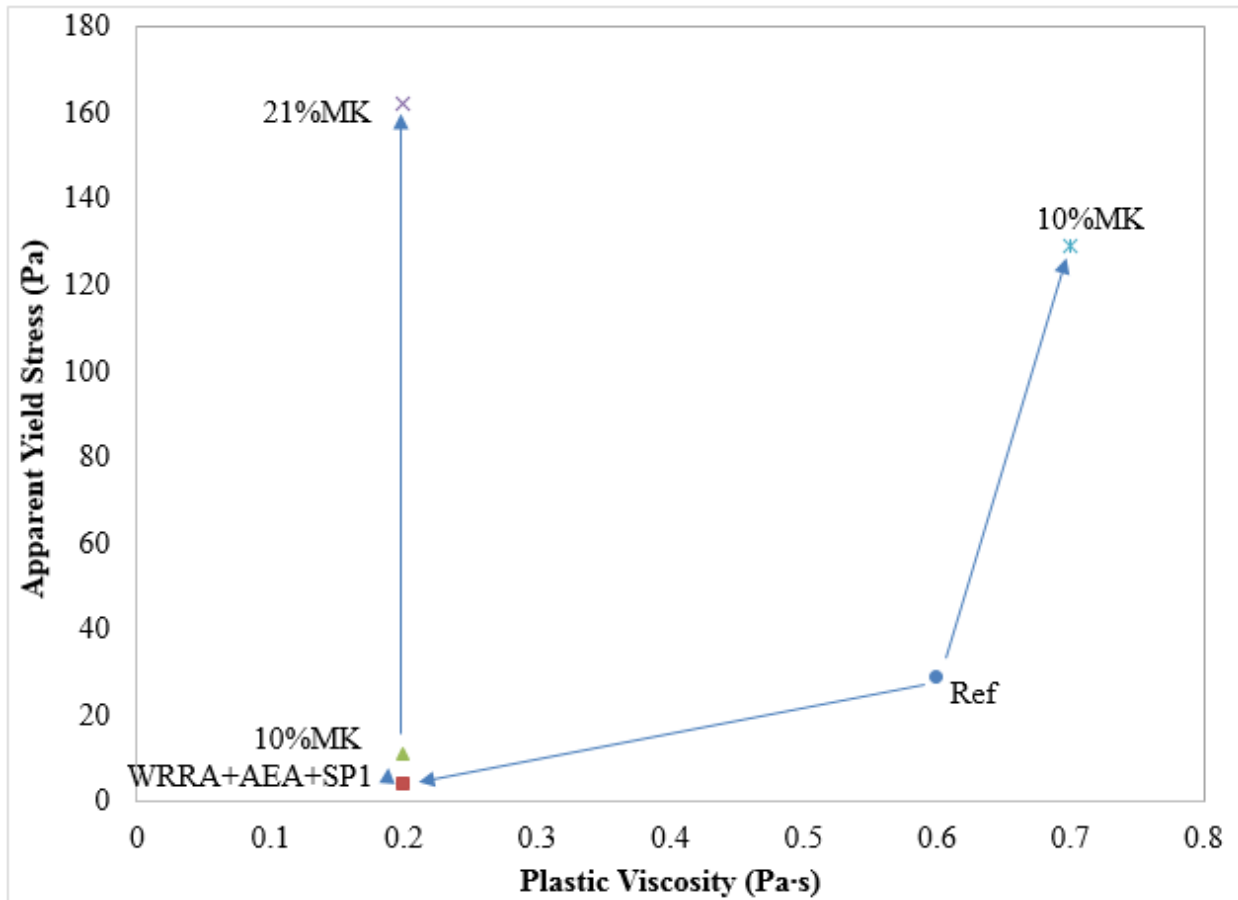


Figure 4.4. Effect of metakaolin on rheology of non-plasticized (Ref) and plasticized pastes

Increased yield stress with silica fume addition has been observed previously and is commonly attributed to increased water demand as SF has a high surface area [30]. Shi et al. [155] observed a decrease in yield stress compared to the control mix with addition of up to 9% silica fume. However, the yield stress increased with increasing SF content and exceeded that of the control mix at 12% SF.

Similar effect was observed with metakaolin addition (Figure 4.4). There was a dramatic increase in τ_0 with 10% MK compared to the reference paste; μ also increased slightly from 0.6 to 0.7. Addition of chemical admixtures lowered both τ_0 and μ and was sufficient to maintain workability at 10% cement replacement by metakaolin. Viscosity of this mixture was identical to that of the reference cement paste with chemical admixtures and the yield stress was only slightly higher. Further increase in MK content of the plasticized mixture did not affect plastic viscosity; the yield stress, however, increased by approximately 150 Pa. The increase in the yield stress points to insufficient SP dosage and a consequent flocculation of particles in the system. Decrease in the workability with MK addition has been noted previously as well as its increased water demand [116], [156], which is consistent with the results of the current study.

Since both fly ash and slag decreased the yield strength while silica fume and metakaolin increased it, the effect of mineral admixture combinations was examined in order to assess the effect of SCM combinations on yield stress. If the effect is additive, as suggested by Banfill [130], combining slag or fly ash with silica fume or metakaolin should result in lower yield stress compared to binary mixtures of OPC/SF or OPC/MK. Addition of fly ash to the binary OPC/10% SF paste did, in fact, improve both the yield stress and viscosity (Figure 4.5); however, the effect was not simply additive. Both of these parameters were lowered beyond simply adding the individual effects of these two SCMs, suggesting a synergistic interaction between SF and FA.

These findings are in agreement with Gesoglu and Ozbay [123], who reported that incorporation of slag or FA in conjunction with SF and OPC resulted in improved rheology.

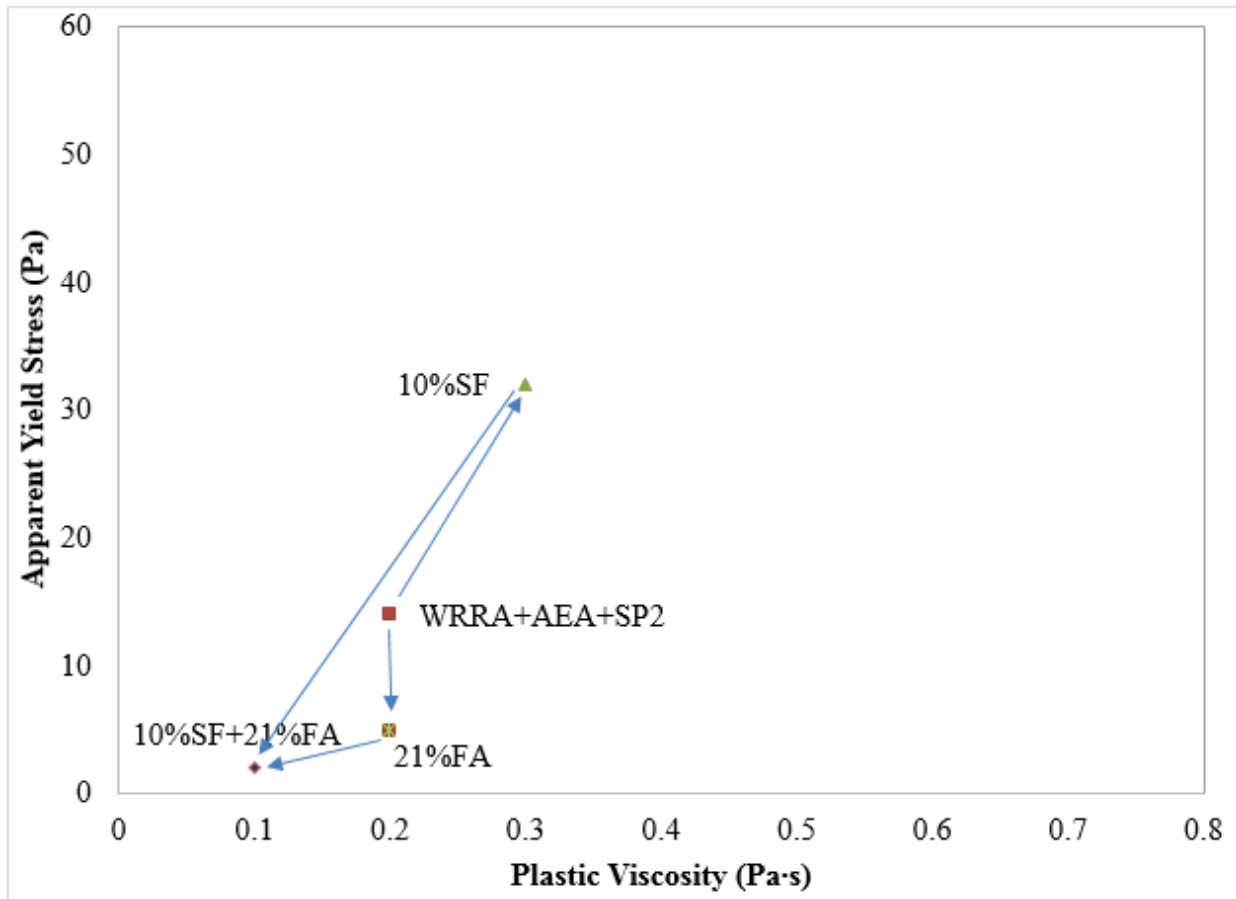


Figure 4.5. Effect of fly ash/silica fume combination on rheology of plasticized paste

The opposite effect was observed when fly ash was added to OPC/MK paste (Figure 4.6). Not only did τ_0 and μ not improve, as would be expected if the effects were additive, but they both increased by 10% fly ash addition from 11 Pa to 25 Pa. Further increase in fly ash content did not affect the yield stress; however, μ increased further.

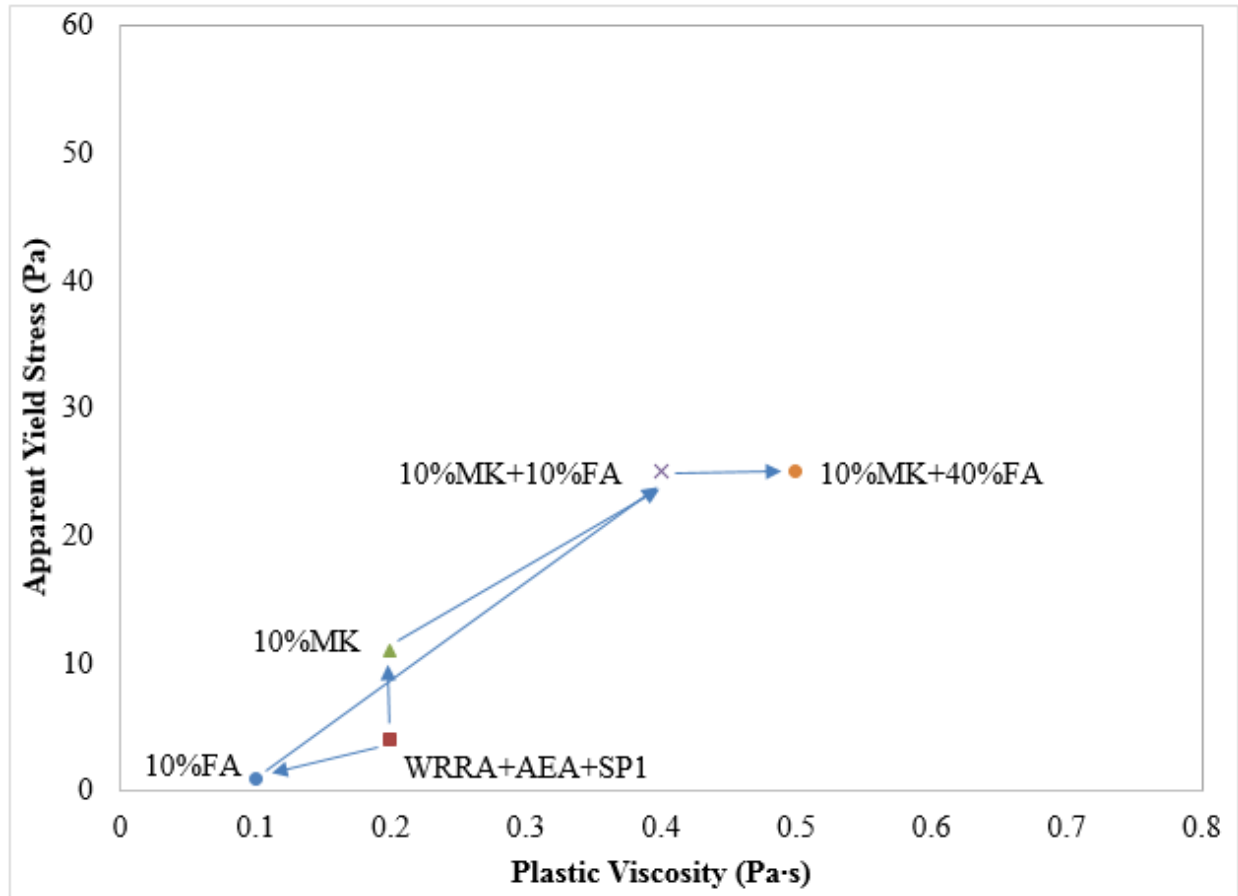


Figure 4.6. Effect of fly ash/metakaolin combination on rheology of plasticized paste

Addition of slag to the OPC/MK mixture also results in an increase in τ_0 and μ , similar to fly ash, although this increase is lower (Figure 4.7). This is contrary to Li and Ding [116], who observed that addition of slag to OPC/MK blends reduces water demand and superplasticizer dosage of the mixtures, which implies improved workability. MK used in their study was very coarse, similar Blaine fineness and median particle size to that of cement, while slag was significantly finer. Workability was measured in terms of slump. Workability reduction cannot be attributed to the increased fineness as of the OPC/MK blend. The authors state that metakaolin “tends to absorb water” [116]. This does not explain improvement of workability with slag addition as MK amounts were maintained constant (10%) in all the mixtures containing slag and no OPC/slag mixtures were tested.

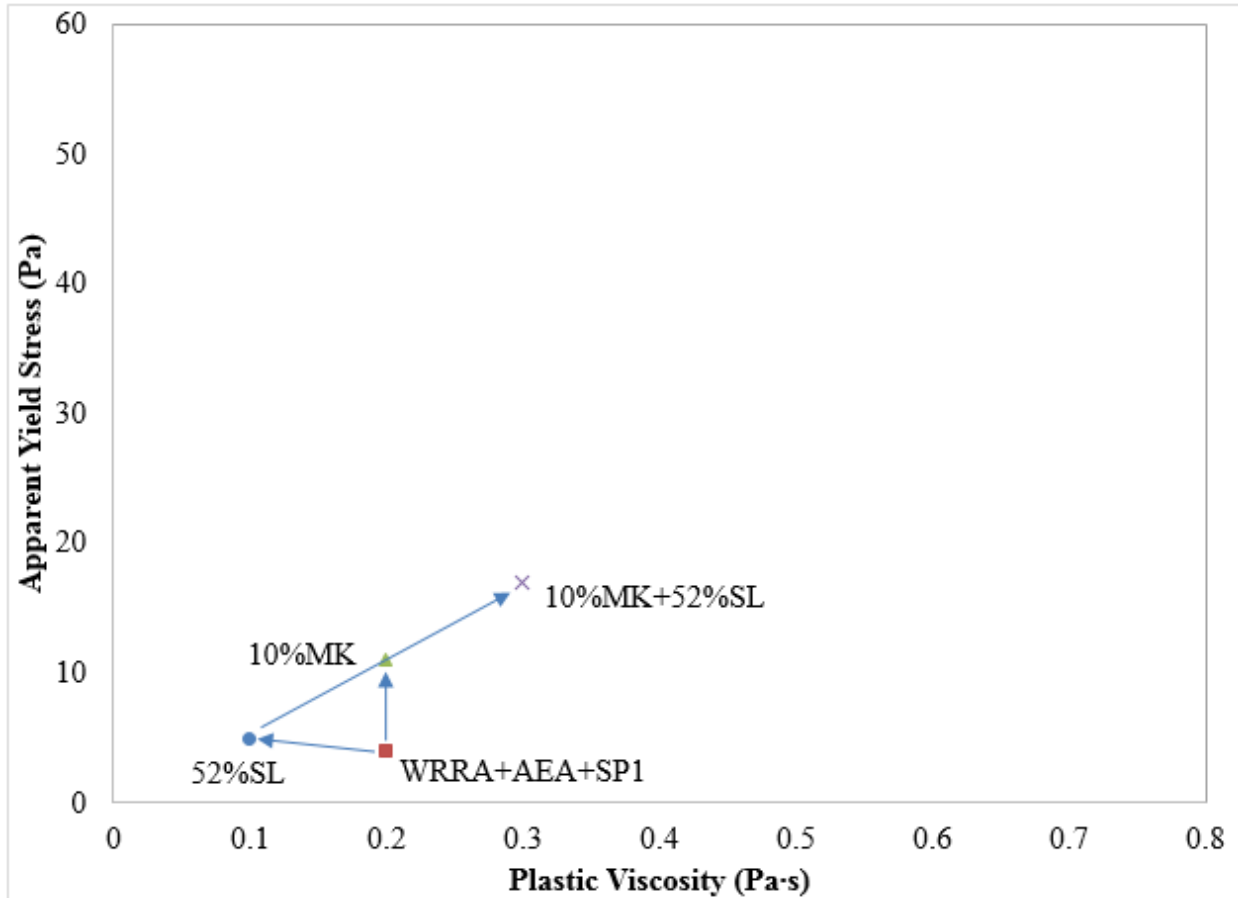


Figure 4.7. Effect of slag/metakaolin combination on rheology of plasticized paste

A quaternary combination of cement, metakaolin, silica fume and slag was also investigated (Figure 4.8). Compared to the binary combinations, both the yield stress and viscosity of this quaternary combination are higher. While the viscosity for the binary combinations of cement with metakaolin or slag or silica fume ranged from 0.1 to 0.3 Pa·s, the viscosity of the quaternary mixture is 0.5 Pa·s. As for the yield stress, it ranged from 6 to 32 Pa for the binary mixtures, while in the quaternary it increased to 57 Pa.

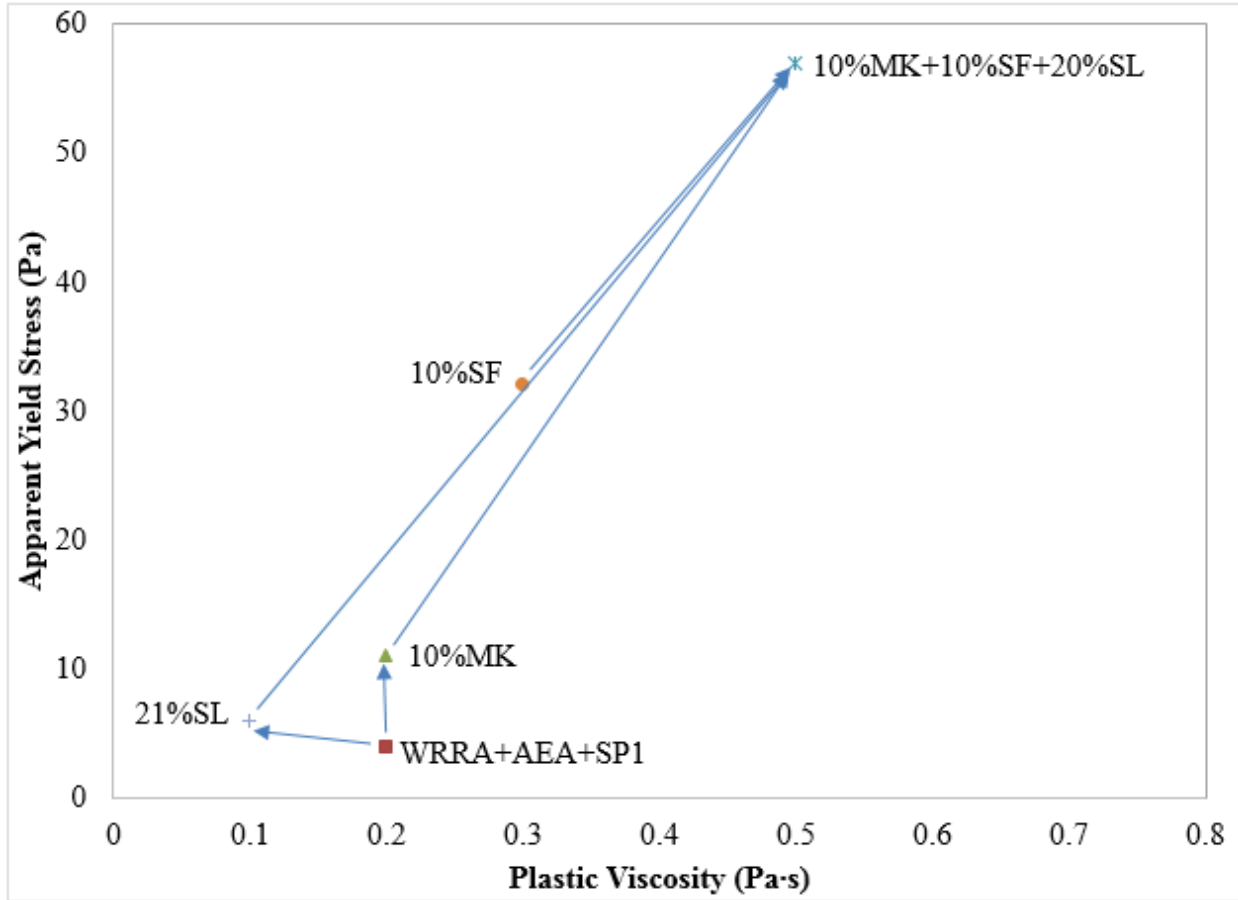


Figure 4.8. Effect of metakaolin/silica fume/slag combination on rheology of plasticized paste

Flocculation has been identified as one of the main parameters affecting the yield stress [130], [156]. Figures 4.9 and 4.10 illustrate the relationship between MPS, which should represent the average size of the flocs, calculated based on Equation 4.2, for each combination and the apparent yield strength (τ_0). In the case where OPC/SCM blends were mixed with water only, (Figure 4.9), there is an exponential relationship between MPS and τ_0 for the binary blends of OPC with FA, SL and SF. However, the apparent yield stress of the OPC/MK blend, which was only measured at 10% cement replacement, does not follow this relationship. Moulin et al. [156] observed a significant increase in the yield stress of OPC/MK pastes mixed with water compared

to the plain OPC paste at w/cm ratio of 0.4, although no other SCMs were examined and no explanation was offered by the authors for this behavior.

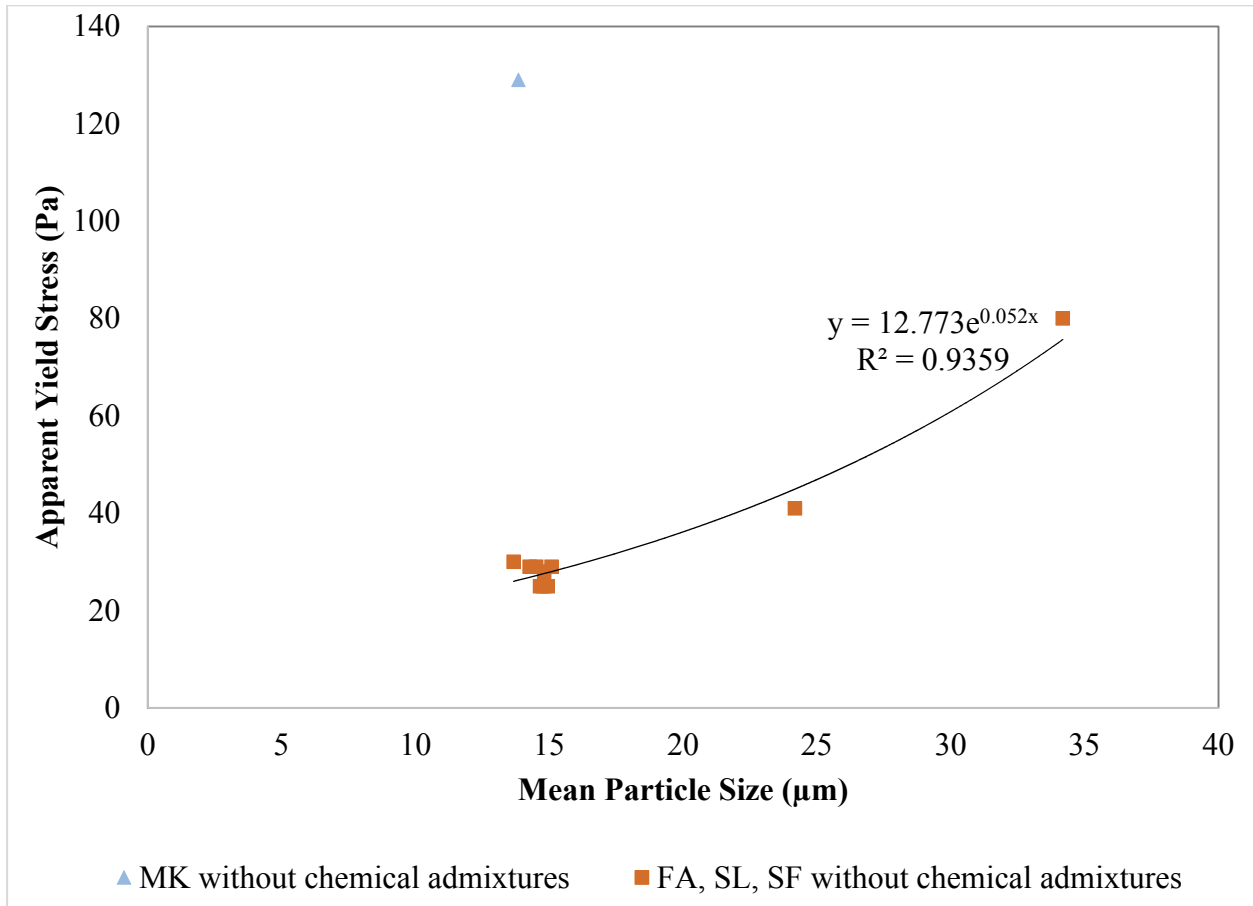


Figure 4.9. Relationship between mean particle size of the OPC and OPC/SCM binary blends and apparent yield stress in the absence of chemical admixtures

In the presence of chemical admixtures, however, the relationship between τ_0 and MPS changes and appears to be linear, (Figure 4.10). This is not surprising, as additions of WRR and SPs result in deflocculation of cement particles [130], [133], [137]. It should be noted that at 10% cement replacement, the binary OPC/MK blend follows the same trend as the rest of the binary mixtures. However, the paste with 21% cement replacement does not follow this trend, most likely due to insufficient amount of SP, as discussed previously. The ternary combinations of OPC/SL/FA follow the same trend as well. It is interesting to note that the OPC/SF/FA ternary

blend appears to be an outlier. It is possible that addition of FA improved the dispersion of densified silica fume and that the calculated MPS is not representative of the average floc size in this particular paste (OPC/SF/FA). It should also be noted that although the ternary and quaternary blends containing MK (Table 4.2) also show a linear relationship between MPS and τ_0 , it is different from that of the other blends.

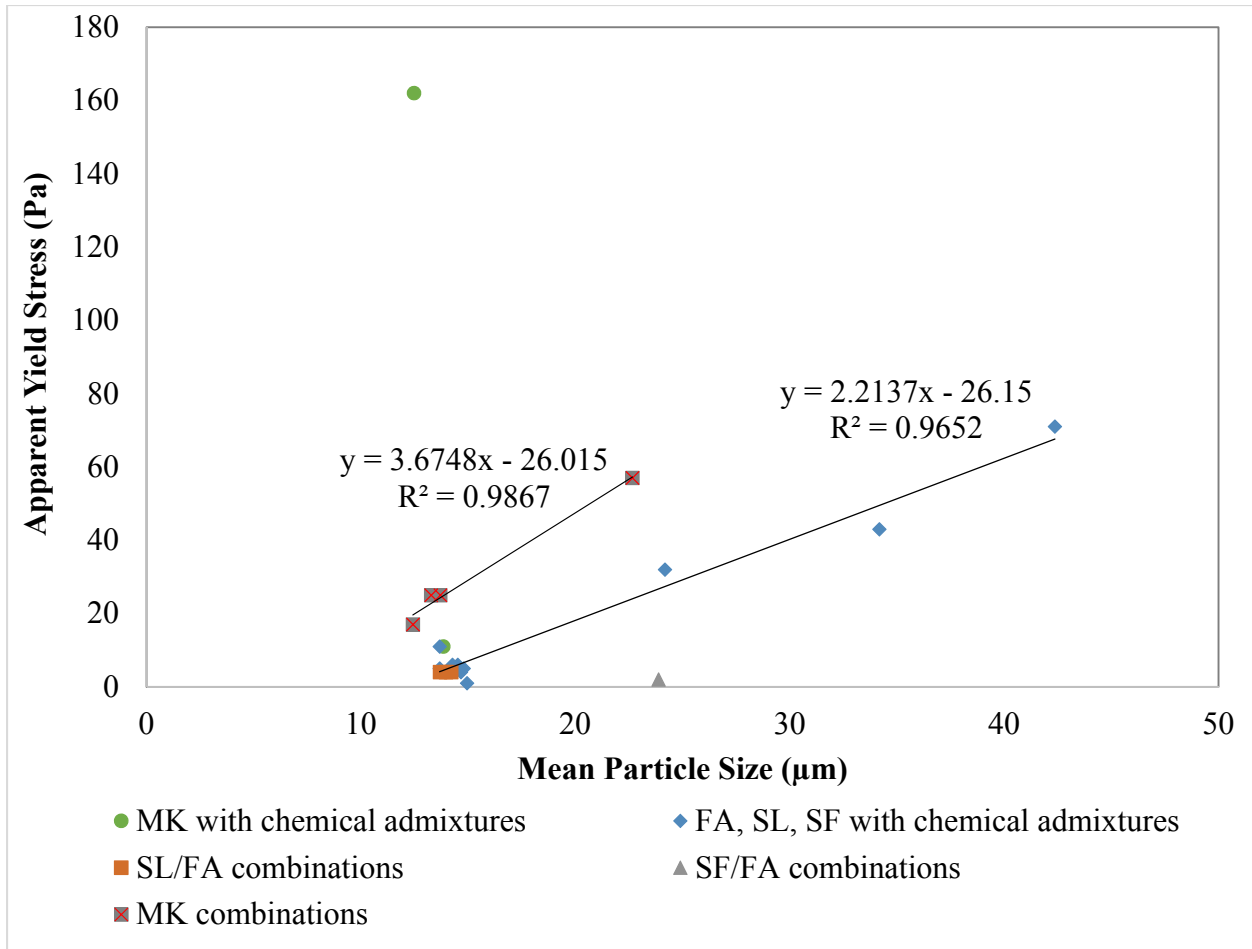


Figure 4.10. Relationship between mean particle size of the OPC/SCM binary, ternary and quaternary blends and apparent yield stress in the presence of chemical admixtures

Since deflocculation is expected to occur with addition of chemical admixtures, the effect of fineness, expressed in terms of the calculated BET specific surface area of the blends on the apparent yield stress was evaluated as well. As BET fineness is not affected by the presence of

chemical admixtures, it was expected to provide a more universal relationship with τ_0 in the presence of AEA, WRRRA and SPs. Yamada et al. [157] reported a direct linear relationship between concrete slump and the amount of adsorbed polycarboxyate-based SP per area of hydration products measured by one-point BET method. As the amount of adsorbed SP increased, so did the slump. This parameter had a direct linear relationship with mortar flow as well [157].

First, the relationship between BET specific surface area and τ_0 was evaluated in the absence of chemical admixtures. Figure 4.11 shows that it is very similar to that of MPS and τ_0 for pastes only containing water. Again, the OPC+10MK paste was an outlier and did not follow the general trend.

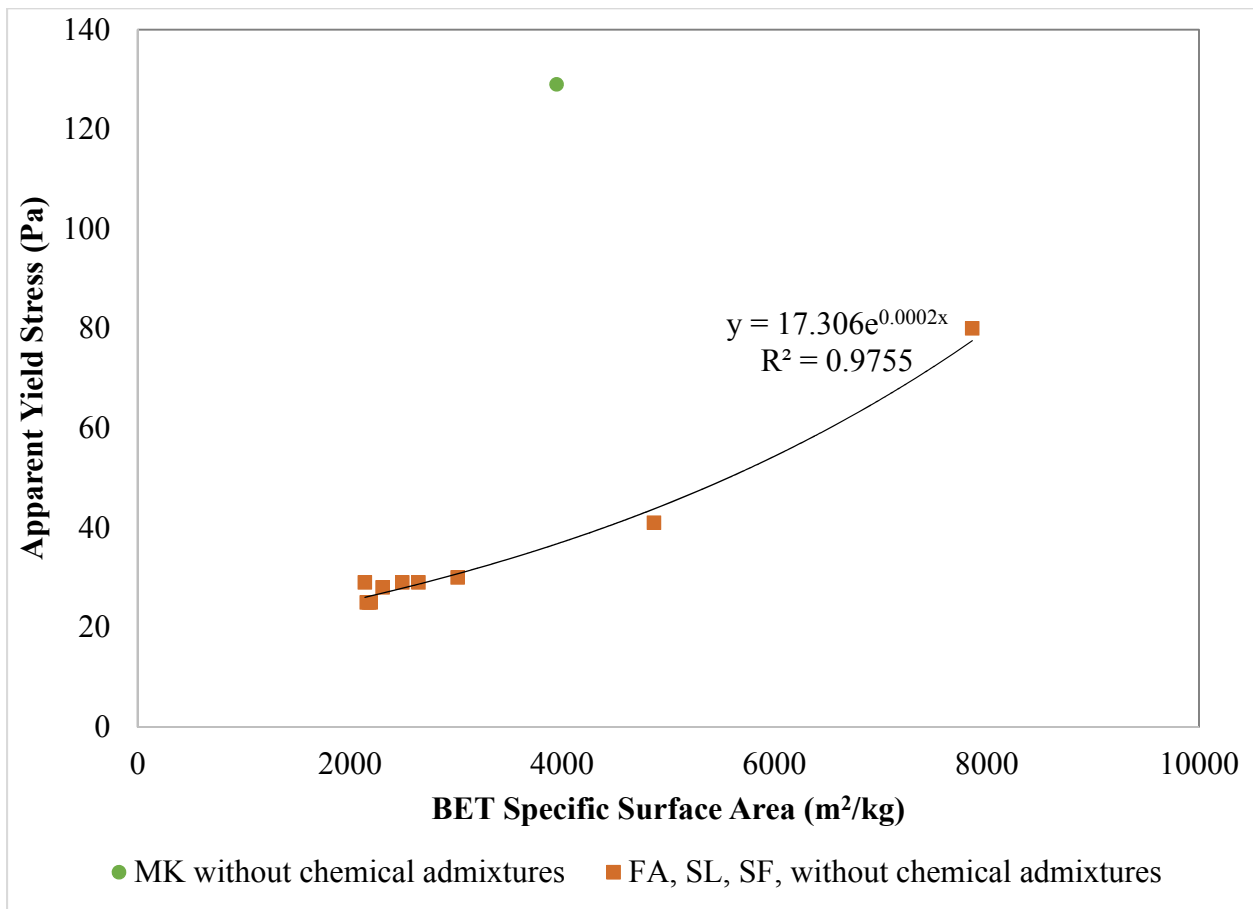


Figure 4.11. Relationship between BET specific surface area of the OPC and OPC/SCM binary blends and apparent yield stress in the absence of chemical admixtures

Figure 4.12 presents the relationship between BET SSA and τ_0 in the presence of WRRRA, AEA and SP. Again, there is a single trend between BET SSA and τ_0 for all the mixtures including OPC+10MK, except for OPC+21MK, most likely due to the insufficient dosage of SP to provide complete defloculation as discussed previously. It is hypothesized that increasing SP dosage for the OPC+21MK mixture would have likely decreased τ_0 making this mixture part of the trend as well; however, the intent of the study was to measure rheology changes with SCM addition at constant w/cm ratio and constant chemical admixture dosages.

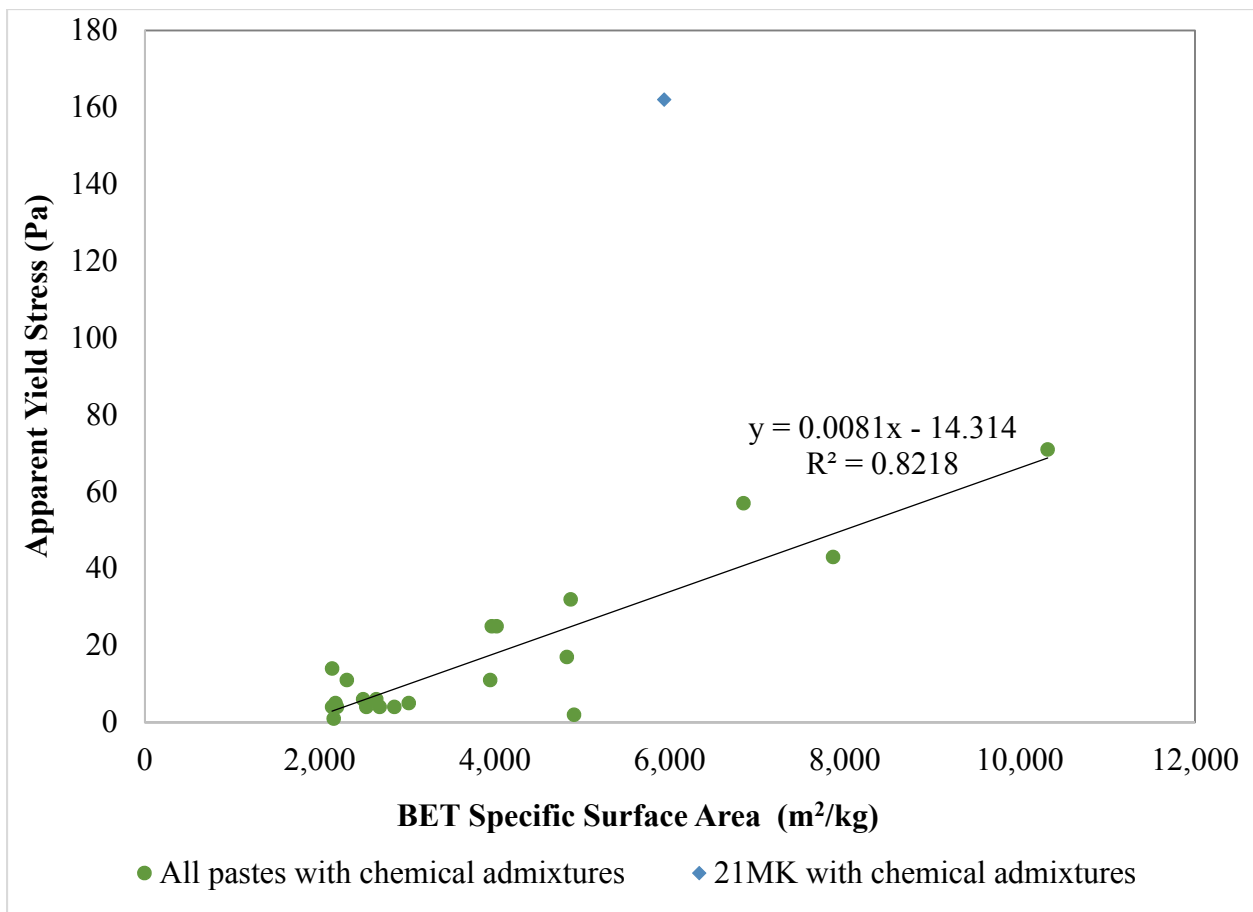


Figure 4.12. Relationship between BET specific surface area of the OPC/SCM binary, ternary and quaternary blends and apparent yield stress in the presence of chemical admixtures

Since a fixed dosage of SP was used in this study, and the amount of SP adsorbed per unit area is expected to decrease with increasing the surface area of the cementitious materials in the mixture, the apparent yield stress was expected to increase with increasing BET SSA. This was confirmed by the experimental results (Figure 4.12). It appears that BET SSA is a better predictor of the apparent yield stress of a mixture than MPS, especially in the presence of chemical admixtures.

Although BET SSA provided more generalized trends with τ_0 , both with and without chemical admixtures, compared to MPS, it still did not provide a unified trend that included all the metakaolin mixtures. The trends themselves are expected to be different for pastes with and without chemical admixtures due to the different interparticle interactions, which are dominated by van der Waals forces in the absence of chemical admixtures [158] and by steric repulsion in the presence of PC-based superplasticizers [159], [160]. While the non-conformance of the OPC+21MK mixture with WRRR, AEA and SP1 to the general trend (Figure 4.12) is attributed to insufficient SP dosage, the non-conformance of OPC+10MK to the general trend (Figure 4.11) in the absence of chemical admixtures is puzzling. Recently, Knop and Peled [161] observed that the setting behavior of the OPC/limestone blends of various fineness was dependent not only of the surface area of blend, but also on the packing density. To this effect, the formula in Equation 4.3 [162] was used to calculate packing density (Φ) for the OPC/SCM combinations:

$$\Phi = \frac{1}{1 + \rho_p \frac{w}{p}} \quad \text{Equation 4.3}$$

where ρ_p is the density of the dry powder calculated based on the measured density for each material (Table 4.4) divided by the density of water and using their respective weighted fractions, w is the volume of water required to obtain normal consistency and p is the mass of cementitious materials. When τ_0 was plotted against Φ (Figure 4.13), a single trend was obtained for all the

non-plasticized pastes, including OPC+10MK with no outliers. The high apparent yield stress of the OPC+10MK mixture was due to its low packing density, which appears to be the best predictor of the apparent yield stress for pastes in the absence of chemical admixtures. It appears that around $\Phi=0.55$ the yield stress diverges to 25-28 Pa. This low value of Φ at divergence indicates a flocculated system [128], which was as expected. There was no definitive relationship between Φ and yield stress in the presence of chemical admixtures.

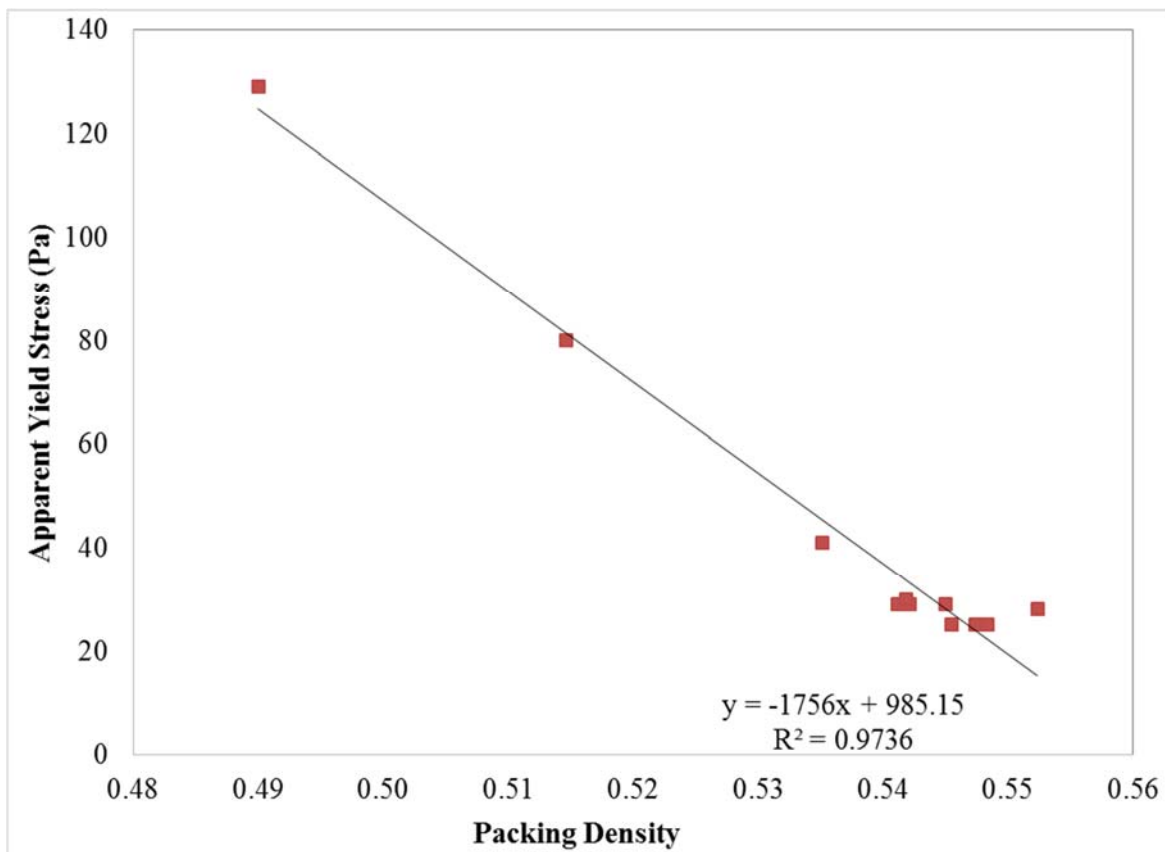


Figure 4.13. Relationship between packing density of the OPC and OPC/SCM binary blends and apparent yield stress in the absence of chemical admixtures

Sabir et al. [163] state that “no detailed examinations have been reported to-date on the water demand of MK and its influence on the flow properties.” Figures 4.14 and 4.15 show the water demand as a function of total cement replacement as well as BET surface area. It should be

noted that the spread in the normal consistency values of cement observed in these figures is due to the addition of chemical admixtures and their combinations.

He et al. [164] observed that w/c ratio had a “broad linear correlation” with BET surface area. Although they examined a variety of calcined clays, only one metakaolin was used at a fixed cement replacement of 30%. Even though MK was calcined at different temperatures, its BET fineness was very similar, and the specific relationship between BET SSA of OPC/MK mixtures could not be established in that study.

Water demand increases with increasing percentage of metakaolin and silica fume as well as with increasing BET surface area of cementitious mixtures. As for FA and slag, as well as their combinations, their water demand does not appear to be affected by the total cement replacement percentage. It should be noted that the increase in water demand is notably higher for mixtures containing MK compared to SF. Based on Figure 4.13, this can be attributed to their lower packing densities.

It appears that the effect of combining MK with FA or slag or combining SF with FA has an additive effect on water demand; that is, the water demand remains at the level of the binary OPC/MK or OPC/SF paste and is not affected by further cement replacement with slag or FA. In addition to particle-type effects, such as surface area and packing density discussed previously, it is possible that addition of SCMs modifies the initial dissolution and precipitation reactions affecting rheology. Talero et al. [165] compared the water demand of two portland cement pastes of similar fineness and suggested that the higher water demand was due to the higher C_3A content of one of the cements and consequently increased formation of hydration products of C_3A . The researchers also observed that the setting time for the high- C_3A cement was shorter. Again, this was attributed to the hydration reaction of this compound. Talero [166], [167] also demonstrated

that Al_2O_3 present in metakaolin is not only reactive at early ages, but that it is even more reactive than C_3A present in cement. This is in line with the increased water demand of the OPC/MK blends (Figure 4.14).

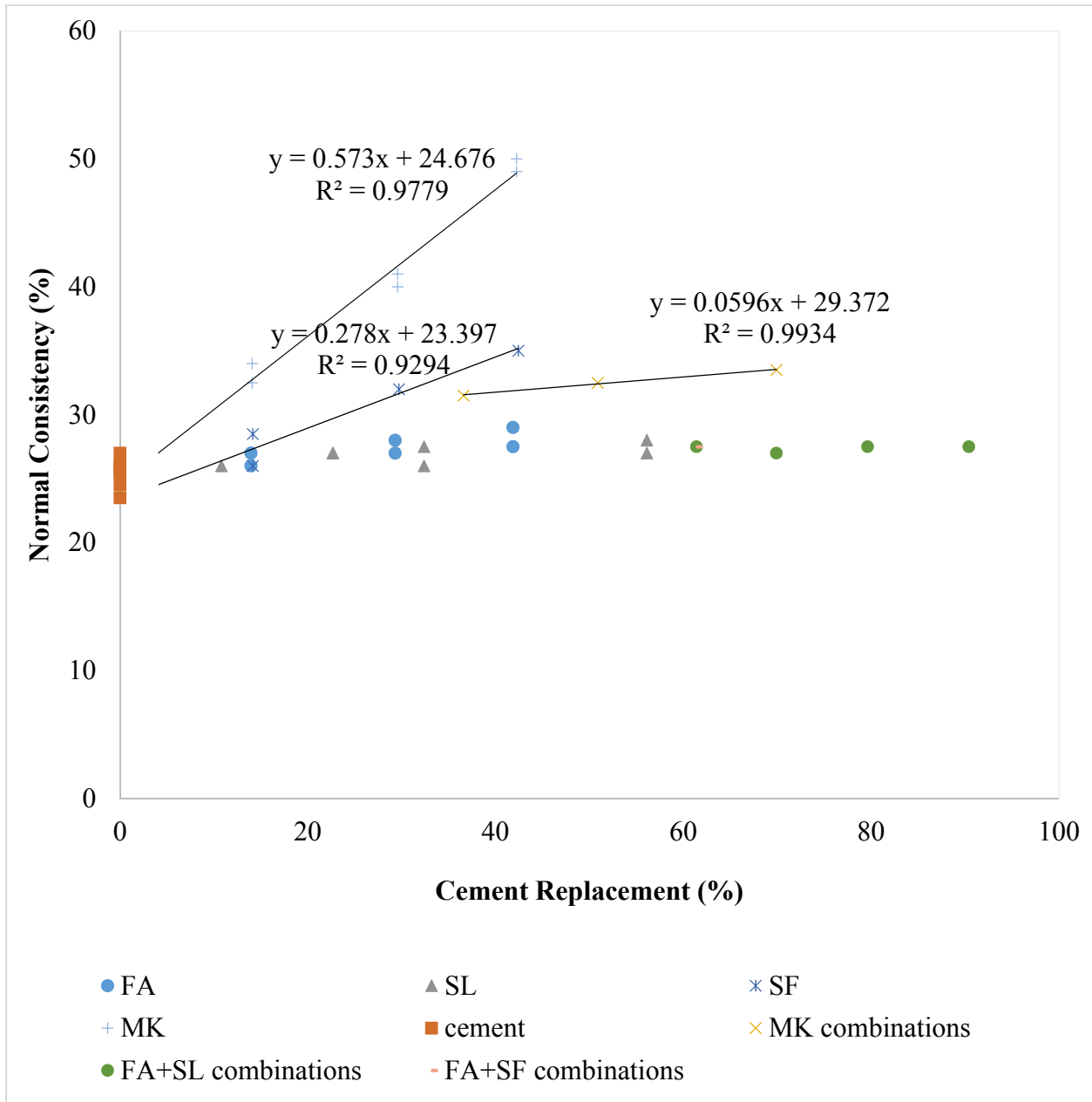


Figure 4.14. Relationship between percent cement replacement and normal consistency for all the pastes

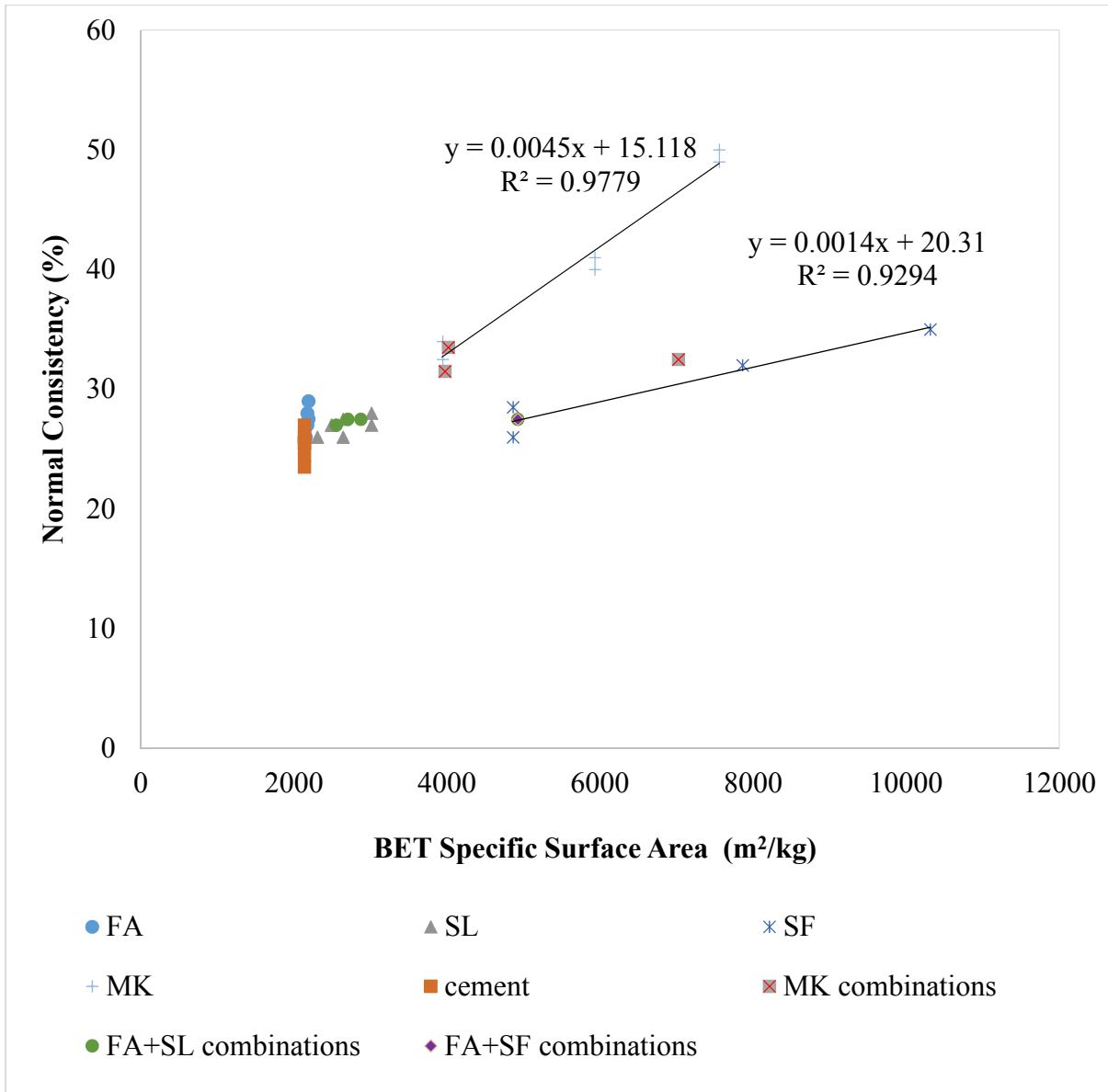


Figure 4.15. Relationship between BET surface area and normal consistency for all the pastes

4.5 Conclusions

The results of this study show that there is a synergistic effect of SCM combinations on yield stress of pastes for ternary and quaternary OPC/SCM blends. It is clear that the effect of SCM combinations on paste rheology is not additive and cannot be predicted from the results obtained for their respective binary combinations.

At a fixed w/cm ratio and a fixed dosage of chemical admixtures, a linear relationship was observed between apparent yield stress and BET surface area of the mixtures. Only binary mixtures were tested without chemical admixtures; in this case, the packing density determined based on normal consistency measurements appeared to be the best predictor of the apparent yield stress. The high yield stress of the OPC/MK paste without chemical admixtures was explained by its lower packing density.

It was also observed that for fly ash and slag binary and ternary mixtures, with and without chemical admixtures, there was no significant change in water demand with increasing cement replacement. This was not the case with metakaolin and silica fume, for which normal consistency was measured at 10, 20 and 30% cement replacement levels. For these mixtures the water demand increased with increasing cement replacement level. Binary OPC/MK pastes had the highest water demand regardless of the presence of chemical admixtures. The water demand of the ternary and quaternary mixtures remained at the level of the binary OPC/MK or OPC/SF mixtures and was not affected by further cement replacement with fly ash or slag. In this case, the effect of SCM combinations appears to be additive.

Since only one source was used for each of the SCMs, further work is needed to confirm the observed trends between yield stress and packing density as well as surface area. When SCMs from different sources with different chemistries, densities and surface areas are analyzed, these conclusions can be extended to SCMs as a whole.

CHAPTER 5: MODELING HEAT OF HYDRATION REDUCTION FOR CEMENT REPLACEMENT BY SCMs⁴

5.1 Introduction

Considerable amounts of heat liberated during cement hydration lead to an increase in temperature which typically occurs several hours after concrete placement. Since thermal conductivity of concrete is low, large temperature gradients can develop between the surface exposed to ambient temperature conditions and the core of the structure. These temperature gradients are of particular concern for mass concrete structures, where thermal stresses can lead to early-age cracking. In Florida, due to the warmer climate, thermal gradients can lead to cracking even in structures which would not normally be considered mass concrete, such as concrete pavement [25]. Reduction of early-age cracking risk is typically achieved by reducing the heat of hydration and, therefore concrete temperature rise. The recommended strategies for reducing the amount of heat generated during cement hydration include the use of low-heat portland cements, blended cements and partial cement replacement with supplementary cementitious materials (SCMs) [168].

Prediction and control of concrete temperature rise due to cement hydration is of great significance for mass concrete structures since large temperature gradients between the surface and the core of the structure can lead to cracking thus reducing durability of the structure. A

⁴ This chapter has been submitted as a manuscript to the Journal of Thermal Analysis and Calorimetry.

number of models have been proposed to predict heat evolution from cement hydration reactions [38], [169]–[171].

However, it has been well established that incorporation of SCMs affects the heat evolution concrete and temperature development [12], [26], [172]. This effect depends not only on the total amount of cement replacement, but also on the type of SCM used. Both fly ash (FA) and blast furnace slag (SL) have low reactivity at early hydration ages, although slag is believed to be more reactive than fly ash [173]. Therefore, addition of both of these SCMs is expected to decrease the heat of hydration at early ages and concrete temperature rise [11], [12], [174]–[176]. Nevertheless, Pane and Hansen [176] noted that although both FA and SL at 25% cement replacement result in lower total heat evolution during early ages compared to the plain cement sample, the total heat generated by BSF samples appears to exceed that of the control mixture beyond 3 days.

Silica fume (SF) and metakaolin (MK) are generally believed to increase the heat evolution. However, contradictory reports can be found in the literature regarding the effect of both of these materials on heat of hydration and temperature rise. Kadri and Duval [177] observed an increase in the total heat with SF addition up to 30% in the first 24 hours. This increase was more pronounced at low w/cm ratios. On the contrary, Mostafa and Brown [178] reported a slight reduction in the total heat during the first 24 hours with 10, 20 and 30% SF addition. After this time, there was a slight increase in the total heat for the mixture containing 10% SF, while the others continued to exhibit total heat below that of the plain cement sample. Pane and Hansen [176] confirmed that the effect of SF is dependent on the w/cm ratio of the mixture.

Frias et al. [179] reported a slight increase in the heat of hydration with MK addition compared to OPC. Kadri et al. [180] recorded a more notable increase in the heat of hydration and temperature rise with 10% MK. Increase in heat flow and temperature rise in 10% cement

replacement with MK was also observed by Williams et al. [181]. Ambroise et al. [182] and Bai and Wild [183] observed an increase in the maximum temperature rise during hydration with up to 20% MK addition, while Kim et al. [184] reported a slight decrease in the maximum adiabatic temperature with addition of 10% MK. Jiang et al. [185] found the effect of cement replacement with MK on heat evolution to be dosage-dependent. At 6% MK addition, the total heat was significantly increased compared to the OPC mixture up to approximately 48 hours, while at 10 and 14% cement replacement a decrease in total heat was observed. Bai and Wild [183] reported that an increase in temperature rise with MK addition can be counteracted by incorporation equal amounts of pulverized-fuel ash (PFA). The idea of combining several mineral admixtures in order to reduce heat evolution and concrete temperature rise is attractive, especially in the case of MK, as its addition can improve the low early-age compressive strengths typically associated with cement replacement by SL or FA [116], [117].

Several models have been proposed for predicting heat release by blended cements. Most of these models have been developed for binary combinations of OPC and slag [186]–[190]. A model incorporating SF and superplasticizer has been proposed as well [191]. Wang et al. [192] proposed an equation for total heat release for mixtures incorporating both slag and fly ash. Schindler and Folliard [26] also proposed a model incorporating the effects of slag and fly ash, which was later modified to incorporate silica fume as well [193]. Poole et al. [194] and Riding et al. [172] demonstrated that chemical admixtures can impact hydration as well and should be taken into account when modeling hydration processes. However, none of the models to date address the effect of MK on heat evolution. The only guidance regarding the heat of hydration (HOH) of MK comes from Gajda [29] who states that it can be approximated as “100% to 125% that of Portland cement.” This, however, applies only to OPC/MK mixtures, and it is unclear how

the total heat evolution of a ternary or quaternary system will be modified by the addition of MK with chemical admixtures.

Additionally, all of the above models consider the effects of each SCM and each chemical admixture on hydration to be additive. However, there are indications in the literature that there may be more complex interactions between SCMs and also possibly chemical admixtures. Han et al. [195] investigated the effect of cement replacement with slag and cement replacement with low-CaO fly ash (binary combinations of OPC and each SCM) on heat release. Although the authors did not model the heat release of these binary systems, they observed that the heat reduction is “not proportional to the dosage of mineral admixtures.” Palou et al. [196] also observed in the OPC-SL-SF-MK systems that the total heat of hydration is not proportional to cement content reduction.

The absence of a predictive equation for heat evolution incorporating MK as well as the possibility of interactions between certain SCM and/or chemical admixture combinations served as a motivation for this study. The goal was to assess the effect of commonly used SCMs and chemical admixtures as well as their potential interactions on the cumulative heat evolution and to develop a set of equations that will allow engineers to estimate the potential heat reduction resulting from the incorporation of different SCMs and chemical admixtures combinations into a concrete mixture.

5.2 Experimental Procedures

Type I/II commercial portland cement, four mineral admixtures (FA, SL, SF and MK) and three chemical admixtures, air-entraining admixture (AEA), water-reducing and retarding admixture (WRRR) and superplasticizer (SP), that are typically used in structural concrete in Florida were selected for this study. X-ray fluorescence spectroscopy (XRF) was used to

determine the chemical oxide composition of cement and mineral admixtures following ASTM C114. Mineralogical composition of cement was determined from x-ray diffraction (XRD) measurements in accordance with ASTM C1365. Prior to XRD measurements, cement was wet-ground in ethanol in a McCrone micronizing mill to a particle size between 1 and 10 μm . The wet grinding method was used to avoid the effect of temperature on gypsum and its possible phase transformation to hemihydrate or anhydrite. The samples were then dried in an oven at 43°C. XRD scans were collected using the Phillips X'Pert PW3040 Pro diffractometer equipped with the X'Celerator Scientific detector and a Cu-K α x-ray source. Tension and current were set to 45 kV and 40 mA respectively; 5 mm divergence and anti-scatter slits were used in the automatic mode. Phase quantification was performed using the Rietveld refinement functionality of the Panalytical HighScore Plus 3.0 software.

Factorial design was used to evaluate the effect of the selected SCMs and chemical admixtures on heat evolution. Factorial designs are commonly used in screening experiments to identify significant factors (mineral and chemical admixtures in this study) using the smallest number of experiments [197]. In concrete research, factorial designs have been previously used for mix design optimization [198]–[205]. The advantage of factorial designs is not only they allow reducing the number of experiments compared to “one factor at a time” approach, they also are able to evaluate the potential for factors interactions.

Seven admixtures (factors) were identified for this study: Class F FA, SL, SF, MK, AEA, WRRRA, and SP. At first, a fractional factorial design was performed (design matrix is listed in Table 5.2). Fractional factorial designs are commonly used in screening experiments to identify significant factors using the smallest number of experiments [197]. The fractional factorial design

was a resolution III design, which means that the effect of each factor could not be separated from the effect of two-factor interactions.

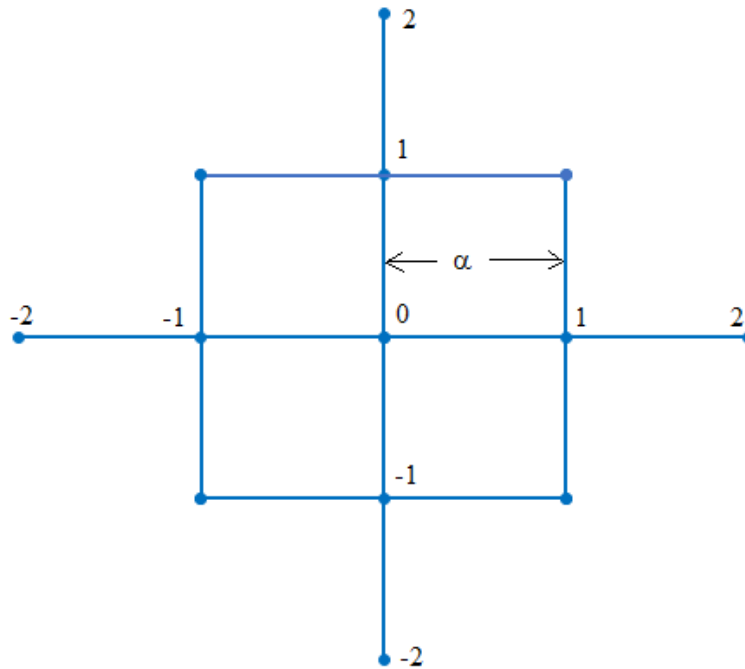


Figure 5.1. Two-dimensional central composite design (CCD) representation

In order to improve the resolution, axial points and a center point were added to create central composite design (CCD) with $\alpha = 2$, where α is the distance from the center point for each factor. A 2D graphical illustration of CCD is presented in Figure 5.1. Both experimental designs were created using JMP software from SAS. One run was performed for each mixture, except for the center point, where two runs were performed to assess the error associated with experimental results. CCD was a resolution IV design, in which the main effects were not compounded with any two-factor interactions, but the two-factor interactions were compounded with each other. Additionally, since the CCD used five levels of each factor, it can be used to assess whether or not the response changed linearly with changing factor level.

Coded values for each factor were used in the experimental design, which were calculated using the following general equation [197]:

$$Coded\ value = \frac{(actual\ value - \frac{(\alpha_{-1} + \alpha_1)}{2})}{\frac{\alpha_1 - \alpha_{-1}}{2}} \quad \text{Equation 5.1}$$

Therefore, individual coded values for each variable were calculated as follows:

$$FA_{coded} = SL_{coded} = \frac{actual\ value - 0.20}{0.10} \quad \text{Equation 5.2}$$

$$SF_{coded} = MK_{coded} = \frac{actual\ value - 0.10}{0.05} \quad \text{Equation 5.3}$$

$$AEA_{coded} = \frac{actual\ value - 23}{11.5} \quad \text{Equation 5.4}$$

$$WRR_{coded} = \frac{actual\ value - 200}{100} \quad \text{Equation 5.5}$$

$$SP_{coded} = \frac{actual\ value - 100}{50} \quad \text{Equation 5.6}$$

The dosages of each chemical and mineral admixture corresponding to each coded design value are listed in Table 5.1. A constant w/cm ratio of 0.485 was maintained for all the mixtures.

The use of coded variables is preferable in the initial analysis over actual (natural) values. Since the levels of each factor can differ greatly from each other, converting natural values to coded values allows the relative effect of each factor to be evaluated [197]. Additionally, the use of coded variables ensures that the root mean square error (RMSE) is the same for all the variables.

Table 5.1. Experimental design addition levels

Design Level	2	1	0	-1	-2
FA (fraction of total cementitious content)	0.40	0.30	0.20	0.10	0.00
SF (fraction of total cementitious content)	0.20	0.15	0.10	0.05	0.00
MK (fraction of total cementitious content)	0.20	0.15	0.10	0.05	0.00
SL (fraction of total cementitious content)	0.40	0.30	0.20	0.10	0.00
AEA (ml/100 kg cementitious)	46	34.5	23	11.5	0
WRR (ml/100 kg cementitious)	400	300	200	100	0
SP (ml/100 kg cementitious)	200	150	100	50	0

Table 5.2. Fractional factorial design matrix

Mix #	FA	SF	MK	SL	AEA	WRRR	SP
1	1	-1	-1	-1	-1	1	1
2	-1	-1	1	-1	-1	1	-1
3	1	1	-1	-1	1	1	-1
4	-1	1	-1	-1	1	-1	1
5	-1	1	1	1	1	1	-1
6	-1	-1	-1	-1	-1	-1	-1
7	1	-1	1	-1	1	-1	1
8	1	1	1	-1	-1	-1	-1
9	1	-1	-1	1	1	-1	-1
10	-1	-1	-1	1	1	1	1
11	-1	1	-1	1	-1	1	-1
12	1	1	-1	1	-1	-1	1
13	1	1	1	1	1	1	1
14	-1	-1	1	1	-1	-1	1
15	1	-1	1	1	1	-1	-1
16	-1	1	1	-1	-1	1	1

Table 5.3. Additional axial points design matrix

Mix #	FA	SF	MK	SL	AEA	WRRR	SP
17	2	0	0	0	0	0	0
18	-2	0	0	0	0	0	0
19	0	2	0	0	0	0	0
20	0	-2	0	0	0	0	0
21	0	0	2	0	0	0	0
22	0	0	-2	0	0	0	0
23	0	0	0	2	0	0	0
24	0	0	0	-2	0	0	0
25	0	0	0	0	2	0	0
26	0	0	0	0	-2	0	0
27	0	0	0	0	0	2	0
28	0	0	0	0	0	-2	0
29	0	0	0	0	0	0	2
30	0	0	0	0	0	0	-2
31	0	0	0	0	0	0	0
32	0	0	0	0	0	0	0

Heat flow measurements were performed following external mixing protocol, Method B of ASTM C1702. All measurements were carried out at an isothermal temperature of 23°C. Pastes were mixed with an IKA WERKE mixer for a total of 7 min following the procedure described in [206]. WRRRA was added to the mixing water. After combining water and cementitious materials, the paste was mixed for 1 minute prior to the addition of AEA, after which it was mixed for an additional 2 minutes. The mixture was then rested for 2 minutes. After the rest period, SP was added to the mixture, and the sample was mixed for an additional 2 minutes at 1200 rpm rather than 2000 rpm as reported by Muller et al. [206]. Upon completion of mixing, samples were immediately placed into the iCal-8000 Calmetrix isothermal calorimeter.

The cumulative heat values at 12, 24, 48 and 72 hours were extracted from the collected data for each mixture. Since only one cement was used in this study, reduction of the total heat compared to the plain cement-water paste ($\Delta Q/Q_{OPC}$, where ΔQ is the difference between cumulative heat of the plain OPC-water mixture, Q_{OPC} , and the mixture modified by addition of SCM and/or chemical admixtures) was selected as a response variable rather than the total heat. Several studies demonstrated that the total heat evolution depends on cement fineness and mineral composition [38], [169], [207], [208]. Therefore, it is expected that equations that model total heat reduction with SCM incorporation compared to the plain cement mixture would be more useful than those modeling the total heat based only on one OPC composition.

$\Delta Q/Q_{OPC}$ values calculated for each mixture were analyzed with JMP software to identify significant factors. A significance level of 95% was used in this study. In addition to the 32 mixtures that were used to generate the models, 35 additional mixtures were prepared for validation of these models. Admixture addition rates and their corresponding coded levels for the validation mixtures are listed in Tables 5.4 and 5.5 respectively.

Table 5.4. Admixture addition rates for validation mixtures

Mix#	FA	SF	MK	SL	AEA	WRRA	SP
	(fraction of total cementitious content)				(ml/100 kg cementitious)		
1	0.10	0.15	0.05	0.30	11.5	100	150
2	0.10	0.05	0.05	0.30	34.5	100	50
3	0.30	0.15	0.15	0.10	11.5	300	150
4	0.20	0.10	0.10	0.20	0	200	0
5	0.20	0.10	0.10	0.20	23	0	0
6	0.20	0.10	0.10	0.20	0	0	100
7	0.20	0.10	0.00	0.20	0	0	0
8	0.20	0.10	0.10	0.20	0	0	0
9	0.20	0.00	0.10	0.20	0	0	0
10	0.20	0.00	0.10	0.00	0	0	0
11	0.40	0.00	0.10	0.00	0	0	0
12	0.40	0.00	0.20	0.00	0	0	0
13	0.20	0.00	0.10	0.00	0	0	0
14	0.40	0.00	0.10	0.00	0	0	0
15	0.40	0.00	0.20	0.00	0	0	0
16	0.00	0.00	0.10	0.20	0	0	0
17	0.00	0.00	0.10	0.40	0	0	0
18	0.20	0.20	0.00	0.00	0	0	0
19	0.20	0.00	0.00	0.20	0	0	0
20	0.20	0.00	0.00	0.40	0	0	0
21	0.00	0.00	0.10	0.30	0	0	0
22	0.00	0.00	0.20	0.30	0	0	0
23	0.30	0.20	0.00	0.00	0	0	0
24	0.21	0.08	0.00	0.00	0	0	0
25	0.21	0.08	0.00	0.00	0	0	0
26	0.21	0.08	0.00	0.00	0	0	0
27	0.21	0.00	0.10	0.00	0	0	0
28	0.21	0.00	0.10	0.00	0	0	0
29	0.21	0.00	0.00	0.30	0	0	0
30	0.21	0.00	0.00	0.30	0	0	0
31	0.21	0.00	0.00	0.30	0	0	0
32	0.00	0.00	0.00	0.00	23	200	100
33	0.00	0.00	0.00	0.00	0	0	100
34	0.00	0.00	0.00	0.00	0	0	200
35	0.00	0.00	0.00	0.00	46	300	

Table 5.5. Validation mixtures coded levels for each factor

Mix #	FA	SF	MK	SL	AEA	WRRA	SP
1	-1	1	-1	1	-1	-1	1
2	-1	-1	-1	1	1	-1	-1
3	1	1	1	-1	-1	1	1
4	0	0	0	0	-2	0	-2
5	0	0	0	0	0	-2	-2
6	0	0	0	0	-2	-2	0
7	0	0	-2	0	-2	-2	-2
8	0	0	0	0	-2	-2	-2
9	0	-2	0	0	-2	-2	-2
10	0	-2	0	-2	-2	-2	-2
11	2	-2	0	-2	-2	-2	-2
12	2	-2	2	-2	-2	-2	-2
13	0	-2	0	-2	-2	-2	-2
14	2	-2	0	-2	-2	-2	-2
15	2	-2	2	-2	-2	-2	-2
16	-2	-2	0	0	-2	-2	-2
17	-2	-2	0	2	-2	-2	-2
18	0	2	-2	-2	-2	-2	-2
19	0	-2	-2	0	-2	-2	-2
20	0	-2	-2	2	-2	-2	-2
21	-2	-2	0	1	-2	-2	-2
22	-2	-2	2	1	-2	-2	-2
23	1	2	-2	-2	-2	-2	-2
24	0.1	-0.4	-2	-2	-2	-2	-2
25	0.1	-0.4	-2	-2	-2	-2	-2
26	0.1	-0.4	-2	-2	-2	-2	-2
27	0.1	-2	0	-2	-2	-2	-2
28	0.1	-2	0	-2	-2	-2	-2
29	0.1	-2	-2	1	-2	-2	-2
30	0.1	-2	-2	1	-2	-2	-2
31	0.1	-2	-2	1	-2	-2	-2
32	-2	-2	-2	-2	0	0	0
33	-2	-2	-2	-2	-2	-2	0
34	-2	-2	-2	-2	-2	-2	2
35	-2	-2	-2	-2	2	1	-2

5.3 Results and Discussion

5.3.1 Model Development

Based on the fractional factorial design, only FA and SL were identified as significant factors at 12 and 24 hours. SF had a p-value of 0.0502 at 24 hours, so its significance was very close to 95%. All three of these factors had p-values below 0.05 at 48 and 72 hours. However, each of these individual factors was aliased with a number of factor combinations. Additionally, coefficients of determination (R^2 values) for the linear models varied from 0.72 to 0.83 depending on the hydration age, indicating that the fit could possibly be improved by addition of factor interactions or quadratic terms.

Addition of axial points and a center point increased the resolution of the design so that individual factors were no longer aliased with factor combinations and allowed quadratic effects to be evaluated as well. Statistical analysis showed that significant factors and factor combinations varied depending on the age of paste (Tables 5.6 and 5.7).

Response surface methodology with least squares fitting was used to obtain coefficients (listed in Estimates columns of Tables 5.6 and 5.7) for the significant factors and factor interactions. R^2 values for the models at each hydration age were significantly improved compared to those obtained from linear models based on the fractional factorial design.

The analysis was first performed using coded variables (Table 5.6). Since the modeled response was the reduction of total heat with addition of different admixtures, positive coefficients in Table 5.6 indicate that an increase in those factors will result in a further decrease in the total heat. Negative coefficients, on the other hand, signify an increase in total heat with an increase in the factor level.

Table 5.6. Parameter estimates of the statistical models based on coded values

	12 hrs / R ² =0.96			24 hrs / R ² =0.93			48 hrs / R ² =0.93			72 hrs / R ² =0.92		
	Estimate	Prob. >	t	Estimate	Prob. >	t	Estimate	Prob. >	t	Estimate	Prob. >	t
β_0 Intercept	0.407	0.000		0.421	0.000		0.396	0.000		0.376	0.000	
β_1 FA	0.117	0.000		0.109	0.000		0.105	0.000		0.104	0.000	
β_2 SL	0.114	0.000		0.106	0.000		0.089	0.000		0.083	0.000	
β_3 SF	0.052	0.000		0.056	0.000		0.055	0.000		0.055	0.000	
β_4 MK	0.037	0.000		0.050	0.000		0.044	0.000		0.043	0.000	
β_5 SL ²	0.023	0.003		0.018	0.041		0.017	0.042		0.017	0.035	
β_6 FA*SL	0.027	0.008		0.027	0.031		0.024	0.039		0.024	0.039	
B_7 MK*SL	0.031	0.004		-	-		-	-		-	-	
β_8 WRRRA	0.020	0.015		-	-		-	-		-	-	
β_9 AEA	-0.020	0.015		-	-		-	-		-	-	
β_{10} SF*MK	0.024	0.017		-	-		-	-		-	-	

Table 5.7. Parameter estimates of the statistical models based on natural values

	12 hrs / R ² =0.97			24 hrs / R ² =0.93			48 hrs / R ² =0.93			72 hrs / R ² =0.92		
	Estimate	Prob. >	t	Estimate	Prob. >	t	Estimate	Prob. >	t	Estimate	Prob. >	t
β_0 Intercept	-0.231	0.000		-0.226	0.000		-0.191	0.000		-0.196	0.000	
β_1 FA	1.166	0.000		1.095	0.000		1.053	0.000		1.045	0.000	
β_2 SL	1.135	0.000		1.061	0.000		0.888	0.000		0.827	0.000	
β_3 SF	1.047	0.000		1.130	0.000		1.103	0.000		1.109	0.000	
β_4 MK	0.730	0.000		1.002	0.000		0.887	0.000		0.863	0.000	
β_5 (SL-0.2) ²	2.299	0.002		1.846	0.041		1.712	0.035		1.758	0.000	
β_6 (FA-0.2)*(SL-0.2)	2.734	0.005		2.683	0.031		2.385	0.039		2.358	0.001	
B_7 (MK-0.1)*(SL-0.2)	6.140	0.002		-	-		-	-		-	-	
β_8 WRRRA	0.0002	0.009		-	-		-	-		-	-	
β_9 AEA	-0.002	0.010		-	-		-	-		-	-	
β_{10} (SF-0.1)*(MK-0.1)	9.750	0.011		-	-		-	-		-	-	
β_{11} (FA-0.2)*(AEA-23)	-0.016	0.043		-	-		-	-		-	-	

While significant factors at 12 hours included both mineral and chemical admixtures, the contribution of chemical admixtures was determined to be insignificant after this age. The lack of significant effect of chemical admixtures on heat evolution after 12 hour has been previously reported by [209]. At all ages, the largest reduction in the total heat is achieved by increasing FA and SL content. At 12 and 24 hours, their coefficients are approximately the same, while at 48 and 72 hours the coefficient for BFS begins to decrease. This decrease in the slag coefficient may possibly indicate that at these ages the hydration reaction of slag starts to contribute to the total heat evolution, therefore lowering the total heat reduction compared to the plain OPC mixture.

It is of interest that the statistical analysis identified SL^2 as a significant factor. The non-linear effect of slag on total heat is in line with the results reported by Han et al. [188], [195], who also observed a non-linear reduction in heat with increasing cement replacement by SL. As for the other SCMs, their effect on the total heat evolution was linear.

Same factors and factor interactions, namely FA, SL, SF, MK, SL^2 and the interaction of FA and SL, were identified as significant at 24, 48, and 72 hours. Since the model coefficients were similar at these ages, a combined model for predicting total heat reduction at 24, 48 or 72 hours was created as well:

$$\Delta Q/Q_{OPC \text{ coded}} = 0.398 + 0.106 \cdot C_{FA} + 0.092 \cdot C_{SL} + 0.056 \cdot C_{SF} + 0.046 \cdot C_{MK} + 0.018 \cdot C_{SL}^2 + 0.025 \cdot C_{FA} \cdot C_{SL} \quad \text{Equation 5.7}$$

where C_i is the i th coded level of each factor. It should be noted that the significance of all the coefficients in the combined model was 99% or greater.

Although the use of coded variable is very helpful for statistical analysis, an equation based on natural values of each factor is more convenient, practically. In addition to the coded variables,

the analysis was also carried out based on the natural variables (Table 5.7). Again, a combined equation for the 24, 48 and 72 hours total heat reduction was calculated as well:

$$\Delta Q/Q_{OPC} = -0.034 + 0.569 \cdot P_{FA} - 0.279 \cdot P_{SL} + 1.114 \cdot P_{SF} + 0.917 \cdot P_{MK} + 1.772 \cdot P_{SL}^2 + 2.475 \cdot P_{FA} \cdot P_{SL} \quad \text{Equation 5.8}$$

Figures 5.2 and 5.3 show the relationship between the BSF and FA content of the mixture and the total heat reduction. These figures clearly illustrate the non-linear effect of SL on heat reduction. It is interesting to note that at small cement replacement levels, below 3% for FA and below 22% for SL, there is no reduction in cumulative heat.

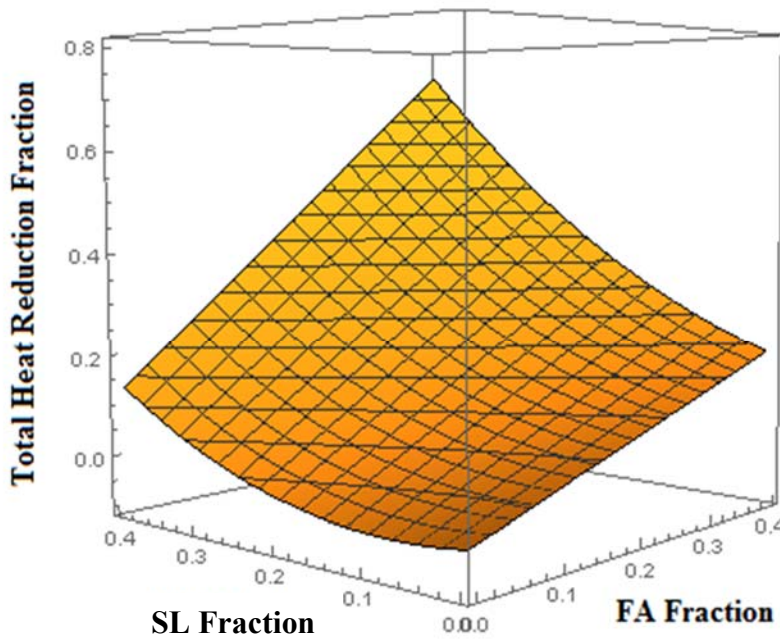


Figure 5.2. Response surface plot for the change in FA and SL content using Equation 5.8

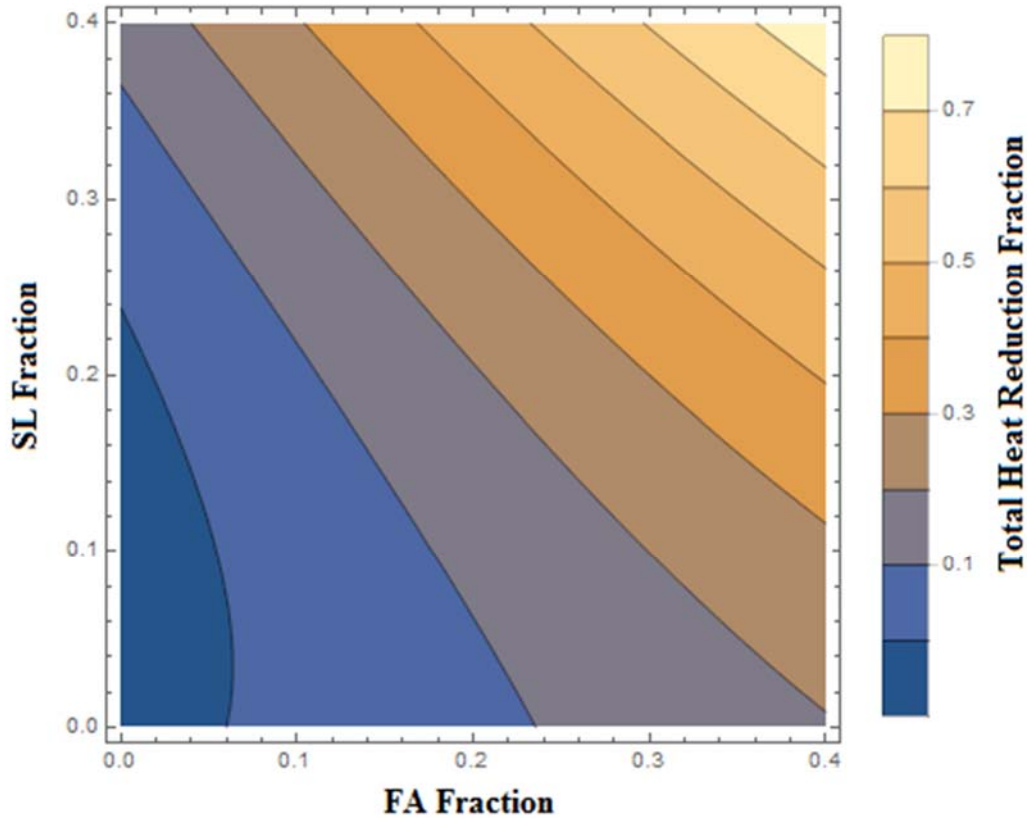


Figure 5.3. Contour plot of the total heat reduction with the change in FA and SL content

Since it is not possible to generate a response surface plot for an equation with more than three variables, Figures 5.4-5.6 present three-dimensional contour plots for combinations of 3 SCMs resulting in a specified cumulative heat reduction. These figures illustrate that there are multiple SCM combinations that can produce the required reduction in heat evolution. Therefore, a lower hydration heat need not be the only consideration when selecting supplementary cementitious materials for cement replacement, and other concrete fresh and hardened properties can be taken into account in order to select the optimum SCM combination.

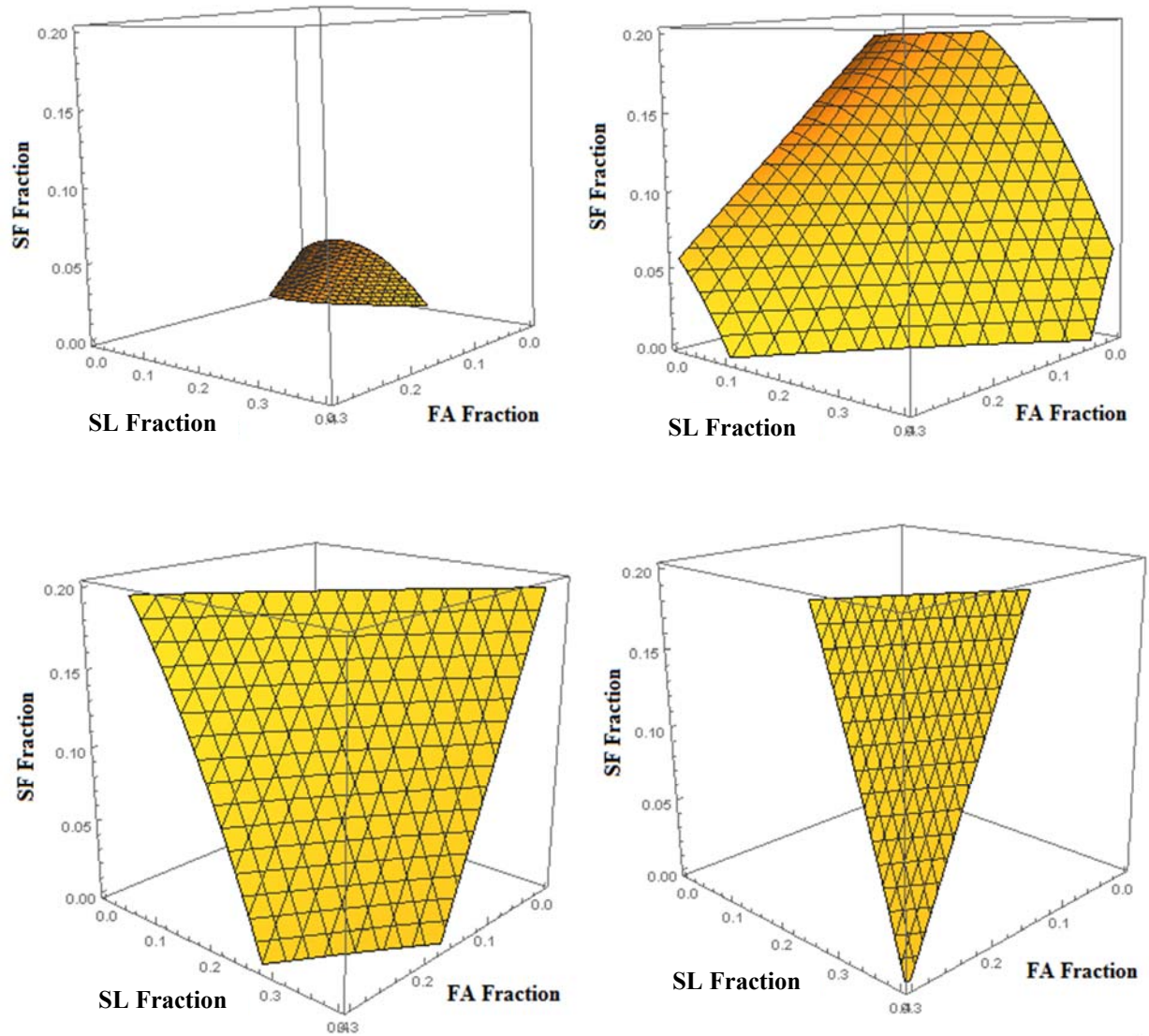


Figure 5.4. Contour plot for the change in FA, SL and SF content using Equation 5.8. a) no change in cumulative heat evolved compared to the plain OPC-water mixture, b) 20% cumulative heat reduction, c) 40% cumulative heat reduction, d) 60% cumulative heat reduction

It is interesting to note that Figures 5.4a illustrates there are certain FA-SL-SF combinations that will not result in cumulative heat reduction at 24, 48 or 72 hours. Essentially the same plots are generated for the FA-SL-MK combinations, since the coefficients for MK and

SF in Equation 5.8 are very similar. Figures 5.5a and 5.6a also show regions of 0% heat reduction with addition of small amounts of SCMs.

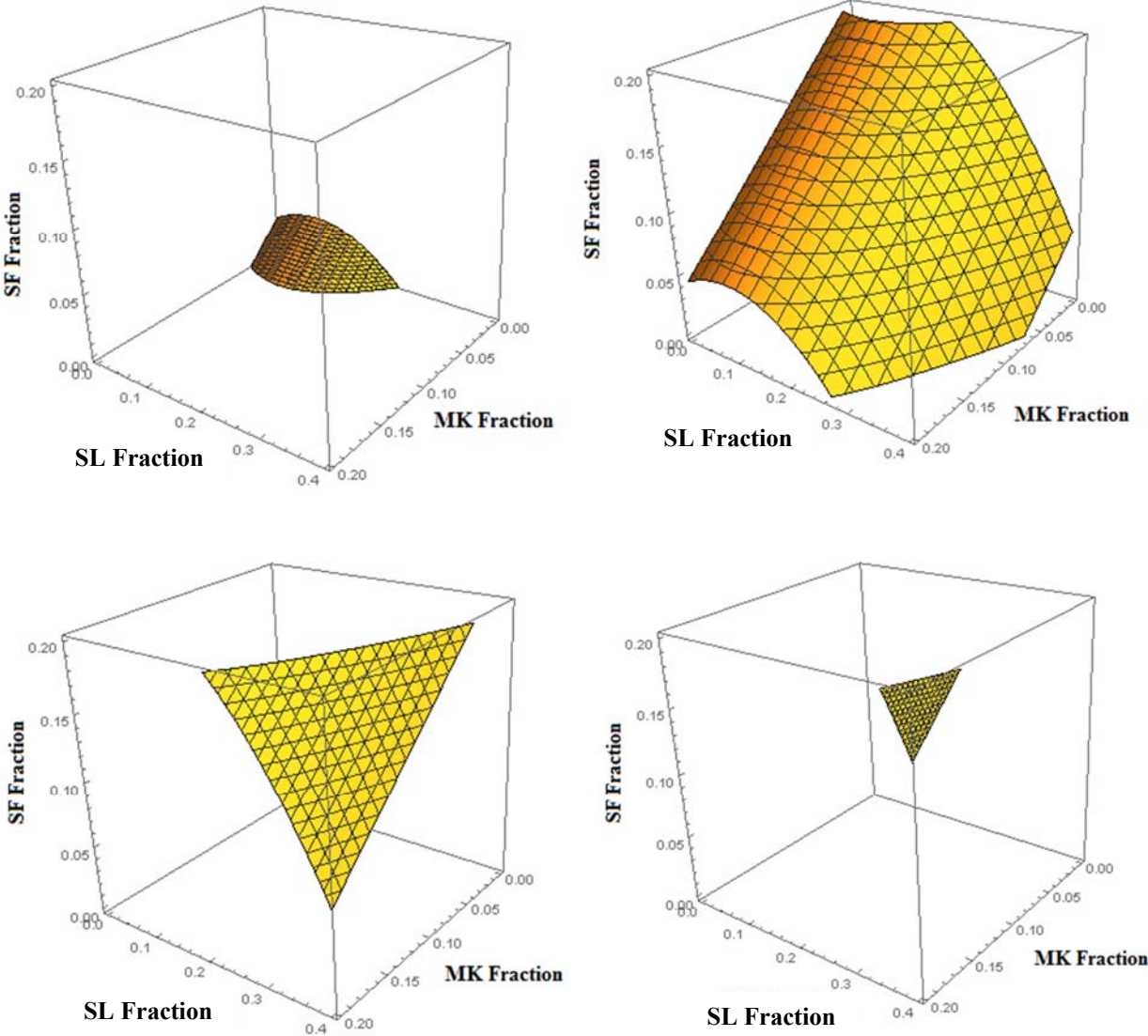


Figure 5.5. Contour plot of the total heat reduction with the change in MK, SL and SF content using Equation 5.8. a) no change in cumulative heat evolved compared to the plain OPC-water mixture, b) 20% cumulative heat reduction, c) 40% cumulative heat reduction, d) 50% cumulative heat reduction.

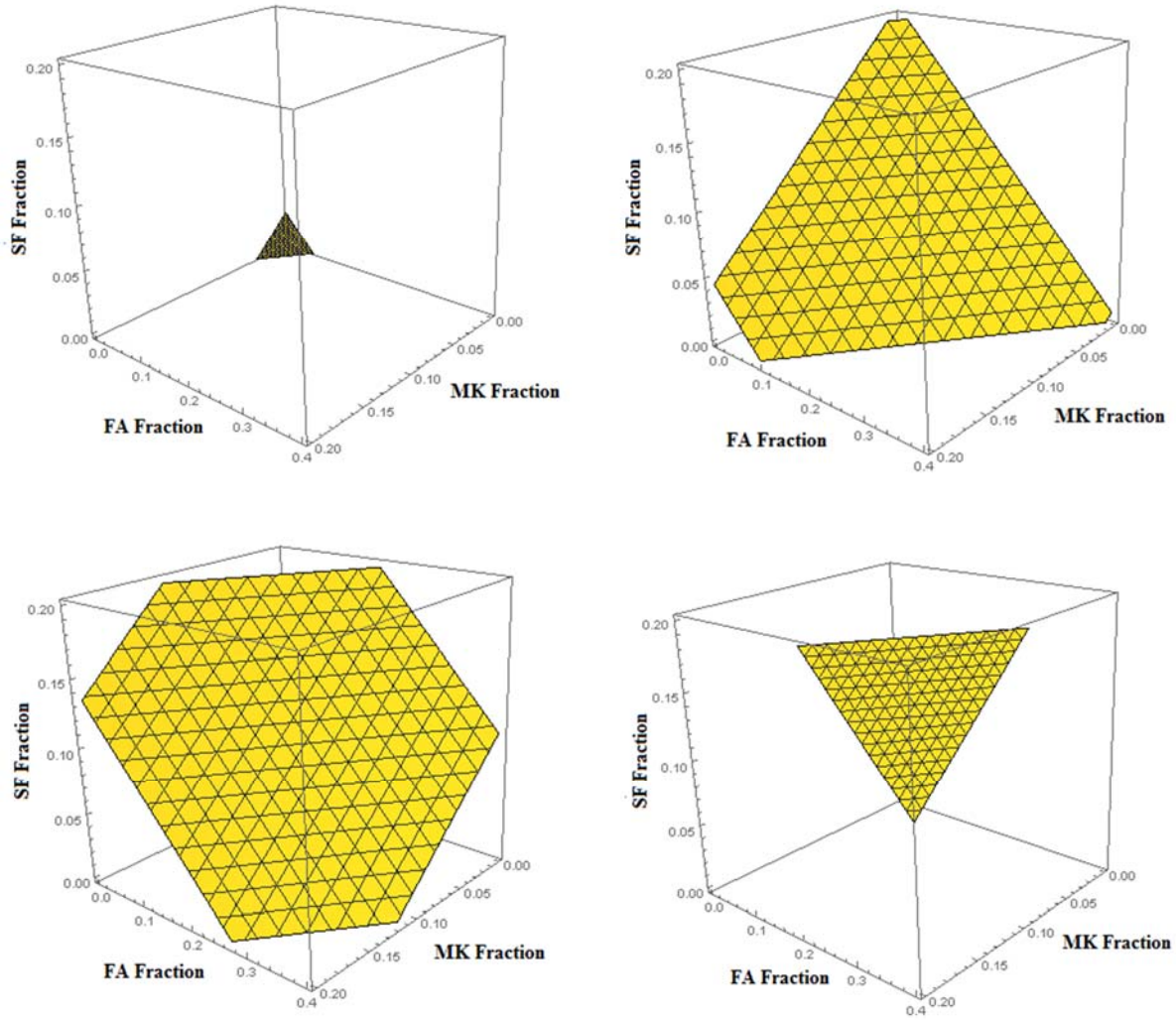


Figure 5.6. Contour plot of the total heat reduction with the change in MK, FA and SF content using Equation 5.8. a) no change in cumulative heat evolved compared to the plain OPC-water mixture, b) 20% cumulative heat reduction, c) 30% cumulative heat reduction, d) 50% cumulative heat reduction.

5.3.2 Model Validation

The model presented in Equation 5.8 was validated by comparing heat reduction measured experimentally against the predicted values. The majority of the values lie within the 95% confidence interval (Figure 5.7). Additionally, the data is evenly distributed around the line of fit, which indicates that there is no consistent bias in the model. Identical plot was obtained for

Equation 5.7 as this equation can be converted to Equation 5.8 by substituting Equations 5.2 and 5.3 for the appropriated coded variables.

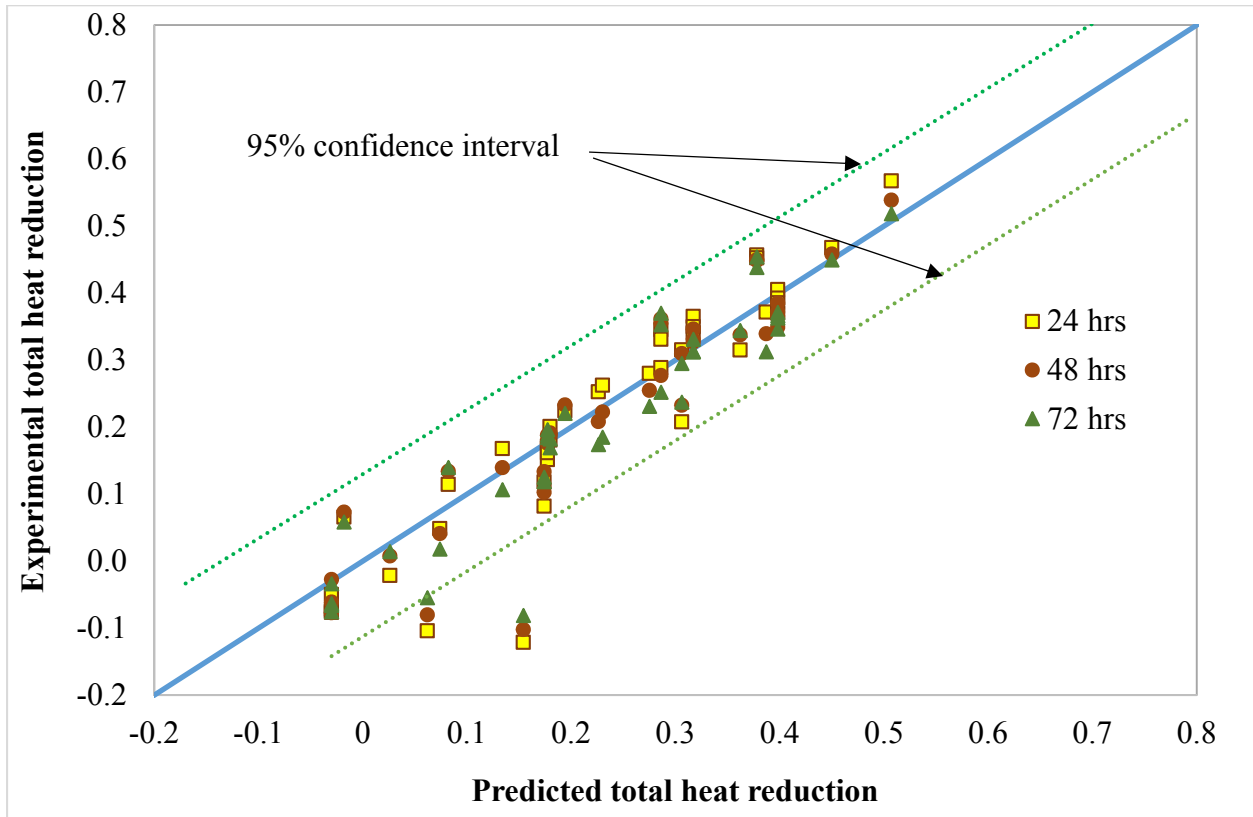


Figure 5.7. Measured versus predicted total heat reduction calculated using Equation 5.8

5.4 Conclusions

Statistical analysis of isothermal calorimetry data indicated that chemical admixtures do not have a significant effect on heat evolution beyond the hydration age of 12 hours. SCMs investigated in this study (FA, SL, SF and MK), on the other hand, were found to have a significant effect at hydration ages of 12, 24, 48 and 72 hours. While the effect of FA, SF and MK on the total heat reduction with increasing cement replacement appeared to be linear, the effect of SL was quadratic. The models proposed in this study were successful in predicting the total heat reduction with incorporation of chemical admixtures and SCMs compared to a plain OPC mixture. Since the proposed models predict the fraction of cumulative heat reduction compared to a plain OPC-

water mixture, only one isothermal calorimetry measurement needs to be carried out. These models will allow practitioners to estimate heat reduction with the use of different SCM/chemical admixture combinations while avoiding multiple experimental testing.

CHAPTER 6: MULTI-TECHNIQUE INVESTIGATION OF METAKAOLIN AND SLAG BLENDED PORTLAND CEMENT PASTES⁵

6.1 Introduction

Metakaolin (MK) is a relatively new supplementary cementitious material (SCM) that has been introduced in the 1990s [210]. MK is a pozzolanic material obtained by subjecting kaolin clay to heat treatment (calcination) at 500-800°C. Upon heating, kaolinite ($\text{SiO}_2 \cdot 2\text{Al}_2\text{O}_3 \cdot 2\text{H}_2\text{O}$) is dehydroxylated and transformed into a more disordered metakaolin phase [211]. MK generally consists of 50% SiO_2 and 40% Al_2O_3 , although its exact composition varies depending on the source of kaolin clay [211]–[214]. Incorporation of MK into concrete has been gaining popularity due to the increase in early compressive strength and reduced permeability [215]–[218]. MK is typically added to concrete at cement replacement level of 10% in order to maximize compressive strength [182], [219], [220]. It has been established that maximum contribution of MK to compressive strength occurs at approximately 14 days, after which the pozzolanic reaction of MK slows down [210], [221]. Therefore, early-age properties of the OPC/MK mixtures are of particular interest in studying the effect of MK.

While the effect of metakaolin on hardened concrete properties has been the topic of a large number of studies, its effect on paste microstructure has not been explored in as much detail. Incorporation of MK is known to alter the chemical composition of C-S-H [182], [222], which is the main hydration product and is primarily responsible for concrete compressive strength. This

⁵ This chapter has been submitted as a manuscript to the Applied Clay Science Journal and is currently under review.

change in C-S-H composition implies a possible change in its microstructure and mechanical response. Recently, Rodriguez et al. [223] demonstrated that C-S-H morphology changes from fibrillar to foil-like as Ca/Si ratio decreased from 1.63 to 1.33. Several molecular simulations showed a change in mechanical properties of C-S-H with the change in Ca/Si ratio [99]–[101].

Nanoindentation has been extensively used to ascertain mechanical properties of C-S-H, which is the main hydration product and is primarily responsible for concrete compressive strength. It has been established that the mechanical response of C-S-H depends on the packing density of C-S-H globules [224]–[227]. Values of elastic moduli have been published for a number of C-S-H morphologies, which are summarized in Table 6.1. It can be seen that there exists a very porous phase, the elastic modulus of which is affected by capillary porosity [224], [228], [229], with a modulus of approximately 8-13 GPa, low-density or outer product C-S-H with an elastic modulus \approx 21 GPa, high-density or inner product C-S-H with a modulus \approx 30 GPa, and CH or a mixture of C-S-H and CH also referred to as ultra-high-density C-S-H with a modulus 36-40 GPa.

While nanoindentation has been applied to C₃S and OPC pastes, there are few studies on nanoindentation of OPC/MK samples. He et al. [230] investigated the effect of SCMs, including MK, on the elastic moduli of the hydration products and the volume fractions of LD and HD C-S-H. Samples containing SCMs were prepared with a water to binder (w/b) ratio of 0.3, while the control sample had a w/b ratio of 0.35 in order to obtain similar 28-day compressive strengths. The authors reported that at the age of 60 days the control sample had the smallest fraction of HD C-S-H, while for the samples containing SCMs the HD C-S-H fraction appeared to increase with an increase in the molar fraction of (Al+Si)/Ca in the OPC-SCM blend. However, the control sample did not fit this relationship, possibly due to a difference in the w/b ratio. The authors concluded that the (Al+Si)/Ca ratio can be used in place of nanoindentation tests for cementitious

mixtures with the same w/b ratio and similar 28-day compressive strengths in order to predict the fraction of HD C-S-H. Only two types of C-S-H, LD and HD, were observed in this study, with no significant difference in their values regardless of SCM addition.

Barbhuiya and Chow [231] reported nanoindentation modulus and hardness values for PC and PC+10%MK pastes. The calculated volume fractions of LD and HD C-S-H ($\approx 36\%$ each) in the PC+10%MK sample were only slightly higher than those of the PC sample ($\approx 33\%$ for each). However, the age or degree of hydration of the samples was not reported, and it remains unclear whether these results are indicative of early-age or later-age characteristics on the MK-containing pastes.

Table 6.1. Summary of published elastic moduli values for C-S-H and CH

Phase	Mean \pm Standard Deviation (GPa)	Reference
Low stiffness phase	8.1	[224]
Porous phase	9.4 ± 3.4	[228]
Very porous (VP) C-S-H	13.6 ± 1.0	[229]
Low stiffness C-S-H	16.5 ± 4.7 22.89 ± 0.76	[228] [232]
Low-density (LD) C-S-H	18.2 ± 4.2 21.7 ± 2.2 22.39 ± 4.84 22.5 ± 5.0	[224] [233] [234] [235]
Outer product (OP) C-S-H	20.8 ± 3.2	[229]
Medium stiffness C-S-H	31.16 ± 2.51	[232]
High stiffness C-S-H	27.1 ± 3.5 41.45 ± 1.75	[228] [232]
High-density (HD) C-S-H	29.1 ± 4.0 29.4 ± 2.4 30.4 ± 2.9 34.82 ± 5.25	[224] [233] [235] [234]
Inner product (IP) C-S-H	31.0 ± 3.1	[229]
Ultra-high-density (UHD) C-S-H	40.9 ± 7.7	[235]
CH	40.3 ± 4.2 36.9 ± 3.5 38 ± 5.0 $39.77-44.89$	[224] [228] [233] [236]

In addition to a change in C-S-H composition, a change in porosity with MK addition has been reported as well. Ambroise et al. [182] reported an increased amount of pores in the 6-20 nm range with 20-30% MK addition. Poon et al. [220] also reported that addition of metakaolin at a constant w/cm ratio decreases the average pore diameter for any age and at any cement replacement level up to 20%.

The effect of chemical and mineral admixtures on pore size distribution is of great interest as pores of different sizes will have an impact on different concrete properties. Juenger and Jennings [22] observed that an increase in the nitrogen accessible pore volume and surface area corresponded to increased drying shrinkage. Jennings et al. [237] also state that creep is affected by gel porosity.

Porosity of the OPC/MK mixtures has been predominantly studied using mercury intrusion porosimetry (MIP) [182], [215], [216], [220], [238], [239]. Although MIP can measure a wide range of pore sizes from approximately 2 nm to 100 μm [142], this technique measures the pore entry sizes rather than actual pore diameters. Nitrogen (N_2) adsorption is another technique that can be used to measure porosity although it is limited to the 1.5-40 nm range. However, unlike MIP, it is not affected by pore network effects when the adsorption branch is used [142]. Only one study [240] to date has been published that utilized nitrogen adsorption to measure porosity of the OPC/MK samples. However, the authors reported only percent of total pore volume for pores less than 10 nm, 10-20 nm and greater than 20 nm diameters, which provides limited information on how pore size distributions compare between plain OPC samples and those containing MK. No information was found on the effect of SL incorporation on porosity as measured by N_2 adsorption.

The goal of this study was to investigate the effect of cement replacement with 10%MK on hydration products, nanoindentation characteristics and porosity at the age of 7 days and

compare the effect of MK to that of SL as well as to the plain OPC paste at ambient temperature. Additionally, since nanoindentation modulus depends on C-S-H packing density and packing density determines C-S-H porosity, a possible relationship between nanoindentation modulus and porosity was investigated as well.

6.2 Experimental Procedures

6.2.1 Materials

A Type I/II commercial Portland cement and two SCMs, metakaolin (MK) and blast furnace slag (SL) were selected for this study. Additionally, four chemical admixtures that are commonly used in structural concrete mixtures, air-entraining admixture (AEA), water-reducing and retarding admixture (WRRRA) and two superplasticizers (SP), were used. According to the manufacturer's safety data sheets, WRRRA was lignosulfonate-based and both SP1 and SP2 were polyacrylate-based with SP1 being more concentrated. In the field, SP1 is used in concrete containing MK, while SP2 is used with SL. Since MK is expected to be finer than SL, a more concentrated SP is needed to achieve proper particle dispersion with the incorporation of MK.

6.2.2 Methodology

6.2.2.1 Isothermal Calorimetry

Table 6.2 lists mixture designs used in this study. A constant w/cm ratio of 0.485 was used for all the mixtures taking into account the water added as part of the chemical admixtures. Heat of hydration of the mixtures was measured using TAM Air 8-twin channel isothermal calorimeter manufactured by TA Instruments. The measurements were performed at 23°C following the ASTM C1702 Method A, internal mixing.

Table 6.2. Mixture proportions

Sample	Mineral Admixture	Mineral Admixture (% Cement Replacement)	WRA Dosage	AEA Dosage	SP2 Dosage	SP1 Dosage
			(ml/100 kg cementitious)			
CN+SP1	None	0	110	2.5	0	155
10MK	Metakaolin	10	110	2.5	0	155
52SL	Blast Furnace Slag	52	110	2.5	110	0

The degree of hydration, $\alpha(t)$, for each mixture was calculated based on isothermal calorimetry measurements. $\alpha(t)$ was calculated following Equation 6.1:

$$\alpha(t) = \frac{H(t)}{H_u} \quad \text{Equation 6.1}$$

where $H(t)$ is the total heat released by each mixture at time (t) and H_u is the total available heat that can be generated by the cementitious components of the mixture. For pastes without SCMs, $H_u = H_{cem}$.

$$H_{cem} = 500P_{C3S} + 260P_{C2S} + 866P_{C3A} + 420P_{C4AF} + 624P_{SO3} + 1186P_{FreeCaO} + 850P_{MgO} \quad \text{Equation 6.2}$$

where H_{cem} is the total heat of hydration of portland cement and P_i is the mass of i^{th} component to total cement content ratio. For the 52SL sample, H_u was calculated using the equation provided by [26], but eliminating the fly ash contribution:

$$H_u = H_{cem} P_{cem} + 461 P_{slag} \quad \text{Equation 6.3}$$

The current models proposed in the literature to predict hydration behavior of OPC/SCM systems [26]–[28] do not include metakaolin. The only guidance regarding the HOH of MK mixtures comes from Gajda [29] who states that it can be approximated as “100% to 125% that of Portland cement.” For the 10MK mix, H_u was calculated using the upper limit proposed by Gajda [29]:

$$H_u = H_{cem} P_{cem} + 1.25 H_{cem} P_{MK} \quad \text{Equation 6.4}$$

There is no mention of the effect of chemical admixtures on H_u in [26]. Therefore, it was assumed in this study that chemical admixtures do not affect the ultimate heat of hydration.

6.2.2.2 Sample Preparation for X-Ray Diffraction, Nanoindentation and Nitrogen

Adsorption

Samples were mixed using the IKA WERKE mixer. The WRRRA was added to the mixing water; AEA was introduced after mixing for 1 minute at 300 rpm, which was followed by 30 seconds of mixing at 600 rpm. Superplasticizer (SP1 or SP2) was added after a 90 second rest period, after which the paste was mixed for an additional 60 seconds at 600 rpm. After mixing, paste samples were sealed and cured under isothermal conditions at 23°C.

6.2.2.3 X-Ray Diffraction and Rietveld Analysis

For x-ray diffraction (XRD), demolded samples were ground by hand with an agate mortar and pestle. Paste samples were mixed with a standard reference material, (SRM) 676a, obtained from the National Institute of Standards and Technology (NIST). SRM 676a was used as an internal standard (IS) at 20% replacement in order to determine the amorphous unidentified content of each sample [241], [242]. SRM 676a was mixed with the paste by hand with the mortar and pestle to in order to avoid increasing the amorphous content of paste during grinding [243]–[245]. No specific technique was used to stop the hydration, as samples were prepared immediately after demolding and loaded into the diffractometer.

XRD measurements were performed using the Phillips X'Pert PW3040 Pro diffractometer equipped with the X'Celerator Scientific detector and a Cu-K α x-ray source ($\lambda=1.540598 \text{ \AA}$). Tension and current were set to 45 kV and 40 mA respectively. Scans were performed in the range of 7 - 70° 2 θ , with a step size of 0.0167° 2 θ and counting time per step was 130.2. 5 mm divergence and anti-scatter slits were used in the automatic mode. Samples were loaded into the sample holder

using a back-loading technique in order to minimize preferred orientation, and placed onto a spinner stage that was rotating at 30 rpm in order to improve counting statistics [246]. Mineralogical analysis of the collected diffraction patterns was carried out using Panalytical HighScore Plus 3.0 software. Quantification was performed using the Rietveld refinement functionality built into the software.

6.2.2.4 Nitrogen Adsorption

Samples for porosity measurement by nitrogen adsorption were mixed and cured as described in section 2.2.2 until the age of 7 days at 23°C. Immediately after demolding, the samples were crushed and sieved to separate the particles in the range of 1-3 mm, and dried at 105°C under vacuum for 2 hours using the outgasser built into Autosorb-1 analyzer manufactured by Quantachrome Instruments. This drying procedure was selected as drying at a lower temperature may accelerate the hydration process [88] and is not suitable at early ages. Slow removal of water by procedures such as D-drying does not quickly arrest the hydration [142]. Drying at 105°C was limited to 2 hours to avoid damaging the C-S-H microstructure, which is typically a concern with drying at this temperature for 24 hours [247]. Beaudoin [89] suggests that limiting oven-drying at 105°C to 2-3 hours results in a microstructure that is similar to D-drying, which would be most suitable for nitrogen adsorption. In this work, samples were dried for 2 hours, after which nitrogen isotherms were collected using Autosorb-1.

Pore size distribution calculations were performed using the Barrett, Joyner, Halenda (BJH) method [248], adsorption branch. Since the adsorption branch measures the size of the interior of the pore it was selected over the desorption branch, which measures the pore entry size [93], [94]. Additionally, the adsorption branch is not influenced by the pore network effects to the

same degree as the desorption branch [93], [95]. Brunauer, Emmett, Teller (BET) method [141] was used to calculate specific surface area, which is typically attributed to C-S-H [249].

6.2.2.5 Nanoindentation

Nanoindentation samples were demolded at the age of 7 days, crushed and placed in isopropanol for 48 hours to stop hydration. After 48 hours, the samples were dried under vacuum and cast in SPECIFIX-40 two part epoxy from Struers. Samples were polished using MD-Piano series polishing discs #200, 500, 1200, followed by diamond suspensions of 3, 1, and 0.25 μm . The diamond suspensions were used with MD-Dur polishing cloths. As a final step, the samples were polished with 0.5 alumina powder suspension on an MD-Nap polishing cloth. Samples were washed in ethanol in an ultrasonic bath for 10 minutes between each polishing step.

Indentation measurements were performed using the Hysitron Ti 900 Triboindenter with a Berkovich tip. A trapezoidal loading function was used with a 5 second loading time, 3 second hold period and a 5 second unloading period and a maximum load (P_{max}) of 2 mN. Instrument compliance and tip area function calibrations were performed using a fused quartz standard prior to sample measurements. A minimum of 50 points were indented for each sample. Constantinides and Ulm [224] showed that 50 nanoindentation points were sufficient to identify correct volume fractions of HD and LD C-S-H and no further improvement was achieved by increasing the number of indentations. Points were indented in a grid of 10x10 points, spaced 20 μm apart.

The data were analyzed based on the Oliver and Pharr method [250] using the TriboScan 6.0 software. After analyzing the indentation results, the data was normalized by the number of indents in each sample and deconvoluted to obtain the modulus of individual phases as described in [251].

6.3 Results and Discussion

6.3.1 Isothermal Calorimetry

The degree of hydration for each of the paste samples obtained from isothermal calorimetry was calculated at the age of 7 days using Equations 6.1-6.4 and is listed in Table 6.3. Total heat evolution used for calculating the degree of hydration are presented in Figure 6.1. As expected, the higher substitution of cement by slag shows the lowest total heat at 7 days of hydration while the total heat for 10MK and CN are similar.

Table 6.3. Degree of hydration calculated from isothermal calorimetry at 7 days

Mix ID	Degree of Hydration
CN+ SP1	0.72
10MK	0.68
52SL	0.46

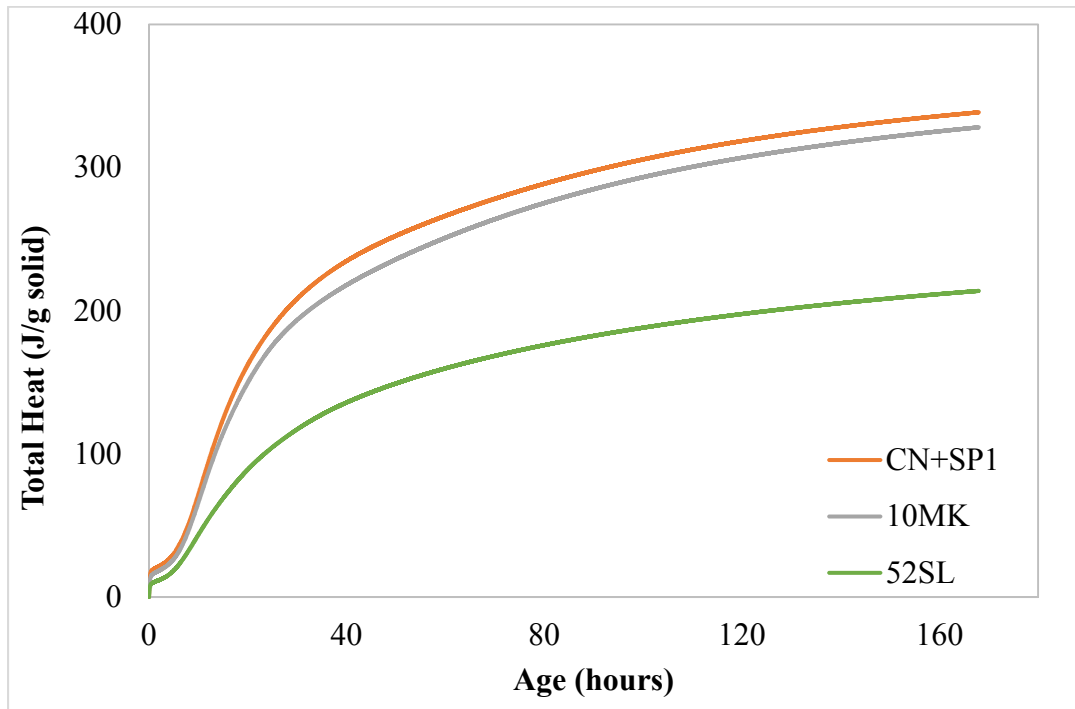


Figure 6.1. Total heat of hydration

6.3.2 Hydration Products

The main hydration phases identified in the control sample at the age of 7 days were CH, ettringite and hemicarboaluminate (Table 6.4). The presence of hemicarboaluminate is attributed to the reaction of C₃A and CH with limestone, which was present in the cement used in this study. Examination of the as-received cement revealed the presence of 2.0% calcite, which is consistent with the limestone addition reported on the mill certificate for this cement. Limestone powder has been reported to react with C₃A during cement hydration forming hemicarboaluminate (C₄AC_{0.5}H₁₂) and with C₃A and CH forming monocarboaluminate (C₄A_{CH}₁₁) as shown by [252].

Table 6.4. Rietveld analysis of the pastes at the age of 7 days

Phase	ICSD #	CN+SP1	10MK	52SL
Alite	94742	2.0	1.4	0.1
Belite	81096	13.9	13.3	6.0
C ₃ A	1841	1.6	1.3	0.0
C ₄ AF	9197	3.0	1.7	0.0
Portlandite	15471	12.9	8.0	4.2
Quartz	41414	0.8	0.4	0.8
Calcite	80869	1.0	0.9	0.6
Ettringite	155395	8.6	6.6	3.1
Tobermorite 9A	87689	1.0	1.5	2.8
Hemicarboaluminate	263124	2.8	4.0	3.8
Monocarboaluminate	59327	0.4		
0.8-Carboaluminate	263123	0.2		
Amorphous/Unidentified		51.8	61.1	78.3

There are a number of publications detailing the hydration products in the OPC/MK systems [253]–[256]. However, these studies have not attempted to quantify hydration phases, therefore, our results can only be compared qualitatively. In the current study, only hemicarboaluminate was identified in the 10MK sample as opposed to the results obtained by Antoni et al. [253], who reported the presence of both hemi- and monocarboaluminate, most likely due to significantly lower CaCO₃ content in the as-received cement (2.1%) compared to that used

by [253] (15%). Strätlingite was not present in 10MK sample, which is more in line with Antoni's [253] results for the 30%MK with no limestone. The broad diffused peak observed by [253] in the 30%MK with no LS sample was also present in the 9-10° 2 θ region in the 10MK sample in this study and was followed by a hemicarboaluminate peak. A small tobermorite peak was also found in this area. The fitted pattern generated by Rietveld refinement with the inclusion of these phases (ettringite, tobermorite, monosulfoaluminate and hemicarboaluminate) did not completely fit the collected XRD pattern. It is possible that inclusion of some other calcium aluminate hydrate as suggested by Cassagnabère et al. [255] would improve the fit in this region.

Addition of mineral admixtures did not appear to change the main hydration products. Generally, no significant effect on phase consumption (Table 6.5) was observed with addition of mineral admixtures, except in the case of 52SL, where consumption of all phases was increased, likely due to the small amount of cement present in this mixture and a much higher effective w/c ratio.

Table 6.5. Consumption of individual clinker phases at the age of 7 days

Phase	CN+SP1	10MK	52SL
C ₃ S	0.94	0.95	0.99
C ₃ A	0.75	0.78	1
C ₄ AF	0.44	0.65	1

6.3.3 Porosity Measurement with Nitrogen Adsorption

Nitrogen-accessible porosity increased with addition of MK and SL (Figures 6.2 and 6.3). This can be attributed to two factors: lower degree of hydration and changes in porosity of C-S-H. While the degree of hydration (Table 6.3) of the 52SL sample is significantly lower than that of CN+SP1 and a higher amount of LD C-S-H is expected at lower degrees of hydration, the degree of hydration of 10MK and CN+SP1 are similar, so the observed differences in the pore size

distributions in the 1.5-10 nm range of CN+SP1 and 10MK samples are likely due to the changes in the porosity of C-S-H, possibly due to the changes in its chemical composition.

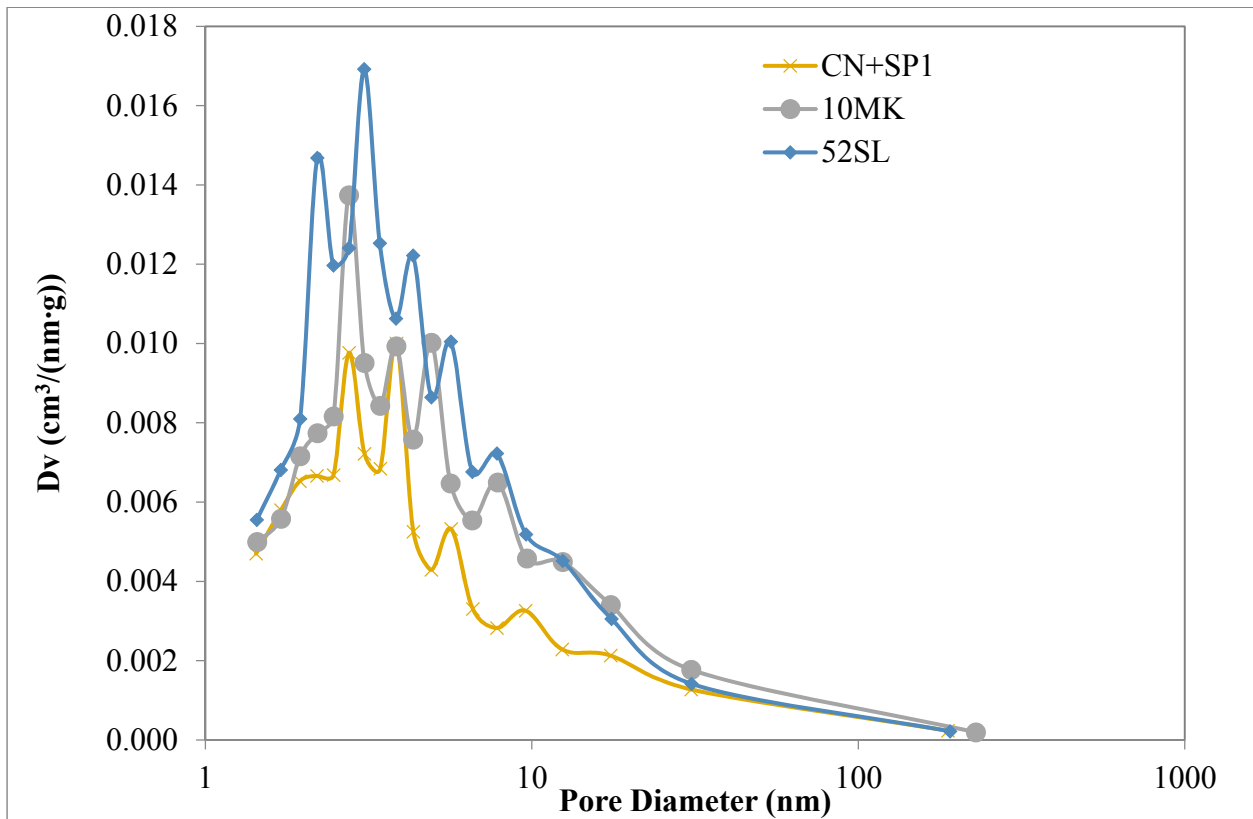


Figure 6.2. BJH pore size distribution at 7 days

It is difficult to compare these results to previous studies, as the study by Justice and Kurtis [240], who used N₂ adsorption to measure porosity, reported % pore volumes rather than actual volumes for pore diameters below 10 nm, 10-20 nm and above 20 nm at 1 and 28 days. The rest of the studies utilized MIP, reporting the total pore volume and break through diameters, which cannot be related to the N₂ adsorption data. Even so, the results are contradictory. Poon [215], [220] and Duan et al. [216] reported lower total porosity compared to the control in 10%MK mixtures at 7 days, while Khatib and Wild [238] observed an increase in the total pore volume at 7 days with 10% cement replacement with MK. Additionally, Khatib and Wild [238] reported that the percentage of pores with radii less than 20nm was greater in the 10%MK sample than in the

control at all ages, while the amount of pores with radii greater than 20 nm was always lower. Since N₂ adsorption is limited to the 1.5-40 nm diameter range, the higher total pore volume of the 10MK sample compared to the control is in agreement with the findings by [238].

Several pore size classifications have been proposed for concrete [142]. In this study, CM-II model [104] was predominantly used to separate pore size distribution into specific pore volumes. The CM-II model distinguishes two types of C-S-H pores: small gel pores (SGP) representing the space within C-S-H particles and large gel pores (LGP) between the C-S-H particles. It estimates the size of SGPs to be below 3 nm, and the size of LGPs to be in the range of 3-12 nm. Recent NMR study reported 10 nm pores between C-S-H particles [257]. Others [258] report clustering of pores around the following average values: 1.8, 7, 50 and 600 nm. The authors attributed 1.8 nm pores to the pores inside C-S-H (SGP pores proposed by Jennings [104]) and 7 nm pores to the pores between C-S-H particles. Reconciling these studies as well as the pore size classification proposed by Mindess et al. [7], pore size distributions of the samples analyzed in this study were compared for the following pore ranges: < 3nm (SGP pores), 3-10 nm (LGP pores) and > 10 nm (fraction of capillary pores measured by N₂ sorption) (Figure 6.3).

No significant differences were observed in the SGP pore volumes of the samples (Figure 6.3). The LGP porosity, however, increased with addition of SCMs and was the highest for the 52SL sample. This indicates that 52SL paste had the highest LD/HD C-S-H ratio, which could be attributed to the lower degree of hydration of this sample. Although lower than that of 52SL, the LD/HD ratio for the 10MK sample was also notably higher than that of the control paste, in spite of their similar degree of hydration.

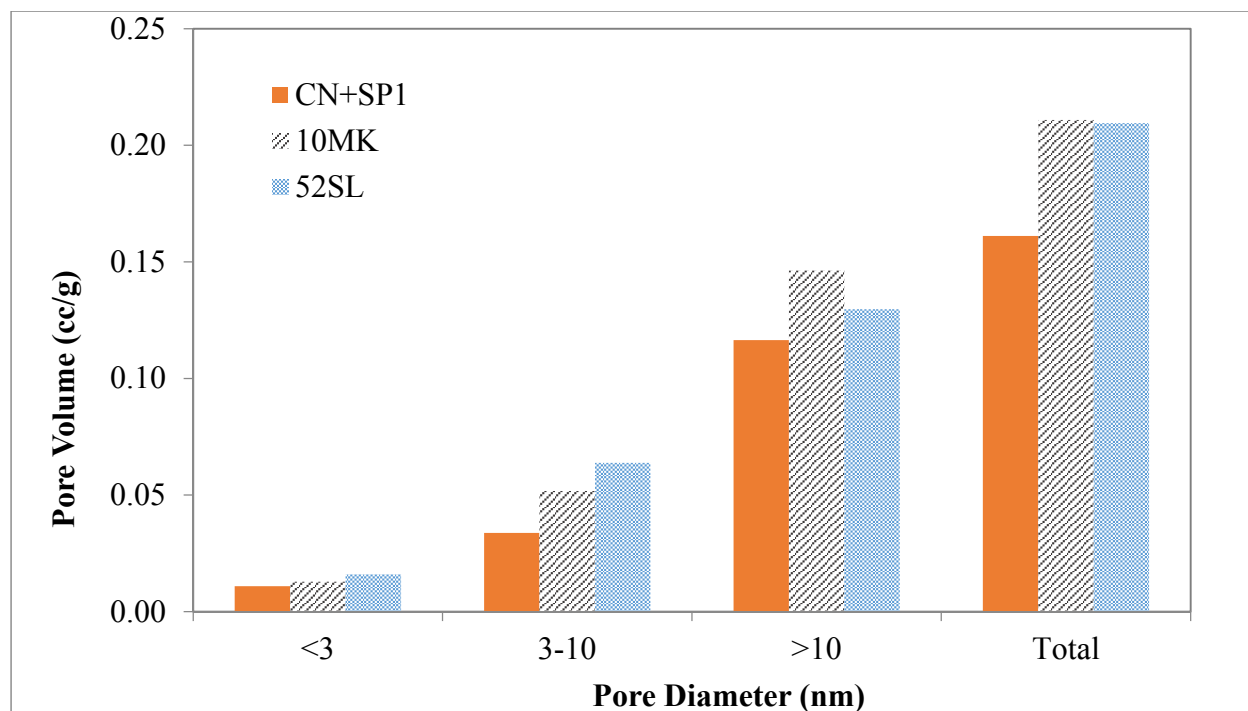


Figure 6.3. BJH pore volumes for each paste sample at 7 days

BET predominantly measures porosity of C-S-H, and there is a general agreement in the literature that N₂ molecules can enter the pores of low-density (LD) C-S-H, but only a small fraction of the high-density (HD) C-S-H porosity, while water can enter the pores of both LD and HD C-S-H [104], [259], [260]. Jennings and Thomas [260] state that because of this, N₂ BET surface areas are much more sensitive to the microstructural differences than those obtained with water vapor. As with the pore size distribution, the highest BET surface area was observed for the 52SL sample followed by 10MK (Table 6.6). Surface area of the control sample was significantly lower implying a presence of less porous C-S-H. The ration of LD/HD C-S-H is known to affect shrinkage and creep of concrete [70].

Table 6.6. BET surface areas at 7 days

Mix ID	5-point BET Surface Area (m ² /g)
CN+ SP1	53.35
10MK	72.18
52SL	86.37

6.3.4 Nanoindentation

The results obtained from grid indentation were used to calculate the average elastic modulus, hardness and average maximum depth of penetration (h_{max}) for each sample. First, the average E , H and h_{max} were calculated based on the data obtained from all the indents, which would include both the hydration products and the unhydrated clinker phases (Table 6.7). The average maximum penetrations depths are very similar and indicate that the majority of the indents were made in the C-S-H phase [225]. However, large differences can be observed between the average elastic moduli and average hardness values for these samples. The CN+SP1 sample had the highest elastic modulus, followed by 52SL, and 10MK sample had the lowest. The average hardness of the 10MK sample was also significantly lower than that of the other samples.

The elastic modulus of individual clinker phases is known to be significantly higher than that of hydration products [261]. Despite a large difference in the degree of hydration of 10MK and 52SL samples (Table 6.3), their average elastic moduli are similar, while there is a large difference in the E values for 10MK and CN+SP1 samples in spite of their similar degree of hydration. This indicates that the average E values in Table 6.7 are heavily influenced by the presence of unhydrated clinker phases and may not be the best way to evaluate the mechanical properties of the hydrated paste.

Table 6.7. Average nanoindentation values

Sample	Average E (GPa)	Average H (GPa)	Average h_{max} (nm)
10MK	19.7	0.5	323
CN+SP1	30.1	1.2	294
52SL	23.0	1.4	323

In order to evaluate the influence of MK and SL addition on the average mechanical properties of the hydration products and eliminate the effect of the large difference in the degree of hydration, the average E , H , and h_{max} values were recalculated excluding indents with E greater

than 40 GPa (Table 6.8). A number of E and H values for C-S-H and CH have been reported in the literature by [229], [233], [236], [262]–[265]. Němeček et al. [266] reported a modulus of approximately 44 GPa for unreacted MK and 26 GPa for unreacted SL. Therefore, 40 GPa was selected as a cutoff point to ensure that all the possible C-S-H packing arrangements were included in the adjusted average values, but the unreacted MK, if any may be present in the 10MK sample, was excluded. Since the expected value for unreacted SL modulus was between those reported for LD and HP C-S-H, it could not be excluded. However, based on Figure 6.6 it appears that minimal number of indents were made in the unreacted SL particles and they are not expected to have a significant effect on the values calculated for the 52SL sample in Table 6.8.

Table 6.8. Adjusted average values after excluding indentations with E above 40 GPa

Sample	Average E (GPa)	Average H (GPa)	Average h_{\max} (nm)
CN+SP1	21.6	0.5	327
10MK	19.7	0.5	323
52SL	14.7	0.5	370

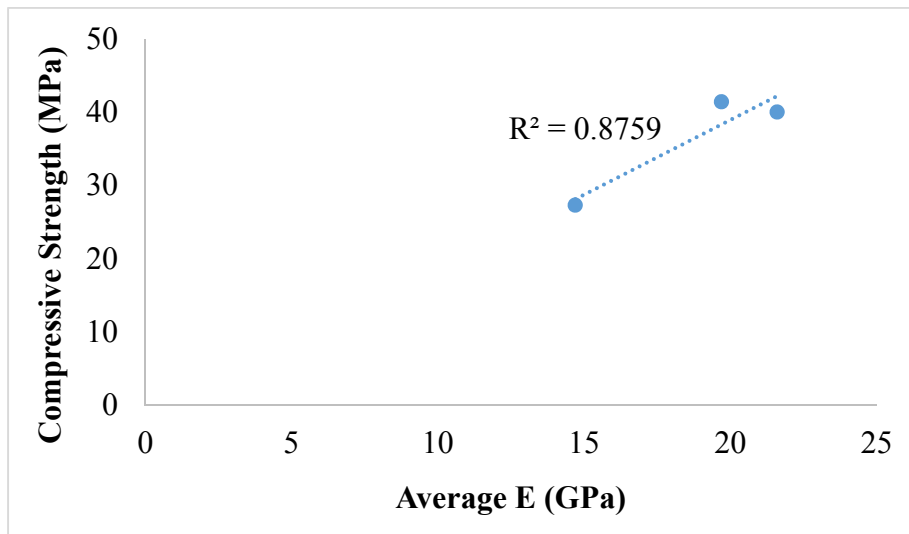


Figure 6.4. Relationship between compressive strength and average nanoindentation modulus of hydration products at 7 days

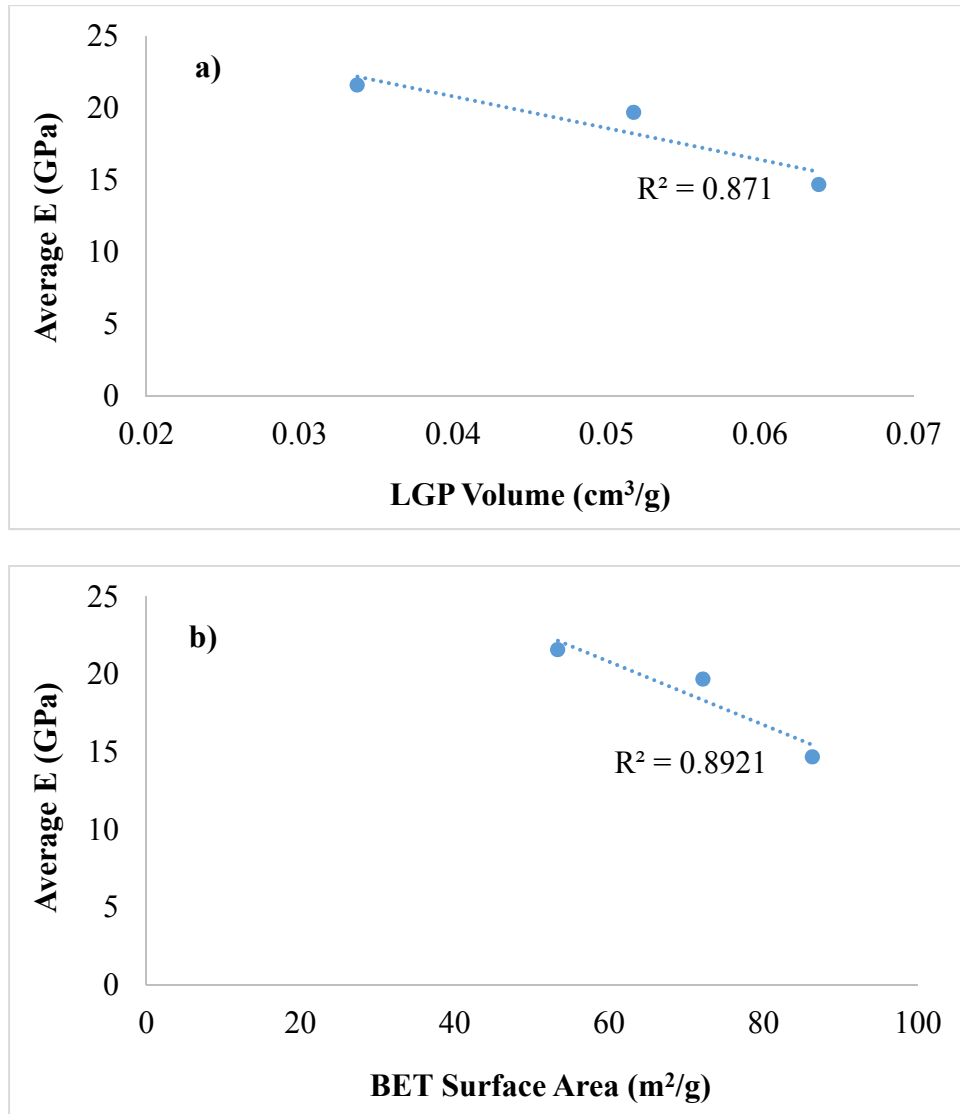


Figure 6.5. Relationship between a) LGP pore volume and b) BET surface area and average nanoindentation modulus of hydration products at 7 days

The adjusted average E values in Table 6.8 correlate with compressive strength results (Figure 6.4); compressive strength appears to increase with an increase in average elastic modulus computed for values below 40 GPa. Additionally, there is good agreement between the adjusted average E values and porosity results, specifically LGP pore volume; as the LGP volume increased, the adjusted average E decreased (Figure 6.5a). Same trend was observed with the BET surface area as well (Figure 6.5b).

Further analysis of nanoindentation data was carried out by plotting the probability distributions of the elastic moduli (below 40 GPa) for each sample as depicted in Figure 6.6. The results of the deconvolution analysis and the volume fractions of each phase are listed in Table 6.9. The obtained values of elastic moduli are in general agreement with the published literature (see Table 6.1).

The probability plot for the 10MK sample (Figure 6.6b) is significantly different from that of CN+SP1 (Figure 6.6a). While the control sample is showing presence of low stiffness, LD and HD C-S-H, the microstructure of the 10MK sample appears to be dominated by low stiffness C-S-H. A presence of a porous phase has also been identified in the 10MK sample. 52SL sample contained a significantly higher amount of the porous phase (Figure 6.6c), and C-S-H morphology was dominated by low stiffness C-S-H with very small amount of HD C-S-H present. Vandamme et al. [235] illustrated a relationship between w/c ratio and relative volumes of LD, HD and UHD C-S-H; as w/c ratio increases, so does the volume of LD C-S-H at the expense of HD C-S-H. The volume fractions of low stiffness-LD C-S-H observed in this study appears to be affected by the effective w/c ratios of the mixtures. Although the w/b ratio was maintained constant, the w/c ratio of the 52SL mixture was significantly higher, especially taking into account the low reactivity of SL compared to MK at 7 days.

There are no indents with elastic moduli in the CH range for the 52SL sample. The absence of clear indication of CH presence by nanoindentation is not surprising, as Rietveld refinement identified minimal amounts of CH compared to the other samples. Generally, the volume fraction of CH is in agreement with the XRD results (Figure 6.7). It appears that at 4 weight percent measured by XRD analysis, CH is difficult to detect with grid nanoindentation.

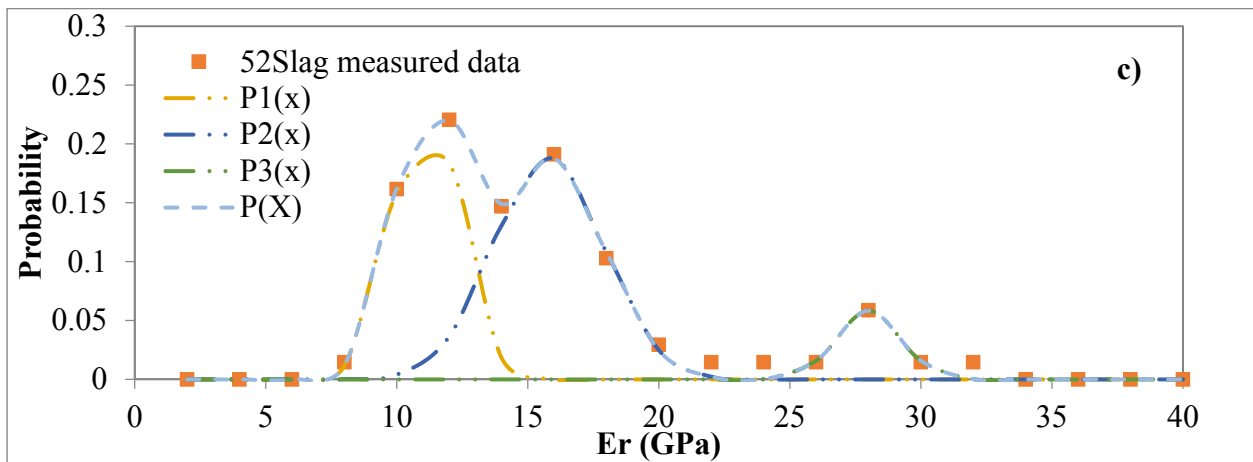
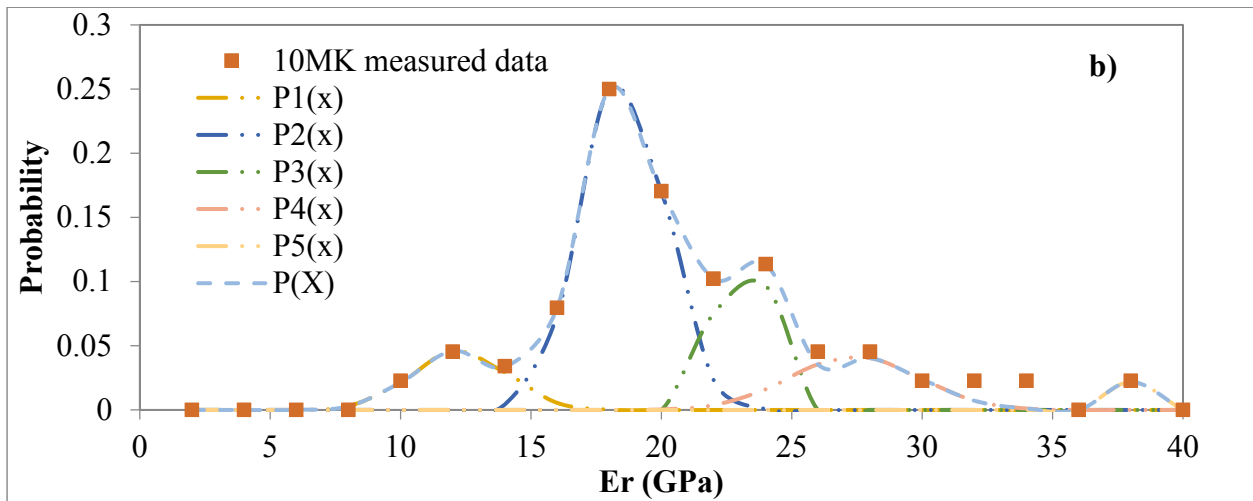
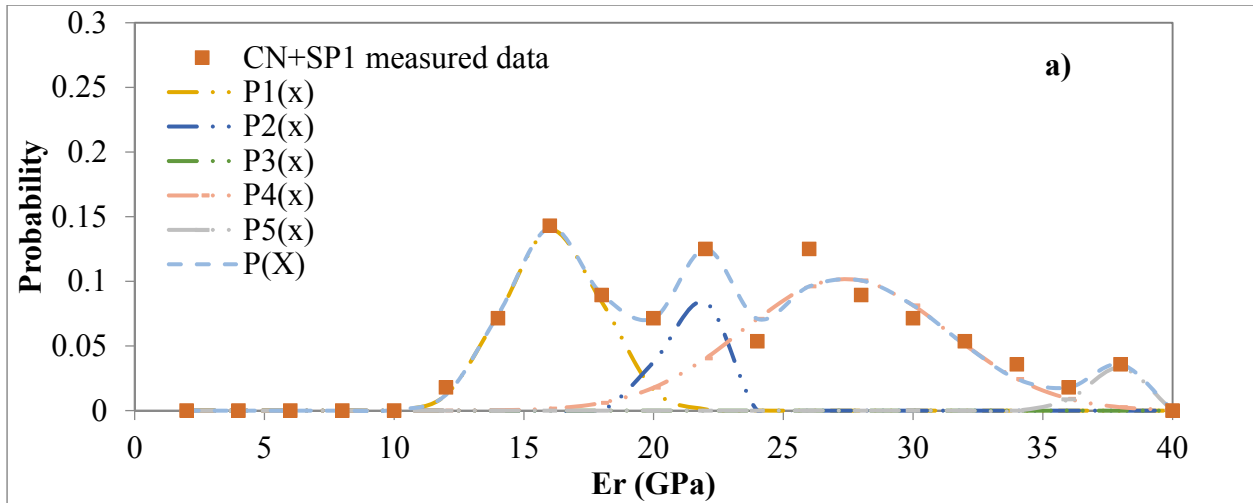


Figure 6.6. Probability density functions of a) control, b) 10MK and c) 52SL paste at 7 days

Table 6.9. Results of the deconvolution analysis

Sample	Phase	Mean \pm Standard Deviation (GPa)	Volume Fraction
CN+SP1	Low stiffness C-S-H	16.1 \pm 1.9	0.31
	LD C-S-H	21.1 \pm 0.6	0.17
	HD C-S-H	27.4 \pm 3.9	0.48
	CH	37.3 \pm 0.7	0.04
10MK	Porous phase	12.3 \pm 1.8	0.10
	Low stiffness C-S-H	18.5 \pm 1.6	0.48
	LD C-S-H	23.0 \pm 0.6	0.28
	HD C-S-H	27.4 \pm 2.5	0.12
	CH	38.3 \pm 0.1	0.02
52SL	Porous phase	11.1 \pm 1.3	0.39
	Low stiffness C-S-H	15.8 \pm 2.1	0.52
	HD C-S-H	28.00 \pm 1.2	0.09

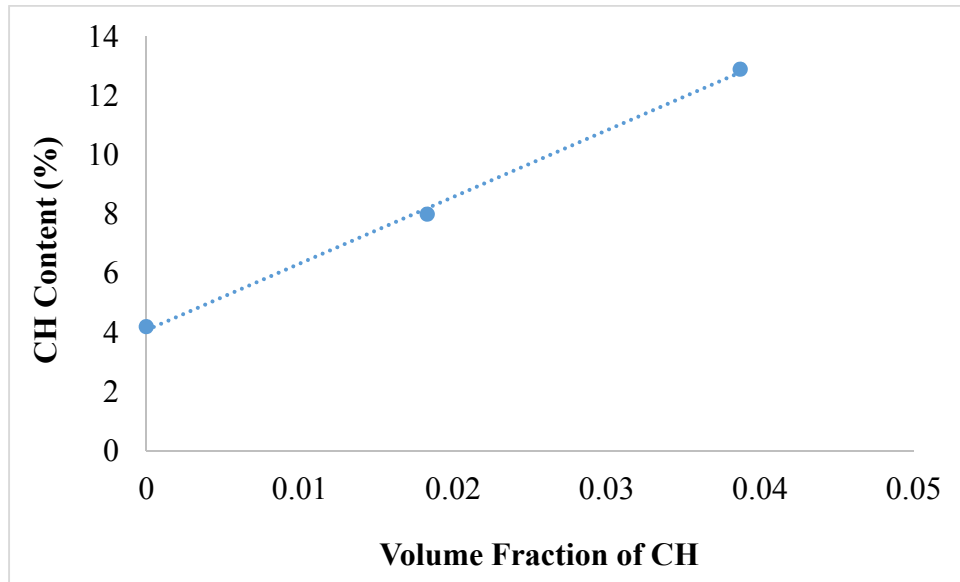


Figure 6.7. Relationship between volume fraction of CH obtained from nanoindentation and weight percent of CH calculated from XRD measurements

6.4 Conclusions

The following conclusions can be made based on the findings of this study:

- Generally, addition of chemical and mineral admixtures did not change the main hydration products for mixtures cured at 23°C. No significant differences in phase consumption were observed with addition of 10% metakaolin or 52% SL compared to the control paste at 7 days.
- Despite the similarity in phase consumption and the hydration products formed, nitrogen adsorption measurements indicated an increase in LGP volume with addition of 10% MK and 52% SL as well as increase in the fraction of capillary pores accessible by nitrogen adsorption technique.
- Nanoindentation measurements also indicated an increase in C-S-H porosity with 10% MK and 52% SL addition, the highest increase resulting from SL incorporation which is in agreement with nitrogen adsorption measurements.
- Additionally, a linear relationship was observed between the average elastic modulus of hydration products obtained from nanoindentation and the volume of LGP from N₂ adsorption. A linear relationship was also observed between the average elastic modulus and compressive strength.

The results indicate that phase quantification by QXRD of hydrated pastes may not be sufficient to assess the impact of metakaolin or SL addition on hydrating cementitious systems, and a multi-technique approach that provides information not only on the amount of hydration products, but also their morphology is preferable.

CHAPTER 7: CONCLUSIONS

The undertaken research investigated a broad range of interactions than can occur between chemical admixtures and cements of variable mineralogy, between chemical admixtures and cement containing different SCMs. The following conclusions can be drawn based on the presented results.

Analysis of the heat flow measurements for three different cements and the doped samples accelerated with pure CaCl_2 or commercial accelerator it can be concluded that pure CaCl_2 showed a slight sensitivity to the variation in C_3A and gypsum content of cement, while this variation had no effect on the performance of commercial CaCl_2 -based accelerator. However, the presence of alkalis resulted in a reduced magnitude of the main hydration peak of the accelerated samples, whether with pure CaCl_2 or Type E commercial admixture, and a shift in the position of the peak to a later age. Further investigation is needed to determine the cause of this reduction in the accelerating efficiency in the presence of alkalis.

Cement alkali content needs to be taken into account prior to accelerator selection as reduced heat release in high-alkali cements with chloride-based accelerator is expected to correlate with reduced compressive strength.

The addition of lignosulfonate-based water-reducing and retarding admixture changed little the autogenous shrinkage rate of concrete when the rate was compared on a degree of hydration basis. However, addition of CaCl_2 -based accelerator increased autogenous shrinkage in concretes containing water-reducing and air-entraining admixtures, when compared on a degree of hydration basis.

There was good agreement between autogenous deformation at 3 days and pore volume in the 10-20 nm range as determined by MIP on concrete and by nitrogen adsorption on paste samples. This increase in porosity appears to be dosage dependent; porosity increases with initial accelerator addition, however, it remains constant until a “critical” dosage is reached that results in a further porosity increase. This large increase in autogenous shrinkage with the larger dosages of accelerator highlights the importance of controlling accelerator additions on field sites for rapid repair concrete mixtures to reduce the risk of cracking.

The results of this study show that there is a synergistic effect of SCM combinations on yield stress and plastic viscosity of pastes for ternary and quaternary OPC/SCM blends. It is clear that the effect of SCM combinations on paste rheology is not additive and cannot be predicted from the results obtained for their respective binary combinations.

At a fixed w/cm ratio and a fixed dosage of chemical admixtures, a linear relationship was observed between apparent yield stress and BET surface area of the mixtures. Only binary mixtures were tested without chemical admixtures; in this case, the packing density determined based on normal consistency measurements appeared to be the best predictor of the apparent yield stress. The high yield stress of the OPC/MK paste without chemical admixtures was explained by its lower packing density.

It was also observed that for fly ash and slag binary and ternary mixtures, with and without chemical admixtures, there was no significant change in water demand with increasing cement replacement. This was not the case with metakaolin and silica fume, for which the water demand increased with increasing cement replacement. Binary OPC/MK pastes had the highest water demand regardless of the presence of chemical admixtures. The water demand of the ternary and quaternary mixtures remained at the level of the binary OPC/MK or OPC/SF mixtures and was not

affected by further cement replacement with fly ash or slag. In this case, the effect of SCM combinations appears to be additive.

Since only one source was used for each of the SCMs, further work is needed to confirm the observed trends between yield stress and packing density as well as surface area. When SCMs from different sources with different chemistries, densities and surface areas are analyzed, these conclusions can be extended to SCMs as a whole.

Statistical analysis of isothermal calorimetry data indicated that chemical admixtures do not have a significant effect on heat evolution beyond the hydration age of 12 hours. SCMs investigated in this study (Class F FA, BFS, SF and MK), on the other hand, were found to have a significant effect at all ages. While the effect of FA, SF and MK on the total heat reduction with increasing cement replacement appeared to be linear, the effect of BFS was quadratic. The models proposed in this study were successful in predicting the total heat reduction with incorporation of chemical admixtures and SCMs compared to a plain OPC mixture.

Generally, addition of metakaolin and slag with chemical admixtures did not change the main hydration products for mixtures cured at 23°C. No significant differences in phase consumption were observed with addition of 10% metakaolin or 52% SL compared to the control paste at 7 days.

Despite the similarity in phase consumption and the hydration products formed, nitrogen adsorption measurements indicated an increase in LGP volume with addition of 10% MK and 52% SL as well as increase in the fraction of capillary pores accessible by nitrogen adsorption technique.

Nanoindentation measurements also indicated an increase in C-S-H porosity with 10% MK and 52% SL addition, the highest increase resulting from SL incorporation which is in agreement with nitrogen adsorption measurements.

Additionally, a linear relationship was observed between the average elastic modulus of hydration products obtained from nanoindentation and the volume of LGP from N₂ adsorption. A linear relationship was also observed between the average elastic modulus and compressive strength.

Phase quantification by QXRD of hydrated pastes may not be sufficient to assess the impact of metakaolin or SL addition on hydrating cementitious systems, and a multi-technique approach that provides information not only on the amount of hydration products, but also their morphology is preferable.

REFERENCES

- [1] F. Jackson, “The durability of concrete in service,” *ACI J. Proc.*, vol. 43, no. 165, pp. 165–180, 1946.
- [2] L. Tuthill, R. Adams, S. N. Bailey, and R. W. Smith, “A Case of Abnormally Slow Hardening Concrete for Tunnel Lining,” *J. Am. Concr. Inst.*, vol. 57, no. March, pp. 1091–1110, 1961.
- [3] L. Roberts and P. Taylor, “Understanding cement-SCM-admixture interaction issues,” *Concr. Int.*, pp. 33–41, 2007.
- [4] H. Wang, C. Qi, H. Farzam, and J. I. M. Turici, “Interaction of Materials Used in Concrete,” *Concr. Int.*, vol. 28, no. 4, pp. 47–52, 2006.
- [5] T. Oey, J. Stoian, J. Li, C. Vong, M. Balonis, A. Kumar, W. Franke, and G. Sant, “Comparison of Ca(NO₃)₂ and CaCl₂ Admixtures on Reaction, Setting, and Strength Evolutions in Plain and Blended Cementing Formulations,” *J. Mater. Civ. Eng.*, vol. 27, no. 10, p. 04014267, Oct. 2015.
- [6] D. P. Bentz, T. Barrett, I. De la Varga, and W. J. Weiss, “Relating Compressive Strength to Heat Release in Mortars,” *Adv. Civ. Eng. Mater.*, vol. 1, no. 1, p. 20120002, 2012.
- [7] S. Mindess, J. F. Young, and D. Darwin, *Concrete*, 2nd ed. Upper Saddle River, NJ: Prentice Hall, 2003.
- [8] P. Lura, O. M. Jensen, and K. van Breugel, “Autogenous shrinkage in high-performance cement paste: An evaluation of basic mechanisms,” *Cem. Concr. Res.*, vol. 33, no. 2, pp. 223–232, Feb. 2003.
- [9] C. Hua, P. Acker, and A. Ehrlacher, “Analyses and models of the autogenous shrinkage of hardening cement paste I. Modelling at macroscopic scale,” *Cem. Concr. Res.*, vol. 25, no. 7, pp. 1457–1468, 1995.
- [10] C. Hua, A. Ehrlacher, and P. Acker, “Analyses and models of the autogenous shrinkage of hardening cement paste II. Modelling at scale of hydrating grains,” *Cem. Concr. Res.*, vol. 27, no. 2, pp. 245–258, 1997.
- [11] P. K. Mehta and P. J. M. Monteiro, *Concrete: Microstructure, Properties and Materials*, 3rd ed. New York, NY: McGraw-Hill, 2006.
- [12] D. P. Bentz, “A review of early-age properties of cement-based materials,” *Cem. Concr. Res.*, vol. 38, no. 2, pp. 196–204, Feb. 2008.

- [13] A. C. Jupe, A. P. Wilkinson, K. Luke, and G. P. Funkhouser, "Slurry Consistency and In Situ Synchrotron X-Ray Diffraction During the Early Hydration of Portland Cements With Calcium Chloride," *J. Am. Ceram. Soc.*, vol. 90, no. 8, pp. 2595–2602, Aug. 2007.
- [14] J. J. Shideler, "Calcium Chloride in Concrete," *J. Am. Concr. Inst.*, vol. 23, no. 7, pp. 537–559, 1952.
- [15] W. Price, "Factors influencing concrete strength," *ACI J. Proc.*, vol. 47, no. 2, pp. 417–432, 1951.
- [16] A. Suryavanshi, J. Scantlebury, and S. Lyon, "Pore Size Distribution of OPC & SRPC Mortars in Presence of Chlorides," *Cem. Concr. Res.*, vol. 25, no. 5, pp. 980–988, 1995.
- [17] C. M. Hansson, T. Frolund, and J. Markussen, "The Effect of Chloride Cation Type on the Corrosion of Steel in Concrete by Chloride Salts," *Cem. Concr. Res.*, vol. 15, no. 1, pp. 65–73, 1985.
- [18] E. A. Kishar, D. A. Ahmed, M. R. Mohammed, and R. Noury, "Effect of calcium chloride on the hydration characteristics of ground clay bricks cement pastes," *Beni-Suef Univ. J. Basic Appl. Sci.*, vol. 2, no. 1, pp. 20–30, Mar. 2013.
- [19] J. Young, "Capillary Porosity in Hydrated Tricalcium Silicate Pastes," *Powder Technol.*, vol. 9, no. 4, pp. 173–179, 1974.
- [20] V. Gouda, W. Mourad, and R. Mikhail, "Additives to Cement Pastes: Simutaneous Effects on Pore Structure and Corrosion of Steel Reinforcement," *J. Colloid Interface Sci.*, vol. 43, no. 2, pp. 294–302, 1973.
- [21] M. C. G. Juenger, P. J. M. Monteiro, E. M. Gartner, and G. P. Denbeaux, "A Soft X-ray Microscope Investigation into the Effects of Calcium Chloride on Tricalcium Silicate Hydration," *Cem. Concr. Res.*, vol. 35, no. 1, pp. 19–25, Jan. 2005.
- [22] M. C. G. Juenger and H. M. Jennings, "Examining the relationship between the microstructure of calcium silicate hydrate and drying shrinkage of cement pastes," *Cem. Concr. Res.*, vol. 32, no. 2, pp. 289–296, Feb. 2002.
- [23] D. A. Buidens, "Effects of Mix Design Using Chloride-Based Accelerator on Concrete Pavement Cracking Potential," University of South Florida, Tampa, FL, Mater's thesis, 2014.
- [24] N. Shanahan, D. Buidens, K. Riding, and A. Zayed, "Effect of Chloride-Based Accelerator in the Presence of Water-Reducing and Retarding Admixture on Autogenous Shrinkage," *J. Am. Ceram. Soc.*, pp. 1–12, Mar. 2016.
- [25] A. Zayed, K. A. Riding, C. Ferraro, A. J. Bien-Aime, N. Shanahan, D. Buidens, T. Meagher, V. Tran, J. Henika, J. Paris, C. Tibbetts, and B. Watts, "Long-Life Slab Replacement Concrete," University of South Florida, Tampa, FL, 2015.

- [26] A. K. Schindler and K. J. Folliard, "Heat of hydration models for cementitious materials," *ACI Mater. J.*, vol. 102, no. 1, pp. 24–33, 2005.
- [27] J. Poole, K. Riding, K. Folliard, M. C. G. Juenger, and A. K. Schindler, "Hydration study of cementitious materials using semi-adiabatic calorimetry," *ACI Spec. Publ. SP-241-5*, pp. 59–76, 2007.
- [28] K. Riding, J. Poole, K. J. Folliard, M. C. G. Juenger, and A. K. Schindler, "Modeling Hydration of Cementitious Systems," *ACI Mater. J.*, vol. 109, no. 2, pp. 225–234, 2012.
- [29] J. Gajda, *Mass Concrete for Buildings and Bridges*. Skokie, IL: Portland Cement Association, 2007.
- [30] C. F. Ferraris, K. H. Obla, and R. Hill, "The influence of mineral admixtures on the rheology of cement paste and concrete," *Cem. Concr. Res.*, vol. 31, no. 2, pp. 245–255, Feb. 2001.
- [31] T. Danner, H. Justnes, M. Geiker, and R. Andreas, "Phase changes during the early hydration of Portland cement with Ca-lignosulfonates," *Cem. Concr. Res.*, vol. 69, pp. 50–60, Mar. 2015.
- [32] A. Zingg, L. Holzer, A. Kaech, F. Winnefeld, J. Pakusch, S. Becker, and L. Gauckler, "The microstructure of dispersed and non-dispersed fresh cement pastes — New insight by cryo-microscopy," *Cem. Concr. Res.*, vol. 38, no. 4, pp. 522–529, Apr. 2008.
- [33] M. Whittaker, M. Zajac, M. Ben Haha, F. Bullerjahn, and L. Black, "The role of the alumina content of slag, plus the presence of additional sulfate on the hydration and microstructure of Portland cement-slag blends," *Cem. Concr. Res.*, vol. 66, pp. 91–101, Dec. 2014.
- [34] V. Tydlitát, A. Trník, L. Scheinherrová, R. Podoba, and R. Černý, "Application of isothermal calorimetry and thermal analysis for the investigation of calcined gypsum–lime–metakaolin–water system," *J. Therm. Anal. Calorim.*, 2015.
- [35] J. Cabrera and M. F. Rojas, "Mechanism of hydration of the metakaolin–lime–water system," *Cem. Concr. Res.*, vol. 31, no. 2, pp. 177–182, Feb. 2001.
- [36] V. Ramachandran, "Accelerators," in *Concrete Admixtures Handbook: Properties, Science and Technology*, 2nd ed., V. Ramachandran, Ed. Park Ridge, NJ: Noyes Publications, 1995, pp. 185–285.
- [37] O. Mendoza, C. Giraldo, S. S. Camargo, and J. I. Tobón, "Structural and nano-mechanical properties of Calcium Silicate Hydrate (C-S-H) formed from alite hydration in the presence of sodium and potassium hydroxide," *Cem. Concr. Res.*, vol. 74, pp. 88–94, 2015.

- [38] A. Sedaghat, N. Shanahan, and A. Zayed, “Predicting One-Day, Three-Day, and Seven-Day Heat of Hydration of Portland Cement,” *J. Mater. Civ. Eng.*, vol. 27, no. 9, p. 04014257, Dec. 2015.
- [39] J. L. Poole, K. A. Riding, K. J. Folliard, M. C. G. Juenger, and A. K. Schindler, “Methods for Calculating Activation Energy for Portland Cement,” *ACI Mater. J.*, vol. 104, no. 1, pp. 303–311, 2007.
- [40] I. Odler, “Hydration, Setting and Hardening of Portland Cement,” in *Lea’s Chemistry of Cement and Concrete*, 4th ed., P. C. Hewlett, Ed. New York, NY: Arnold, 1998, pp. 241–297.
- [41] W. Lerch, *The Influence of Gypsum on the Hydration and Properties of Portland Cement Pastes*. Chicago, IL: Research Laboratory of the Portland Cement Association, 1946.
- [42] A. Quennoz and K. L. Scrivener, “Interactions between alite and C3A-gypsum hydrations in model cements,” *Cem. Concr. Res.*, vol. 44, pp. 46–54, Feb. 2013.
- [43] V. Peterson and M. Juenger, “Hydration of tricalcium silicate: effects of CaCl₂ and sucrose on reaction kinetics and product formation,” *Chem. Mater.*, vol. 18, no. 24, pp. 5798–5804, 2006.
- [44] V. K. Peterson and M. C. Garci Juenger, “Time-resolved quasielastic neutron scattering study of the hydration of tricalcium silicate: Effects of CaCl₂ and sucrose,” *Phys. B Condens. Matter*, vol. 385–386, pp. 222–224, Nov. 2006.
- [45] J. Thomas, A. Allen, and H. Jennings, “Hydration kinetics and microstructure development of normal and CaCl₂-accelerated tricalcium silicate pastes,” *J. Phys. Chem.*, vol. 113, no. 46, pp. 19836–19844, 2009.
- [46] A. Traetteberg and P. Sereda, “Strength of C3A paste containing gypsum and CaCl₂,” *Cem. Concr. Res.*, vol. 6, no. 4, pp. 461–474, 1976.
- [47] I. Odler and S. Abdul-Maula, “Effect of Chemical Admixtures on Portland Cement Hydration,” *Cem. Concr. Aggregates*, vol. 9, no. 1, pp. 38–43, 1987.
- [48] H. F. W. Taylor, *Cement Chemistry*, 2nd ed. London, UK: Thomas Telford Publishing, 1997.
- [49] C. Bedard and N. Mailvaganam, “The Use of Chemical Admixtures in Concrete. Part I: Admixture-Cement Compatibility,” *J. Perform. Constr. Facil.*, vol. 19, no. 4, pp. 263–267, 2005.
- [50] H. Wang, D. De Leon, and H. Farzam, “C4AF Reactivity—Chemistry and Hydration of Industrial Cement,” *ACI Mater. J.*, vol. 111, no. 2, pp. 201–210, 2014.

- [51] C. Hesse, F. Goetz-Neunhoeffler, and J. Neubauer, "A new approach in quantitative in-situ XRD of cement pastes: Correlation of heat flow curves with early hydration reactions," *Cem. Concr. Res.*, vol. 41, no. 1, pp. 123–128, Jan. 2011.
- [52] V. K. Peterson, D. Neumann, and R. Livingston, "Effect of NaOH on the kinetics of tricalcium silicate hydration: A quasielastic neutron scattering study," *Chem. Phys. Lett.*, vol. 419, no. 1–3, pp. 16–20, Feb. 2006.
- [53] V. Ramachandran, J. Beaudoin, S. Sarkar, and X. Aimin, "Physico-Chemical and Microstructural Investigations of the Effect of NaOH on the Hydration of $3\text{CaO}\cdot\text{SiO}_2$," *Cem.*, vol. 90, no. 2, pp. 73–84, 1993.
- [54] Y. Bu and J. Weiss, "The Influence of Alkali Content on the Electrical Resistivity and Transport Properties of Cementitious Materials," *Cem. Concr. Compos.*, vol. 51, pp. 49–58, Mar. 2014.
- [55] M. C. G. Juenger and H. M. Jennings, "Effects of high alkalinity on cement pastes," *ACI Mater. J.*, vol. 98, no. 3, pp. 251–255, 2001.
- [56] I. Jawed and J. Skalny, "Alkalies in Cement: A Review II. Effect of alkalies on hydration and performance of portland cement," *Cem. Concr. Res.*, vol. 8, no. 1, pp. 37–51, 1978.
- [57] B. Samet and S. L. Sarkar, "The influence of calcium sulfate form on the initial hydration of clinkers containing different alkali combinations," *Cem. Concr. Res.*, vol. 27, no. 3, pp. 369–380, 1997.
- [58] I. Odler and R. Wonnemann, "Effect of alkalies on portland cement hydration II. Alkalies present in the form of sulfates," *Cem. Concr. Res.*, vol. 13, no. 6, pp. 771–777, 1983.
- [59] D. P. Bentz, E. J. Garboczi, C. J. Haecker, and O. M. Jensen, "Effects of cement particle size distribution on performance properties of Portland cement-based materials," *Cem. Concr. Res.*, vol. 29, pp. 1663–1671, 1999.
- [60] D. D. P. Bentz, G. Sant, and J. Weiss, "Early-age properties of cement-based materials. I: Influence of cement fineness," *J. Mater. Civ. Eng.*, vol. 20, no. 7, pp. 502–508, 2008.
- [61] M. Balonis, B. Lothenbach, G. Le Saout, and F. P. Glasser, "Impact of chloride on the mineralogy of hydrated Portland cement systems," *Cem. Concr. Res.*, vol. 40, no. 7, pp. 1009–1022, Jul. 2010.
- [62] A. Suryavanshi, J. Scantlebury, and S. Lyon, "Mechanism of Friedel's Salt Formation in Cements Rich in Tri-Calcium Aluminate," *Cem. Concr. Res.*, vol. 26, no. 5, pp. 717–727, 1996.
- [63] N. Tenoutasse, "The Hydration Mechanism of C3A and C3S in the Presence of Calcium Chloride and Calcium Sulphate," in *V International Symposium of Chemistry of Cement*, 1968, pp. 372–378.

- [64] M. A. G. Aranda, A. G. De la Torre, and L. Leon-Reina, "Rietveld Quantitative Phase Analysis of OPC Clinkers, Cements and Hydration Products," *Reviews in Mineralogy and Geochemistry*, vol. 74, no. 1, pp. 169–209, 2012.
- [65] C. Peng, F. Zhang, and Z. Guo, "Gypsum crystallization and potassium chloride regeneration by reaction of calcium chloride solution with potassium sulfate solution or solid," *Trans. Nonferrous Met. Soc. China*, vol. 20, no. 4, pp. 712–720, 2010.
- [66] C. Labbez, I. Pochard, B. Jönsson, and A. Nonat, "C-S-H/solution interface: Experimental and Monte Carlo studies," *Cem. Concr. Res.*, vol. 41, no. 2, pp. 161–168, 2011.
- [67] J. J. Beaudoin, V. S. Ramachandran, and R. Feldman, "Interaction of chloride and C-S-H," *Cem. Concr. Res.*, vol. 20, no. 6, pp. 875–883, 1990.
- [68] G. Plusquellec, A. Nonat, and I. Pochard, "Anion uptake by calcium silicate hydrate," *32nd Cem. Concr. Sci. Conf.*, p. 4, 2012.
- [69] H. Viallis, P. Faucon, J. C. Petit, and A. Nonat, "Interaction between salts (NaCl, CsCl) and calcium silicate hydrates (C-S-H)," *J. Phys. Chem. B*, vol. 103, no. 25, pp. 5212–5219, 1999.
- [70] M. . Zhang, C. . Tam, and M. . Leow, "Effect of water-to-cementitious materials ratio and silica fume on the autogenous shrinkage of concrete," *Cem. Concr. Res.*, vol. 33, no. 10, pp. 1687–1694, Oct. 2003.
- [71] V. Baroghel-Bouny, P. Mounanga, A. Khelidj, A. Loukili, and N. Rafaï, "Autogenous deformations of cement pastes," *Cem. Concr. Res.*, vol. 36, no. 1, pp. 123–136, Jan. 2006.
- [72] T. Aly and J. G. Sanjayan, "Effect of Pore-Size Distribution on Shrinkage of Concretes," *J. Mater. Civ. Eng.*, vol. 22, no. 5, pp. 525–532, 2010.
- [73] S. Slatnick, K. Riding, K. J. Folliard, M. C. G. Juenger, and A. K. Schindler, "Evaluation of Autogenous Deformation of Concrete at Early Ages.," *ACI Mater. J.*, vol. 108, no. 1, pp. 21–28, 2011.
- [74] J. Brooks and M. Johari, "Effect of metakaolin on creep and shrinkage of concrete," *Cem. Concr. Compos.*, vol. 23, pp. 495–502, 2001.
- [75] Y. Li, J. Bao, and Y. Guo, "The relationship between autogenous shrinkage and pore structure of cement paste with mineral admixtures," *Constr. Build. Mater.*, vol. 24, no. 10, pp. 1855–1860, Oct. 2010.
- [76] S. W. Yoo, S.-J. Kwon, and S. H. Jung, "Analysis technique for autogenous shrinkage in high performance concrete with mineral and chemical admixtures," *Constr. Build. Mater.*, vol. 34, pp. 1–10, Sep. 2012.
- [77] E. Tazawa and S. Miyazawa, "Influence of cement and admixture on autogenous shrinkage of cement paste," *Cem. Concr. Res.*, vol. 25, no. 2, pp. 281–287, 1995.

- [78] A. N. M. Lopes, E. F. Silva, D. C. C. D. Molin, and R. D. T. Filho, “Shrinkage-Reducing Admixture : Effects on Durability of High-Strength Concrete,” no. 110, pp. 365–374, 2014.
- [79] J. Weiss, P. Lura, F. Rajabipour, and G. Sant, “Performance of Shrinkage-Reducing Admixtures at Different Humidities and at Early Ages,” no. 105, 2009.
- [80] G. Sant, “The Influence of Temperature on Autogenous Volume Changes in Cementitious Materials Containing Shrinkage Reducing Admixtures,” *Cem. Concr. Compos.*, vol. 34, no. 7, pp. 855–865, Aug. 2012.
- [81] M. José Oliveira, A. B. Ribeiro, and F. G. Branco, “Combined effect of expansive and shrinkage reducing admixtures to control autogenous shrinkage in self-compacting concrete,” *Constr. Build. Mater.*, vol. 52, pp. 267–275, 2014.
- [82] T. Meagher, N. Shanahan, D. Buidens, K. A. Riding, and A. Zayed, “Effects of chloride and chloride-free accelerators combined with typical admixtures on the early-age cracking risk of concrete repair slabs,” *Constr. Build. Mater.*, vol. 94, pp. 270–279, 2015.
- [83] T. J. VanDam, K. R. Peterson, L. L. Sutter, A. Panguluri, and J. Sytsma, “Guidelines for Early-Opening to Traffic Portland Cement Concrete for Pavement Rehabilitation, NCHRP Report 540,” Washington, DC, 2005.
- [84] G. B. Wallace and E. L. Ore, “Structural and Lean Mass Concrete as Affected by Water-Reducing, Set-Retarding Agents,” *ASTM Spec. Tech. Publ. 266*, pp. 38–94, 1960.
- [85] E. Holt, “Contribution of mixture design to chemical and autogenous shrinkage of concrete at early ages,” *Cem. Concr. Res.*, vol. 35, no. 3, pp. 464–472, 2005.
- [86] V. Ramachandran and R. Feldman, “Time-Dependent and Intrinsic Characteristics of Portland Cement Hydrated in the Presence of Calcium Chloride,” *Cem.*, vol. 75, no. 3, pp. 311–322, 1978.
- [87] M. C. G. Juenger and H. M. Jennings, “The use of nitrogen adsorption to assess the microstructure of cement paste,” *Cem. Concr. Res.*, vol. 31, no. 6, pp. 883–892, May 2001.
- [88] A. Korpa and R. Trettin, “The influence of different drying methods on cement paste microstructures as reflected by gas adsorption: Comparison between freeze-drying (F-drying), D-drying, P-drying and oven-drying methods,” *Cem. Concr. Res.*, vol. 36, no. 4, pp. 634–649, Apr. 2006.
- [89] J. Beaudoin, “A discussion on, ‘ The use of nitrogen adsorption to assess the microstructure of cement paste’ by MCG Juenger and HM Jennings,” *Cem. Concr. Res.*, vol. 32, pp. 831–832, 2002.

- [90] R. Mikhail, L. E. Copeland, and S. Brunauer, "Pore structures and surface areas of hardened Portland cement pastes by nitrogen adsorption," *Can. J. Chem.*, vol. 42, pp. 426–438, 1964.
- [91] I. Maruyama, Y. Nishioka, G. Igarashi, and K. Matsui, "Microstructural and bulk property changes in hardened cement paste during the first drying process," *Cem. Concr. Res.*, vol. 58, pp. 20–34, 2014.
- [92] J. M. Justice, "Evaluation of Metakaolins for Use as Supplementary Cementitious Materials," Georgia Institute of Technology, 2005.
- [93] E. Bodor, J. Skalny, S. Brunauer, J. Massy, and M. Yudenfreund, "Pore structures of hydrated calcium silicates and Portland cements by nitrogen adsorption," *J. Colloid Interface Sci.*, vol. 34, no. 4, pp. 560–570, 1970.
- [94] G. W. Scherer, "Drying, Shrinkage, and Cracking of Cementitious Materials," *Transp. Porous Media*, vol. 110, no. 2, pp. 311–331, Nov. 2015.
- [95] J. C. Groen, L. A. A. Peffer, and J. Pérez-Ramírez, "Pore size determination in modified micro- and mesoporous materials. Pitfalls and limitations in gas adsorption data analysis," *Microporous Mesoporous Mater.*, vol. 60, pp. 1–17, 2003.
- [96] T. Oey, J. Stoian, J. Li, and C. Vong, "Comparison of Ca (NO₃)₂ and CaCl₂ Admixtures on Reaction, Setting, and Strength Evolutions in Plain and Blended Cementing Formulations," *J. Mater. ...*, no. 3, pp. 1–12, 2014.
- [97] V. S. Ramachandran, "Kinetics of hydration of tricalcium silicate in presence of calcium chloride by thermal methods," *Thermochim. Acta*, vol. 2, no. 1, pp. 41–55, 1971.
- [98] K. De Weerd, a. Colombo, L. Coppola, H. Justnes, and M. R. Geiker, "Impact of the associated cation on chloride binding of Portland cement paste," *Cem. Concr. Res.*, vol. 68, pp. 196–202, Feb. 2015.
- [99] D. Hou, T. Zhao, H. Ma, and Z. Li, "Reactive Molecular Simulation on Water Confined in the Nanopores of the Calcium Silicate Hydrate Gel: Structure, Reactivity, and Mechanical Properties," *J. Phys. Chem. C*, vol. 119, pp. 1346–1358, 2015.
- [100] M. Bauchy, M. J. Abdolhosseini Qomi, C. Bichara, F. J. Ulm, and R. J. M. Pellenq, "Nanoscale structure of cement: Viewpoint of rigidity theory," *J. Phys. Chem. C*, vol. 118, pp. 12485–12493, 2014.
- [101] M. J. Abdolhosseini Qomi, K. J. Krakowiak, M. Bauchy, K. L. Stewart, R. Shahsavari, D. Jagannathan, D. B. Brommer, A. Baronnet, M. J. Buehler, S. Yip, F.-J. Ulm, K. J. Van Vliet, and R. J. M. Pellenq, "Combinatorial molecular optimization of cement hydrates," *Nat. Commun.*, vol. 5, pp. 1–9, Sep. 2014.

- [102] H. Chen, M. Wyrzykowski, K. Scrivener, and P. Lura, "Prediction of self-desiccation in low water-to-cement ratio pastes based on pore structure evolution," *Cem. Concr. Res.*, vol. 49, pp. 38–47, Jul. 2013.
- [103] J. Lai, L. Zhang, X. Qian, C. Shen, and J. Zhang, "Influence of superplasticizers on early age drying shrinkage of cement paste with the same consistency," *J. Wuhan Univ. Technol. Sci. Ed.*, vol. 29, no. 6, pp. 1201–1207, Dec. 2014.
- [104] H. M. Jennings, "Refinements to colloid model of C-S-H in cement: CM-II," *Cem. Concr. Res.*, vol. 38, no. 3, pp. 275–289, Mar. 2008.
- [105] H. M. Jennings, "A model for the microstructure of calcium silicate hydrate in cement paste," *Cem. Concr. Res.*, vol. 30, pp. 101–116, 2000.
- [106] I. Maruyama, G. Igarashi, and Y. Nishioka, "Bimodal behavior of C-S-H interpreted from short-term length change and water vapor sorption isotherms of hardened cement paste," *Cem. Concr. Res.*, vol. 73, pp. 158–168, 2015.
- [107] I. Maruyama, "Origin of Drying Shrinkage of Hardened Cement Paste: Hydration Pressure," *J. Adv. Concr. Technol.*, vol. 8, no. 2, pp. 187–200, 2010.
- [108] F. Beltzung and F. H. Wittmann, "Role of disjoining pressure in cement based materials," *Cem. Concr. Res.*, vol. 35, no. 12, pp. 2364–2370, 2005.
- [109] O. M. Jensen and P. F. Hansen, "Influence of temperature on autogenous deformation and relative humidity change in hardening cement paste," *Cem. Concr. Res.*, vol. 29, no. 4, pp. 567–575, 1999.
- [110] Z. Jiang, Z. Sun, and P. Wang, "Autogenous relative humidity change and autogenous shrinkage of high-performance cement pastes," *Cem. Concr. Res.*, vol. 35, no. 8, pp. 1539–1545, Aug. 2005.
- [111] F. Beltzung, F. Wittmann, and L. Holzer, "Influence of composition of pore solution on drying shrinkage," in *Creep, Shrinkage and Durability Mechanics of Concrete and Other Quasi-Brittle Materials, Proceedings of the Sixth International Conference, CONCREEP-6@MIT*, 2001, pp. 39–48.
- [112] R. Rixom and N. Mailvaganam, *Chemical Admixtures for Concrete*, 3rd ed. New York, NY: Routledge, 1999.
- [113] W. Kurdowski, *Cement and Concrete Chemistry*. Dordrecht: Springer Netherlands, 2014.
- [114] B. Hope and D. Manning, "Creep of Concrete Influenced by Accelerators," *ACI J. Proc.*, vol. 68, no. 5, pp. 361–365, 1971.
- [115] M. Alexander and B. Magee, "Durability performance of concrete containing condensed silica fume," *Cem. Concr. Res.*, vol. 29, no. 6, pp. 917–922, 1999.

- [116] Z. Li and Z. Ding, "Property improvement of Portland cement by incorporating with metakaolin and slag," *Cem. Concr. Res.*, vol. 33, no. 4, pp. 579–584, Apr. 2003.
- [117] J. M. Khatib and J. J. Hibbert, "Selected engineering properties of concrete incorporating slag and metakaolin," *Constr. Build. Mater.*, vol. 19, no. 6, pp. 460–472, Jul. 2005.
- [118] B. W. Langan, K. Weng, and M. A. Ward, "Effect of silica fume and fly ash on heat of hydration of Portland cement," *Cem. Concr. Res.*, vol. 32, pp. 1045–1051, 2002.
- [119] M. I. Khan and C. J. Lynsdale, "Strength, permeability, and carbonation of high-performance concrete," *Cem. Concr. Res.*, vol. 32, no. 1, pp. 123–131, Jan. 2002.
- [120] M. Codina, C. Cau-dit-Coumes, P. Le Bescop, J. Verdier, and J. P. Ollivier, "Design and characterization of low-heat and low-alkalinity cements," *Cem. Concr. Res.*, vol. 38, no. 4, pp. 437–448, Apr. 2008.
- [121] E. Güneyisi, M. Gesoğlu, and E. Özbay, "Strength and drying shrinkage properties of self-compacting concretes incorporating multi-system blended mineral admixtures," *Constr. Build. Mater.*, vol. 24, no. 10, pp. 1878–1887, Oct. 2010.
- [122] P. A. M. Basheer, P. R. V. Gilleece, A. E. Long, and W. J. Mc Carter, "Monitoring Electrical Resistance of Concretes Containing Alternative Cementitious Materials to Assess Their Resistance to Chloride Penetration," *Cem. Concr. Compos.*, vol. 24, no. 5, pp. 437–449, Oct. 2002.
- [123] M. Gesoğlu, E. Güneyisi, and E. Özbay, "Properties of self-compacting concretes made with binary, ternary, and quaternary cementitious blends of fly ash, blast furnace slag, and silica fume," *Constr. Build. Mater.*, vol. 23, no. 5, pp. 1847–1854, May 2009.
- [124] R. Bleszynski and R. Hooton, "Durability of ternary blend concrete with silica fume and blast-furnace slag: laboratory and outdoor exposure site studies," *ACI Mater. J.*, vol. 99, pp. 499–508, 2002.
- [125] M. D. A. Thomas, M. H. Shehata, S. G. Shashiprakash, D. S. Hopkins, and K. Cail, "Use of ternary cementitious systems containing silica fume and fly ash in concrete," *Cem. Concr. Res.*, vol. 29, no. 8, pp. 1207–1214, Aug. 1999.
- [126] T. K. Erdem and Ö. Kirca, "Use of binary and ternary blends in high strength concrete," *Constr. Build. Mater.*, vol. 22, no. 7, pp. 1477–1483, Jul. 2008.
- [127] N. Bouzoubaâ, A. Bilodeau, V. Sivasundaram, B. Fournier, and D. M. Golden, "Development of Ternary Blends for High- Performance Concrete," *ACI Mater. J.*, vol. 101, no. 1, pp. 19–29, 2004.
- [128] N. Roussel, A. Lemaître, R. J. Flatt, and P. Coussot, "Steady state flow of cement suspensions: A micromechanical state of the art," *Cem. Concr. Res.*, vol. 40, no. 1, pp. 77–84, 2010.

- [129] B. Patzák and Z. Bittnar, “Modeling of fresh concrete flow,” *Comput. Struct.*, vol. 87, no. 15–16, pp. 962–969, 2009.
- [130] P. Banfill, “Rheology of fresh cement and concrete,” *Rheol. Rev.*, pp. 61–130, 2006.
- [131] N. Roussel, “Rheology of fresh concrete: from measurements to predictions of casting processes,” *Mater. Struct.*, vol. 40, no. 10, pp. 1001–1012, 2007.
- [132] S. Hanehara and K. Yamada, “Rheology and early age properties of cement systems,” *Cem. Concr. Res.*, vol. 38, no. 2, pp. 175–195, 2008.
- [133] R. Flatt, “Towards a prediction of superplasticized concrete rheology,” *Mater. Struct.*, vol. 37, no. June, pp. 289–300, 2004.
- [134] O. H. Wallevik and J. E. Wallevik, “Rheology as a tool in concrete science: The use of rheographs and workability boxes,” *Cem. Concr. Res.*, vol. 41, no. 12, pp. 1279–1288, Dec. 2011.
- [135] R. S. Ahari, T. K. Erdem, and K. Ramyar, “Effect of various supplementary cementitious materials on rheological properties of self-consolidating concrete,” *Constr. Build. Mater.*, vol. 75, pp. 89–98, 2015.
- [136] C. Ferraris and F. de Larrard, *Testing and modelling of fresh concrete rheology*. 1998.
- [137] R. J. Flatt and P. Bowen, “Yodel: A Yield Stress Model for Suspensions,” *J. Am. Ceram. Soc.*, vol. 89, no. 4, pp. 1244–1256, Apr. 2006.
- [138] R. J. Flatt and P. Bowen, “Yield Stress of Multimodal Powder Suspensions: An Extension of the YODEL (Yield Stress mODEL),” *J. Am. Ceram. Soc.*, vol. 90, no. 4, pp. 1038–1044, Apr. 2007.
- [139] J. Z. Q. Zhou, P. H. T. Uhlherr, and F. T. Luo, “Yield stress and maximum packing fraction of concentrated suspensions,” *Rheol. Acta*, vol. 34, no. 6, pp. 544–561, 1995.
- [140] Z. Zhou, M. J. Solomon, P. J. Scales, and D. V. Boger, “The yield stress of concentrated flocculated suspensions of size distributed particles,” *J. Rheol. (N. Y. N. Y.)*, vol. 43, no. 3, p. 651, 1999.
- [141] S. Brunauer, P. H. Emmett, and E. Teller, “Adsorption of Gases in Multimolecular Layers,” *J. Am. Chem. Soc.*, vol. 60, no. 1, pp. 309–319, 1938.
- [142] K. K. Aligizaki, *Pore Structure of Cement-Based Materials: Testing, Interpretation and Requirements*. New York, NY: Taylor & Francis, 2006.
- [143] R. Pileggi, A. Betioli, F. Cardoso, and V. John, “Entended rheological chracterization of cement pastes: squeeze flow plus rotational rheometry,” in *Proceedings of the 12th International Congress on the Chemistry of Cement*, 2007.

- [144] E. Brito-de La Fuente, L. Choplin, and P. A. Tanguy, "Mixing with Helical Ribbon Impellers : Effect of Highly Shear Thinning Behaviour and Impeller Geometry," no. 1.
- [145] R. Siddique and M. I. Khan, *Supplementary Cementing Materials*, vol. 37. Berlin, Germany: Springer, 2011.
- [146] A. Buchwald, R. Tatarin, and D. Stephan, "Reaction progress of alkaline-activated metakaolin-ground granulated blast furnace slag blends," *J. Mater. Sci.*, vol. 44, no. 20, pp. 5609–5617, Aug. 2009.
- [147] F. Curcio, B. . DeAngelis, and S. Pagliolico, "Metakaolin as a pozzolanic microfiller for high-performance mortars," *Cem. Concr. Res.*, vol. 28, no. 6, pp. 803–809, Jun. 1998.
- [148] J. Yajun and J. H. Cahyadi, "Effects of densified silica fume on microstructure and compressive strength of blended cement pastes," *Cem. Concr. Res.*, vol. 33, no. 10, pp. 1543–1548, Oct. 2003.
- [149] E. P. Koehler and D. W. Fowler, "Development of a Portable Rheometer for Fresh Portland Cement Concrete," Washington, DC, 2004.
- [150] A. K. H. Kwan and Y. Li, "Effects of fly ash microsphere on rheology, adhesiveness and strength of mortar," *Constr. Build. Mater.*, vol. 42, pp. 137–145, May 2013.
- [151] C. K. Park, M. H. Noh, and T. H. Park, "Rheological properties of cementitious materials containing mineral admixtures," *Cem. Concr. Res.*, vol. 35, no. 5, pp. 842–849, May 2005.
- [152] L. Rudzinski, "The effect of fly ashes on the rheological behaviour of cement pastes," *Matériaux Constr.*, vol. 17, no. 5, pp. 369–373, 1984.
- [153] X. Zhang and J. Han, "The effect of ultra-fine admixture on the rheological property of cement paste," *Cem. Concr. Res.*, vol. 30, no. 5, pp. 827–830, May 2000.
- [154] M. Palacios, F. Puertas, P. Bowen, and Y. F. Houst, "Effect of PCs superplasticizers on the rheological properties and hydration process of slag-blended cement pastes," *J. Mater. Sci.*, vol. 44, no. 10, pp. 2714–2723, Mar. 2009.
- [155] Y. Shi, I. Matsui, and N. Feng, "Effect of compound mineral powders on workability and rheological property of HPC," *Cem. Concr. Res.*, vol. 32, no. 1, pp. 71–78, Jan. 2002.
- [156] E. Moulin, P. Blanc, and D. Sorrentino, "Influence of key cement chemical parameters on the properties of metakaolin blended cements," *Cem. Concr. Compos.*, vol. 23, pp. 463–469, 2001.
- [157] K. Yamada, T. Sugamata, and H. Nakanishi, "Fluidity Performance Evaluation of Cement and Superplasticizer," *J. Adv. Concr. Technol.*, vol. 4, no. 2, pp. 241–249, 2006.

- [158] T. Tadros, “Interparticle interactions in concentrated suspensions and their bulk (rheological) properties.,” *Adv. Colloid Interface Sci.*, vol. 168, no. 1–2, pp. 263–77, Oct. 2011.
- [159] L. Ferrari, J. Kaufmann, F. Winnefeld, and J. Plank, “Interaction of cement model systems with superplasticizers investigated by atomic force microscopy, zeta potential, and adsorption measurements,” *J. Colloid Interface Sci.*, vol. 347, no. 1, pp. 15–24, Jul. 2010.
- [160] S. Hanehara and K. Yamada, “Interaction between Cement and Chemical Admixture from the Point of Cement Hydration, Absorption Behaviour of Admixture, and Paste Rheology,” *Cem. Concr. Res.*, vol. 29, no. 8, pp. 1159–1165, Aug. 1999.
- [161] Y. Knop and A. Peled, “Setting behavior of blended cement with limestone: influence of particle size and content,” *Mater. Struct.*, vol. 49, no. 1–2, pp. 439–452, Jan. 2016.
- [162] A. Lecomte, J. M. Mechling, and C. Diliberto, “Compaction index of cement paste of normal consistency,” *Constr. Build. Mater.*, vol. 23, no. 10, pp. 3279–3286, 2009.
- [163] B. Sabir, S. Wild, and J. Bai, “Metakaolin and calcined clays as pozzolans for concrete: a review,” *Cem. Concr. Compos.*, vol. 23, no. 6, pp. 441–454, Dec. 2001.
- [164] C. He, B. Osbaeck, and E. Makovicky, “Pozzolanic Reactions of Six Principal Clay Minerals: Activation, Reactivity Assessments and Technological Effects,” *Cem. Concr. Res.*, vol. 25, no. 8, pp. 1691–1702, 1995.
- [165] R. Talero, C. Pedrajas, and V. Rahhal, “Performance of Fresh Portland Cement Pastes - Determination of Some Specific Rheological Parameters,” in *Rheology - New Concepts, Applications and Methods*, R. Durairaj, Ed. InTech, 2013, pp. 57–79.
- [166] R. Talero, “Kinetic and morphological differentiation of Ettringites in plain and blended Portland cements using Metakaolin and the ASTM C 452-68 test. Part I : kinetic differentiation,” *Mater. Construcción*, vol. 58, no. 292, pp. 45–66, 2008.
- [167] R. Talero, “Kinetic and morphological differentiation of ettringites in plain and blended Portland cements with metakaolin and the ASTM C 452-68 test. Part II : Morphological differentiation by SEM and XRD analysis,” *Mater. Construcción*, vol. 59, no. 293, pp. 35–51, 2009.
- [168] ACI Committee 207, *ACI 207.2R-07 Report on Thermal and Volume Change Effects on Cracking of Mass Concrete*. Farmington Hills, MI: American Concrete Institute, 2007.
- [169] T. Poole, “Predicting Seven-Day Heat of Hydration of Hydraulic Cement from Standard Test Properties,” *J. ASTM Int.*, vol. 6, no. 6, pp. 1–10, 2009.
- [170] T. Kishi and K. Maekawa, “Multi-Component Model for Hydration Heat of Portland Cement,” *Concr. Libr. JSCE*, vol. 28, no. 1, pp. 97–115, 1996.

- [171] S. Swaddiwudhipong, D. Chen, and M. H. Zhang, "Simulation of the exothermic hydration process of Portland cement," *Adv. Cem. Res.*, vol. 14, no. 2, pp. 61–69, 2002.
- [172] K. A. Riding, J. L. Poole, K. J. Folliard, M. C. G. Juenger, and A. K. Schindler, "Modeling Hydration of Cementitious Systems," *ACI Mater. J.*, vol. 109, no. 2, pp. 225–234, 2012.
- [173] B. Lothenbach, K. Scrivener, and R. D. Hooton, "Supplementary cementitious materials," *Cem. Concr. Res.*, vol. 41, no. 12, pp. 1244–1256, Dec. 2011.
- [174] A. M. Neville, *Properties of Concrete*, 4th ed. Harlow, England: Pearson Education Limited, 2006.
- [175] G. Osborne, "Durability of Portland blast-furnace slag cement concrete," *Cem. Concr. Compos.*, vol. 21, pp. 11–21, 1999.
- [176] I. Pane and W. Hansen, "Investigation of blended cement hydration by isothermal calorimetry and thermal analysis," *Cem. Concr. Res.*, vol. 35, no. 6, pp. 1155–1164, Jun. 2005.
- [177] E.-H. Kadri and R. Duval, "Hydration heat kinetics of concrete with silica fume," *Constr. Build. Mater.*, vol. 23, no. 11, pp. 3388–3392, Nov. 2009.
- [178] N. Y. Mostafa and P. W. Brown, "Heat of hydration of high reactive pozzolans in blended cements: Isothermal conduction calorimetry," *Thermochim. Acta*, vol. 435, no. 2, pp. 162–167, 2005.
- [179] M. Frías, M. S. de Rojas, and J. Cabrera, "The effect that the pozzolanic reaction of metakaolin has on the heat evolution in metakaolin-cement mortars," *Cem. Concr. Res.*, vol. 30, pp. 209–216, 2000.
- [180] E.-H. Kadri, S. Kenai, K. Ezziane, R. Siddique, and G. De Schutter, "Influence of metakaolin and silica fume on the heat of hydration and compressive strength development of mortar," *Appl. Clay Sci.*, vol. 53, no. 4, pp. 704–708, Oct. 2011.
- [181] A. Williams, A. Markandeya, Y. Stetsko, K. Riding, and A. Zayed, "Cracking potential and temperature sensitivity of metakaolin concrete," *Constr. Build. Mater.*, vol. 120, pp. 172–180, 2016.
- [182] J. Ambroise, S. Maximilien, and J. Pera, "Properties of metakaolin blended cements," *Adv. Cem. Based Mater.*, vol. 1, no. 4, pp. 161–168, 1994.
- [183] J. Bai and S. Wild, "Investigation of the temperature change and heat evolution of mortar incorporating PFA and metakaolin," *Cem. Concr. Compos.*, vol. 24, no. 2, pp. 201–209, 2002.

- [184] H.-S. Kim, S.-H. Lee, and H.-Y. Moon, “Strength properties and durability aspects of high strength concrete using Korean metakaolin,” *Constr. Build. Mater.*, vol. 21, no. 6, pp. 1229–1237, Jun. 2007.
- [185] G. Jiang, Z. Rong, and W. Sun, “Effects of metakaolin on mechanical properties, pore structure and hydration heat of mortars at 0.17 w/b ratio,” *Constr. Build. Mater.*, vol. 93, pp. 564–572, 2015.
- [186] K. Meinhard and R. Lackner, “Multi-phase hydration model for prediction of hydration-heat release of blended cements,” *Cem. Concr. Res.*, vol. 38, no. 6, pp. 794–802, 2008.
- [187] G. De Schutter and L. Taerwe, “General hydration model for portland cement and blast furnace slag cement,” *Cem. Concr. Res.*, vol. 25, no. 3, pp. 593–604, 1995.
- [188] F. Han, Z. Zhang, D. Wang, and P. Yan, “Hydration kinetics of composite binder containing slag at different temperatures,” *J. Therm. Anal. Calorim.*, vol. 121, no. 2, pp. 815–827, 2015.
- [189] B. Kolani, L. Buffo-Lacarrière, A. Sellier, G. Escadeillas, L. Boutillon, and L. Linger, “Hydration of slag-blended cements,” *Cem. Concr. Compos.*, vol. 34, no. 9, pp. 1009–1018, 2012.
- [190] Y. Luan, T. Ishida, T. Nawa, and T. Sagawa, “Enhanced Model and Simulation of Hydration Process of Blast Furnace Slag in Blended Cement,” *J. Adv. Concr. Technol.*, vol. 10, no. 1, pp. 1–13, 2012.
- [191] S. Swaddiwudhipong, H. Wu, and M. H. Zhang, “Numerical simulation of temperature rise of highstrength concrete incorporating silica fume and superplasticiser,” *Adv. Cem. Res.*, vol. 15, no. 4, pp. 161–169, 2003.
- [192] X. Y. Wang, H. K. Cho, and H. S. Lee, “Prediction of temperature distribution in concrete incorporating fly ash or slag using a hydration model,” *Compos. Part B Eng.*, vol. 42, no. 1, pp. 27–40, 2011.
- [193] K. J. Folliard, M. Juenger, A. Schindler, K. A. Riding, J. L. Poole, L. Kallivokas, S. Slatnick, J. Whigham, and J. L. Meadows, “Prediction Model for Concrete Behavior - Final Report,” Center for Transportation Research, the University of Texas at Austin, Austin, TX, 2008.
- [194] J. J. L. Poole, K. A. K. Riding, M. C. G. Juenger, K. J. Folliard, and A. K. Schindler, “Effect of Chemical Admixtures on Apparent Activation Energy of Cementitious Systems,” *J. Mater. Civ. Eng.*, vol. 23, no. 12, pp. 1654–1662, Dec. 2011.
- [195] F. Han, R. Liu, D. Wang, and P. Yan, “Characteristics of the hydration heat evolution of composite binder at different hydrating temperature,” *Thermochim. Acta*, vol. 586, pp. 52–57, Jun. 2014.

- [196] M. T. Palou, E. Kuzielová, R. Novotný, F. Šoukal, and M. Žemlička, “Blended cements consisting of Portland cement–slag–silica fume–metakaolin system,” *J. Therm. Anal. Calorim.*, Mar. 2016.
- [197] D. C. Montgomery, *Design and Analysis of Experiments*, 6th ed. Hoboken, NJ: John Wiley & Sons, Inc., 2005.
- [198] M. Sonebi, L. Svermova, and P. J. M. Bartos, “Factorial Design of Cement Slurries Containing Limestone Powder for Self-Consolidating Slurry-Infiltrated Fiber Concrete,” *ACI Mater. J.*, vol. 101, no. 2, pp. 136–145, 2005.
- [199] A. Ghezal and K. H. Khayat, “Optimizing Self-Consolidating Concrete with Limestone Filler by using Statistical Factorial Design Methods,” *ACI Mater. J.*, vol. 99, no. 3, pp. 264–272, 2002.
- [200] K. H. Khayat, A. Ghezal, and M. S. Hadriche, “Factorial design models for proportioning self-consolidating concrete,” *Mater. Struct.*, vol. 32, no. 9, pp. 679–686, 1999.
- [201] K. Soudki, E. F. El-Salakawy, and N. Elkum, “Full factorial optimization of concrete mix design for hot climates,” *J. Mater. Civ. Eng.*, vol. 13, no. 6, pp. 427–433, 2001.
- [202] R. Patel, K. Hossain, and M. Shehata, “Development of statistical models for mixture design of high-volume fly ash self-consolidating concrete,” *ACI Mater. J.*, vol. 101, no. 4, pp. 294–302, 2004.
- [203] L. Ferrara, Y.-D. Park, and S. P. Shah, “A method for mix-design of fiber-reinforced self-compacting concrete,” *Cem. Concr. Res.*, vol. 37, no. 6, pp. 957–971, Jun. 2007.
- [204] C. B. Srinivasan, N. L. Narasimhan, and S. V. Ilango, “Development of rapid-set high-strength cement using statistical experimental design,” *Cem. Concr. Res.*, vol. 33, no. 9, pp. 1287–1292, Sep. 2003.
- [205] M. Sonebi, “Factorial design modelling of mix proportion parameters of underwater composite cement grouts,” *Cem. Concr. Res.*, vol. 31, no. 11, pp. 1553–1560, Nov. 2001.
- [206] A. C. A. Muller, K. L. Scrivener, A. M. Gajewicz, and P. J. McDonald, “Use of bench-top NMR to measure the density, composition and desorption isotherm of C-S-H in cement paste,” *Microporous Mesoporous Mater.*, vol. 178, pp. 99–103, 2013.
- [207] G. Verbeck and C. Foster, “Long-time study of cement performance in concrete: The heats of hydration of the cements,” in *Proceedings of the American Society for Testing Materials*, vol. 50, Philadelphia, PA, 1950, pp. 1235–1262.
- [208] A. Zayed, A. Sedaghat, A. J. Bien-Aime, and N. Shanahan, “Effects of portland cement particle size on heat of hydration,” University of South Florida, Tampa, FL, 2013.

- [209] C. Medina, I. F. Sáez del Bosque, E. Asensio, M. Frías, and M. I. Sánchez de Rojas, “New additions for eco-efficient cement design. Impact on calorimetric behaviour and comparison of test methods,” *Mater. Struct.*, Jan. 2016.
- [210] A. A. Ramezaniyanpour, “Metakaolin,” in *Cement Replacement Materials*, Berlin, Germany: Springer-Verlag Berlin Heidelberg, 2014, p. 336.
- [211] A. Shvarzman, K. Kovler, G. . Grader, and G. . Shter, “The effect of dehydroxylation/amorphization degree on pozzolanic activity of kaolinite,” *Cem. Concr. Res.*, vol. 33, no. 3, pp. 405–416, Mar. 2003.
- [212] C. Bich, J. Ambroise, and J. Péra, “Influence of degree of dehydroxylation on the pozzolanic activity of metakaolin,” *Appl. Clay Sci.*, vol. 44, no. 3–4, pp. 194–200, May 2009.
- [213] G. Kakali, T. Perraki, S. Tsivilis, and E. Badogiannis, “Thermal treatment of kaolin: the effect of mineralogy on the pozzolanic activity,” *Appl. Clay Sci.*, vol. 20, no. 1–2, pp. 73–80, Sep. 2001.
- [214] T. Ramlochan, M. Thomas, and K. a Gruber, “The effect of metakaolin on alkali–silica reaction in concrete,” *Cem. Concr. Res.*, vol. 30, no. 3, pp. 339–344, Mar. 2000.
- [215] C. S. Poon, S. C. Kou, and L. Lam, “Compressive strength, chloride diffusivity and pore structure of high performance metakaolin and silica fume concrete,” *Constr. Build. Mater.*, vol. 20, no. 10, pp. 858–865, 2006.
- [216] P. Duan, Z. Shui, W. Chen, and C. Shen, “Effects of metakaolin, silica fume and slag on pore structure, interfacial transition zone and compressive strength of concrete,” *Constr. Build. Mater.*, vol. 44, pp. 1–6, 2013.
- [217] J. M. Justice, L. H. Kennison, B. J. Mohr, S. L. Beckwith, L. E. McCormick, B. Wiggins, Z. Z. Zhang, and K. E. Kurtis, “Comparison of Two Metakaolins and a Silica Fume Used as Supplementary Cementitious Materials,” in *Proceedings of the ACI 7th International Symposium on Utilization of High-Strength/High-Performance Concrete*, 2005, pp. 213–236.
- [218] K. A. Gruber, T. Ramlochan, A. Boddy, R. . Hooton, and M. D. A. Thomas, “Increasing concrete durability with high-reactivity metakaolin,” *Cem. Concr. Compos.*, vol. 23, no. 6, pp. 479–484, Dec. 2001.
- [219] G. Batis, P. Pantazopoulou, S. Tsivilis, and E. Badogiannis, “The effect of metakaolin on the corrosion behavior of cement mortars,” *Cem. Concr. Compos.*, vol. 27, no. 1, pp. 125–130, Jan. 2005.
- [220] C.-S. Poon, L. Lam, S. . Kou, Y.-L. Wong, and R. Wong, “Rate of pozzolanic reaction of metakaolin in high-performance cement pastes,” *Cem. Concr. Res.*, vol. 31, no. 9, pp. 1301–1306, Sep. 2001.

- [221] S. Wild, J. M. Khatib, and A. Jones, "Relative strength, pozzolanic activity and cement hydration in superplasticised metakaolin concrete," *Cem. Concr. Res.*, vol. 26, no. 10, pp. 1537–1544, 1996.
- [222] I. G. Richardson, "Tobermorite/jennite- and tobermorite/calcium hydroxide-based models for the structure of C-S-H: applicability to hardened pastes of tricalcium silicate, β -dicalcium silicate, Portland cement, and blends of Portland cement with blast-furnace slag, metakaol," *Cem. Concr. Res.*, vol. 34, no. 9, pp. 1733–1777, 2004.
- [223] E. T. Rodriguez, I. G. Richardson, L. Black, E. Boehm-Courjault, A. Nonat, and J. Skibsted, "Composition, silicate anion structure and morphology of calcium silicate hydrates (C-S-H) synthesised by silica-lime reaction and by controlled hydration of tricalcium silicate (C3S)," *Adv. Appl. Ceram.*, vol. 114, no. 7, pp. 362–371, 2015.
- [224] G. Constantinides and F. J. Ulm, "The nanogranular nature of C-S-H," *J. Mech. Phys. Solids*, vol. 55, no. 1, pp. 64–90, 2007.
- [225] F.-J. Ulm, M. Vandamme, H. M. Jennings, J. Vanzo, M. Bentivegna, K. J. Krakowiak, G. Constantinides, C. P. Bobko, and K. J. Van Vliet, "Does microstructure matter for statistical nanoindentation techniques?," *Cem. Concr. Compos.*, vol. 32, no. 1, pp. 92–99, Jan. 2010.
- [226] F. J. Ulm, M. Vandamme, C. Bobko, J. Alberto Ortega, K. Tai, and C. Ortiz, "Statistical indentation techniques for hydrated nanocomposites: Concrete, bone, and shale," *J. Am. Ceram. Soc.*, vol. 90, no. 9, pp. 2677–2692, 2007.
- [227] K. Ioannidou, K. J. Krakowiak, M. Bauchy, C. G. Hoover, E. Masoero, S. Yip, F. J. Ulm, P. Levitz, R. J.-M. Pellenq, and E. Del Gado, "Mesoscale texture of cement hydrates," *Proc. Natl. Acad. Sci.*, vol. 113, no. 8, pp. 2029–2034, 2016.
- [228] P. Mondal, S. P. Shah, L. D. Marks, and J. J. Gaitero, "Comparative Study of the Effects of Microsilica and Nanosilica in Concrete," *Transp. Res. Rec. J. Transp. Res. Board*, vol. 2141, no. -1, pp. 6–9, 2010.
- [229] C. Hu, Y. Han, Y. Gao, Y. Zhang, and Z. Li, "Property investigation of calcium-silicate-hydrate (C-S-H) gel in cementitious composites," *Mater. Charact.*, vol. 95, pp. 129–139, 2014.
- [230] Z. He, C. Qian, Y. Zhang, F. Zhao, and Y. Hu, "Nanoindentation characteristics of cement with different mineral admixtures," *Sci. China Technol. Sci.*, vol. 56, no. 5, pp. 1119–1123, 2013.
- [231] S. Barbhuiya and P. Chow, "Effects of Metakaolin on Nanomechanical Properties of Cement Paste," in *Calcined Clays for Sustainable Concrete, Proceedings of the 1st International Conference on Calcined Clays for Sustainable Concrete*, 2015, pp. 459–466.

- [232] P. Mondal, S. P. Shah, and L. Marks, “A reliable technique to determine the local mechanical properties at the nanoscale for cementitious materials,” *Cem. Concr. Res.*, vol. 37, no. 10, pp. 1440–1444, Oct. 2007.
- [233] G. Constantinides and F.-J. Ulm, “The effect of two types of C-S-H on the elasticity of cement-based materials: Results from nanoindentation and micromechanical modeling,” *Cem. Concr. Res.*, vol. 34, no. 1, pp. 67–80, Jan. 2004.
- [234] M. Vandamme and F. J. Ulm, “Nanoindentation investigation of creep properties of calcium silicate hydrates,” *Cem. Concr. Res.*, vol. 52, pp. 38–52, 2013.
- [235] M. Vandamme, F. J. Ulm, and P. Fonollosa, “Nanogranular packing of C-S-H at substoichiometric conditions,” *Cem. Concr. Res.*, vol. 40, no. 1, pp. 14–26, 2010.
- [236] P. J. M. Monteiro and C. T. Chang, “The elastic moduli of calcium hydroxide,” *Cem. Concr. Res.*, vol. 25, no. 8, pp. 1605–1609, 1995.
- [237] H. M. Jennings, J. W. Bullard, J. J. Thomas, J. E. Andrade, J. J. Chen, and G. W. Scherer, “Characterization and Modeling of Pores and Surfaces in Cement Paste: Correlations to Processing and Properties,” *J. Adv. Concr. Technol.*, vol. 6, no. 1, pp. 5–29, 2008.
- [238] J. Khatib and S. Wild, “Pore size distribution of metakaolin paste,” *Cem. Concr. Res.*, vol. 26, no. 10, pp. 1545–1553, 1996.
- [239] P. Duan, Z. Shui, W. Chen, and C. Shen, “Influence of metakaolin on pore structure-related properties and thermodynamic stability of hydrate phases of concrete in seawater environment,” *Constr. Build. Mater.*, vol. 36, pp. 947–953, 2012.
- [240] J. M. Justice and K. E. Kurtis, “Influence of Metakaolin Surface Area on Properties of Cement-Based Materials,” *J. Mater. Civ. Eng.*, vol. 19, no. 9, pp. 762–771, 2007.
- [241] R. Snellings, A. Bazzoni, and K. Scrivener, “The existence of amorphous phase in Portland cements: Physical factors affecting Rietveld quantitative phase analysis,” *Cem. Concr. Res.*, vol. 59, pp. 139–146, 2014.
- [242] I. C. Madsen, N. V. Y. Scarlett, and A. Kern, “Description and survey of methodologies for the determination of amorphous content via X-ray powder diffraction,” *Zeitschrift für Krist.*, vol. 226, no. 12, pp. 944–955, Dec. 2011.
- [243] D. Jansen, F. Goetz-Neunhoeffler, C. Stabler, and J. Neubauer, “A remastered external standard method applied to the quantification of early OPC hydration,” *Cem. Concr. Res.*, vol. 41, no. 6, pp. 602–608, Jun. 2011.
- [244] D. Jansen, S. T. Bergold, F. Goetz-Neunhoeffler, and J. Neubauer, “The hydration of alite: A time-resolved quantitative XRD approach using the G-factor method compared with heat release,” *J. Appl. Crystallogr.*, vol. 44, pp. 895–901, 2011.

- [245] D. Jansen, C. Stabler, F. Goetz-Neunhoeffler, S. Dittrich, and J. Neubauer, “Does Ordinary Portland Cement Contain Amorphous Phase? A Quantitative Study Using an External Standard Method,” *Powder Diffr.*, vol. 26, no. 01, pp. 31–38, Mar. 2012.
- [246] D. Bish and R. J. Reynolds, “Sample Preparation for X-Ray Diffraction,” in *Modern Powder Diffraction*, D. Bish and J. Post, Eds. Washington, DC: The Mineralogical Society of America, 1989, pp. 73–99.
- [247] R. Detwiler, L. Powers, U. Jakobsen, W. U. Ahmed, K. L. Scrivener, and K. O. Kjellsen, “Preparing specimens for microscopy,” *Concr. Int.*, vol. 23, no. 11, pp. 51–58, 2001.
- [248] E. P. Barrett, L. G. Joyner, and P. P. Halenda, “The Determination of Pore Volume and Area Distributions in Porous Substances. I. Computations from Nitrogen Isotherms,” *J. Am. Ceram. Soc.*, vol. 73, no. 1, pp. 373–380, 1951.
- [249] G. J. G. Gluth and B. Hillemeier, “Pore structure and permeability of hardened calcium aluminate cement pastes of low w/c ratio,” *Mater. Struct.*, vol. 46, no. 9, pp. 1497–1506, Dec. 2012.
- [250] W. C. Oliver and G. M. Pharr, “An Improved Technique for Determining Hardness and Elastic-Modulus Using Load and Displacement Sensing Indentation Experiments,” *J. Mater. Res.*, vol. 7, no. 6, pp. 1564–1583, 1992.
- [251] G. Constantinides, K. S. Ravi Chandran, F.-J. Ulm, and K. J. Van Vliet, “Grid indentation analysis of composite microstructure and mechanics: Principles and validation,” *Mater. Sci. Eng. A*, vol. 430, no. 1–2, pp. 189–202, 2006.
- [252] K. De Weerd, M. Ben Haha, G. Le Saout, K. O. Kjellsen, H. Justnes, and B. Lothenbach, “Hydration mechanisms of ternary Portland cements containing limestone powder and fly ash,” *Cem. Concr. Res.*, vol. 41, no. 3, pp. 279–291, 2011.
- [253] M. Antoni, J. Rossen, F. Martirena, and K. Scrivener, “Cement substitution by a combination of metakaolin and limestone,” *Cem. Concr. Res.*, vol. 42, no. 12, pp. 1579–1589, Dec. 2012.
- [254] R. Snellings, a. Salze, and K. L. Scrivener, “Use of X-ray diffraction to quantify amorphous supplementary cementitious materials in anhydrous and hydrated blended cements,” *Cem. Concr. Res.*, vol. 64, pp. 89–98, 2014.
- [255] F. Cassagnabère, G. Escadeillas, and M. Mouret, “Study of the reactivity of cement/metakaolin binders at early age for specific use in steam cured precast concrete,” *Constr. Build. Mater.*, vol. 23, no. 2, pp. 775–784, 2009.
- [256] M. Boháč, M. Palou, R. Novotný, J. Másilko, D. Všianský, and T. Staněk, “Investigation on early hydration of ternary Portland cement-blast-furnace slag–metakaolin blends,” *Constr. Build. Mater.*, vol. 64, pp. 333–341, Aug. 2014.

- [257] A. Valori, P. J. McDonald, and K. L. Scrivener, “The morphology of C–S–H: Lessons from 1H nuclear magnetic resonance relaxometry,” *Cem. Concr. Res.*, vol. 49, pp. 65–81, Jul. 2013.
- [258] J. P. Korb, L. Monteilhet, P. J. McDonald, and J. Mitchell, “Microstructure and texture of hydrated cement-based materials: A proton field cycling relaxometry approach,” *Cem. Concr. Res.*, vol. 37, no. 3, pp. 295–302, 2007.
- [259] I. Odler, “The BET-specific surface area of hydrated Portland cement and related materials,” *Cem. Concr. Res.*, vol. 33, no. 12, pp. 2049–2056, Dec. 2003.
- [260] H. M. Jennings and J. J. Thomas, “A discussion of the paper ‘The BET-specific surface area of hydrated Portland cement and related materials’ by Ivan Odler,” *Cem. Concr. Res.*, vol. 34, no. 10, pp. 1959–1960, Oct. 2004.
- [261] K. Velez, S. Maximilien, D. Damidot, G. Fantozzi, and F. Sorrentino, “Determination by nanoindentation of elastic modulus and hardness of pure constituents of Portland cement clinker,” *Cem. Concr. Res.*, vol. 31, no. 4, pp. 555–561, Apr. 2001.
- [262] J. J. Hughes and P. Trtik, “Micro-mechanical properties of cement paste measured by depth-sensing nanoindentation: a preliminary correlation of physical properties with phase type,” *Mater. Charact.*, vol. 53, no. 2–4, pp. 223–231, Nov. 2004.
- [263] F. Pelisser, P. J. P. Gleize, and A. Mikowski, “Effect of the Ca/Si molar ratio on the micro/nanomechanical properties of synthetic C-S-H measured by nanoindentation,” *J. Phys. Chem. C*, vol. 116, no. 32, pp. 17219–17227, 2012.
- [264] C. Hu and Z. Li, “Property investigation of individual phases in cementitious composites containing silica fume and fly ash,” *Cem. Concr. Compos.*, Dec. 2014.
- [265] H. M. Jennings, J. J. Thomas, J. S. Gevrenov, G. Constantinides, and F.-J. Ulm, “A multi-technique investigation of the nanoporosity of cement paste,” *Cem. Concr. Res.*, vol. 37, no. 3, pp. 329–336, Mar. 2007.
- [266] J. Němeček, V. Šmilauer, and L. Kopecký, “Nanoindentation characteristics of alkali-activated aluminosilicate materials,” *Cem. Concr. Compos.*, vol. 33, no. 2, pp. 163–170, 2011.

APPENDIX A: COPYRIGHT PERMISSIONS


Below is permission from the Florida Department of Transportation to use the material presented in this dissertation. This refers to the data presented in Chapters 3 through 6.

Permission to use reports for dissertation



Inbox x



 **Natallia Shanahan** <nkashalo@mail.usf.edu>

Jan 19 ☆



to Harvey, Abia ▾

Dr. Deford,

I am in the process of writing my dissertation, and would like to ask for your permission and approval to use the reports from the Long-Life Slab Replacement project, contract number BDV25-977-01, and from the Chemical and Mineral Admixtures project in my dissertation.

Thank you,

Natalya

 **DeFord, Harvey** <Harvey.DeFord@dot.state.fl.us>

Jan 19 ☆



to Research, me, Abia ▾

Natalya,

You have FDOT permission to use the results presented in the reports submitted for the BDV25-977-01 and BDV25-977-02 projects for which Prof. Zayed was Principal Investigator and I was Project Manager.

Hope the writing goes well.

Dale

Dale DeFord, PhD
Structural Materials Research Specialist
Office: [352-955-6671](tel:352-955-6671), Fax: [850-412-8355](tel:850-412-8355)
Office Hours: M-Th 7:00 AM-5:30 PM
harvey.deford@dot.state.fl.us

Note: Most written communications to or from state officials are public records available to the public and media upon request (Florida Statute, Chapter 119).

Below is permission for use of the article published in the Journal of the American Ceramic Society included as Chapter 3. The relevant section is circled in red.

COPYRIGHT TRANSFER AGREEMENT



Date: 02/23/2016 Contributor name: Natallia Shanahan

Contributor address: 4202 E Fowler Ave, Tampa, FL 33620, USA

Manuscript number (if known): JACE14221

Re: Manuscript entitled Effect of Chloride-Based Accelerator in the Presence of Water-Reducing and Retarding Admixture on Autogenous Shrinkage (the "Contribution")

for publication in the Journal of the American Ceramic Society (the "Journal")

published by Wiley-Blackwell ("Wiley-Blackwell").

Dear Contributor(s):

Thank you for submitting your Contribution for publication. In order to expedite the editing and publishing process and enable Wiley-Blackwell to disseminate your Contribution to the fullest extent, we need to have this Copyright Transfer Agreement signed and returned as directed in the Journal's instructions for authors as soon as possible. If the Contribution is not accepted for publication, or if the Contribution is subsequently rejected, this Agreement shall be null and void. **Publication cannot proceed without a signed copy of this Agreement.**

A. COPYRIGHT

1. The Contributor assigns to Wiley-Blackwell, during the full term of copyright and any extensions or renewals, all copyright in and to the Contribution, and all rights therein, including but not limited to the right to publish, republish, transmit, sell, distribute and otherwise use the Contribution in whole or in part in electronic and print editions of the Journal and in derivative works throughout the world, in all languages and in all media of expression now known or later developed, and to license or permit others to do so.

2. Reproduction, posting, transmission or other distribution or use of the final Contribution in whole or in part in any medium by the Contributor as permitted by this Agreement requires a citation to the Journal and an appropriate credit to Wiley-Blackwell as Publisher, and/or the Society if applicable, suitable in form and content as follows: (Title of Article, Author, Journal Title and Volume/Issue, Copyright © [year], copyright owner as specified in the Journal). Links to the final article on Wiley-Blackwell's website are encouraged where appropriate.

B. RETAINED RIGHTS

Notwithstanding the above, the Contributor or, if applicable, the Contributor's Employer, retains all proprietary rights other than copyright, such as patent rights, in any process, procedure or article of manufacture described in the Contribution.

3. **Final Published Version.** Wiley-Blackwell hereby licenses back to the Contributor the following rights with respect to the final published version of the Contribution:

a. Copies for colleagues. The personal right of the Contributor only to send or transmit individual copies of the final published version to colleagues upon their specific request provided no fee is charged, and further-provided that there is no systematic distribution of the Contribution, e.g. posting on a listserve, website or automated delivery. For those Contributors who wish to send high-quality e-prints, purchase reprints, or who wish to distribute copies more broadly than allowed hereunder (e.g. to groups of colleagues or mailing lists), please contact the publishing office.

b. Re-use in other publications. The right to re-use the final Contribution or parts thereof for any publication authored or edited by the Contributor (excluding journal articles) where such re-used material constitutes less than half of the total material in such publication. In such case, any modifications should be accurately noted.

c. Teaching duties. The right to include the Contribution in teaching or training duties at the Contributor's institution/place of employment including in course packs, e-reserves, presentation at professional conferences, in-house training, or distance learning. The Contribution may not be used in seminars outside of normal teaching obligations (e.g. commercial seminars). Electronic posting of the final published version in connection with teaching/training at the Contributor's institution/place of employment is